Supporting Information

Sky-blue emitting bridged diiridium complexes: beneficial effects of intramolecular π–π stacking

Daniel G. Congrave, Yu–Ting Hsu, Andrei S. Batsanov, Andrew Beeby, and Martin R. Bryce*

Department of Chemistry, Durham University, Durham DH1 3LE, U.K.

Email: m.r.bryce@durham.ac.uk

Contents **Page**

Experimental Section

General

^{1}H, ^{13}C and ^{19}F NMR spectra were recorded on Bruker Avance 400 MHz, Varian Mercury 200, and 400 MHz, Varian Inova 500 MHz or Varian VNMRS 600 and 700 MHz spectrometers. All spectra were either referenced against the residual solvent signal or tetramethylsilane (TMS) and peak shifts are reported in ppm. Where assigned, cyclohexyl protons are labelled 'e' or 'a' to denote equatorial or axial positions, respectively. The labels 'ap. t' and 'bs' denote an apparent triplet and a broad singlet, respectively. For ^{13}C NMR assignment the labels * and # denote 2 and 3 overlapping signals, respectively. Electrospray ionisation (ESI) mass spectra were recorded on a Waters Ltd. TQD spectrometer. Atmospheric solids analysis probe (ASAP) mass spectra were recorded on a LCT premier XE spectrometer. Matrix-assisted laser desorption time-of-flight (MALDI–TOF) mass spectra were recorded on a Bruker Daltonik Autoflex II spectrometer running in positive ion reflectron mode. MALDI–TOF samples were prepared in CH_2Cl_2 (DCM) with *trans*-2-[3-(4-*tert*-butylphenyl)-2-methyl-2-propenylidene]malononitrile (DCTB) as the matrix. Elemental analyses were obtained on an Exeter Analytical Inc. CE-440 elemental analyser. Thermal analysis was run under a helium atmosphere at a rate of 10 °C min^{-1} using a Perkin-Elmer Pyris 1 instrument. Reactions requiring an inert atmosphere were carried out under argon which was first passed through a phosphorus pentoxide column. Thin layer chromatography (TLC) was carried out on silica gel (Merck, silica gel 60, F254) or alumina (Merck, neutral alumina 60 type E, F254) plates and visualized using UV light (254, 315, 365 nm). Flash chromatography was carried out using either glass columns or a Biotage® Isolera OneTM automated flash chromatography machine on 60 micron silica gel purchased from Fluorochem Ltd.

Chemicals

All commercial chemicals were of ≥95% purity and were used as received without further purification. $[Ir(ppy)_2\mu\text{–}Cl]_2$[1] and 4-(2,4,6-trimethylphenyl)-2-chloropyridine[2] were synthesised according to literature procedures. All solvents used were of analytical reagent grade or higher. Anhydrous solvents were dried through a HPLC column on an Innovative Technology Inc. solvent purification system or purchased from Acros (dry diglyme).

Calculations

All calculations were carried out with the Gaussian 09 package.[3] All optimized S_0 geometries of the diiridium complexes were carried out using B3LYP[4,5] with the pseudopotential (LANL2DZ)[6–8] for iridium and 3–21G* basis set for all other atoms.[9,10]All S_0 geometries were true minima based on no imaginary frequencies found. Electronic structure calculations were also carried out on the optimised geometries at B3LYP/LANL2DZ:3–21G*. The MO diagrams and orbital contributions were generated with the aid of Gabedit[11] and GaussSum[12] packages, respectively.

X-ray Crystallography

X-ray diffraction experiments were carried out at 120 K on a Bruker 3-circle diffractometer D8 Venture with a PHOTON 100 CMOS area detector, using Mo-*K*α radiation from a IμS microsource with focussing mirrors and a Cryostream (Oxford Cryosystems) open-flow N_2 gas cryostat. The absorption correction was carried out by numerical integration based on crystal face indexing, using SADABS program.[13] The structures were solved by Patterson (**7**, **11**, **12**) or direct methods using SHELXS 2013/1 software[14] and refined in anisotropic approximation by full matrix least squares against F^2 off all data, using OLEX2[15] and SHELXL 2016/6 software.[16]

Electrochemistry

Cyclic voltammetry experiments were recorded using either BAS CV50W electrochemical analyzer or a a PalmSens EmStat^2 potentiostat with PSTrace software. A three-electrode system consisting of a Pt disk (Ø = 1.8 mm) as the working electrode, a Pt wire as an auxiliary electrode and an Pt wire as a quasireference electrode was used. Cyclic voltammetry experiments were conducted at a scan rate of 100 mV/s. Experiments were conducted in dry, degassed DCM with *n*-Bu_4NPF_6 (0.1 M) as the supporting electrolyte and were referenced internally to ferrocene. Oxidation processes are assigned as being electrochemically reversible based on the equal magnitudes of corresponding oxidation and reduction peaks.

Photophysics

General The absorption spectra were measured on either a Unicam UV2-100 spectrometer operated with the Unicam Vision software or a Thermo Scientific Evolution 220 spectrometer with the Thermo Scientific Insight software in quartz cuvettes with a path length of 20 mm. The pure solvent was used for the baseline correction. The extinction coefficients were calculated using the Beer-Lambert Law, $A = \varepsilon cl$. The photoluminescence spectra were recorded on a Horiba Jobin Yvon SPEX Fluorolog 3-22 spectrofluorometer in quartz cuvettes with a path length of 10 mm. All Ir complexes were measured in degassed DCM (repeated freeze-pump-thaw cycles using a turbomolecular pump). The quantum yields of all samples were determined by the comparative method relative to. quinine sulphate in 0.5 M H_2SO_4 (Φ = 0.546[17]) following the literature procedure.[18] The quantum yields of complexes doped into poly(methyl methacrylate) (PMMA) thin films were recorded on a Horiba Jobin Yvon SPEX Fluorolog 3 using a calibrated Quanta-Φ integrating sphere and were calculated according to the literature method.[19] Solid state PLQY data were obtained in triplicate from three samples that were prepared in parallel: the calculated standard error values were ≤10%. Lifetime measurements were recorded using an N_2 laser (337 nm, 10 μJ, 10 Hz) as an excitation source in a custom spectrometer which produced a 1 kHz train of pulses of 20 ns duration. The luminescence was collected at 90° and focused onto the entrance slit of a monochromator (Bethan TM 300V). The emission was detected by a photon counting PMT and the arrival times of photons at the detector determined using a multichannel scaler. The data were transferred to a PC and analysed using non-linear regression. The decay data were fitted to exponential functions. Low temperature emission spectra and lifetime data were measured in a DN1704 optical cryostat (Oxford Instruments) with a ITC601 temperature controller (Oxford Instruments).

PMMA film preparation An adaptation of our previously reported method was used.[20] This adaptation was possible due to the improved solubility of the complexes studied here in chlorobenzene (CB) and is experimentally simpler. 100 μL of a 1 mg mL^{-1} solution of the diiridium complex in DCM was added to 1 mL of a 10 mg mL^{-1} solution of PMMA in CB and the resulting solution was stirred open to air at room temperature (*ca.* 2 h). The solution was then drop-cast using a Gilson precision pipette onto a 10 × 1 mm circular quartz disk (UQG Optics Ltd., UK) in a single. 150 μL portion. The substrate was heated to *ca.* 40 ºC overnight on a hot plate under air. Photophysical analysis was then immediately carried out. The PLQY values obtained using films prepared in this manner were the same (within experimental error) as those obtained using our previously reported method.

Synthesis

The synthesis of **21** (Scheme S1) started with etherification of the xylenol **23** with bromomethylcyclohexane to obtain the aryl ether **24** in 98% yield. Subsequent trapping of the lithiated derivative of **24** with $SnBu_3Cl$ afforded the stannane **25**. This was coupled with 4-iodo-2-chloropyridine in a Stille reaction to chemoselectively obtain the 2-chloropyridine derivative **26**. Finally, Suzuki-Miyaura coupling of **26** with 2,4-difluorophenylboronic acid afforded **21** in 90% yield. **22** was synthesised from **27** via a sequential etherification and cross coupling strategy analogous to ligand **21**

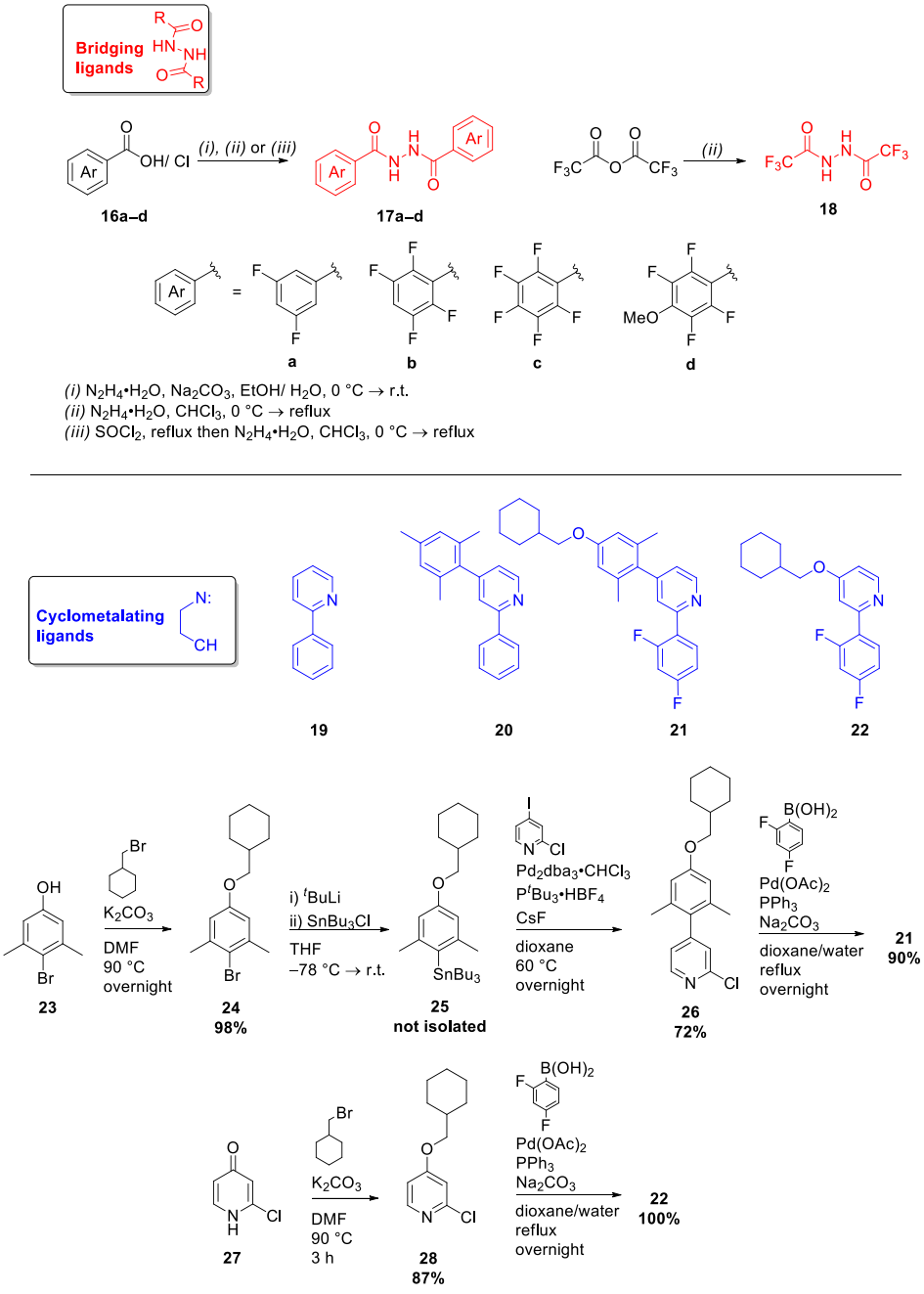

Scheme S1. Structures and synthetic schemes for the bridging and cyclometalating ligands studied in this work.

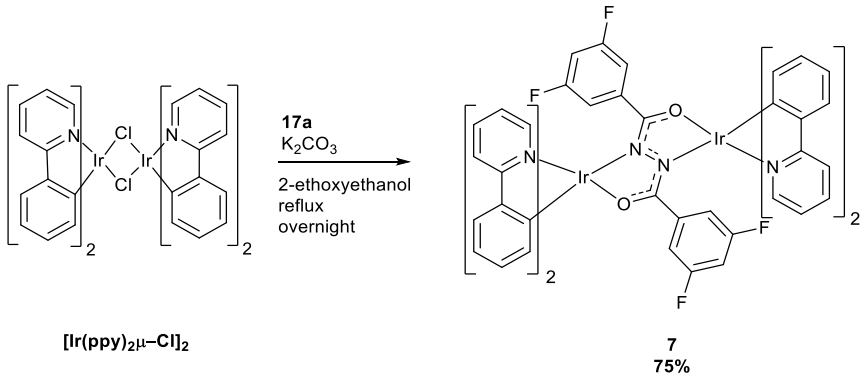

Complex 7. *N*,*N*′-Bis(3,5-difluorobenzoyl)hydrazide (**17a**) (87 mg, 0.28 mmol, 1.00 eq.), $[Ir(ppy)_2\mu\text{-}Cl]_2$ (300 mg, 0.28 mmol, 1.00 eq.) and K_2CO_3 (116 mg, 0.84 mmol, 3.00 eq.) were added to 2-ethoxyethanol (15 mL) under and argon atmosphere and heated to reflux overnight. The reaction mixture was then cooled to room temperature and the solvent was removed under reduced pressure. The residue was then dissolved in DCM and suspended onto celite (*c.a.* 2 g) under reduced pressure, before being subjected to flash chromatography on silica gel (eluent: gradient *n*-hexane/ DCM sat. K_2CO_3 3:7 – 0:1). The yellow band was collected and after removing the solvent under reduced pressure, the residue was dissolved in a minimal amount of DCM (*ca*. 20 mL). Addition of methanol (*ca*. 20 mL) followed by reducing the volume of the mixture to 20 mL afforded complex **7** (275 mg, 0.21 mmol, 75%) as a yellow precipitate which was isolated via filtration and washed sequentially with methanol followed by pentane. The isolated product was a mixture of diastereomers in a *ca.* 9:1 ratio. MS (MALDI–TOF): *m/z* 1312.2 [M^+]. Calcd. for $C_{58}H_{38}F_4Ir_2N_6O_2^+$: 1312.2; Anal. Calcd. for $C_{58}H_{38}F_4Ir_2N_6O_2$: C, 53.12; H, 2.92; N, 6.41, Calcd. for $C_{58}H_{38}F_4Ir_2N_6O_2{\cdot}0.2CH_2Cl_2$: C, 52.62; H, 2.91; N, 6.33. Found: C, 52.62; H, 2.95; N, 6.27.;

Major diastereomer: ^{1}H NMR (600 MHz, CD_2Cl_2, TMS) δ (ppm) = 9.00 (ddd, *J* = 5.7, 1.6, 0.8 Hz, $2H_A$), 8.70 (dt, *J* = 5.6, 1.2 Hz, $2H_B$), 8.02 – 7.89 (m, $4H_{2A}$), 7.85 – 7.76 (m, $4H_{2B}$), 7.54 – 7.45 (m, $4H_{A,D}$), 7.36 (dd, *J* = 7.8, 1.4 Hz, $2H_C$), 7.10 (ddd, *J* = 6.7, 5.7, 2.2 Hz, $2H_B$), 6.80 (td, *J* = 7.5, 1.3 Hz, $2H_D$), 6.68 – 6.58 (m, $4H_{C,D}$), 6.41 (td, *J* = 7.5, 1.4 Hz, $2H_C$), 6.17 (tt, *J* = 9.1, 2.4 Hz, $2H_{E2}$), 6.07 – 6.00 (m, $2H_D$), 5.91 (dd, *J* = 7.8, 1.2 Hz, $2H_C$), 5.88 (s, $4H_{E4}$); ^{19}F {^{1}H} NMR (376 MHz, CD_2Cl_2) δ (ppm) = -110.65 (s, 2F).

Due to poor solubility in organic solvents, a solution sufficiently concentrated to obtain a ^{13}C NMR spectrum of the diastereomeric mixture could not be obtained. The ^{1}H NMR spectrum of the minor diastereomer could not be completely deconvoluted due to its low concentration and the presence of overlapping signals. The ^{1}H NMR spectrum of the mixture is shown as Figure S1. Single crystals of the *meso* diastereomer suitable for X-ray diffraction were grown by vapour diffusion of methanol into a DCM solution of the complex.

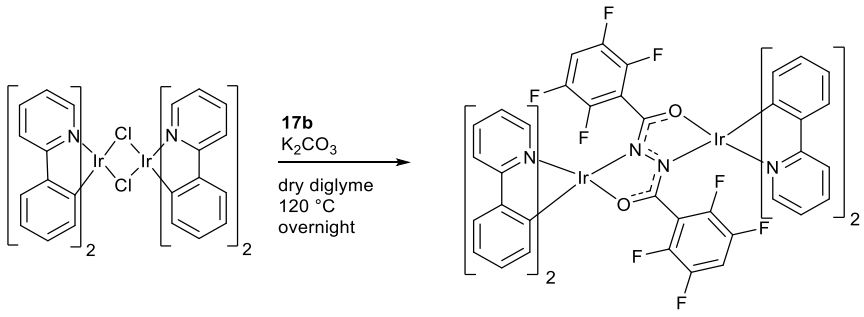

[Ir(ppy)$_2$μ–Cl]$_2$ **8** 53%

Complex 8. *N*,*N*′-Bis(2,3,5,6-tetrafluorobenzoyl)hydrazide (**17b**) (108 mg, 0.28 mmol, 1.00 eq.) was added to dry diglyme (10 mL) with K_2CO_3 (200 mg, 1.45 mmol, 5.18 eq.) and heated to 50 °C under an argon atmosphere for 30 min to obtain a pale yellow suspension. [Ir(ppy)$_2$μ-Cl]$_2$ (300 mg, 0.28 mmol, 1.00 eq.) was then added and the mixture was heated to 120 °C overnight. The reaction mixture was then cooled to room temperature and the solvent was removed under reduced pressure. The residue was dissolved in DCM and suspended onto celite (*c.a.* 2 g) under reduced pressure, before being subjected to flash chromatography on silica gel (eluent: DCM sat. K_2CO_3). The glowing yellow band was collected and after removing the solvent under reduced pressure, the residue was dissolved in a minimal amount of DCM (*ca*. 10 mL). Addition of hexane (*ca*. 20 mL) followed by reducing the volume of the mixture to 25 mL afforded complex **8** (207 mg, 0.15 mmol, 53%) as a yellow precipitate which was isolated via filtration and washed with pentane. The product was isolated as a mixture of diastereomers in a *ca*. 9:1 ratio. MS (MALDI–TOF): *m/z* 1384.2 [M^+]. Calcd. for $C_{58}H_{34}F_8Ir_2N_6O_2^+$: 1384.2; Anal. Calcd. for $C_{58}H_{34}F_8Ir_2N_6O_2$: C, 50.36; H, 2.48; N, 6.08. Found: C, 50.06; H, 2.47; N, 6.00;

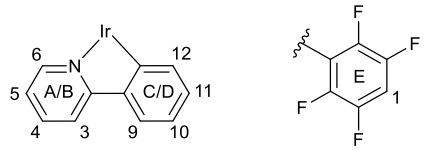

Major diastereomer: ^{1}H NMR (600 MHz, CD_2Cl_2, TMS) δ (ppm) = 9.18 (d, *J* = 5.6 Hz, 2H$_{A6}$), 8.31 (d, *J* = 5.6 Hz, 2H$_{B6}$), 7.97 – 7.94 (m, 2H$_{A4}$), 7.93 – 7.87 (m, 6H$_{A3, B4, B3}$), 7.50 (d, *J* = 7.1 Hz, 2H$_{C9}$), 7.46 (ddd, *J* = 7.5, 5.6, 1.5 Hz, 2H$_{A5}$), 7.37 (d, *J* = 7.2 Hz, 2H$_{D9}$), 7.14 (ddd, *J* = 7.2, 5.6, 1.6 Hz, 2H$_{B5}$), 6.79 (td, *J* = 7.4, 1.2 Hz, 2H$_{C10}$), 6.63 – 6.59 (m, 4H$_{C11, D10}$), 6.47 (td, *J* = 7.5, 1.0 Hz, 2H$_{D11}$), 6.38 – 6.32 (m, 2H$_{E1}$), 6.12 (d, *J* = 7.7 Hz, 2H$_{D12}$), 5.91 (d, *J* = 7.4 Hz, 2H$_{C12}$); ^{19}F {^{1}H} NMR (376 MHz, CD_2Cl_2) δ (ppm) =-138.37 (dd, *J* = 24.5, 12.0 Hz, 2F), -140.73 (dd, *J* = 23.0, 12.4 Hz, 2F), -141.90 (dd, *J* = 24.5, 12.4 Hz, 2F), -145.59 (dd, *J* = 23.0, 12.0 Hz, 2F).

Minor diastereomer: ^{19}F NMR (376 MHz, CD_2Cl_2) δ (ppm) =-139.55 (dd, *J* = 24.2, 11.7 Hz), -139.80 (dd, *J* = 23.4, 12.4 Hz), -143.09 (dd, *J* = 24.2, 11.7 Hz), -144.38 (dd, *J* = 23.4, 12.4 Hz).

Due to poor solubility in organic solvents, a solution sufficiently concentrated to obtain a ^{13}C NMR spectrum of the diastereomeric mixture could not be obtained. The ^{1}H NMR spectrum of the minor diastereomer could not be completely deconvoluted due to its low concentration and the presence of overlapping signals. The ^{1}H NMR spectrum of the mixture is shown as Figure S4.

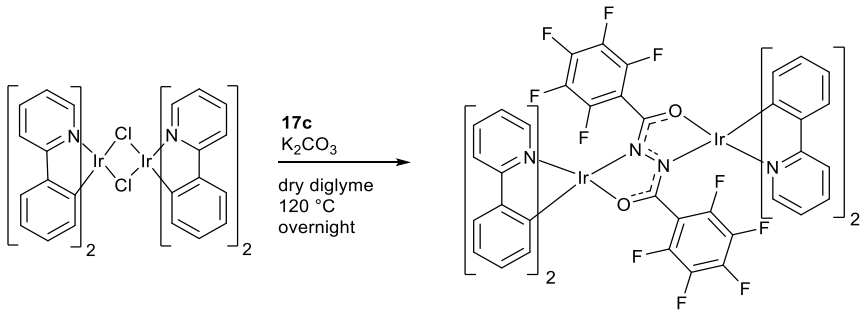

[Ir(ppy)$_2$μ–Cl]$_2$ **9** **33%**

Complex 9. [Ir(ppy)$_2$μ-Cl]$_2$ (160 mg, 0.15 mmol, 1.00 eq.) and *N*,*N*′-bis(pentafluorobenzoyl)hydrazide (**17c**) (63 mg, 0.15 mmol, 1.00 eq.) were added to dry diglyme (20 mL) and heated to 120 °C under an argon atmosphere for 24 h. The reaction mixture was then cooled to room temperature and the solvent was removed under reduced pressure. The residue was then dissolved in DCM and suspended onto celite (*c.a.* 2 g) under reduced pressure, before being subjected to flash chromatography on silica gel (eluent: *n*-hexane/ DCM sat. K_2CO_3 1:1 v/v). The glowing yellow band was collected and after removing the solvent under reduced pressure, the residue was dissolved in a minimal amount of DCM (*ca*. 10 mL). Addition of hexane (*ca*. 20 mL) followed by reducing the volume of the mixture to 25 mL afforded complex **9** (70 mg, 0.05 mmol, 33%) as a yellow precipitate which was isolated via filtration and washed with pentane. The product was isolated as a mixture of diastereomers in a *ca.* 5:4 ratio (*meso:rac*). MS (MALDI–TOF): *m/z* 1420.1 [M^+]. Calcd. for $C_{58}H_{32}F_{10}Ir_2N_6O_2^+$: 1420.2; Anal. Calcd. for $C_{58}H_{32}F_{10}Ir_2N_6O_2$: C, 49.08; H, 2.27; N, 5.92. Found: C, 49.16; H, 2.31; N, 5.89.

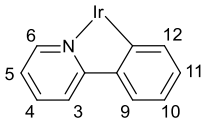

A/B

^{1}H and ^{19}F NMR

Meso diastereomer: ^{1}H NMR (700 MHz, CD_2Cl_2, TMS) δ (ppm) = 8.94 (d, *J* = 5.4 Hz, 2H$_{B6}$), 8.69 (d, *J* = 5.6 Hz, 2H$_{A6}$), 7.98 – 7.88 (m, 4H$_{B4,B3}$), 7.81 – 7.75 (m, 4H$_{A4,A3}$), 7.51 – 7.48 (m, 2H$_{B5}$), 7.47 – 7.44 (m, 2H$_{A9}$), 7.42 – 7.38 (m, 2H$_{B9}$), 7.02 (ddd, *J* = 7.3, 5.6, 2.0 Hz, 2H$_{A5}$), 6.81 – 6.77 (m, 2H$_{A10}$), 6.71 – 6.67 (m, 2H$_{B10}$), 6.64 – 6.59 (m, 2H$_{A11}$), 6.54 – 6.48 (m, 2H$_{B11}$), 6.07 (d, *J* = 7.7 Hz, 2H$_{B12}$), 5.96 (dd, *J* = 7.9, 1.2 Hz, 2H$_{A12}$); ^{19}F {^{1}H} NMR (376 MHz, CD_2Cl_2) δ (ppm) = -142.9 (dd, *J* = 24.2, 7.8 Hz, 2F), -144.0 (dd, *J* = 24.4, 7.8 Hz, 2F), -155.8 – -155.9 (m, 2F), -161.7 (td, *J* = 22.8, 7.8 Hz, 2F), -162.1 (td, *J* = 22.7, 7.7 Hz, 2F).

Rac diastereomer: ^{1}H NMR (700 MHz, CD_2Cl_2, TMS) δ (ppm) = 9.13 (d, *J* = 5.6 Hz, 2H$_{B6}$), 8.27 (d, *J* = 5.4 Hz, 2H$_{A6}$), 7.98 – 7.88 (m, 8H$_{B4,B3,A4,A3}$), 7.51 – 7.48 (m, 2H$_{A9}$), 7.47 – 7.44 (m, 2H$_{B5}$), 7.42 – 7.38 (m, 2H$_{B9}$), 7.14 (ddd, *J* = 7.2, 5.6, 1.5 Hz, 2H$_{A5}$), 6.81 – 6.77 (m, 2H$_{A10}$), 6.71 – 6.67 (m, 2H$_{B10}$), 6.64 – 6.59 (m, 2H$_{A11}$), 6.54 – 6.48 (m, 2H$_{B11}$), 6.12 (d, *J* = 7.8 Hz, 2H$_{B12}$), 5.90 (dd, *J* = 7.6, 1.1 Hz, 2H$_{A12}$); ^{19}F {^{1}H} NMR (376 MHz, CD_2Cl_2) δ (ppm) = -141.6 (d, *J* = 22.6 Hz, 2F), -145.2 (d, *J* = 23.7 Hz, 2F), -155.8 – -155.9 (m, 2F), -160.5 – -160.7 (m, 2F), -162.9 – -163.1 (m, 2F).

^{13}C NMR

Meso diastereomer: ^{13}C NMR (176 MHz, CD_2Cl_2, TMS) δ (ppm) = 149.2 (C$_{A6}$), 147.93 (C$_{B6}$), 131.8 (C$_{B12}$), 131.5 (C$_{A12}$), 129.2 (C$_{A11}$), 128.9 (C$_{B11}$), 123.8 (C$_{A9}$), 123.8 (C$_{B9}$), 121.6 (C$_{A10}$), 121.6 (C$_{B5}$), 121.5 (C$_{A5}$), 119.6 (C$_{B10}$).

Rac diastereomer: ^{13}C NMR (176 MHz, CD_2Cl_2, TMS) δ (ppm) = 149.8 (C$_{B6}$), 148.4 (C$_{A6}$), 131.8 (C$_{A12}$), 131.5 (C$_{B12}$), 129.1 (C$_{A11}$), 128.8 (C$_{B11}$), 123.5 (C$_{B9}$), 121.9 (C$_{A5}$), 121.7 (C$_{A10}$), 121.7 (C$_{A9}$), 121.5 (C$_{B5}$), 120.0 (C$_{B10}$). Due to low solubility in organic solvents, extensive coupling to ^{19}F nuclei and overlapping signals due to the presence of two diastereomers, some of the ^{13}C NMR signals could not be unambiguously assigned. All signals that could be clearly identified in the ^{13}C, ^{1}H–^{13}C

HSQC and ^{1}H–^{13}C HMBC NMR spectra are reported. The spectra are included as Figures S8, S11 and S12. To obtain a sample of the *meso* (ΛΔ) isomer, which was used to grow crystals suitable for X-ray diffraction, the diastereomeric mixture was suspended in toluene at a concentration of 1 mg/ mL. The suspension was refluxed for 20 minutes and then hot filtered to obtain a sample of the *meso* (ΛΔ) isomer as the filtrand. Crystals were grown by layering a near-saturated DCM solution of the complex with hexane.

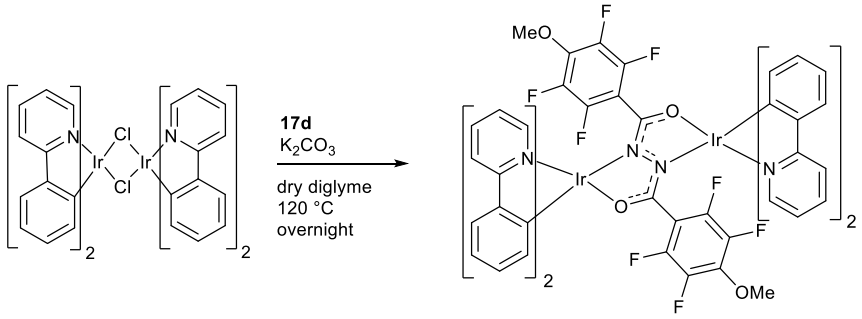

Complex 10. *N*,*N*′-Bis(2,3,5,6-tetrafluoro-4-methoxybenzoyl)hydrazide (**17d**) (62 mg, 0.14 mmol, 1.00 eq.) was added to dry diglyme (5 mL) with K_2CO_3 (96 mg, 0.70 mmol, 5.00 eq.) and heated to 50 °C under an argon atmosphere for 30 min to obtain a pale yellow suspension. $[Ir(ppy)_2\mu\text{-}Cl]_2$ (150 mg, 0.14 mmol, 1.00 eq.) was then added and the mixture was heated to 120 °C overnight. The reaction mixture was then cooled to room temperature and the solvent was removed under reduced pressure. The residue was then dissolved in DCM and suspended onto celite (*c.a.* 2 g) under reduced pressure, before being subjected to flash chromatography on silica gel (eluent: DCM sat. K_2CO_3). The glowing yellow band was collected and after removing the solvent under reduced pressure, the residue was dissolved in a minimal amount of DCM (*ca*. 5 mL). Addition of methanol (*ca*. 20 mL) followed by reducing the volume of the mixture to *ca*. 20 mL afforded complex **10** (57 mg, 0.04 mmol, 28%) as a yellow precipitate which was isolated via filtration and washed with pentane. The product was obtained as a mixture of diastereomers in a *ca.* 5:4 ratio. MS (MALDI–TOF): *m/z* 1444.2 [M^+]. Calcd. for $C_{60}H_{38}F_8Ir_2N_6O_4^+$: 1444.2; Anal. Calcd. for $C_{60}H_{38}F_8Ir_2N_6O_4$: C, 49.93; H, 2.65; N, 5.82, Calcd. for $C_{60}H_{38}F_8Ir_2N_6O_4{\cdot}0.2CH_2Cl_2$: C, 49.51; H, 2.65; N, 5.75. Found: C, 49.50; H, 2.76; N, 5.70.

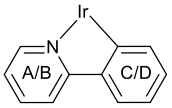

^{1}H and ^{19}F NMR

Major diastereomer: ^{1}H NMR (600 MHz, CD_2Cl_2, TMS) δ (ppm) = 9.16 (d, J = 5.6 Hz, $2H_A$), 8.27 (dt, J = 5.5, 1.2 Hz, $2H_B$), 7.96 – 7.86 (m, $8H_{2A,\ 2B}$), 7.50 – 7.41 (m, $4H_{A,C}$), 7.40 – 7.36 (m, $2H_D$), 7.11 (ddd, J = 7.3, 5.7, 1.7 Hz, $2H_B$), 6.80 – 6.75 (m, $2H_C$), 6.65 – 6.57 (m, $4H_{C,D}$), 6.50 – 6.43 (m, $2H_D$), 6.11 (d, J = 7.7 Hz, $2H_D$), 5.91 (dd, J = 7.8, 1.2 Hz, $2H_C$), 3.86 (s, $6H_{MeO}$); ^{19}F {^{1}H} NMR (376 MHz, CD_2Cl_2) δ (ppm) = -143.2 – -143.5 (m, 2F), -146.6 – -146.8 (m, 2F), -157.7 – -157.9 (m, 2F), -159.4 – -159.7 (m, 2F).

Minor diastereomer: ^{1}H NMR (600 MHz, CD_2Cl_2, TMS) δ (ppm) = 8.95 (dd, J = 5.4, 1.3 Hz, $2H_A$), 8.72 (d, J = 5.7 Hz, $2H_B$), 7.96 – 7.86 (m, H_{2A}), 7.79 – 7.73 (m, $4H_{2B}$), 7.50 – 7.41 (m, $H_{A,C}$), 7.40 – 7.36 (m, $2H_D$), 7.01 (ddd, J = 7.2, 5.7, 2.0 Hz, $2H_B$), 6.80 – 6.75 (m, $2H_C$), 6.65 – 6.57 (m, $4H_{C,D}$), 6.50 – 6.43 (m, $2H_D$), 6.06 (d, J = 7.7 Hz, $2H_D$), 5.96 (dd, J = 7.8, 1.1 Hz, $2H_C$), 3.86 (s, $6H_{MeO}$); ^{19}F {^{1}H} NMR (376 MHz, CD_2Cl_2) δ (ppm) = -144.4 – -144.7 (m, 2F), -145.5 – -145.8 (m, 2F), -158.5 – -158.9 (m, 4F).

^{13}C NMR

Diasteromeric mixture: ^{13}C NMR (151 MHz, CD_2Cl_2, TMS) δ (ppm) = 169.3, 168.8, 168.6, 168.5, 165.2, 151.5 –148.5 (C_{ArF}), 145.0, 144.9, 143.6, 143.5, 138.1, 137.8, 137.6, 132.5, 132.3, 132.1, 132.1, 129.6, 129.6, 129.3, 129.2, 124.3, 124.3, 124.0, 124.0, 122.4, 122.3, 122.1, 122.0, 122.0, 120.2, 120.1, 119.7, 119.3, 119.3, 118.9, 62.0. Due to low solubility in organic

solvents, extensive coupling to ^{19}F nuclei and overlapping signals due to the presence of two diastereomers, some of the ^{13}C NMR signals could not be unambiguously assigned. All signals that could be clearly identified in the ^{13}C, $^{1}H–^{13}C$ HSQC and $^{1}H–^{13}C$ HMBC NMR spectra are reported. The spectra are included as Figures S17, S20 and S21. Single crystals of the *rac* diastereomer suitable for X-ray diffraction were grown by layering a near-saturated DCM solution of the complex with hexane.

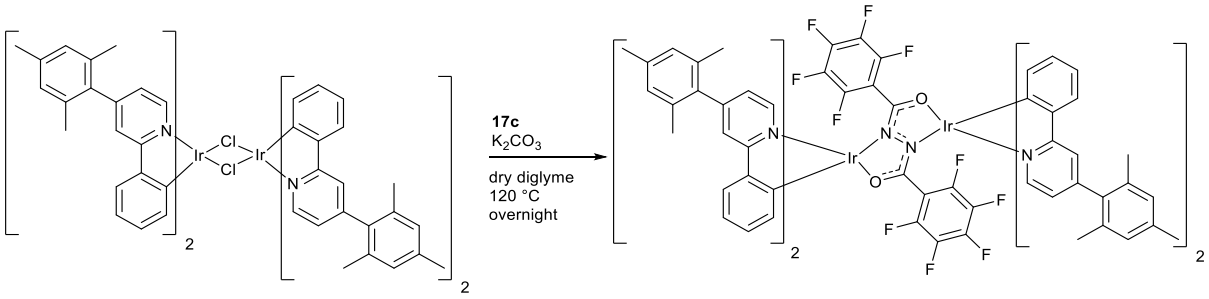

[Ir(mesppy)$_2$μ–Cl]$_2$ ***rac* 11 31%**

Complex *rac* **11.** *N*,*N*′-Bis(pentafluorobenzoyl)hydrazide (**17c**) (82 mg, 0.19 mmol, 1.00 eq.) was added to dry diglyme (15 mL) with K_2CO_3 (80 mg, 0.70 mmol, 2.98 eq.) and heated to 50 °C under an argon atmosphere for 30 min to obtain a pale yellow suspension. [Ir(mesppy)$_2$μ-Cl]$_2$ (300 mg, 0.19 mmol, 1.00 eq.) was then added and the mixture was heated to 120 °C overnight. The reaction mixture was then cooled to room temperature and the solvent was removed under reduced pressure. The residue was then dissolved in DCM and suspended onto celite (*c.a.* 2 g) under reduced pressure, before being subjected to flash chromatography on silica gel (eluent: gradient *n*-hexane/ DCM sat. K_2CO_3 9:1–1:1 v/v). First to elute was the *rac* (ΛΛ/ ΔΔ) diastereomer, which after removal of the solvent was dissolved in a minimal amount of DCM (*ca*. 5 mL). Addition of hexane (*ca*. 20 mL) followed by reducing the volume of the mixture to *ca*. 20 mL afforded complex *rac* **11** as a yellow precipitate which was isolated via filtration and washed with pentane (115 mg, 0.6 mmol, 31%).

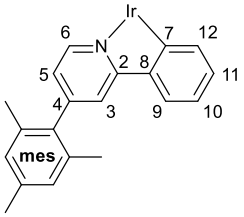

A/B

^{1}H NMR (700 MHz, CD_2Cl_2) δ (ppm) = 9.27 (d, *J* = 5.7 Hz, 2H$_{A6}$), 8.44 (d, *J* = 5.6 Hz, 2H$_{B6}$), 7.71 (s, 2H$_{B3}$), 7.69 (s, 2H$_{A3}$), 7.46 (d, *J* = 7.7 Hz, 2H$_{B9}$), 7.35 (d, *J* = 7.7 Hz, 2H$_{A9}$), 7.21 (dd, *J* = 5.8, 1.7 Hz, 2H$_{A5}$), 7.05 (s, 2H$_{mesAr}$), 7.04 (s, 4H$_{mesAr}$), 7.01 (s, 2H$_{mesAr}$), 6.94 (dd, *J* = 5.7, 1.7 Hz, 2H$_{B5}$), 6.80 (t, *J* = 7.7 Hz, 2H$_{B10}$), 6.70 (t, *J* = 7.3 Hz, 2H$_{A10}$), 6.69 – 6.65 (m, 2H$_{B11}$), 6.62 (t, *J* = 7.4 Hz, 2H$_{A11}$), 6.41 (d, *J* = 7.8 Hz, 2H$_{A12}$), 5.99 (d, *J* = 8.4 Hz, 2H$_{B12}$), 2.37 (s, 6H$_{mesMe}$), 2.36 (s, 6H$_{mesMe}$), 2.29 (s, 6H$_{mesMe}$), 2.21 (s, 6H$_{mesMe}$), 2.13 (s, 6H$_{mesMe}$), 2.09 (s, 6H$_{mesMe}$); ^{19}F NMR {^{1}H} (376 MHz, CD_2Cl_2) δ (ppm) = -141.9 (dd, *J* = 25.2, 7.7 Hz, 2F), -145.1 – -145.2 (m, 2F), -155.9 (t, *J* = 21.6 Hz, 2F), -160.2 – -160.4 (m, 2F), -162.9 (ddd, *J* = 23.3, 21.0, 7.9 Hz, 2F); ^{13}C NMR (176 MHz, CD_2Cl_2) δ (ppm) = 168.1 (C$_{A2}$), 167.9 (C$_{B2}$), 151.9 (C$_{A4}$), 151.6 (C$_{B4}$), 150.8 (C$_{A7}$), 149.8 (C$_{A6}$), 148.4 (C$_{B6}$), 147.7 (C$_{B7}$), 144.7 (C$_{B8}$), 143.0 (C$_{A8}$), 135.0 – 135.8 (C$_{mes\ quart\ carbons}$), 131.8 (C$_{B12}$), 131.7 (C$_{A12}$), 129.1 (C$_{B11}$), 128.9 (C$_{A11}$), 128.4 (C$_{mesAr}$), 128.4$^{\#}$ (C$_{mesAr}$), 123.9 (C$_{B9}$), 123.6 (C$_{A9}$), 123.1 (C$_{A5}$), 122.9 (C$_{B5}$), 121.8 (C$_{B10}$), 120.5 (C$_{A3}$), 119.9 (C$_{B3}$), 119.5 (C$_{A10}$), 20.8* (C$_{mesMe}$), 20.4 (C$_{mesMe}$), 20.3 (C$_{mesMe}$), 20.1 (C$_{mesMe}$), 20.0 (C$_{mesMe}$), Due to low solubility in organic solvents and extensive coupling to ^{19}F nuclei, some of the quaternary ^{13}C NMR signals could not be identified. All signals that could be clearly identified in the ^{13}C, $^{1}H–^{13}C$ HSQC and $^{1}H–^{13}C$ HMBC NMR spectra are reported. The spectra are included as Figures S23, S28 and S29. MS (MALDI–TOF): *m/z* 1892.3 [M$^+$]. Calcd. for $C_{94}H_{72}F_{10}Ir_2N_6O_2^+$: 1892.5; Anal. Calcd. for $C_{94}H_{72}F_{10}Ir_2N_6O_2$: C, 59.67; H, 3.84; N, 4.44, Calcd. for $C_{94}H_{72}F_{10}Ir_2N_6O_2 \cdot 0.4CH_2Cl_2$: C,

58.87; H, 3.81; N, 4.36. Found: C, 58.78; H, 3.73; N, 4.36. Single crystals suitable for X-ray diffraction were grown by vapour diffusion of hexane into a DCM solution of the complex. A second yellow band presumed to contain the *meso* (ΛΔ) diastereomer slowly eluted from the column after the *rac* (ΛΛ/ ΔΔ) diastereomer, but due to very low solubility it could not be isolated in an analytically pure form.

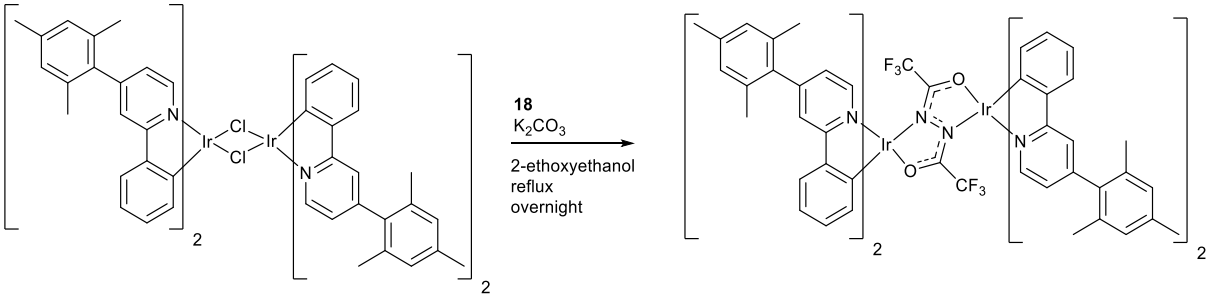

[Ir(mesppy)$_2$μ–Cl]$_2$ **meso 12 61%**

Complex *meso* **12.** Bis(trifluoromethyl)hydrazide (**18**) (43 mg, 0.19 mmol, 1.00 eq.), [Ir(mesppy)$_2$μ-Cl]$_2$ (300 mg, 0.19 mmol, 1.00 eq.) and K_2CO_3 (80 mg, 0.70 mmol, 2.98 eq.) were added to 2-ethoxyethanol (15 mL) under and argon atmosphere and heated to reflux overnight. The reaction mixture was then cooled to room temperature and the solvent was removed under reduced pressure. The residue was then dissolved in DCM and suspended onto celite (*c.a.* 2 g) under reduced pressure, before being subjected to flash chromatography on silica gel (eluent: gradient *n*-hexane/ DCM sat. K_2CO_3 9:1–1:1 v/v). The glowing yellow band was collected and after removing the solvent under reduced pressure, the residue was dissolved in a minimal amount of DCM (*ca*. 5 mL). Addition of hexane (*ca*. 20 mL) followed by reducing the volume of the mixture to *ca*. 20 mL afforded complex *meso* **12** as a yellow precipitate which was isolated via filtration and washed with pentane (200 mg, 0.12 mmol, 61%). A single diastereomer (ΛΔ) was obtained.

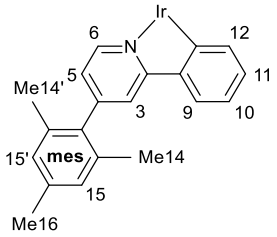

A/B

^{1}H NMR (700 MHz, THF-d_8) δ (ppm) = 8.74 (d, *J* = 5.6 Hz, 2H$_{A6}$), 8.63 (d, *J* = 5.7 Hz, 2H$_{B6}$), 7.84 (d, *J* = 1.8 Hz, 2H$_{A3}$), 7.79 (d, *J* = 1.8 Hz, 2H$_{B3}$), 7.56 (dd, *J* = 7.9, 1.3 Hz, 2H$_{A9}$), 7.53 (dd, *J* = 7.9, 1.3 Hz, 2H$_{B9}$), 7.25 (dd, *J* = 5.7, 1.9 Hz, 2H$_{A5}$), 7.01 – 6.99 (m, 4H$_{A15',B15'}$), 6.97 (s, 2H$_{B15}$), 6.90 – 6.87 (m, 4H$_{A15, B5}$), 6.70 (td, *J* = 7.6, 7.1, 1.2 Hz, 2H$_{B10}$), 6.65 (ddd, *J* = 7.9, 6.9, 1.2 Hz, 2H$_{A10}$), 6.57 (ddd, *J* = 8.2, 7.0, 1.3 Hz, 2H$_{B11}$), 6.53 (ddd, *J* = 8.1, 6.9, 1.3 Hz, 2H$_{A11}$), 6.30 (d, *J* = 7.8 Hz, 2H$_{A12}$), 6.05 (dd, *J* = 7.9, 1.2 Hz, 2H$_{B12}$), 2.35 (s, 6H$_{BMe16}$), 2.32 (s, 6H$_{AMe16}$), 2.18 (s, 6H$_{AMe14'}$), 2.15 (s, 6H$_{BMe14'}$), 1.91 (s, 6H$_{BMe14}$), 1.86 (s, 6H$_{AMe14}$); ^{19}F {^{1}H} NMR (376 MHz, CD_2Cl_2) δ (ppm) = -67.0 (s, 6F); ^{13}C NMR (176 MHz, THF-d_8) δ (ppm) = 170.8 (C$_{A2}$), 169.9 (C$_{B2}$), 152.5 (C$_{B4}$), 152.3 (C$_{A4}$), 150.6 (C$_{B6}$), 150.3 (C$_{A7}$), 149.4 (C$_{A6}$), 146.5 (C$_{B7}$), 145.2 (C$_{B8}$), 145.0 (C$_{A8}$), 138.7 (C$_{mes\ quart}$), 138.5 (C$_{mes\ quart}$), 137.3 – 135.9 (C$_{mes\ quart\ carbons}$), 134.6 (C$_{A12}$), 132.9 (C$_{B12}$), 130.4 (C$_{B11}$), 130.0 (C$_{A11}$), 130.0* (C$_{A15',B15'}$), 129.9 (C$_{B15}$), 129.8 (C$_{A15}$), 125.7 (C$_{B9}$), 125.4 (C$_{A9}$), 124.5 (C$_{B5}$), 124.13 (C$_{A5}$), 122.7 (C$_{B10}$), 121.8 (C$_{B3}$), 121.7 (C$_{A3}$), 121.2 (C$_{A10}$), 22.0* (C$_{A16,B16}$), 21.6 (C$_{A14}$), 21.5 (C$_{B14}$), 21.5 (C$_{A14'}$), 21.4 (C$_{B14'}$), Due to low solubility in organic solvents some of the quaternary ^{13}C NMR signals could not be identified. All signals that could be clearly identified in the ^{13}C, ^{1}H–^{13}C HSQC and ^{1}H–^{13}C HMBC NMR spectra are reported. The spectra are included as Figures S32, S36 and S37. MS (MALDI–TOF): *m/z* 1696.3 [M$^+$]. Calcd. for $C_{84}H_{72}F_6Ir_2N_6O_2^+$: 1696.5; Anal. Calcd. for $C_{84}H_{72}F_6Ir_2N_6O_2$: C, 59.49; H, 4.28; N, 4.96, Calcd. for $C_{84}H_{72}F_6Ir_2N_6O_2 \cdot 0.5CH_2Cl_2$: C, 58.38; H, 4.23; N, 4.83. Found: C, 58.04; H, 4.25; N,

4.71. Single crystals suitable for X-ray diffraction were grown by vapour diffusion of hexane into a THF solution of the complex.

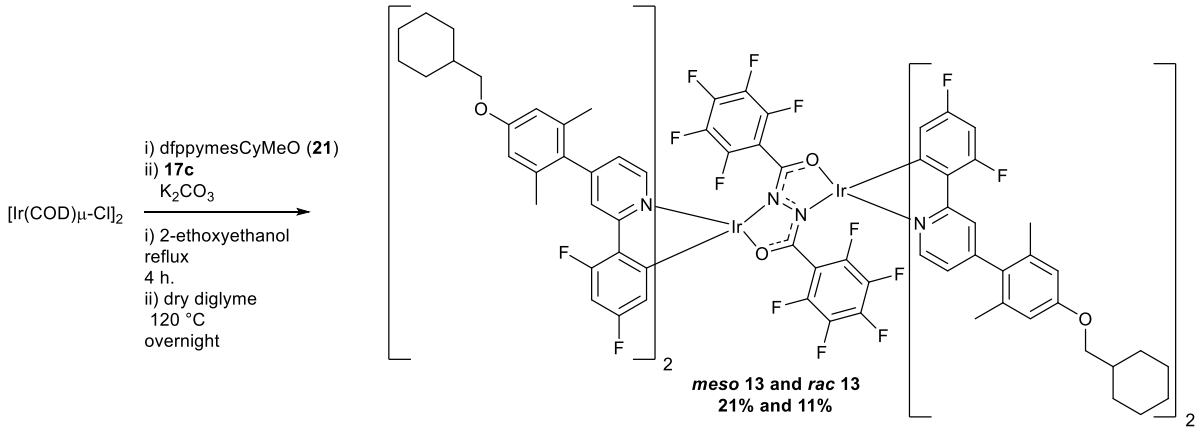

Complexes *meso* **13** and *rac* **13.** [Ir(COD)μ-Cl]$_2$ (200 mg, 0.30 mmol, 1.00 eq.) and 2-(2,4-difluorophenyl)-4-(2,6-dimethyl-4-(methylcyclohexyloxy)phenyl)pyridine (**21**) (534 mg, 1.32 mmol, 4.4 eq.) were added to 2-ethoxyethanol (10 mL) and heated to reflux under an argon atmosphere for 4 h. The reaction mixture was then cooled to room temperature and the solvent removed under reduced pressure. The residue was then dissolved in DCM (*ca.* 10 mL) and hexane was added (*ca*. 30 mL). The solvent volume was reduced to *ca.* 10 mL under reduced pressure. A yellow precipitate formed which was filtered and washed with pentane (*ca.* 20 mL) to isolate the intermediate μ-dichloro-bridged diiridium complex (463 mg, 0.22 mmol, 75%) which was used without further purification (^{1}H NMR data were consistent with the proposed structure – Figure S39). The obtained dichloro dimer was combined with *N,N'*-bis(pentafluorobenzoyl)hydrazide (**17c**) (94 mg, 0.22 mmol, 1.00 eq.) and K_2CO_3 (77 mg, 0.56 mmol, 2.50 eq.) and suspended in dry diglyme (15 mL) under argon. It was subsequently heated to 120 °C overnight. The reaction mixture was then cooled to room temperature and the solvent removed under reduced pressure. To the residue was added DCM (10 mL), and the resulting mixture was sonicated for 5 min. Hexane (30 mL) was then added, before the solvent volume was reduced to *ca.* 30 mL. The mixture was filtered to obtain a yellow powder and a yellow/orange filtrate. Both the filtrate and filtrand were retained.

Filtrand

The filtrand was further purified by flash chromatography on silica gel (eluent: *n*-hexane/ DCM sat. K_2CO_3 4:6 v/v). After evaporation of the column solvent, the residue was precipitated from DCM/ hexane, filtered and washed with pentane to afford the presumed *meso* (ΛΔ) diastereomer *(meso* **13***)* (150 mg, 0.06 mmol, 21% from [Ir(COD)μ-Cl]$_2$).

Filtrate

The filtrate was evaporated and the residue was refluxed in methanol (20 mL) for 5 min. The mixture was then cooled in a freezer (−18 °C) for 1 h before being filtered to obtain a yellow precipitate, which was further purified by flash chromatography on silica gel (eluent: *n*-hexane/ toluene 6:4 v/v). After evaporation of the column solvent, the residue was precipitated from DCM/ hexane, filtered and washed with pentane to afford *rac* **13** (80 mg, 0.03 mmol, 11% from [Ir(COD)μ-Cl]$_2$).

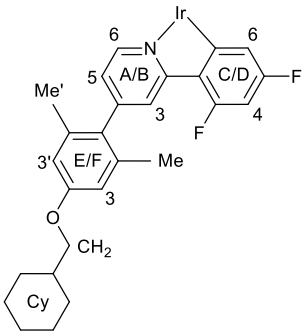

meso **13:** ^{1}H NMR (600 MHz, CD_2Cl_2) δ (ppm) = 8.93 (d, *J* = 5.8 Hz, 2H$_{A6}$), 8.76 (d, *J* = 5.8 Hz, 2H$_{B6}$), 8.10 (s, 2H$_{A3}$), 8.01 (s, 2H$_{B3}$), 7.34 (dd, *J* = 5.7, 1.8 Hz, 2H$_{A5}$), 6.88 (dd, *J* = 5.8, 1.8 Hz, 2H$_{B5}$), 6.78 – 6.72 (m, 6H$_{E3,E3',F3'}$), 6.65 (bs, 2H$_{F3}$), 6.38 – 6.32 (m, 2H$_{C4}$), 6.31 – 6.25 (m, 2H$_{D4}$), 5.66 (dd, *J* = 8.5, 2.0 Hz, 2H$_{D6}$), 5.38 (dd, *J* = 8.9, 2.4 Hz, 2H$_{C6}$), 3.85 (d, *J* = 6.4 Hz, 4H$_{CH2}$), 3.81 (d, *J* = 6.4 Hz, 4H$_{CH2}$), 2.18 (bs, 6H$_{EMe/EMe'}$), 2.16 (bs, 6H$_{FMe/FMe'}$), 1.98 −1.90 (m, 20H$_{Cy,EMe/EMe',FMe/FMe'}$), 1.82 (td, *J* = 7.7, 3.7 Hz, 12H$_{Cy}$), 1.76 (d, *J* = 11.7 Hz, 4H$_{Cy}$), 1.41 – 1.32 (m, 8H$_{Cy}$), 1.29 – 1.26 (m, 4H$_{Cy}$), 1.18 – 1.09 (m, 8H$_{Cy}$) The ^{1}H environments on rings E and F resolve due to restricted rotation. Exchange is observed in ^{1}H−^{1}H NOESY and ^{1}H−^{1}H ROESY experiments (Figures S47 and S48); ^{19}F NMR (376 MHz, CD_2Cl_2) δ (ppm) = -108.0 (d, *J* = 10.2 Hz, 2F), -108.3 (d, *J* = 10.1 Hz, 2F), -109.7 (d, *J* = 10.2 Hz, 2F), -110.0 (d, *J* = 10.2 Hz, 2F), -142.0 (d, *J* = 21.2 Hz, 2F), -143.4 (d, *J* = 20.5 Hz, 2F), -154.7 (t, *J* = 20.8 Hz, 2F), -161.1 (td, *J* = 22.4, 7.8 Hz, 2F), -161.7 (td, *J* = 23.9, 21.7, 7.5 Hz, 2F); ^{13}C NMR (176 MHz, CD_2Cl_2) δ (ppm) = 148.6 (C$_{B6}$), 147.7 (C$_{A6}$), 125.0 (C$_{A3}$), 124.9 (C$_{B3}$), 123.93 (C$_{A5}$), 123.59 (C$_{B5}$), 113.8 (C$_{F3}$), 113.7$^{\#}$ (C$_{F3',E3,E3'}$), 113.6 (C$_{D6}$), 113.5 (C$_{C6}$), 98.2 (C$_{C4}$), 96.0 (C$_{D4}$), 73.5 (C$_{CH2}$), 73.43 (C$_{CH2}$), 37.8* (C$_{Cy}$), 29.9* (C$_{Cy}$), 26.6* (C$_{Cy}$), 25.8* (C$_{Cy}$), 20.7 (C$_{FMe/FMe'}$), 20.6 (C$_{EMe/EMe'}$), 20.4 (C$_{FMe/FMe'}$), 20.3 (C$_{EMe/EMe'}$), Due to low solubility in organic solvents and extensive coupling to ^{19}F nuclei, some quaternary ^{13}C NMR signals could not be identified. All signals that could be clearly identified in the ^{13}C, ^{1}H–^{13}C HSQC and ^{1}H–^{13}C HMBC NMR spectra are reported. The spectra are included as Figures S41, S45 and S46. MS (MALDI–TOF): *m/z* 2428.6 [M^{+}]. Calcd. for $C_{118}H_{104}F_{18}Ir_2N_6O_6^{+}$: 2428.7; Anal. Calcd. for $C_{118}H_{104}F_{18}Ir_2N_6O_6$: C, 58.36; H, 4.32; N, 3.46, Calcd. for $C_{118}H_{104}F_{18}Ir_2N_6O_6{\cdot}0.3CH_2Cl_2$: C, 57.90; H, 4.30; N, 3.42. Found: C, 57.83; H, 4.34; N, 3.36.

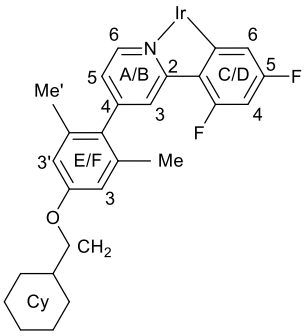

rac **13**: ^{1}H NMR (700 MHz, CD_2Cl_2, TMS) δ (ppm) = 9.18 (d, *J* = 5.8 Hz, 2H$_{A6}$), 8.35 (d, *J* = 5.7 Hz, 2H$_{B6}$), 8.08 (s, 4H$_{A3,B3}$), 7.28 (d, *J* = 5.7 Hz, 2H$_{A5}$), 7.01 – 6.98 (m, 2H$_{B5}$), 6.76 – 6.71 (m, 8H$_{E3,E3',F3,F3'}$), 6.35 (t, *J* = 10.5 Hz, 2H$_{C4}$), 6.29 (t, *J* = 10.6 Hz, 2H$_{D4}$), 5.84 (d, *J* = 8.7 Hz, 2H$_{D6}$), 5.36 – 5.34 (m, 2H$_{C6}$), 3.82 – 3.79 (m, 8H$_{CH2}$), 2.30 (bs, 6H$_{FMe/FMe'}$), 2.22 (bs, 6H$_{EMe/EMe'}$), 2.11 (bs, 6H$_{FMe/FMe'}$), 2.09 (bs, 6H$_{EMe/EMe'}$), 1.89 (d, *J* = 12.8 Hz, 8H$_{Cy}$), 1.79 (d, *J* = 13.8 Hz, 12H$_{Cy}$), 1.73 (d, *J* = 12.8 Hz, 4H$_{Cy}$), 1.34 (q, *J* = 13.1 Hz, 8H$_{Cy}$), 1.29 – 1.22 (m, 4H$_{Cy}$), 1.09 (q, *J* = 12.8 Hz, 8H$_{Cy}$) The ^{1}H environments on rings E and F partially resolve due to restricted rotation. Exchange is suspected from the ^{1}H−^{1}H NOESY experiment (Figure S56); ^{19}F {^{1}H} NMR (376 MHz, CD_2Cl_2) δ (ppm) = -107.9 (d, *J* = 10.2 Hz, 2F), -108.5 (d, *J* = 10.2 Hz, 2F), -109.7 – -109.8 (m, 2F), -109.8 – -109.9 (m, 2F), -141.0 (d, *J* = 24.1 Hz, 2F), -144.5 (d, *J* = 22.6 Hz, 2F), -154.7 (t, *J* = 20.8 Hz, 2F), -159.9 – -160.2 (m, 2F), -161.9 (td, *J* = 22.8, 22.2, 7.7 Hz, 2F);

^{13}C NMR (176 MHz, CD_2Cl_2) δ (ppm) = 164.9 (C_{A2}), 164.4 (C_{B2}), 162.8 (d, *J* = 256 Hz, C_{D5}), 162.4 (d, *J* = 251 Hz, C_{C5}), 153.2 (C_{A4}), 153.1 (C_{B4}), 159.2* ($C_{E/F}$), 148.4 (C_{A6}), 148.1 (C_{B6}), 136.6* ($C_{E/F}$), 130.5* ($C_{E/F}$), 125.1 (C_{A3}), 124.7 (C_{B3}), 123.9 (C_{A5}), 123.7 (C_{B5}), 113.9 (C_{C6}), 113.7* ($C_{E/F}$), 113.7* ($C_{E/F}$), 113.6 (C_{D6}), 98.3 (C_{C4}), 95.9 (C_{D4}), 73.5* (C_{CH2}), 37.7* (C_{Cy}), 29.9* (C_{Cy}), 26.5* (C_{Cy}), 25.8*(C_{Cy}), 20.8 ($C_{EMe/EMe'}$), 20.6 ($C_{FMe/FMe'}$), 20.5 ($C_{FMe/FMe'}$), 20.5 ($C_{EMe/EMe'}$), Due to low solubility in organic solvents and extensive coupling to ^{19}F nuclei, some of the quaternary ^{13}C NMR signals could not be identified. All signals that could be clearly identified in the ^{13}C, ^{1}H–^{13}C HSQC and ^{1}H–^{13}C HMBC NMR spectra are reported. The spectra are included as Figures S50, S54 and S55. MS (MALDI–TOF): *m/z* 2428.6 [M^+]. Calcd. for $C_{118}H_{104}F_{18}Ir_2N_6O_6^+$: 2428.7; Anal. Calcd. for $C_{118}H_{104}F_{18}Ir_2N_6O_6$: C, 58.36; H, 4.32; N, 3.46, Calcd. for $C_{118}H_{104}F_{18}Ir_2N_6O_6{\cdot}0.5CH_2Cl_2$: C, 57.60; H, 4.28; N, 3.40. Found: C, 57.46; H, 4.32; N, 3.42. Crystals suitable for X-ray diffraction fell overnight from a saturated solution of the complex in CD_2Cl_2.

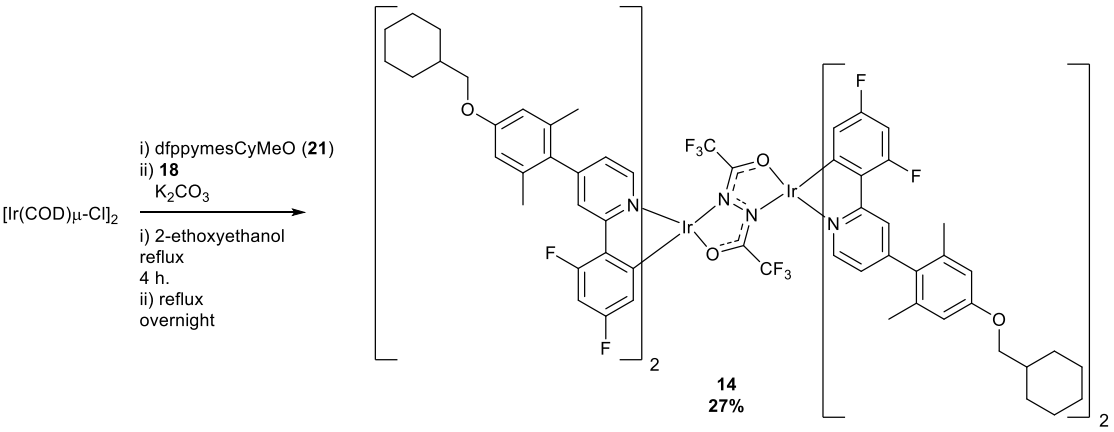

Complex 14. [Ir(COD)μ-Cl]$_2$ (94 mg, 0.14 mmol, 1.00 eq.) and 2-(2,4-difluorophenyl)-4-(2,6-dimethyl-4-(methylcyclohexyloxy)phenyl)pyridine (**21**) (250 mg, 0.62 mmol, 4.4 eq.) were added to 2-ethoxyethanol (5 mL) and heated to reflux under an argon atmosphere for 4 h to generate the μ-dichloro-bridged diiridium complex *in-situ*. The reaction mixture was then cooled to room temperature, before bis(trifluoromethyl)hydrazide (**18**) (34 mg, 0.14 mmol, 1.00 eq.), and K_2CO_3 (58 mg, 0.42 mmol, 3.00 eq.) were added. The reaction mixture was then heated to reflux overnight, before being cooled to room temperature and the solvent removed under reduced pressure. The residue was dissolved in DCM, suspended onto celite (*c.a.* 2 g) under reduced pressure and subjected to flash chromatography on silica gel (eluent: gradient *n*-hexane/ DCM sat. K_2CO_3 8:2–2:8 v/v). The yellow band was collected and the column solvent was removed under reduced pressure. The residue was heated to reflux in THF (25 mL) for 20 min and then hot filtered to obtain a yellow powder (25 mg, 0.01 mmol, 8%). A second crop was obtained by reducing the filtrate to 10 mL and repeating the process (60 mg, 0.03 mmol, 19%). The recovered solids from both filtrations were combined to afford complex (**14**) (85 mg, 0.04 mmol, 27%) as a single diastereomer.

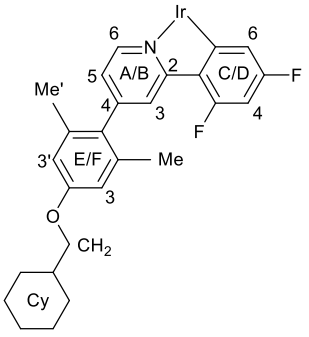

^{1}H NMR (700 MHz, CD_2Cl_2, TMS) δ (ppm) = 8.57 (d, *J* = 5.7 Hz, 2H$_{A6}$), 8.42 (d, *J* = 5.7 Hz, 2H$_{B6}$), 8.13 (s, 2H$_{A3}$), 8.06 (s, 2H$_{B3}$), 7.20 (dd, *J* = 5.7, 1.9 Hz, 2H$_{A5}$), 6.79 (dd, *J* = 5.8, 1.9 Hz, 2H$_{B5}$), 6.73 (bs, 2H$_{E3}$), 6.72 (bs, 2H$_{F3}$), 6.70 (bs, 2H$_{F3'}$), 6.61 (bs, 2H$_{E3'}$), 6.42 (ap. t, *J* = 10.2 Hz, 2H$_{C4}$), 6.36 (ap. t, *J* = 10.6 Hz, 2H$_{D4}$), 5.70 (dd, *J* = 9.1, 2.1 Hz,

$2H_{D6}$), 5.47 (dd, *J* = 9.0, 2.4 Hz, $2H_{C6}$), 3.82 (d, *J* = 6.4 Hz, $4H_{CH2}$), 3.79 (d, *J* = 6.1 Hz, $4H_{CH2}$), 2.17 (bs, $6H_{EMe/EMe'}$), 2.14 (bs, $6H_{FMe/FMe'}$), 1.92 (bs, $6H_{FMe/FMe'}$), 1.91 – 1.81 (m, $8H_{Cy}$), 1.84 (bs, $6H_{EMe/EMe'}$), 1.82 – 1.77 (m, $12H_{Cy}$), 1.74 (d, *J* = 13.0 Hz, $4H_{Cy}$), 1.39 – 1.31 (m, $8H_{Cy}$), 1.29 – 1.23 (m, $4H_{Cy}$), 1.13 – 1.09 (m, $8H_{Cy}$) The ^1H environments on rings E and F resolve due to restricted rotation. Exchange is suspected from the ^1H–^1H NOESY experiment (Figure S64); ^{19}F {^1H} NMR (376 MHz, CD_2Cl_2) δ (ppm) = -67.0 (s, $6F_{CF3}$), -107.6 (d, *J* = 10.2 Hz, $2F_{Ar}$), -109.4 (d, *J* = 9.8 Hz, $2F_{Ar}$), -109.6 (d, *J* = 10.2 Hz, $2F_{Ar}$), -111.2 – -111.3 (m, $2F_{Ar}$); ^{13}C NMR (176 MHz, CD_2Cl_2) δ (ppm) = 165.7 (C_{A2}), 164.6 (C_{B2}), 159.2 ($C_{E\ or\ F}$), 159.1 ($C_{E\ or\ F}$), 152.9 (C_{B4}), 152.7 (C_{A4}), 148.2 (C_{B6}), 146.9 (C_{A6}), 125.1 (C_{B3}), 124.9 (C_{A3}), 123.7 (C_{B5}), 123.3 (C_{A5}), 114.7 (C_{D6}), 113.7# ($C_{E3/E3'/F3'}$), 113.6 (C_{F3}), 113.6 (C_{C6}), 98.4 (C_{C4}), 96.5 (C_{D4}), 73.5 (C_{CH2}), 73.4 (C_{CH2}), 37.8* (C_{Cy}), 29.8* (C_{Cy}), 26.6* (C_{Cy}), 25.8* (C_{Cy}), 20.6 ($C_{EMe/EMe'}$), 20.6 ($C_{FMe/FMe'}$), 20.6 ($C_{FMe/FMe'}$), 20.5 ($C_{EMe/EMe'}$), Due to low solubility in organic solvents, some quaternary ^{13}C NMR signals could not be identified. All signals that could be clearly identified in the ^{13}C, ^1H–^{13}C HSQC and ^1H–^{13}C HMBC NMR spectra are reported. The spectra are included as Figures S58, S62 and S63. MS (MALDI–TOF): *m/z* 2232.2 [M^+]. Calcd. for $C_{108}H_{104}F_{14}Ir_2N_6O_6^+$: 2232.7.

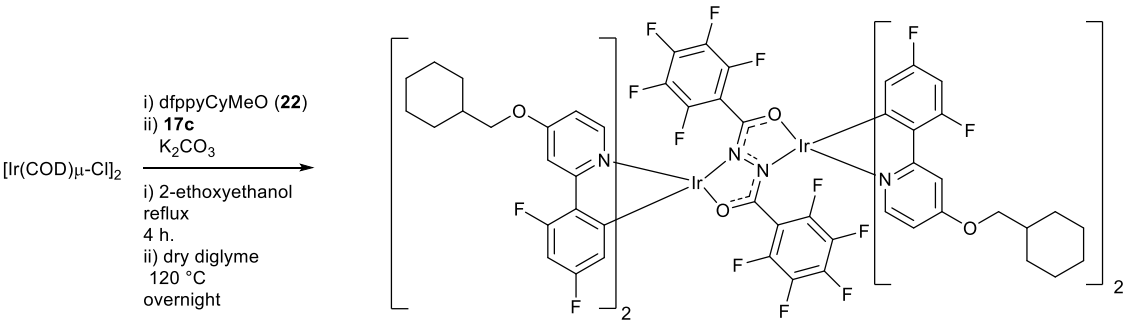

Complex 15. [Ir(COD)μ-Cl]$_2$ (200 mg, 0.30 mmol, 1.00 eq.) and 2-(2,4-difluorophenyl)-4-(methylcyclohexyloxy)phenyl pyridine (**22**) (366 mg, 1.21 mmol, 4.05 eq.) were added to 2-ethoxyethanol (15 mL) and heated to reflux under an argon atmosphere for 4 h. The reaction mixture was then cooled to room temperature and hexane was added (*ca.* 30 mL). The mixture was cooled in a fridge (*ca.* 3 °C) for 1 h. A yellow precipitate formed which was filtered and washed with pentane (*ca.* 20 mL) to isolate the intermediate μ-dichloro-bridged diiridium complex (403 mg, 0.24 mmol, 80%) which was used without further purification (^1H NMR data were consistent with the proposed structure – Figure S65). The obtained dichloro dimer was combined with *N*,*N*′-bis(pentafluorobenzoyl)hydrazide (**17c**) (102 mg, 0.24 mmol, 1.00 eq.) and K_2CO_3 (84 mg, 0.60 mmol, 2.50 eq.) and suspended in dry diglyme (15 mL) under argon. It was subsequently heated to 120 °C overnight. The reaction mixture was then cooled to room temperature and diluted with hexane (*ca.* 70 mL). A yellow precipitate formed which was filtered and washed with pentane (*ca.* 20 mL). The obtained solid was then dissolved in DCM and suspended onto celite (*c.a.* 2 g) under reduced pressure, before being subjected to flash chromatography on silica gel (eluent: *n*-hexane/ DCM sat. K_2CO_3 1:1 v/v). The faint yellow band was collected and after removing the solvent under reduced pressure, the residue was dissolved in minimal DCM (*ca.* 15 mL). Hexane was added (*ca.* 20 mL) and the volume was reduced to 20 mL After collecting the precipitate by filtration and washing with pentane complex **15** was obtained as a yellow solid (130 mg, 0.6 mmol, 22% from [Ir(COD)μ-Cl]$_2$). A single diastereomer was obtained.

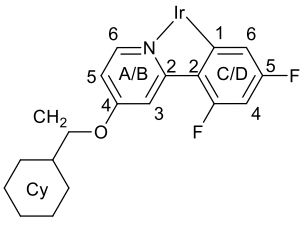

^{1}H NMR (700 MHz, CD_2Cl_2, TMS) δ (ppm)= 8.73 (d, *J* = 6.5 Hz, $2H_{A6}$), 7.94 (d, *J* = 6.5 Hz, $2H_{B6}$), 7.75 (t, *J* = 3.1 Hz, $2H_{A3}$), 7.72 (t, *J* = 2.9 Hz, $2H_{B3}$), 7.00 (dd, *J* = 6.5, 2.8 Hz, $2H_{A5}$), 6.72 (dd, *J* = 6.5, 2.7 Hz, $2H_{B5}$), 6.32 (ddd, *J* = 12.0, 9.0, 2.4 Hz, $2H_{C4}$), 6.24 (ddd, *J* = 11.9, 9.0, 2.4 Hz, $2H_{D4}$), 5.60 (dd, *J* = 9.0, 2.4 Hz, $2H_{D6}$), 5.42 (dd, *J* = 8.7, 2.4 Hz, $2H_{C6}$), 4.08 – 4.05 (m, $8H_{CH2}$), 2.03 – 1.93 (m, $12H_{Cy}$), 1.89 – 1.83 (m, $8H_{Cy}$), 1.80 – 1.74 (m, $4H_{Cy}$), 1.45 – 1.35 (m, $8H_{Cy}$), 1.29 – 1.26 (m, $4H_{Cy}$), 1.25 – 1.16 (m, $8H_{Cy}$); ^{19}F NMR (376 MHz, CD_2Cl_2) δ (ppm) = -108.7 (d, *J* = 10.1 Hz, 2F), -109.4 (d, *J* = 10.0 Hz, 2F), -111.0 (d, *J* = 10.1 Hz, 2F), -111.1 (d, *J* = 10.1 Hz, 2F), -140.4 (d, *J* = 24.5 Hz, 2F), -143.9 (d, *J* = 24.0 Hz, 2F), -155.3 (t, *J* = 20.8 Hz, 2F), -160.5 – -160.8 (m, 2F), -162.1 – -162.4 (m, 2F); ^{13}C NMR (176 MHz, CD_2Cl_2, TMS) δ (ppm) = 167.4 (C_{B2}), 167.2 ($C_{A4\ or\ B4}$), 165.7 (C_{A2}), 165.1 ($C_{A4\ or\ B4}$), 162.6 (d, *J* = 255 Hz, C_{D5}), 162.3 (d, *J* = 251 Hz, C_{C5}), 160.5 (d, *J* = 266 Hz, C_{D3}), 160.4 (d, *J* = 263 Hz, C_{C3}), 150.1 (C_{A6}), 148.7 (B_{B6}), 128. 7 (C_{C1}), 127.15 (C_{D1}), 114.1 (C_{C6}), 113.6 (C_{D6}), 109.7 (C_{A5}), 109.6 (C_{B5}), 108.8 (C_{A3}), 108.4 (C_{B3}), 97.9 (C_{C4}), 95.6 (C_{D4}), 74.3 (C_{CH2}), 74.25 (C_{CH2}), 37.50 (C_{Cy}), 37.44 (C_{Cy}), 29.75 (C_{Cy}), 29.68 (C_{Cy}), 26.39 (C_{Cy}), 26.36 (C_{Cy}), 25.74* (C_{Cy}), Due to low solubility in organic solvents and extensive coupling to ^{19}F nuclei, some of the quaternary ^{13}C NMR signals could not be reported. All signals that could be clearly identified in the ^{13}C, ^{1}H–^{13}C HSQC and ^{1}H–^{13}C HMBC NMR spectra are reported. The spectra are included as Figures S67, S70 and S71. MS (MALDI–TOF): *m/z* 2012.4 [M^+]. Calcd. for $C_{86}H_{72}F_{18}Ir_2N_6O_6^+$: 2012.3; Anal. Calcd. for $C_{86}H_{72}F_{18}Ir_2N_6O_6^+$: C, 51.34; H, 3.61; N, 4.18. Found: C, 51.23; H, 3.60; N, 4.15.

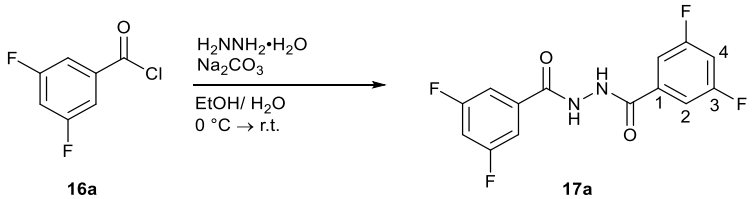

16a **17a** **76%**

***N,N′*-Bis(3,5-difluorobenzoyl)hydrazide (17a).** 3,5-difluorobenzoyl chloride (**16a**) (5.00 g, 28.3 mmol, 2.10 eq.) was added dropwise under air to a stirred solution of hydrazine monohydrate (675 mg, 13.5 mmol, 1.00 eq.) in ethanol (10 mL), which was cooled in an ice bath to maintain the reaction temperature below 15 °C. Formation of a white precipitate was immediately observed. Once the addition was half complete, a further 30 mL of cold ethanol was added to facilitate stirring before a solution of Na_2CO_3 (1.50 g, 14.2 mmol, 1.05 eq.) in water (10 mL) was added dropwise alongside the remaining difluorobenzoyl chloride (**16a**). After the addition of the reagents was completed (*ca*. 20 min), the ice bath was removed and stirring was continued at room temperature for a further 30 min. The reaction mixture was poured into water (50 mL), allowed to settle for 1 h and filtered to collect the crude hydrazide as a white powder which was subsequently refluxed in ethanol (100 mL) for 10 min. The mixture was cooled to room temperature and then filtered to obtain *N,N′*-bis(3,5-difluorobenzoyl)hydrazide (**17a**) (3.19 g, 10.2 mmol, 76%). M.pt. 285–290 °C; ^{1}H NMR (400 MHz, DMSO-d_6) δ (ppm) = 10.84 (s, $2H_{N-H}$), 7.73 – 7.44 (m, $6H_{2+4}$); ^{13}C NMR (101 MHz, DMSO-d_6) δ (ppm) = 163.7 (t, *J* = 2.9 Hz, $C_{C=O}$), 162.8 (dd, *J* = 247.7, 12.7 Hz, C_3), 136.1 (t, *J* = 8.7 Hz, C_1), 111.7 – 111.2 (m, C_2), 108.1 (t, *J* = 25.9 Hz, C_4); ^{19}F{^{1}H} NMR (376 MHz, DMSO-d_6) δ (ppm) = -108.3 (s, 4F); HRMS (ASAP): *m/z* 313.0607 [MH^+]. Calcd. for $C_{14}H_9N_2O_2F_4^+$: 313.0600.

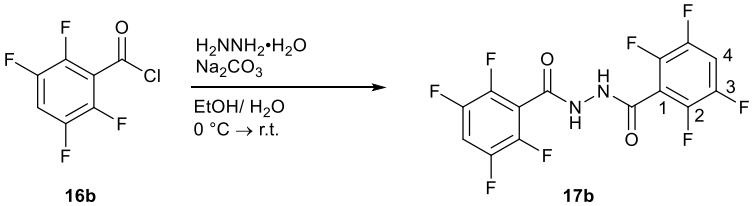

16b **17b** **70%**

***N,N′*-Bis(2,3,5,6-tetrafluorobenzoyl)hydrazide (17b).** 2,3,5,6-tetrafluorobenzoyl chloride (**16b**) (5.00 g, 23.5 mmol, 2.13 eq.) was added dropwise under air to a stirred solution of hydrazine monohydrate (553 mg, 11.0 mmol, 1.00 eq.) in ethanol (10 mL), which was cooled in an ice bath to maintain the reaction temperature below 15 °C. Formation of a white precipitate was immediately observed. Once the addition was half complete, a solution of Na_2CO_3 (1.24 g, 11.7 mmol, 1.06 eq.) in water (10 mL) was added dropwise alongside the remaining 2,3,5,6-tetrafluorobenzoyl chloride (**16b**). After the addition of the reagents was completed (*ca.* 20 min), the ice bath was removed and stirring was continued at room temperature for a further 30 min. The reaction mixture was poured into water (50 mL), allowed to settle for 1 h and filtered to collect the crude hydrazide as a white powder (5.30 g, 13.8 mmol, 125%). The crude material was recrystallised twice from methanol/water and was obtained sufficiently pure for use in the next step (2.95 g, 7.68 mmol, 70%). M.pt. 265–269 °C; ^{1}H NMR (400 MHz, DMSO-d_6) δ (ppm) = 11.36 (s, 2H$_{N–H}$), 8.22 – 8.01 (m, 2H$_4$); ^{13}C NMR (101 MHz, DMSO-d_6) δ (ppm) = 156.7 (C$_{C=O}$), 147.2 – 141.8 (m, C$_{2+3}$), 115.8 (t, J = 20.5 Hz, C$_{1\text{ or }4}$), 109.3 (t, J = 23.5 Hz, C$_{1\text{ or }4}$); ^{19}F {^{1}H} NMR (376 MHz, DMSO-d_6) δ (ppm) = -137.9 – -138.1 (m, 4F), -141.5 – -141.6 (m, 4F); HRMS (ASAP): *m/z* 385.0224 [MH$^+$]. Calcd. for $C_{14}H_5N_2O_2F_8^+$: 385.0223.

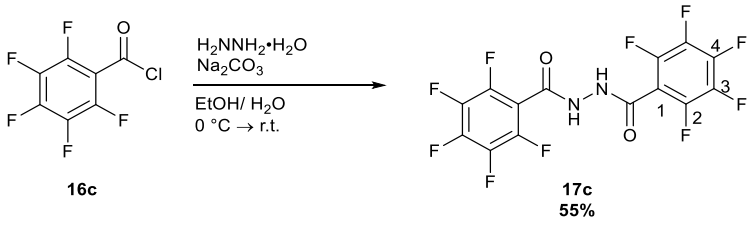

16c **17c** **55%**

***N,N′*-Bis(pentafluorobenzoyl)hydrazide (17c).** Pentafluorobenzoyl chloride (**16c**) (5.00 g, 21.7 mmol, 2.13 eq.) was cautiously added dropwise under air to a stirred solution of hydrazine monohydrate (510 mg, 10.2 mmol, 1.00 eq.) in ethanol (10 mL), which was cooled in an ice bath to maintain the reaction temperature below 15 °C. Formation of a white precipitate was immediately observed. Once the addition was half complete, a further 20 mL of cold ethanol was added to facilitate stirring before a solution of Na_2CO_3 (1.15 g, 10.85 mmol, 1.06 eq.) in water (8 mL) was added dropwise alongside the remaining pentafluorobenzoyl chloride (**16c**). After the addition of the reagents was completed (*ca.* 20 min), the ice bath was removed and stirring was continued at room temperature for a further 30 min. The reaction mixture was poured into water (50 mL), allowed to settle for 1 h and filtered to collect the crude hydrazide as a white powder (3.58 g, 8.57 mmol, 84%). The crude material was recrystallised twice from methanol/water and was obtained sufficiently pure for use in the next step (2.36 g, 5.61 mmol, 55%). M.pt. 264–266 °C (lit. 270 °C[21]); ^{1}H NMR (400 MHz, DMSO-d_6) δ (ppm) = 11.41 (s, 2H$_{N–H}$); ^{13}C NMR (101 MHz, DMSO-d_6) δ (ppm) = 156.0 (C$_{C=O}$), 145.4 – 136.0 (m, C$_{2–4}$), 110.5 (t, J = 21.3 Hz, C$_1$); ^{19}F{^{1}H} NMR (376 MHz, DMSO-d_6) δ (ppm) = -140.8 – -141.0 (m, 2F$_{2\text{ or }3}$), -150.9 (t, J = 22.3 Hz, 1F$_4$), -160.6 – -160.8 (m, 2F$_{2\text{ or }3}$); HRMS (ASAP): *m/z* 421.0035 [MH$^+$]. Calcd. for $C_{14}H_3N_2O_2F_{10}^+$: 421.0035.

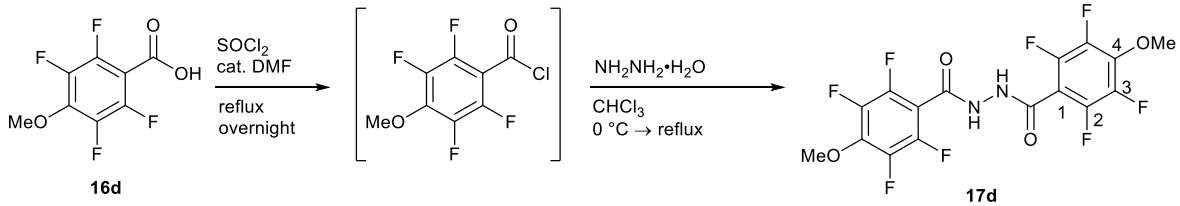

16d **17d** **28%**

***N,N′*-Bis(2,3,5,6-tetrafluoro-4-methoxybenzoyl)hydrazide (17d).** 2,3,5,6-Tetrafluoro-4-methoxybenzoic acid (**16d**) (1.00 g, 4.46 mmol, 1.00 eq.) was heated to reflux in $SOCl_2$ (5 mL) with a drop of *N*,*N*-dimethylformamide overnight under argon. The solvent was then evaporated to obtain crude 2,3,5,6-tetrafluoro-4-methoxybenzoyl

chloride which was dissolved in dry chloroform (30 mL). Hydrazine monohydrate (0.1 mL, 2.09 mmol, 0.47 eq.) was added dropwise to the chloroform solution which was cooled in an ice bath to maintain the reaction temperature below 15 °C. Formation of a white precipitate was immediately observed. After the addition was completed (*ca.* 10 min), the ice bath was removed and the mixture was heated to reflux for 2 h. It was then diluted with *n*-hexane (50 mL), allowed to settle for 1 h and filtered to collect the crude hydrazide as a white powder (650 mg, 1.46 mmol, 70% based on hydrazine monohydrate). The crude material was recrystallised from ethanol and was obtained sufficiently pure for use in the next step (260 mg, 0.59 mmol, 28% based on hydrazine monohydrate). M.pt. 252–256 °C; ^{1}H NMR (400 MHz, DMSO-d_6) δ (ppm) = 11.18 (s, $2H_{N-H}$), 4.14 (s, $6H_{OMe}$); ^{13}C NMR (101 MHz, DMSO-d_6) δ (ppm) = 156.7 ($C_{C=O}$), 145.3 – 139.0 (m, C_{1-3}), 108.3 (t, J = 21 Hz, C_4), 62.8 (C_{OMe}); ^{19}F {^{1}H} NMR (376 MHz, DMSO-d_6) δ (ppm) = -142.4 – -142.5 (m, 4F), -156.9 – -157.2 (m, 4F); HRMS (ASAP): *m/z* 445.0422 [MH^+]. Calcd. for $C_{16}H_9N_2O_4F_8^+$: 445.0435.

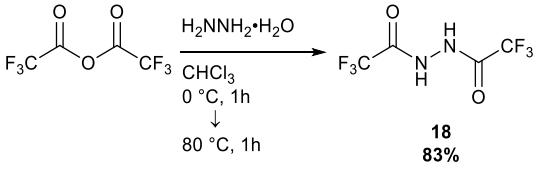

Bis(trifluoromethyl)hydrazide (18). Hydrazine monohydrate (2.5 mL, 51.5 mmol, 1.00 eq.) was added to dry chloroform (10 mL) under argon and cooled in an ice water bath to *ca.* 0 °C. Trifluoroacetic anhydride (21.8 mL, 155 mmol, 3.00 eq.) was then cautiously added to the mixture over the course of 1 h. A white precipitate immediately formed during the addition. Once approximately half had been added, further dry chloroform (10 mL) was added to facilitate stirring. Once the addition was complete, the mixture was refluxed under argon for 1 h, before being cooled to room temperature and filtered. The white precipitate was washed with hexane (*ca.* 50 mL) to obtain bis(trifluoromethyl)hydrazide (**18**) as a white powder (9.6 g, 43 mmol, 83%). Analytical data were in agreement with those previously reported.[22] ^{1}H NMR (400 MHz, Acetone-d_6) δ (ppm) = 10.00 – 11.00 (bs, 2H); ^{19}F {^{1}H} NMR (376 MHz, Acetone-d_6) δ (ppm) = -75.82 (s, 6F).

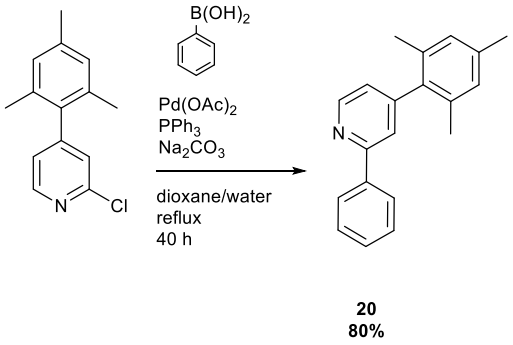

2-Phenyl-4-(2,4,6-trimethylphenyl)pyridine (20). 4-(2,4,6-Trimethylphenyl)-2-chloropyridine (3.36 g, 14.5 mmol, 1.00 eq.), phenyl boronic acid (2.65 g, 21.7 mmol, 1.50 eq.) and PPh_3 (912 mg, 3.48 mmol, 24 mol%) were combined in 1,4-dioxane (45 mL). A solution of Na_2CO_3 (6.14 g, 57.9 mmol, 4.00 eq.) in water (10 mL) was then added and the mixture was degassed for 30 min. $Pd(OAc)_2$ (195 mg, 0.87 mmol, 6 mol%) was then added and the mixture was degassed for a further 10 minutes, before being heated to reflux under argon overnight. The mixture was then allowed to cool to room temperature and evaporated to near-dryness. To the residue was added water (50 mL) and DCM (50 mL). The organic layer was separated and the aqueous later was extracted thrice more with DCM (50 mL). The organic extracts were combined, dried over $MgSO_4$ and evaporated under reduced pressure. The residue was passed through a short column of silica gel (eluent: EtOAc with *ca.* 0.5%

vol. NEt_3 as an additive) before being purified by distillation on a Kugelrohr apparatus (200 °C, *ca.* 9×10^{-2} mbar) to afford 2-phenyl-4-(2,4,6-trimethylphenyl)pyridine (**20**) as a faint yellow viscous oil (3.15 g, 11,52 mmol, 80%). Analytical data were in agreement with those previously reported.[23] ^{1}H NMR (400 MHz, $CDCl_3$) δ (ppm) = 8.77 (dd, *J* = 5.0, 0.9 Hz, 1H), 8.09 – 8.01 (m, 2H), 7.60 (dd, *J* = 1.5, 0.9 Hz, 1H), 7.55 – 7.43 (m, 3H), 7.09 (dd, *J* = 4.9, 1.5 Hz, 1H), 7.01 (d, *J* = 0.7 Hz, 2H), 2.38 (s, 3H), 2.08 (s, 6H).

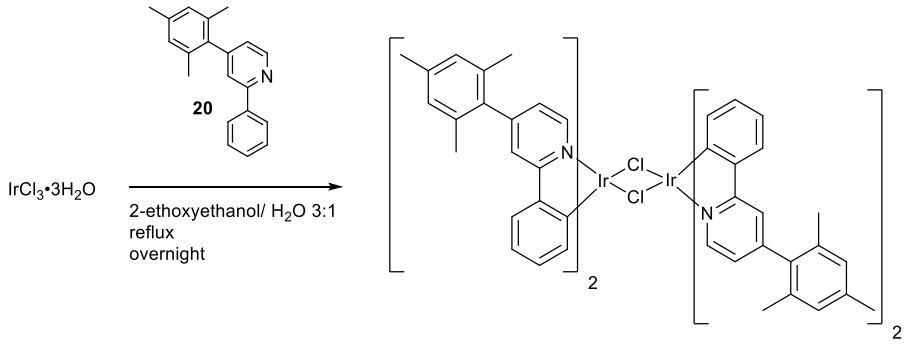

[Ir(mesppy)$_2$μ–Cl]$_2$
94%

Tetrakis(2-phenyl-4-(2,4,6-trimethylphenyl)-pyridine-*C*^{2},*N*')(μ-dichloro)diiridium ([Ir(mesppy)$_2$μ-Cl]$_2$). $IrCl_3 \cdot 3H_2O$ (689 mg, 1.95 mmol, 1.00 eq.) and 2-phenyl-4(2,4,6-trimethylphenyl)-pyridine (**20**) (1.18 g, 4.32 mmol, 2.21 eq.) were added to a mixture of 2-ethoxyethanol (30 mL) and water (10 mL) and heated to reflux under an argon atmosphere for 24 h. The reaction mixture was then cooled to room temperature and poured into water (*ca.* 200 mL) and cooled in a fridge for 1 h. The formed yellow precipitate was then isolated via filtration and washed sequentially with water (*ca.* 50 mL), cold methanol (5 mL), cold *n*-hexane (3 × 20 mL) and cold *n*-pentane (3 × 20 mL) to afford tetrakis(2-phenyl-4-(2,4,6-trimethylphenyl)-pyridine-*C*^{2},*N*')(μ-dichloro)diiridium (**[Ir(mesppy)$_2$μ-Cl]$_2$**). as a yellow powder (1.42 g, 0.92 mmol, 94%). Analytical data were in agreement with those previously reported.[23] ^{1}H NMR (400 MHz, CD_2Cl_2) δ (ppm) = 9.70 (d, *J* = 5.9 Hz, 2H), 7.77 (d, *J* = 1.9 Hz, 2H), 7.54 (dd, *J* = 7.8, 1.4 Hz, 2H), 7.05 (d, *J* = 10.9 Hz, 4H), 6.89 – 6.82 (m, 4H), 6.71 (td, *J* = 7.5, 1.4 Hz, 2H), 5.95 (dd, *J* = 7.9, 1.1 Hz, 2H), 2.42 (s, 6H), 2.16 (s, 6H), 2.15 (s, 6H).

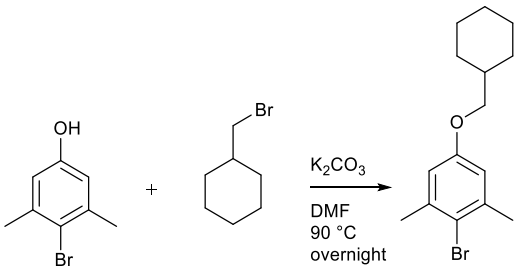

23 **24**
98%

2-Bromo-5-(methylcyclohexyloxy)-*meta*-xylene (24). 2-Bromo-4-hydroxy-*meta*-xylene (**23**) (15.00 g, 74.6 mmol, 1.00 eq.) and K_2CO_3 (20.6 g, 149 mmol mmol, 2.00 eq.) were combined in *N*,*N*-dimethylformamide (100 mL) and heated to 80 °C for 10 min under argon. Bromo(methylcyclohexane) (15.6 mL, 112 mmol, 1.50 eq.) was then added in a single portion and the mixture was heated to 90 °C overnight. The reaction mixture was cooled to room temperature and poured into water (1 L). The mixture was extracted with EtOAc/ toluene 1:1 v/v (3 × 200 mL). The organic layers were combined and washed with $HCl_{(aq)}$ (1 M, 5 × 50 mL) before being dried over $MgSO_4$ and evaporated under reduced pressure to afford a brown oil. The residue was purified via flash chromatography on silica

gel (eluent: *n*-hexane). 2-Bromo-5-(methylcyclohexyloxy)-*meta*-xylene (**24**) eluted as a clear oil (21.7 g, 73.0 mmol, 98%). ^{1}H NMR (400 MHz, $CDCl_3$) δ (ppm) = 6.66 (s, 2H), 3.72 (d, *J* = 6.4 Hz, 2H), 2.40 (S, 6H), 1.93 – 1.67 (m, 6H), 1.39 – 1.17 (m, 3H), 1.05 (qd, *J* = 12.2, 3.4 Hz, 2H); ^{13}C NMR (101 MHz, $CDCl_3$) δ (ppm) = 157.8, 139.0, 117.9, 114.4, 73.6, 37.7, 29.9, 26.5, 25.8, 24.0; HRMS (ASAP): *m/z* 296.0779 [M^+]. Calcd. for $C_{15}H_{21}OBr^+$: 296.0776.

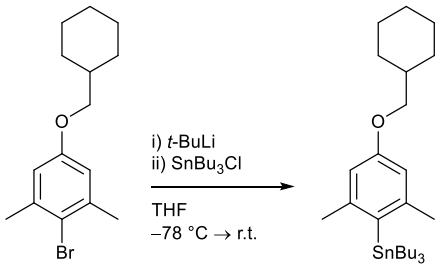

24 **25**

2-Tributylstannyl-5-(methylcyclohexyloxy)-*meta*-xylene (25). 2-Bromo-5-(methylcyclohexyloxy)-*meta*-xylene (**24**) (10.5 g, 33.6 mmol, 1.00 eq.) was dissolved in dry THF (250 mL) and cooled to –78 °C under argon. *t*-BuLi (1.7 M in pentane, 27 mL, 74.8 mmol, 2.22 eq.) was then added over 15 min, keeping the reaction temperature below –65 °C. The thick yellow mixture was then stirred at –78 °C for 45 min before the addition of tributyltin chloride (11.2 mL, 41.2 mmol, 1.23 eq.) over 5 min. The reaction was then warmed to room temperature overnight before being poured into hexane (200 mL). The mixture was washed with sat. $NH_4Cl_{(aq)}$ (3 × 50 mL) before being dried over $MgSO_4$, and the solvent removed under reduced pressure to afford 2-tributylstannyl-5-(methylcyclohexyloxy)-*meta*-xylene (**25**) as a pale yellow oil (17.0 g, 33.5 mmol, 100%) which was used without further purification. ^{1}H NMR (400 MHz, $CDCl_3$) δ (ppm) = 6.59 (s + (d, $^{4}J_{H–Sn}$ = 11.7 Hz), 2H), 3.74 (d, *J* = 6.3 Hz, 2H), 2.38 (s + (d, $^{4}J_{H–Sn}$ = 5.5 Hz), 6H), the aliphatic region (*ca*. 0.5–2 ppm) was not assigned due to the presence of alkyl tin impurities; HRMS (ASAP): *m/z* 505.2808 [MH^+]. Calcd. for $C_{27}H_{49}O^{116}Sn^+$: 505.2801.

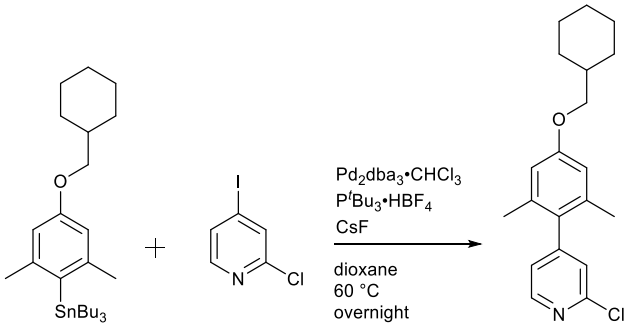

25 **26** **72%**

2-Chloro-4-(2,6-dimethyl-4-(methylcyclohexyloxy)phenyl)pyridine (26). 2-Chloro-4-iodopyridine (3.00 g, 12.5 mmol, 1.00 eq.), 2-tributylstannyl-5-(methylcyclohexyloxy)-*meta*-xylene (**25**) (8.74 g, 17.2 mmol, 1.38 eq.) and tri-*tert*-butylphosphonium tetrafluoroborate (218 mg, 0.75 mmol, 6 mol%) were added to dry dioxane (50 mL) and the resulting mixture was degassed for 40 min. Pd_2dba_3•$CHCl_3$ (388 mg, 0.37 mmol, 3 mol%) was then added to the mixture, which was degassed for a further 10 min before the addition of CsF (4.18 g, 27.5 mmol, 2.20 eq.). The red

reaction mixture was subsequently stirred at room temperature for 2.5 h. Analysis of an aliquot by GC-MS at this point indicated that the desired reaction had not occurred. Further Pd_2dba_3•$CHCl_3$ (130 mg, 0.12 mmol, 1 mol%) and tri-*tert*-butylphosphonium tetrafluoroborate (73 mg, 0.25 mmol, 2 mol%) were added and the mixture was heated to 60 °C for 17 h, after which point analysis of an aliquot by GC-MS revealed complete consumption of 2-chloro-4-iodopyridine. The reaction mixture was cooled to room temperature, diluted with EtOAc (*ca.* 50 mL) and filtered through a plug of celite, which was subsequently washed with further EtOAc (2 × 50 mL). The combined filtrates were evaporated under reduced pressure and the residual crude product was purified via flash chromatography on silica gel (eluent: gradient EtOAc/ *n*-hexane 0:1–1:9 v/v with *ca.* 0.5% vol. NEt_3 as an additive) to obtain 2-chloro-4-(2,6-dimethyl-4-(methylcyclohexyloxy)phenyl)pyridine (**26**) as a brown oil (3.67 g, 11.1 mmol, 89%). Further purification by distillation on a Kugelrohr apparatus (*ca.* 110 °C, 0.1 mbar) afforded a colourless viscous oil which solidified upon standing (2.96 g, 8.97 mmol, 72%). M.pt. 72–75 °C; ^{1}H NMR (400 MHz, $CDCl_3$) δ (ppm) = 8.45 (dd, *J* = 5.0, 0.8 Hz, 1H), 7.18 (dd, *J* = 1.5, 0.7 Hz, 1H), 7.06 (dd, *J* = 5.0, 1.4 Hz, 1H), 6.68 (s, 2H), 3.78 (d, *J* = 6.4 Hz, 2H), 1.93 – 1.70 (m, 6H), 1.41 – 1.19 (m, 3H), 1.15 – 1.02 (m, 2H); ^{13}C NMR (101 MHz, $CDCl_3$) δ (ppm) = 159.0, 152.8, 151.8, 149.7, 136.5, 125.5, 124.1, 113.6, 73.4, 37.8, 29.9, 26.6, 25.8, 20.9; HRMS (ESI): *m/z* 330.1628 [MH^+]. Calcd. for $C_{20}H_{25}NOCl^+$: 330.1625.

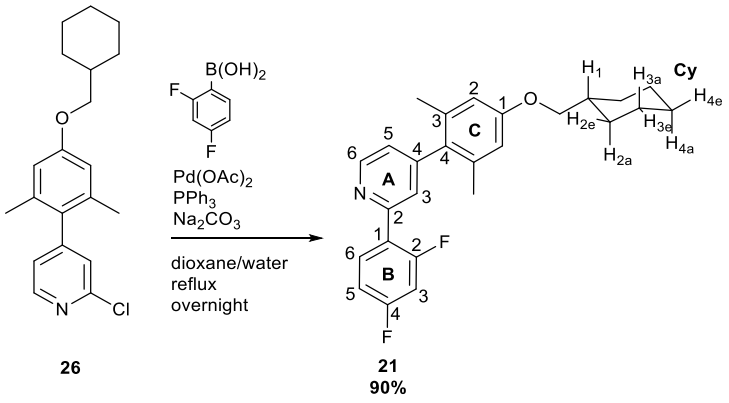

2-(2,4-Difluorophenyl)-4-(2,6-dimethyl-4-(methylcyclohexyloxy)phenyl)pyridine (21). 2-Chloro-4-(2,6-dimethyl-4-(methylcyclohexyloxy)phenyl)pyridine (**26**) (617 g, 1.87 mmol, 1.00 eq.), 2,4-difluorophenyl boronic acid (443 mg, 2.81 mmol, 1.50 eq.) and PPh_3 (20.5 mg, 0.45 mmol, 24 mol%) were combined in 1,4-dioxane (6 mL). A solution of Na_2CO_3 (795 mg, 7.48 mmol, 4.00 eq.) in water (2 mL) was then added and the mixture was degassed for 15 min. $Pd(OAc)_2$ (20.5 mg, 0.11 mmol, 6 mol%) was then added and the mixture was degassed for a further 5 minutes, before being heated to reflux under argon overnight. The mixture was then allowed to cool to room temperature and evaporated to near-dryness. To the residue was added water (30 mL) and DCM (40 mL). The organic layer was separated and the aqueous later was extracted twice more with DCM (40 mL). The organic extracts were combined, dried over $MgSO_4$ and evaporated under reduced pressure. The residue was purified by flash chromatography on silica gel (eluent: gradient EtOAc/ *n*- hexane 1:99–1:9 v/v with *ca.* 0.5% vol. NEt_3 as an additive). 2-(2,4-Difluorophenyl)-4-(2,6-dimethyl-4-(methylcyclohexyloxy)phenyl)pyridine (**21**) was obtained as a white tacky solid (678g, 1.66 mmol, 90%). M.pt. 117–118 °C; ^{1}H NMR (600 MHz, $CDCl_3$) δ (ppm) = 8.74 (dd, *J* = 5.0, 0.9 Hz, $1H_{A6}$), 8.07 (td, *J* = 8.8, 6.6 Hz, $1H_{B6}$), 7.57 (dd, *J* = 1.5, 0.9 Hz, $1H_{A3}$), 7.07 (dd, *J* = 5.0, 1.5 Hz, $1H_{A5}$), 7.02 (dddd, *J* = 8.8, 7.9, 2.6, 1.4 Hz, $1H_{B5}$), 6.90 (ddd, *J* = 11.3, 8.8, 2.6 Hz, $1H_{B3}$), 6.68 (s, $2H_{C2}$), 3.77 (d, *J* = 6.4 Hz, $2H_{CH2Cy}$), 2.06 (s, $6H_{CMe}$), 1.92 – 1.85 (m, $2H_{CyH2e}$), 1.85 – 1.81 (m, $1H_{CyH1}$), 1.77 (dt, *J* = 13.0, 3.4 Hz, $2H_{CyH3e}$), 1.74 – 1.68 (m, $1H_{CyH4e}$), 1.32 (qt, *J* = 12.6, 3.4 Hz, $2H_{CyH3a}$), 1.22 (qt, *J* = 12.7, 3.4 Hz, $1H_{CyH4a}$), 1.07 (qd, *J* = 12.4, 3.5 Hz,

2H$_{CyH2a}$); ^{13}C NMR (151 MHz, $CDCl_3$) δ (ppm) = 163.2 (dd, *J* = 250.9, 12.0 Hz, C$_{B4}$), 160.6 (dd, *J* = 252.8, 12.0 Hz, C$_{B2}$), 158.7 (C$_{C1}$), 152.6 (d, *J* = 2.6 Hz, C$_{A2}$), 149.9 (C$_{A4}$), 149.8 (C$_{A6}$), 136.7 (C$_{C3}$), 132.2 (dd, *J* = 9.7, 4.4 Hz, C$_{B6}$), 131.4 (C$_{C4}$), 125.7 (d, *J* = 9.4 Hz, C$_{A3}$), 123.9 (C$_{A5}$), 123.9 (dd, *J* = 12.0, 3,9 Hz, C$_{B1}$), 113.5 (C$_{C2}$), 111.9 (dd, *J* = 21.1, 3.6 Hz, C$_{B5}$), 104.4 (dd, *J* = 27.0, 25.3 Hz, C$_{B3}$), 73.4 (C$_{CH2}$), 37.7 (C$_{Cy1}$), 29.9 (C$_{Cy2}$), 26.5 (C$_{Cy4}$), 25.8 (C$_{Cy3}$), 21.0 (C$_{Me}$); ^{19}F {^{1}H} NMR (376 MHz, $CDCl_3$) δ (ppm) = -109.2 – -109.5 (m, 1F), -112.7 – - 112.8 (m, 1F); HRMS (ESI): *m/z* 408.2128 [MH^+]. Calcd. for $C_{26}H_{28}NOF_2^+$: 408.2139.

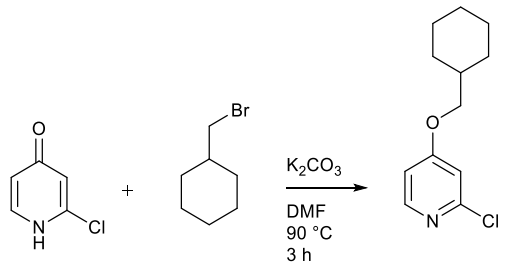

27 **28** **87%**

4-(Methylcyclohexyloxy)-2-chloropyridine (28). 2-Chloro-4-pyridone (**27**) (5.00 g, 38.6 mmol, 1.00 eq.) and K_2CO_3 (10.7 g, 77.2 mmol, 2.00 eq.) were combined in *N,N*-dimethylformamide (50 mL) and heated to 80 °C for 10 min under argon. Bromo(methylcyclohexane) (8.1 mL, 57.9 mmol, 1.50 eq.) was then added in a single portion and the mixture was heated to 90 °C for a further 4 h. The reaction mixture was cooled to room temperature and poured into water (200 mL). The mixture was extracted with EtOAc/ toluene 1:1 v/v (4 × 100 mL). The organic layers were combined and washed with HCl $_{(aq)}$ (1 M, 5 × 50 mL) before being dried over $MgSO_4$ and evaporated under reduced pressure to afford a brown oil. The residue was purified via flash chromatography on silica gel (eluent: EtOAc/ *n*-hexane 3:7 v/v) to obtain 4-(methylcyclohexyloxy)-2-chloropyridine (**28**) as a waxy white solid (7.55 g, 33.4 mmol, 87%). M.pt. 54–55 °C; ^{1}H NMR (400 MHz, $CDCl_3$) δ (ppm) = 8.19 (d, *J* = 5.8 Hz, 1H), 6.84 (d, *J* = 2.2 Hz, 1H), 6.75 (dd, *J* = 5.8, 2.3 Hz, 1H), 3.81 (d, *J* = 6.1 Hz, 2H), 1.93 – 1.59 (m, 6H), 1.40 – 1.15 (m, 3H), 1.14 – 0.99 (m, 2H); ^{13}C NMR (101 MHz, $CDCl_3$) δ (ppm) = 167.0, 152.5, 150.1, 110.1, 109.9, 73.9, 37.3, 29.7, 26.3, 25.7; HRMS (ESI): *m/z* 226.1001 [MH^+]. Calcd. for $C_{12}H_{17}NOCl^+$: 226.0999.

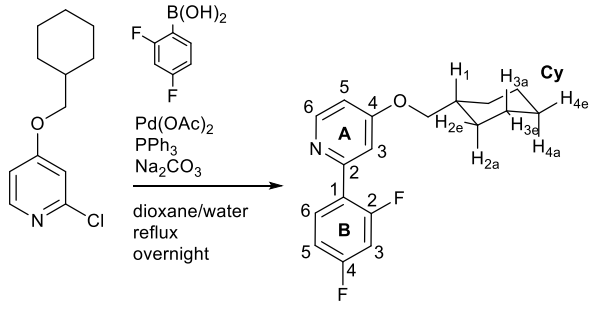

28 **22** **100%**

2-(2,4-Difluorophenyl)-4-(methylcyclohexyloxy)pyridine (22). 4-(Methylcyclohexyloxy)-2-chloropyridine (**28**) (2.00 g, 8.86 mmol, 1.00 eq.), 2,4-difluorophenyl boronic acid (2.10 g, 13.29 mmol, 1.50 eq.) and PPh_3 (558 mg, 2.13 mmol, 24 mol%) were combined in 1,4-dioxane (32 mL). A solution of Na_2CO_3 (3.76 g, 35.4 mmol, 4.00 eq.) in

water (12 mL) was then added and the mixture was degassed for 30 min. $Pd(OAc)_2$ (120 mg, 0.53 mmol, 6 mol%) was then added and the mixture was degassed for a further 10 min, before being heated to reflux under argon overnight. The mixture was then allowed to cool to room temperature and evaporated to near-dryness. To the residue was added water (50 mL) and DCM (50 mL). The organic layer was separated and the aqueous later was extracted twice more with DCM (50 mL). The organic extracts were combined, dried over $MgSO_4$ and evaporated under reduced pressure. The residue was purified by flash chromatography on silica gel (eluent: EtOAc/ *n*- hexane 4:6 v/v with *ca.* 0.5% vol. NEt_3 as an additive). 2-(2,4-Difluorophenyl)-4-(methylcyclohexyloxy)pyridine (**22)** was obtained as a faint yellow oil which solidified on standing (2.68 g, 8.83 mmol, 100%). M.pt. 66–68 °C; ^{1}H NMR (600 MHz, $CDCl_3$) δ (ppm) = 8.49 (d, *J* = 5.7 Hz, $1H_{A6}$), 7.97 (td, *J* = 8.8, 6.6 Hz, $1H_{B6}$), 7.24 (ap. t, *J* = 2.4 Hz, $1H_{A3}$), 6.98 (tdd, *J* = 7.8, 2.5, 1.0 Hz, $1H_{B5}$), 6.90 (ddd, *J* = 11.3, 8.8, 2.5 Hz, $1H_{B3}$), 6.77 (dd, *J* = 5.7, 2.4 Hz, $1H_{A5}$), 3.84 (d, *J* = 6.3 Hz, $2H_{CH2Cy}$), 1.89 – 1.85 (m, $2H_{CyH2e}$), 1.84 – 1.81 (m, $1H_{CyH1}$), 1.78 (dt, *J* = 12.9, 3.4 Hz, $2H_{CyH3e}$), 1.73 – 1.69 (m, $1H_{CyH4e}$), 1.31 (qt, *J* = 12.7, 3.4 Hz, $2H_{CyH3a}$), 1.21 (qt, *J* = 12.8, 3.4 Hz, $1H_{CyH4a}$), 1.07 (qd, *J* = 12.7, 3.6 Hz, $2H_{CyH2a}$); ^{13}C NMR (151 MHz, $CDCl_3$) δ (ppm) = 165.7 (C_{A4}), 163.08 (dd, *J* = 250.7, 12.1 Hz, C_{B4}), 160.45 (dd, *J* = 252.4, 11.9 Hz, C_{B2}), 153.9 (d, *J* = 2.4 Hz, C_{A2}), 150.7 (C_{A6}), 132.1 (dd, *J* = 9.6, 4.5 Hz, C_{B6}), 123.9 (dd, *J* = 11.6, 3.8 Hz, C_{B1}), 111.7 (dd, *J* = 21.0, 3.7 Hz, C_{B5}), 110.9 (d, *J* = 9.1 Hz, C_{A3}), 109.0 (C_{A5}), 104.3 (dd, *J* = 27.1, 25.3 Hz, C_{B3}), 73.4 (C_{CH2}), 37.4 (C_{Cy1}), 29.8 (C_{Cy2}), 26.4 (C_{Cy4}), 25.7 (C_{Cy3}); ^{19}F{^{1}H} NMR (376 MHz, $CDCl_3$) δ (ppm) = -109.4 (d, *J* = 8.5 Hz, 1F), -112.7 (d, *J* = 8.5 Hz, 1F); HRMS (ESI): *m/z* 304.1517 [MH^+]. Calcd. for $C_{18}H_{20}NOF_2^+$: 304.1513.

Copies of NMR Spectra

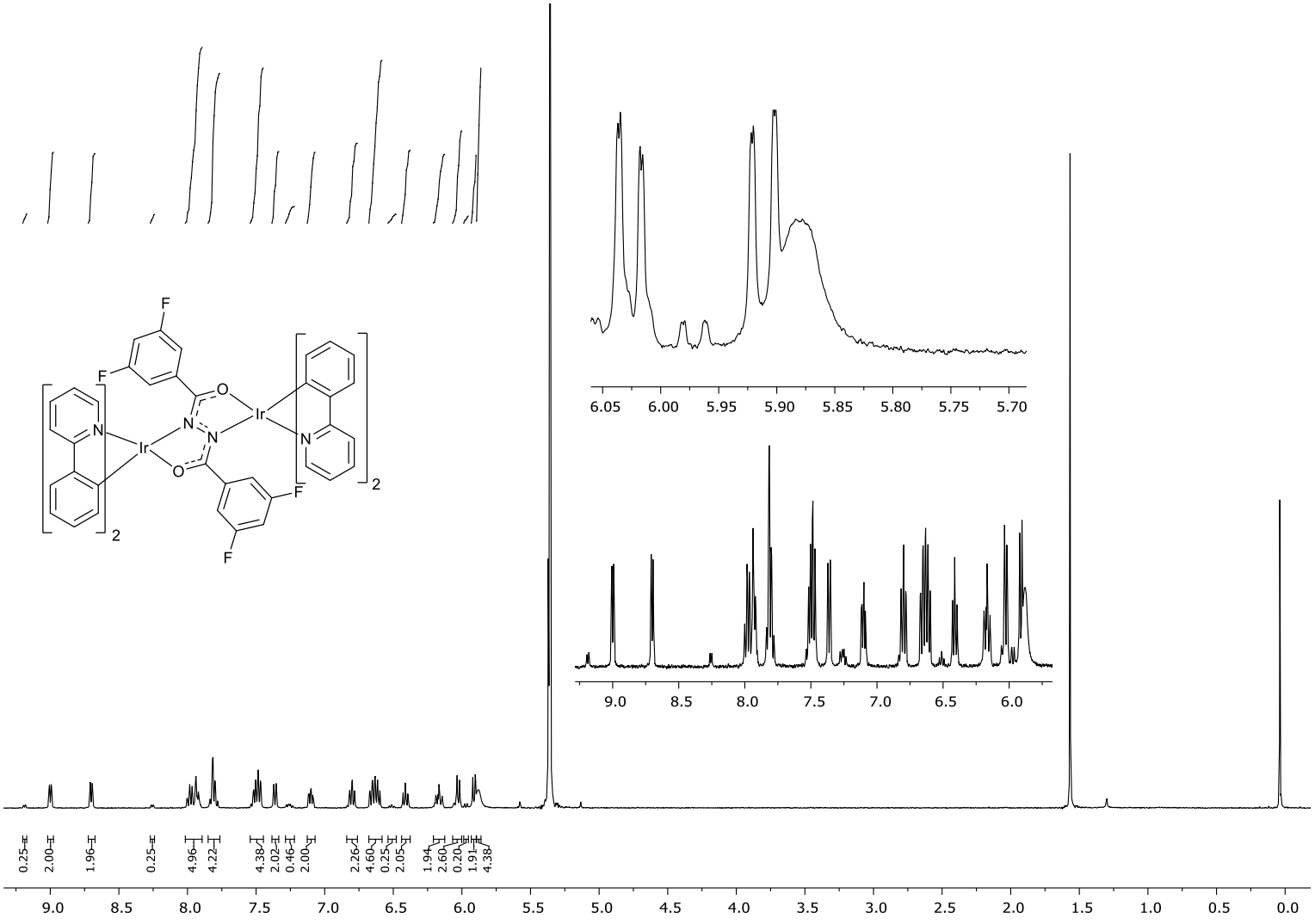

Figure S1. ^{1}H NMR spectrum (600 MHz) of **7** in CD_2Cl_2 (TMS).

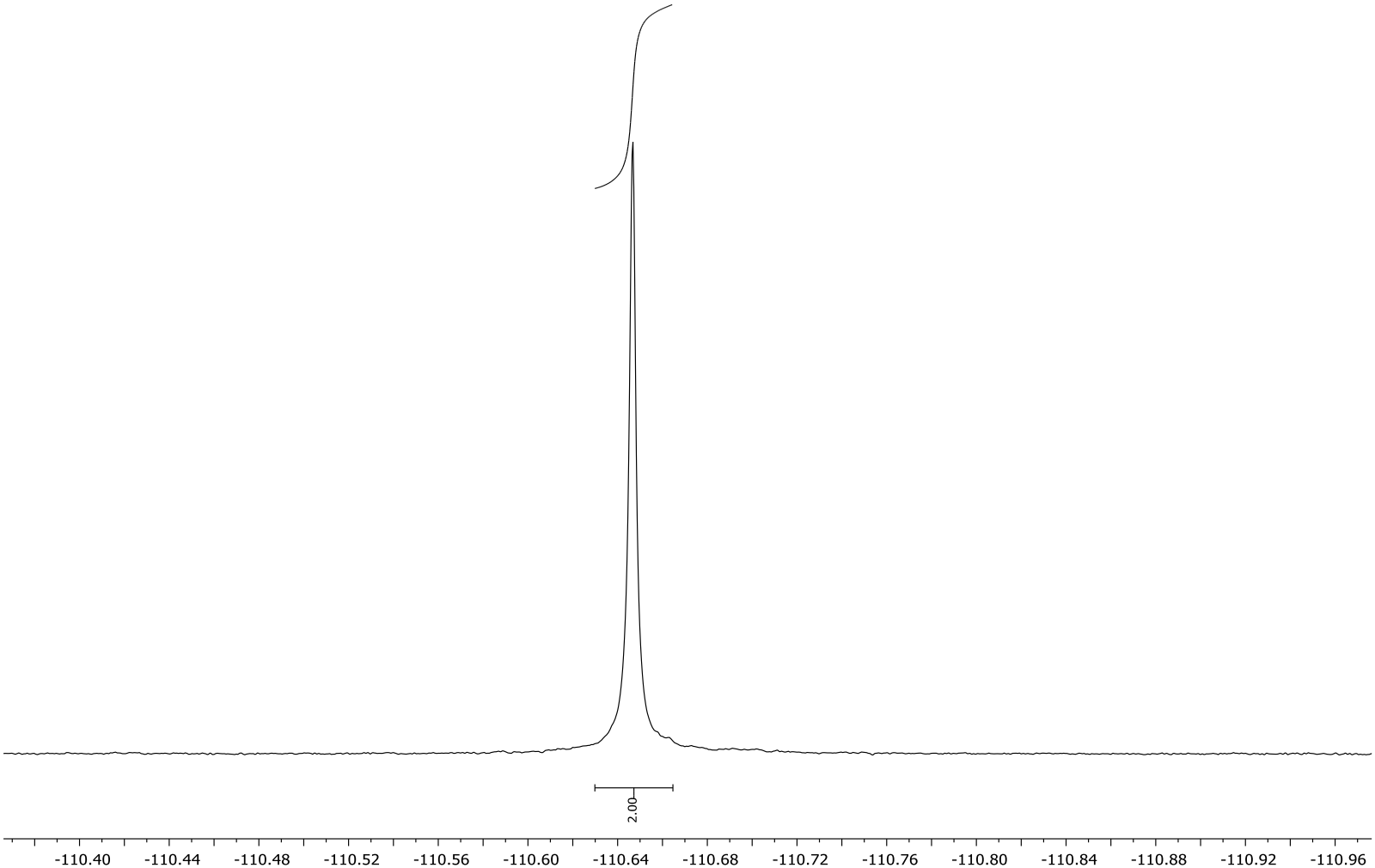

Figure S2. $^{19}F\{^{1}H\}$ NMR spectrum (376 MHz) of **7** in CD_2Cl_2.

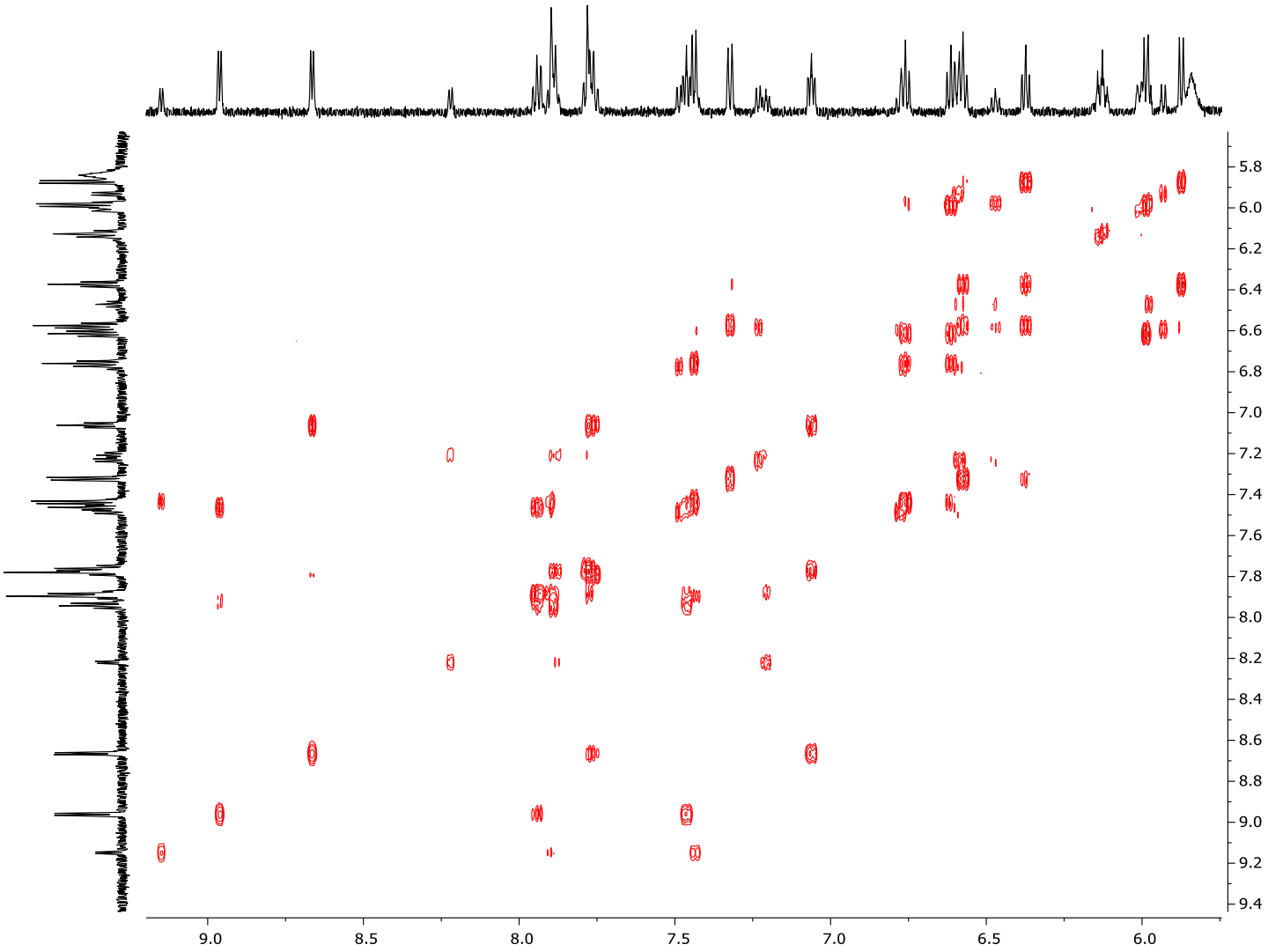

Figure S3. Expansion of the aromatic region of the ^{1}H–^{1}H COSY NMR spectrum of **7** in CD_2Cl_2 (TMS).

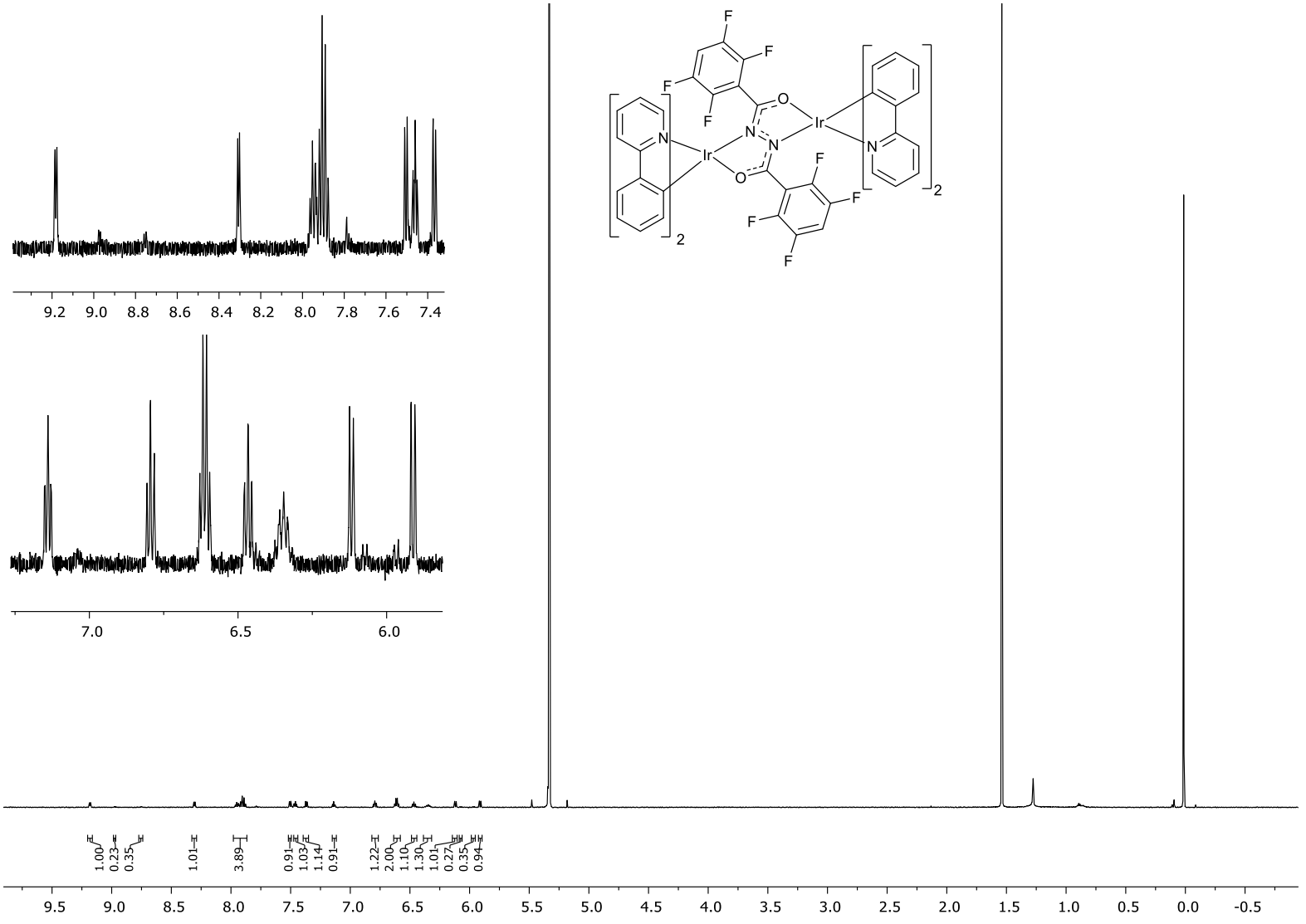

Figure S4. ^{1}H NMR spectrum (600 MHz) of **8** in CD_2Cl_2 (TMS).

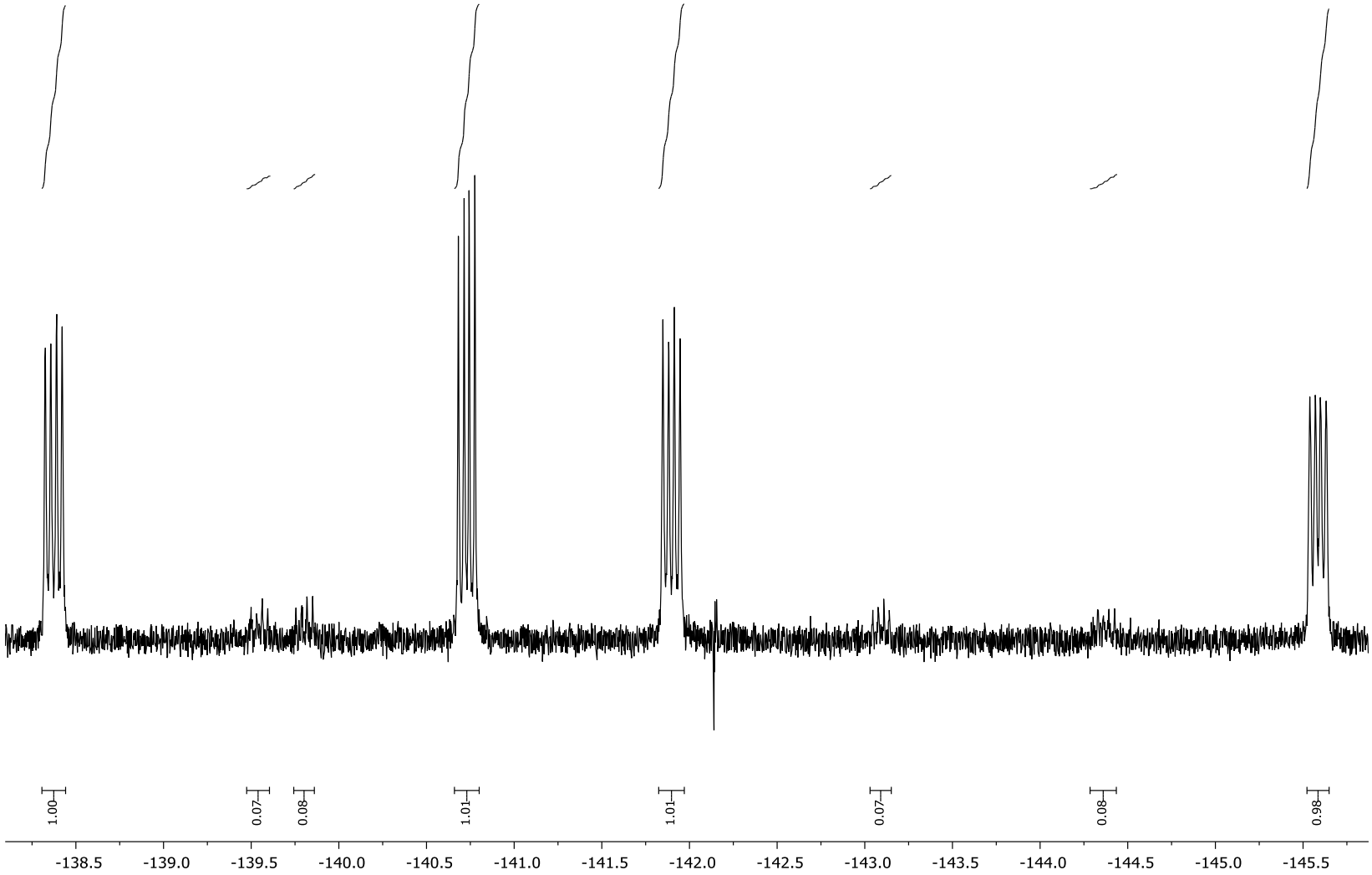

Figure S5. $^{19}F\{^{1}H\}$ NMR spectrum (376 MHz) of **8** in CD_2Cl_2.

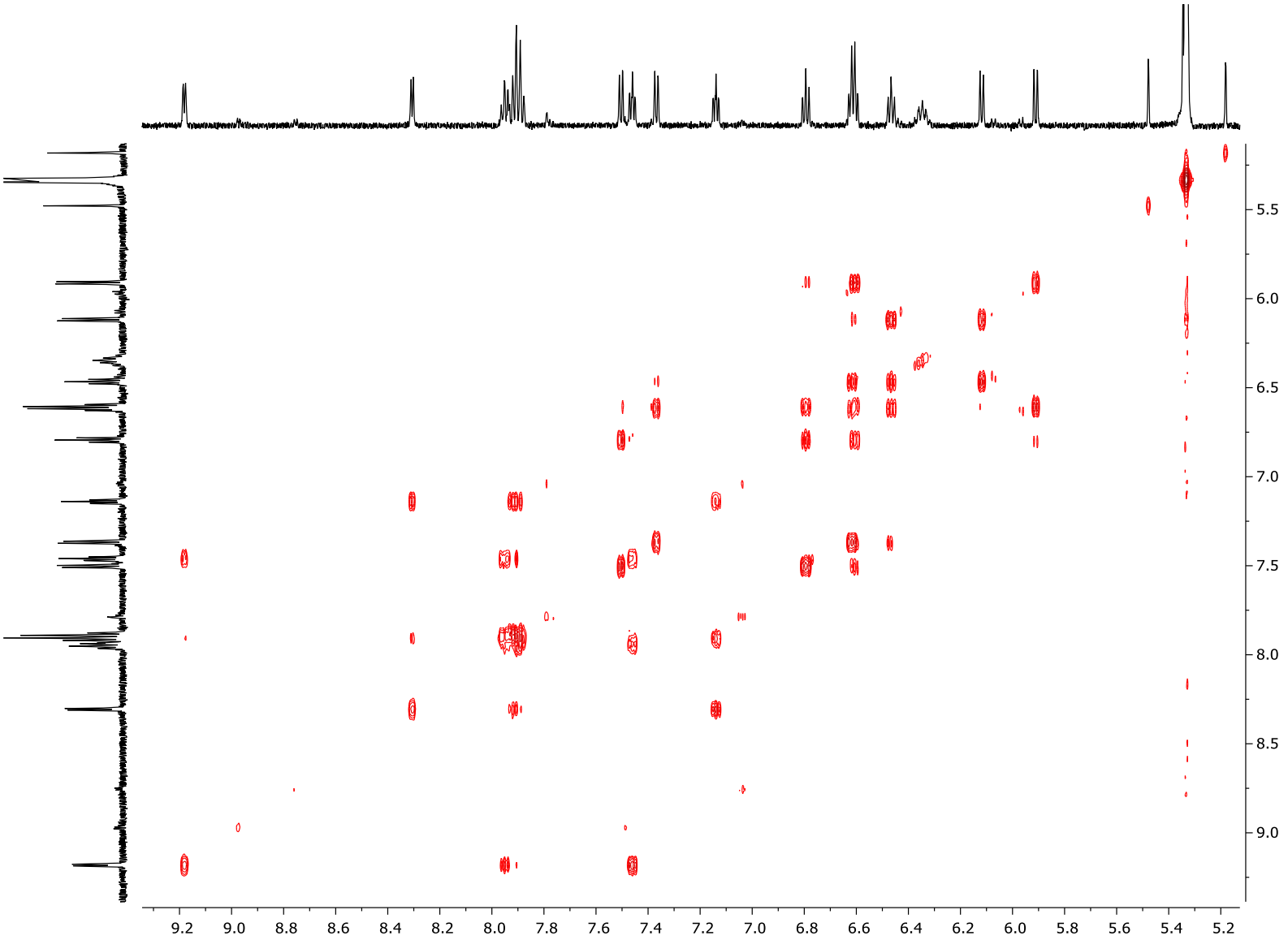

Figure S6. Expansion of the aromatic region of the ^{1}H–^{1}H COSY NMR spectrum of **8** in CD_2Cl_2 (TMS).

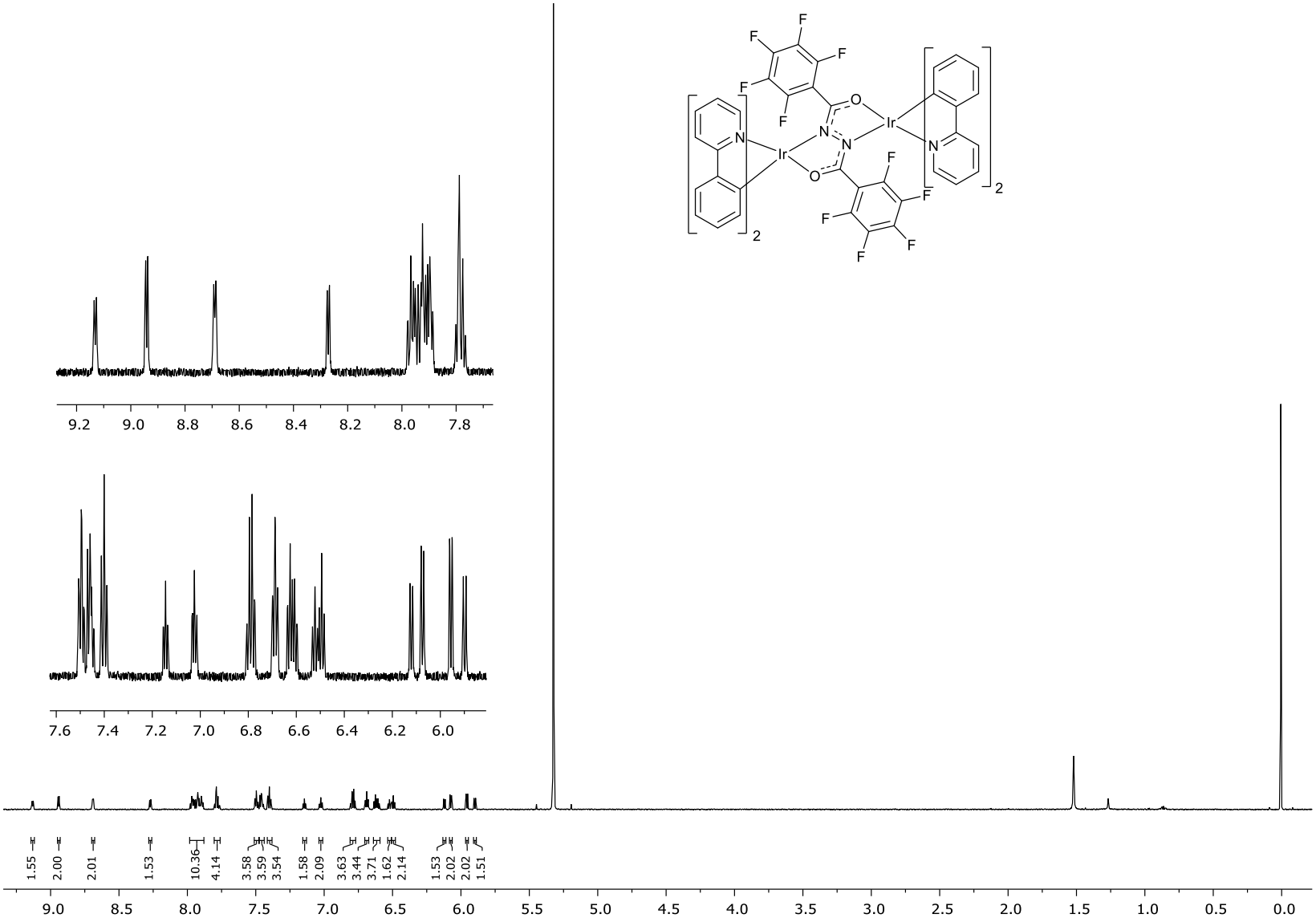

Figure S7. ^{1}H NMR spectrum (700 MHz) of **9** in CD_2Cl_2 (TMS).

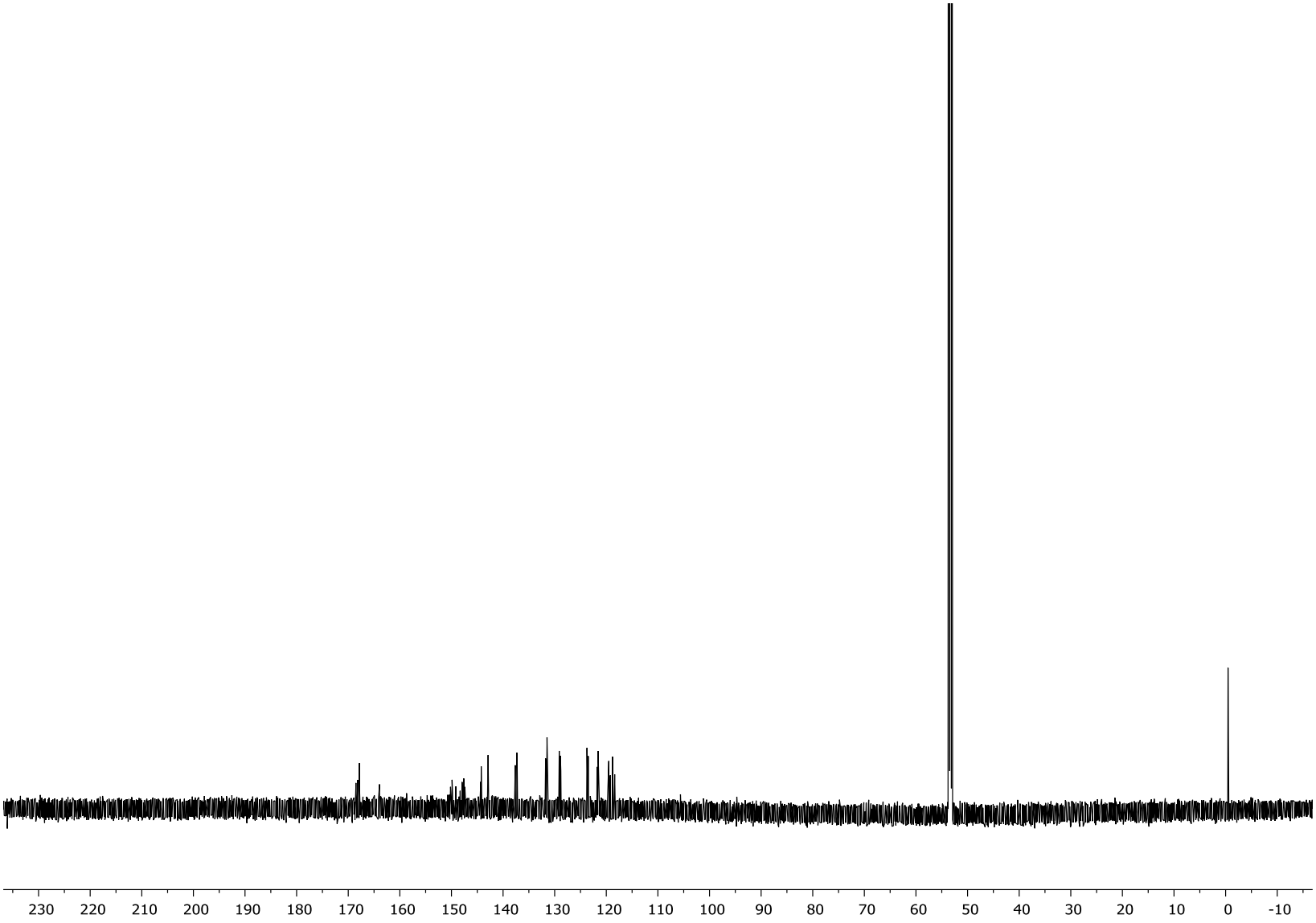

Figure S8. ^{13}C NMR spectrum (151 MHz) of **9** in CD_2Cl_2 (TMS).

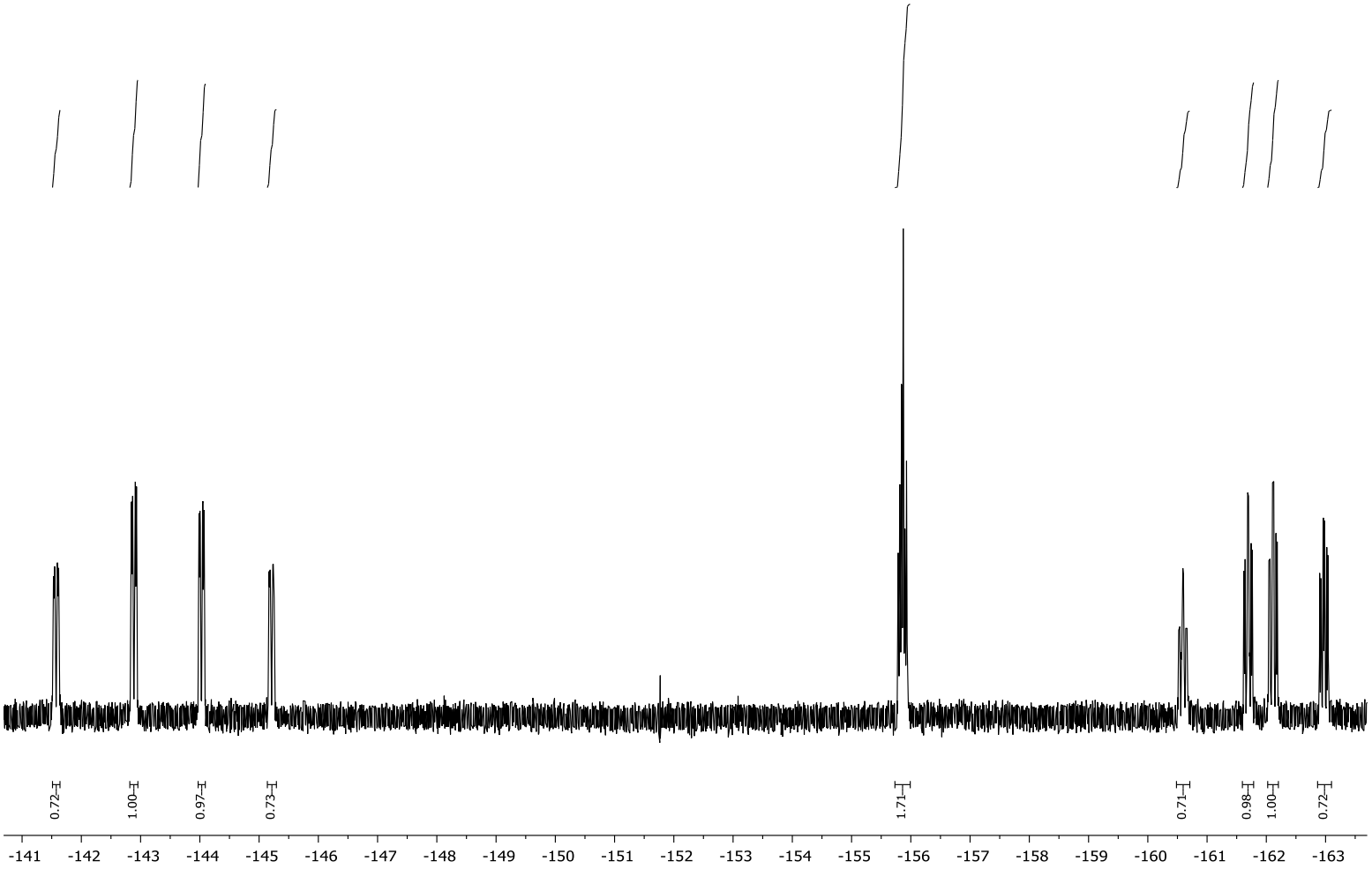

Figure S9. $^{19}F\{^{1}H\}$ NMR spectrum (376 MHz) of **9** in CD_2Cl_2.

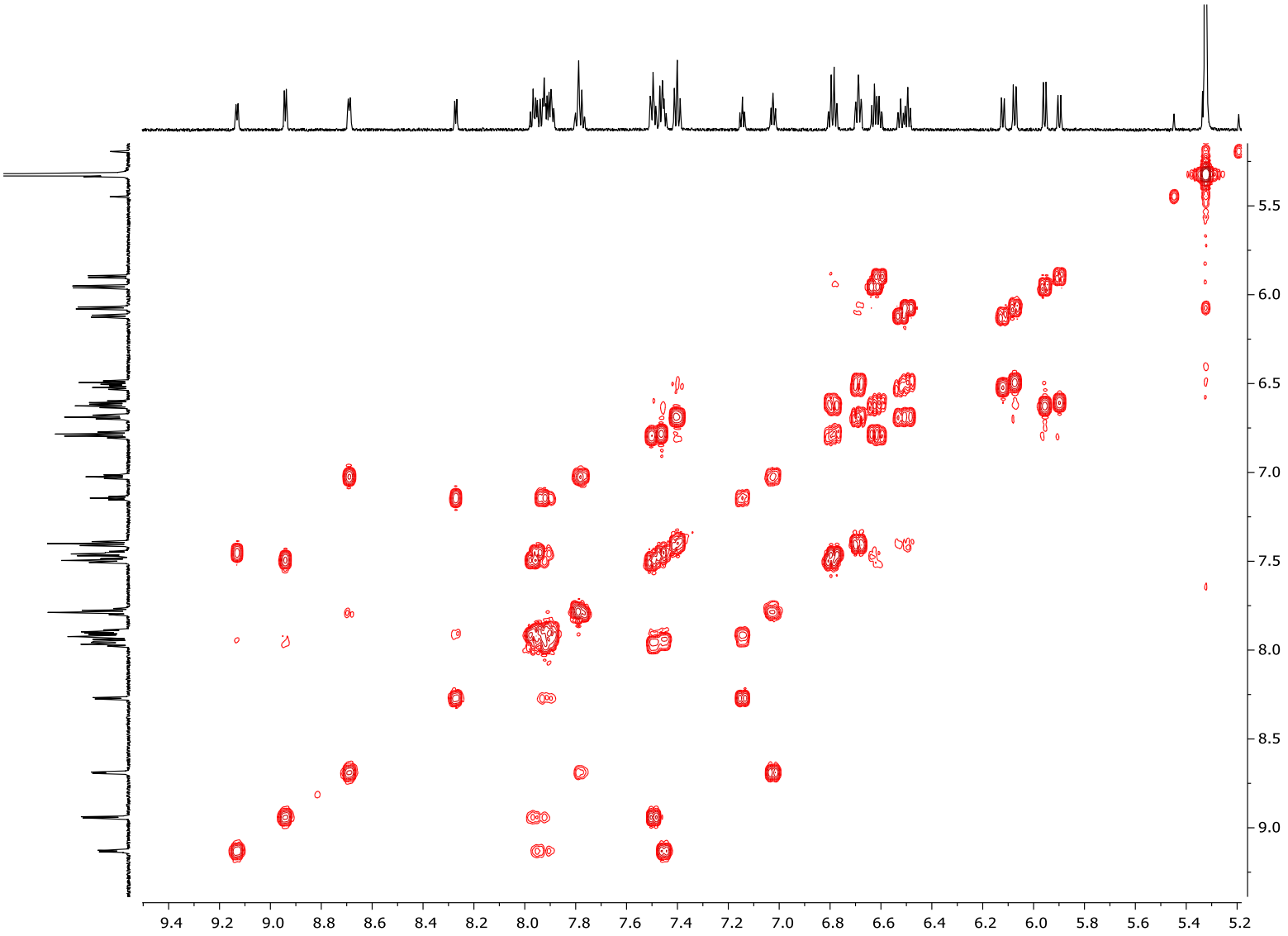

Figure S10. Expansion of the aromatic region of the ^{1}H–^{1}H COSY NMR spectrum of **9** in CD_2Cl_2 (TMS).

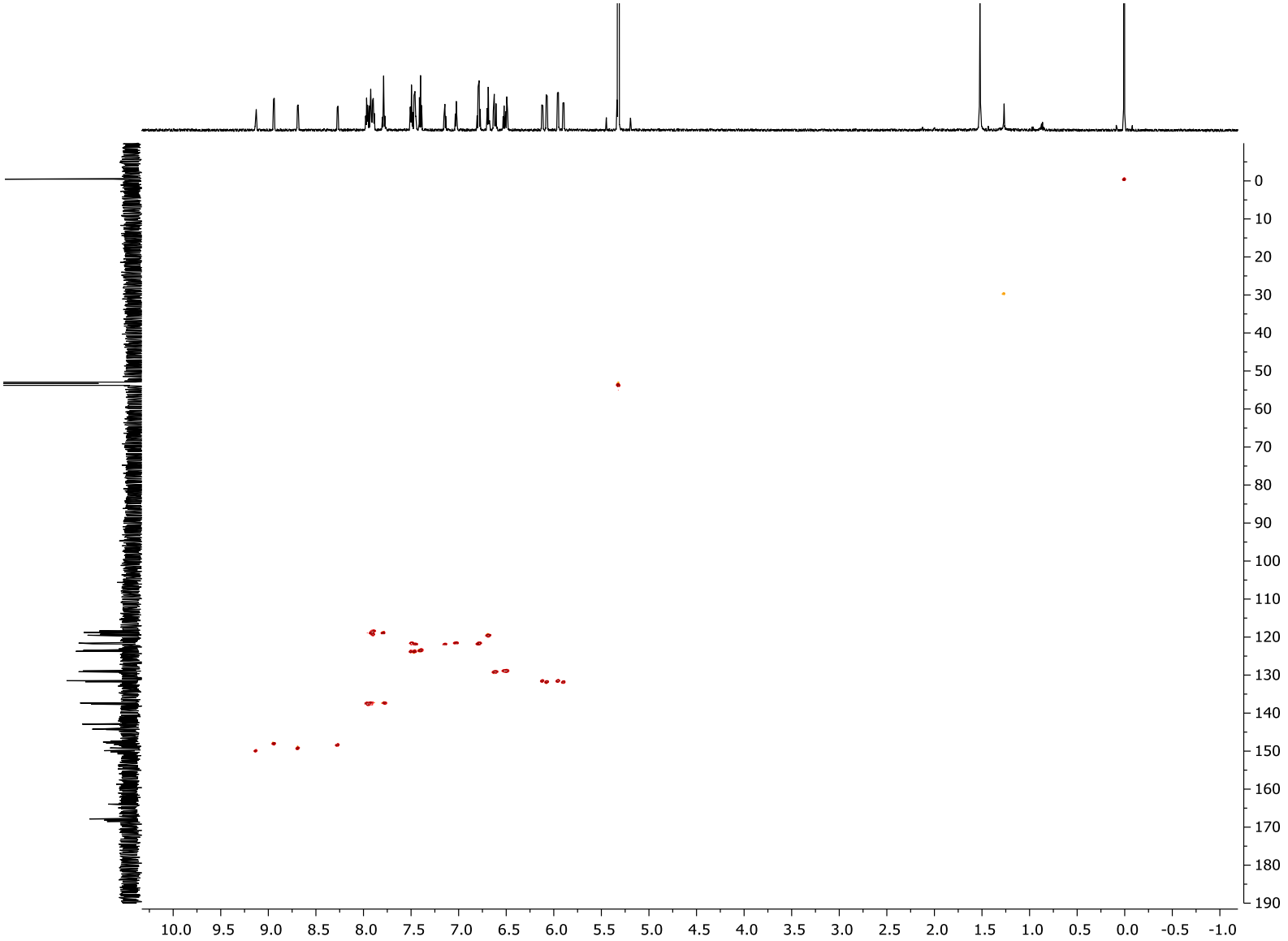

Figure S11. $^{1}H–^{13}C$ HSQC NMR spectrum of **9** in CD_2Cl_2.

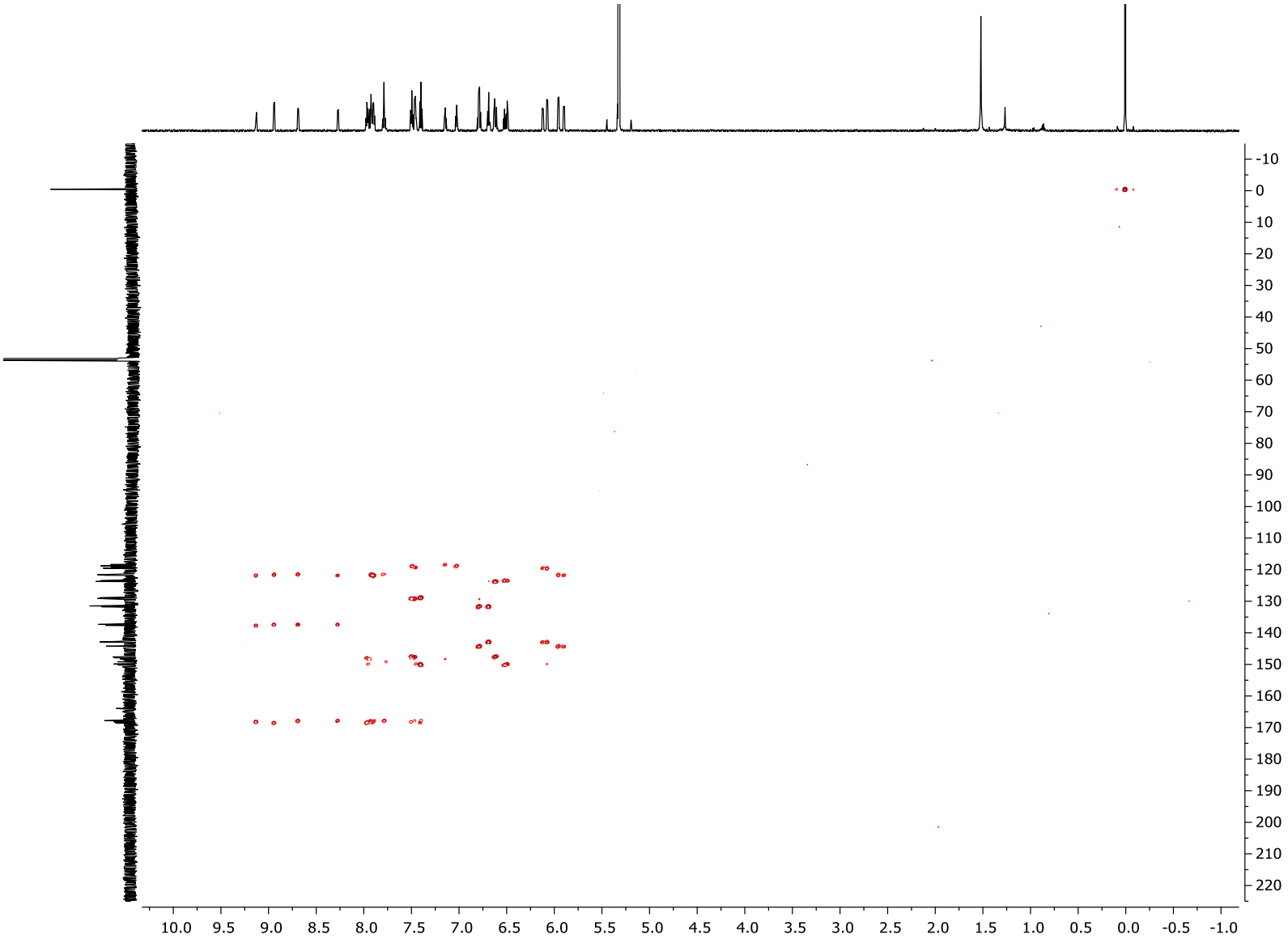

Figure S12. $^{1}H–^{13}C$ HMBC NMR spectrum of **9** in CD_2Cl_2.

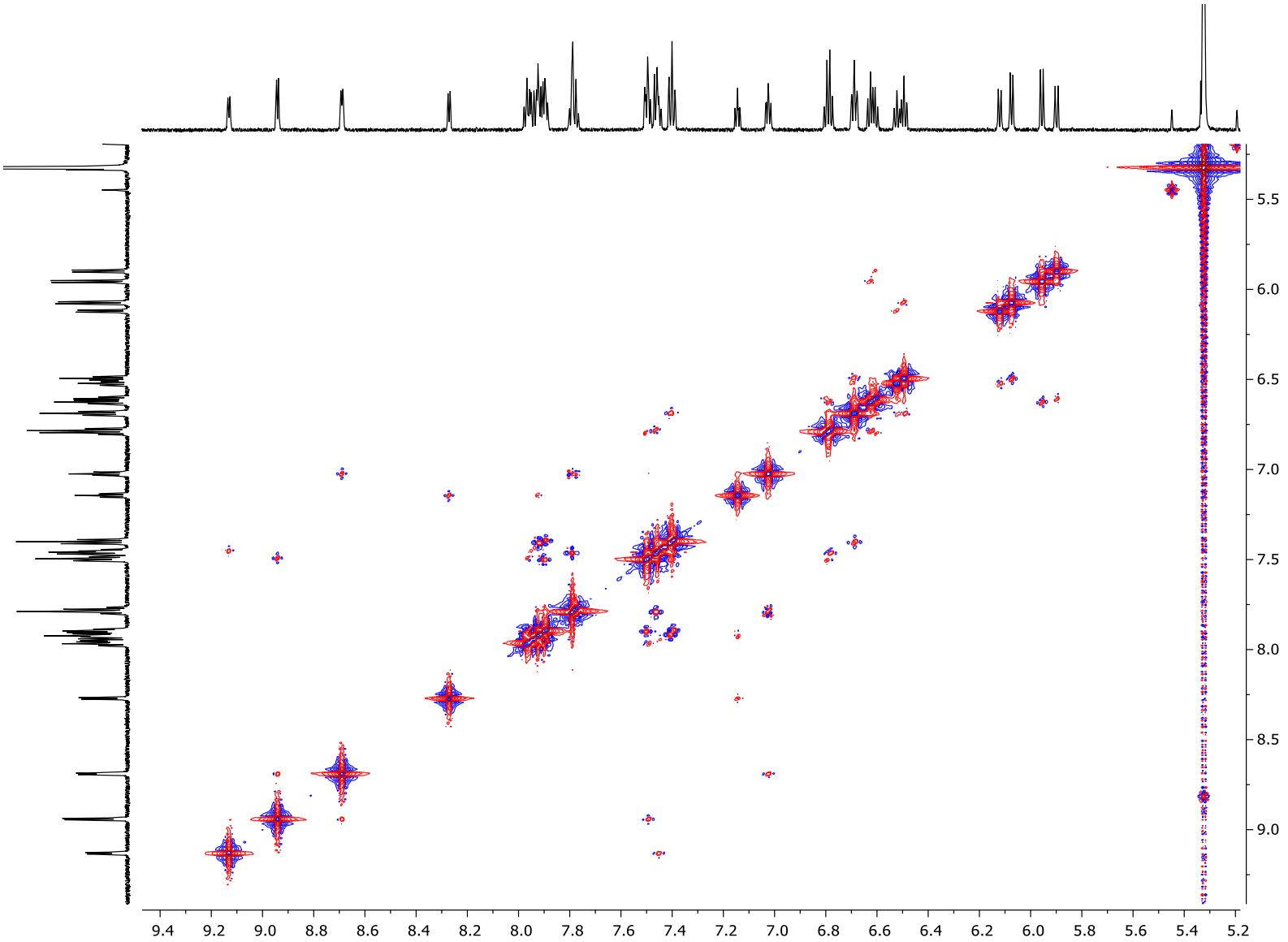

Figure S13. Aromatic region of the ^{1}H–^{1}H NOESY NMR spectrum of **9** in CD_2Cl_2.

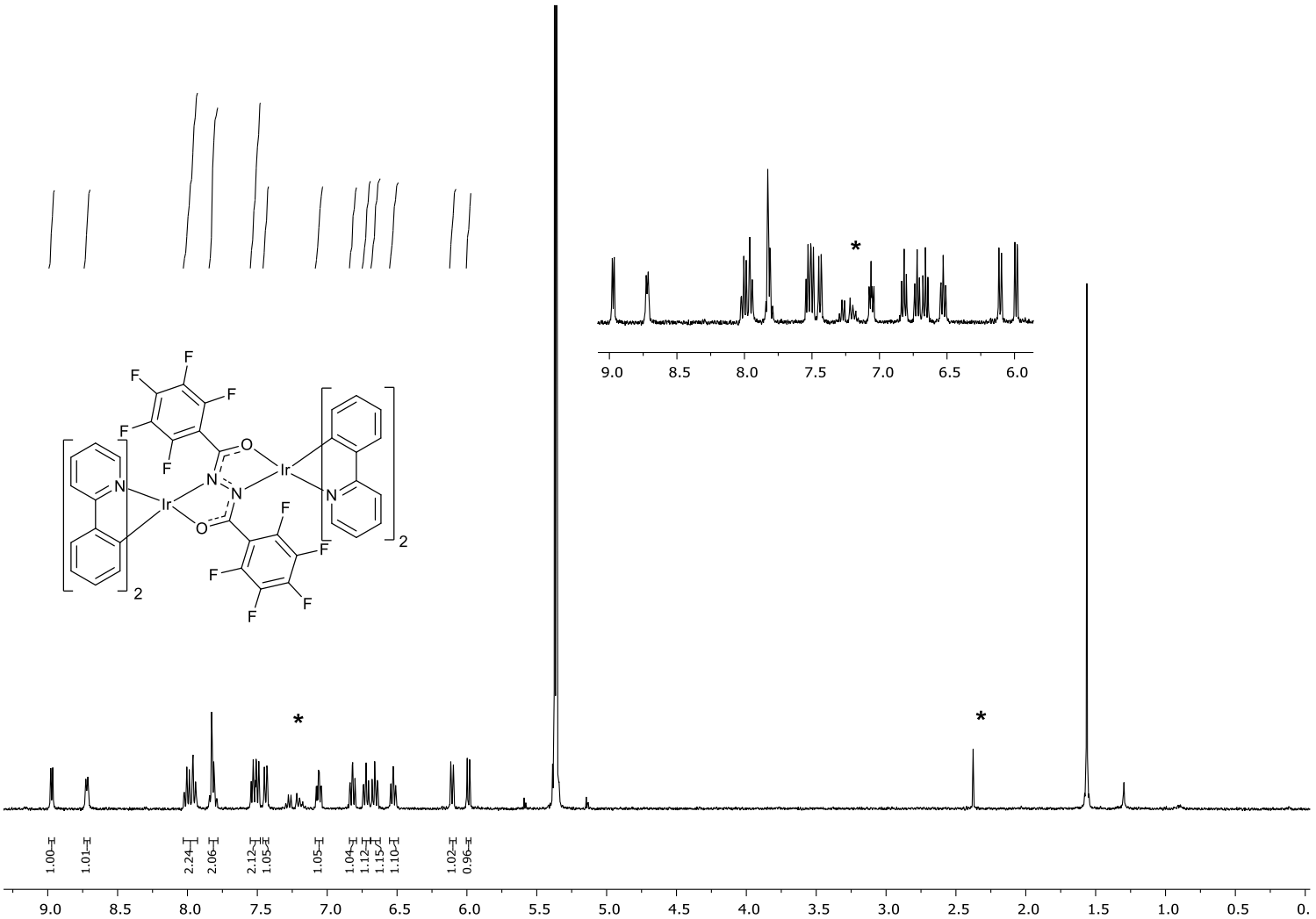

Figure S14. ^{1}H NMR spectrum (700 MHz) of *meso* **9** in CD_2Cl_2.* = Peaks from residual toluene.

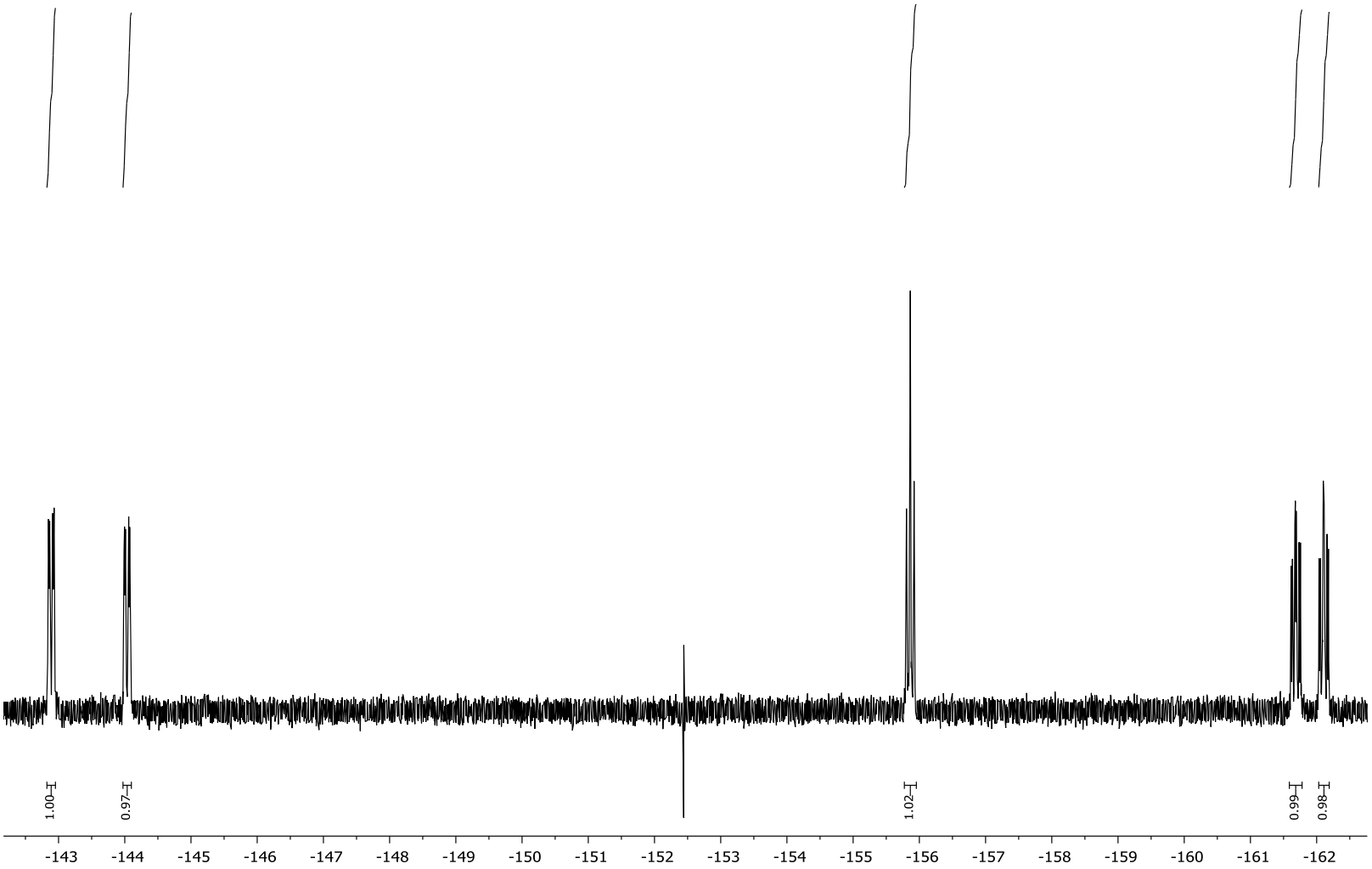

Figure S15. $^{19}F\{^{1}H\}$ NMR spectrum (376 MHz) of *meso* **9** in CD_2Cl_2.

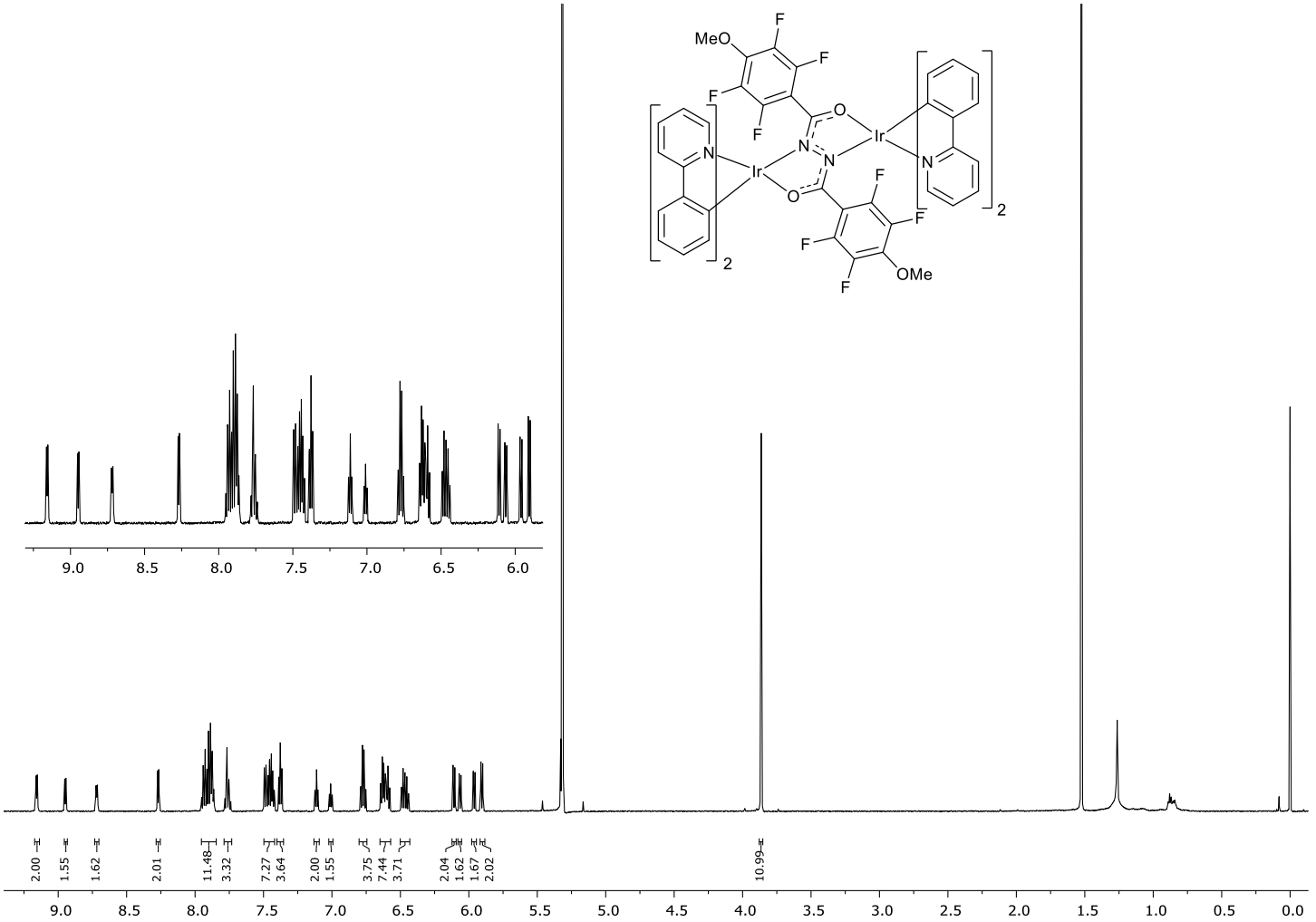

Figure S16. ^{1}H NMR spectrum (600 MHz) of **10** in CD_2Cl_2 (TMS).

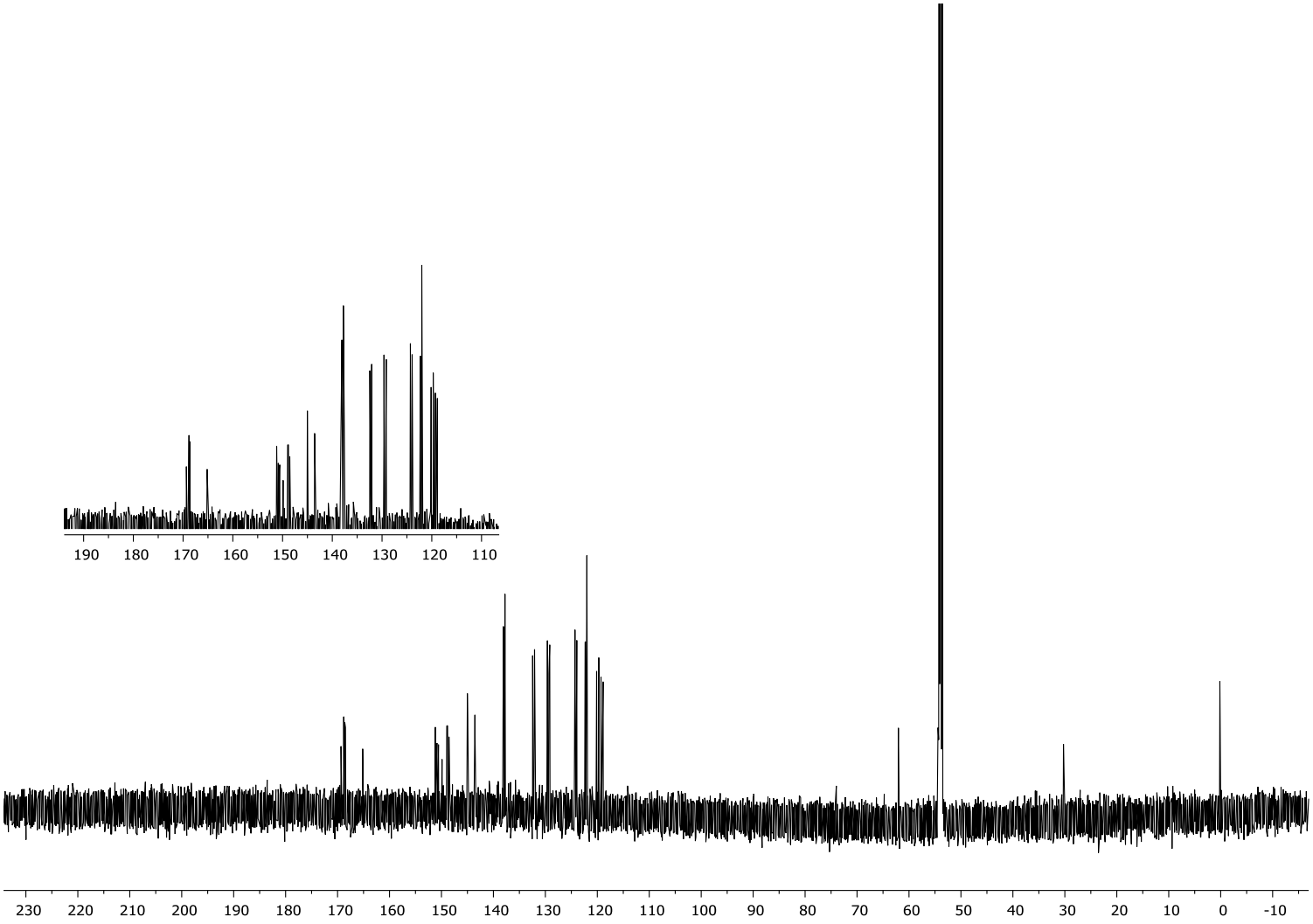

Figure S17. ^{13}C NMR spectrum (151 MHz) of **10** in CD_2Cl_2 (TMS).

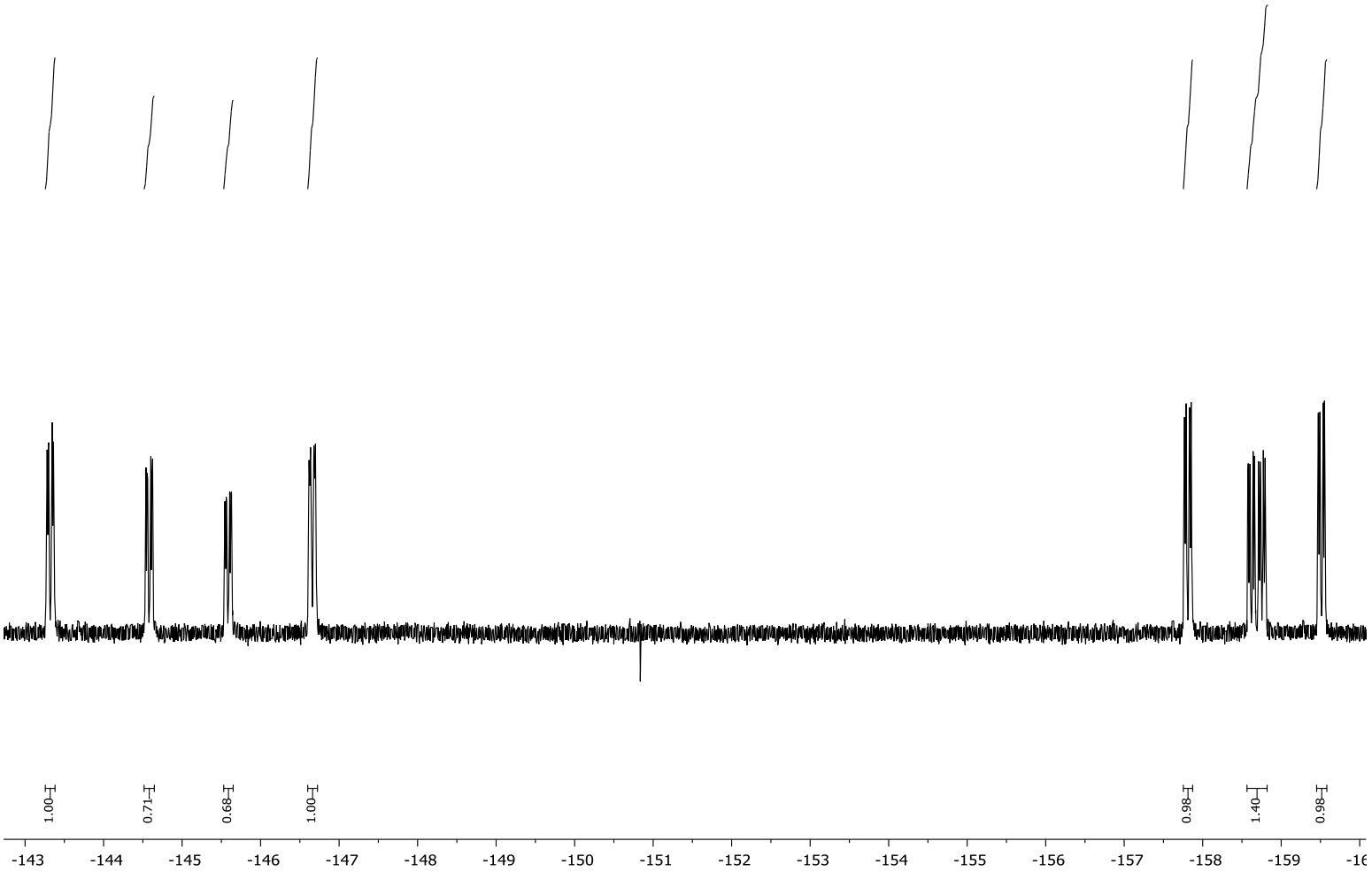

Figure S18. $^{19}F\{^{1}H\}$ NMR spectrum (376 MHz) of **10** in CD_2Cl_2.

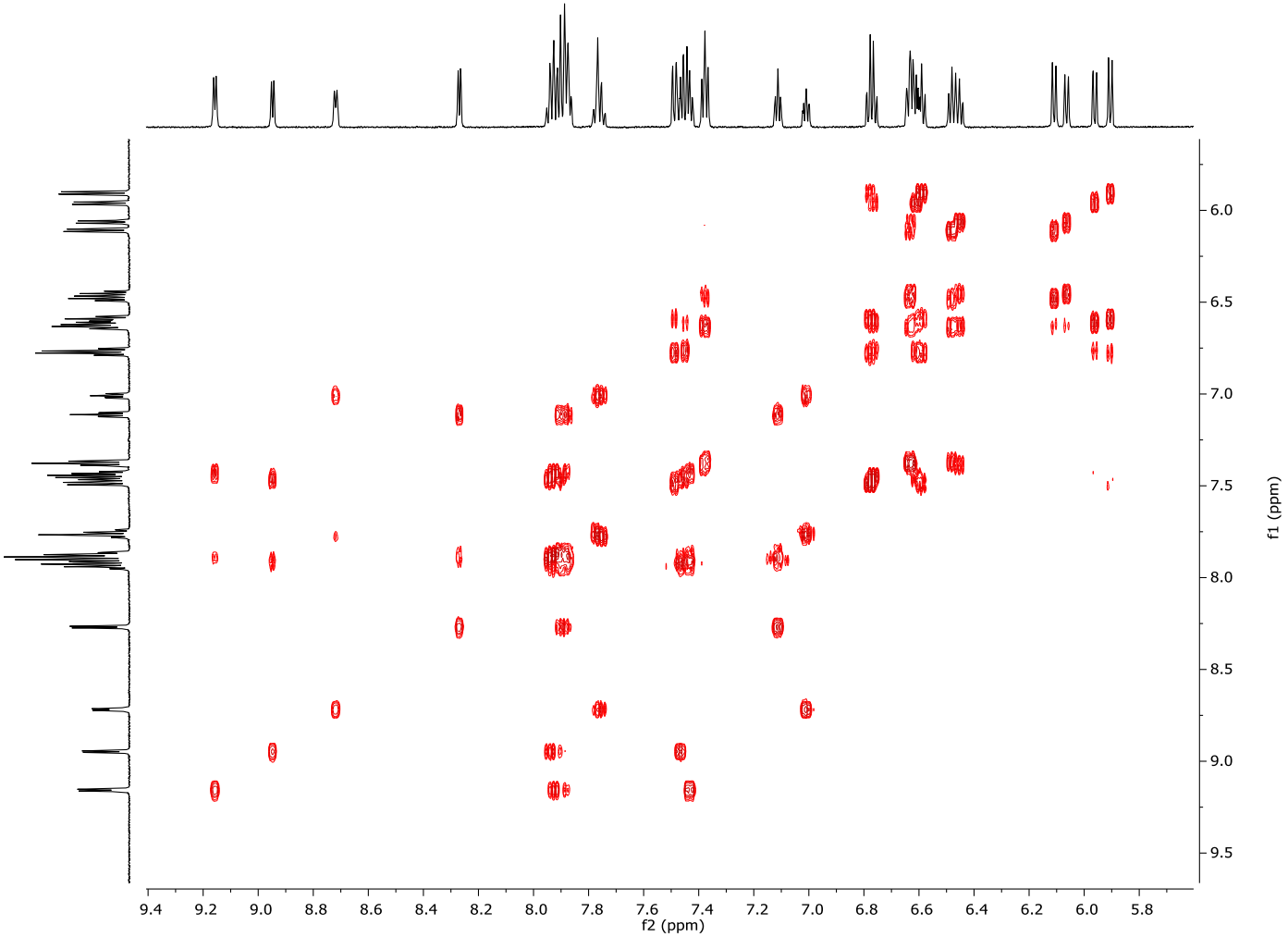

Figure S19. Expansion of the aromatic region of the ^{1}H–^{1}H COSY NMR spectrum of **10** in CD_2Cl_2 (TMS).

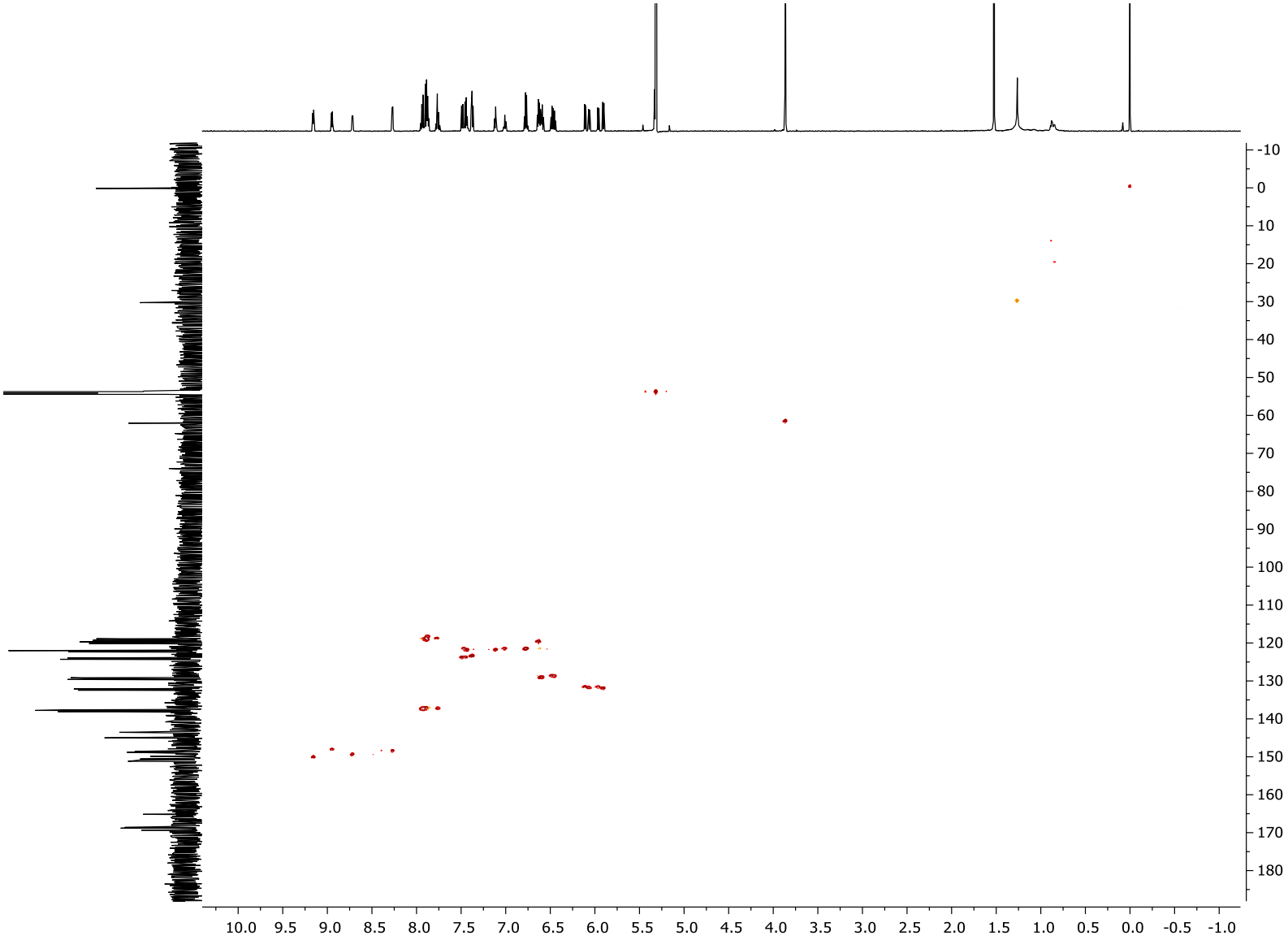

Figure S20. $^{1}H–^{13}C$ HSQC NMR spectrum of **10** in CD_2Cl_2.

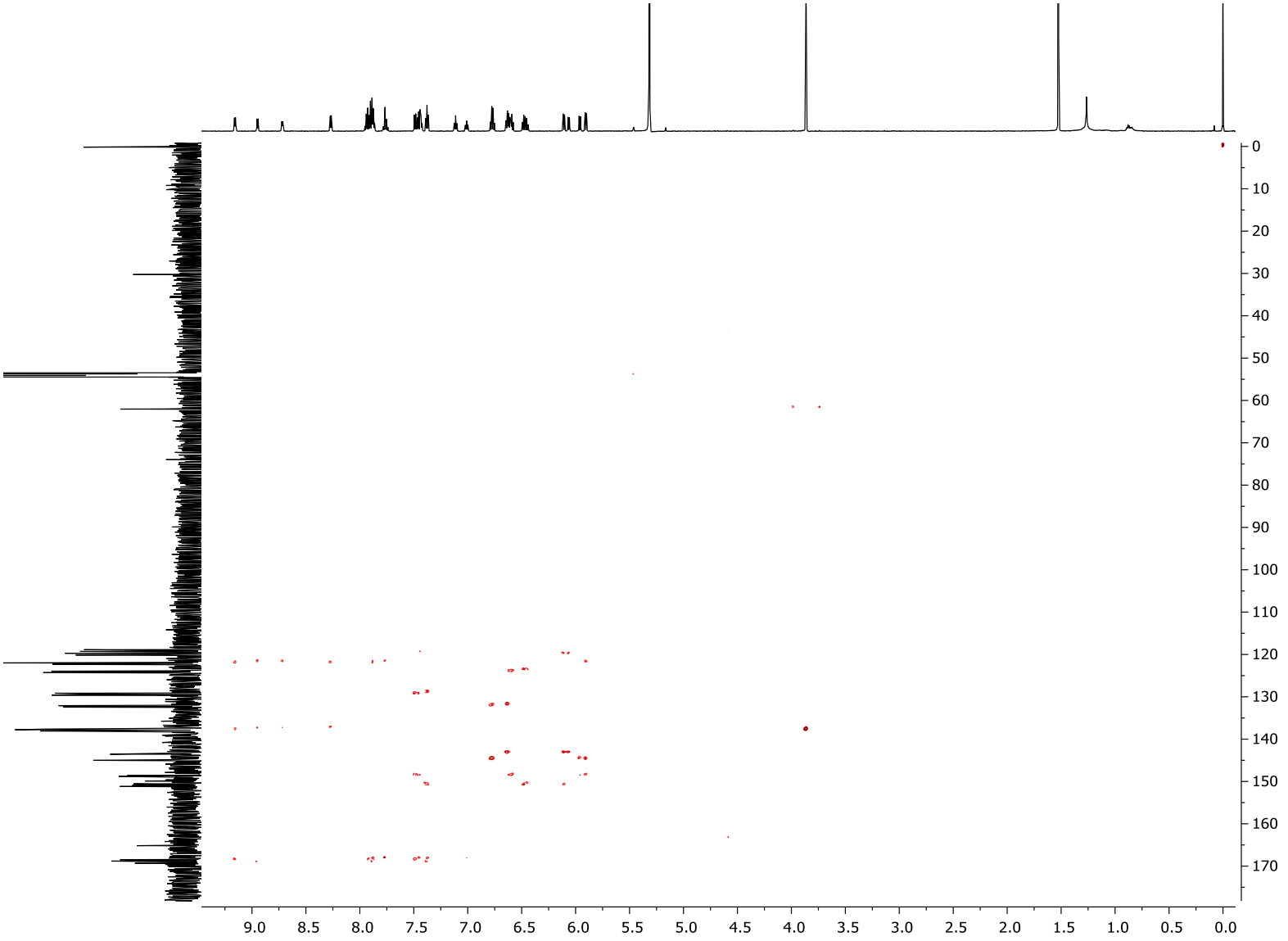

Figure S21. ^{1}H–^{13}C HMBC NMR spectrum of **10** in CD_2Cl_2.

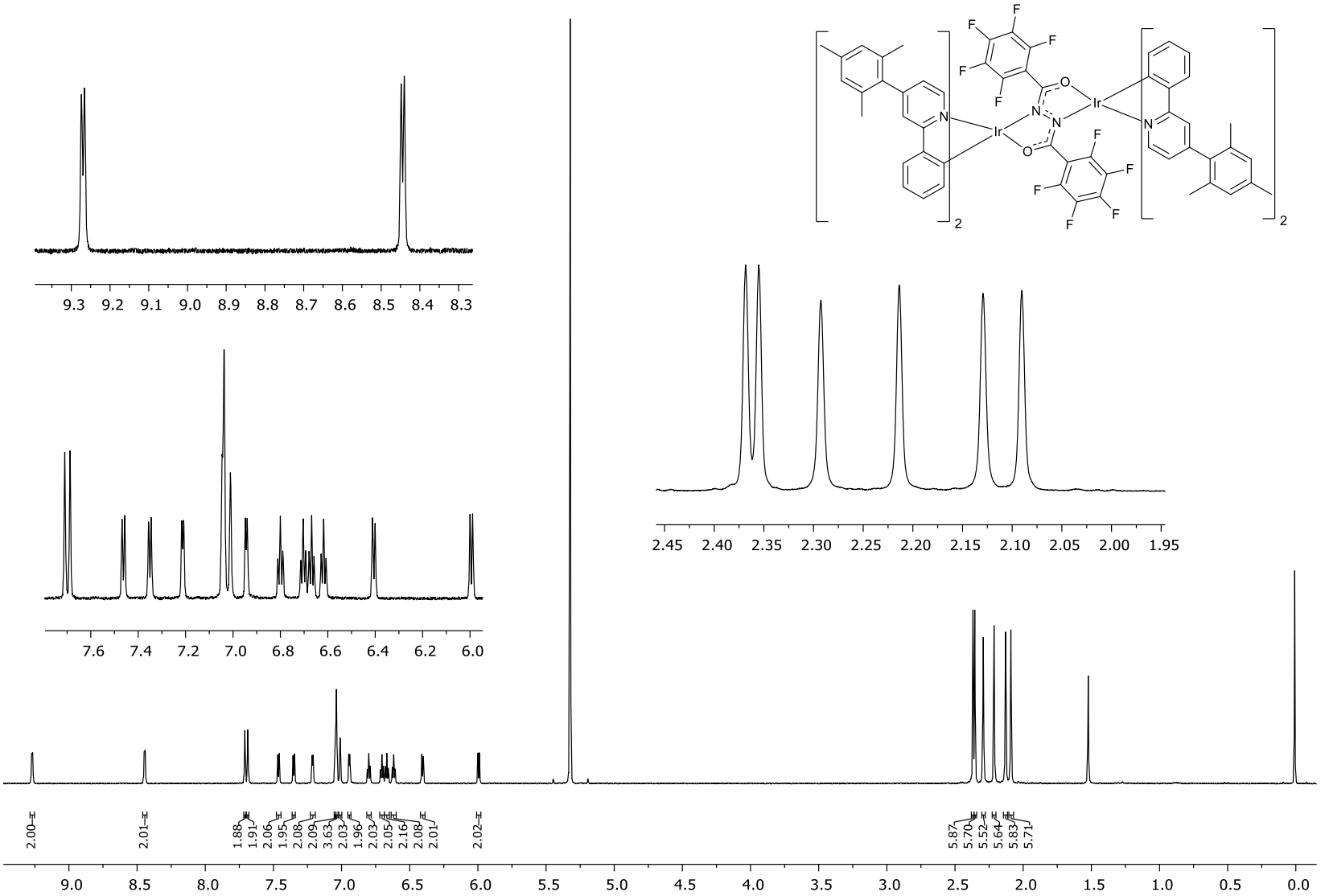

Figure S22. ^{1}H NMR spectrum (700 MHz) of *rac* **11** in CD_2Cl_2 (TMS).

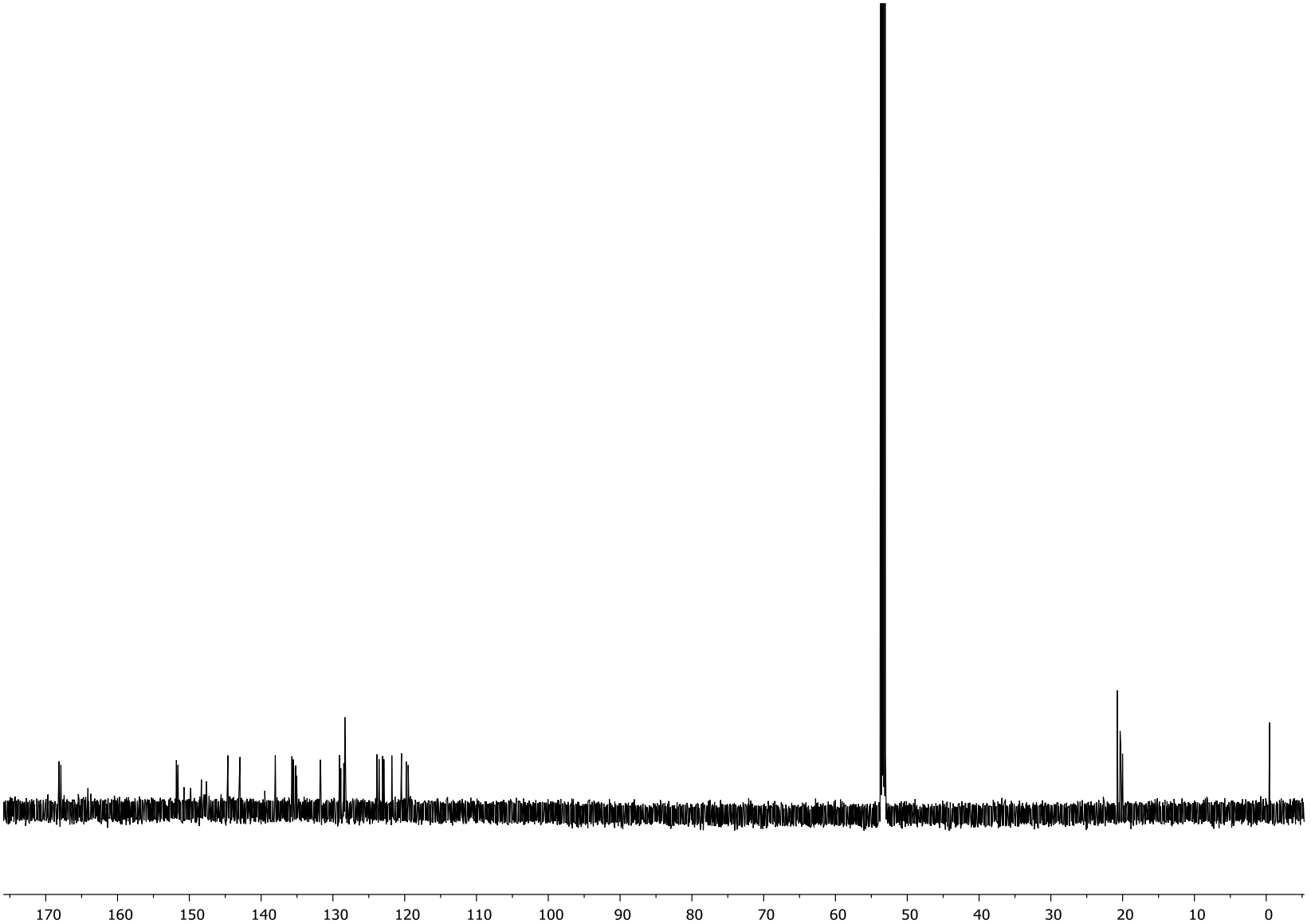

Figure S23. ^{13}C NMR spectrum (151 MHz) of *rac* **11** in CD_2Cl_2 (TMS).

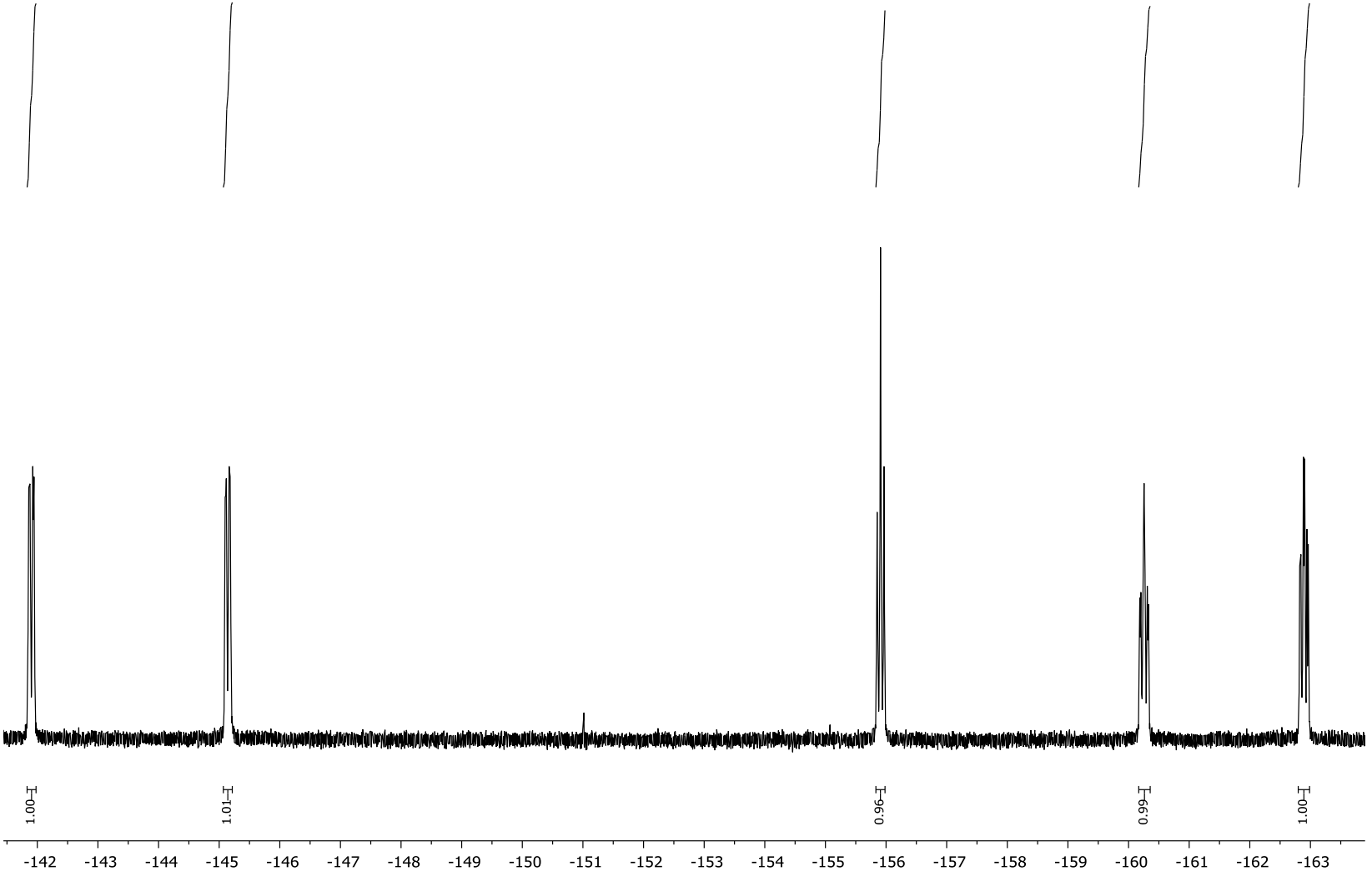

Figure S24. $^{19}F\{^{1}H\}$ NMR spectrum (376 MHz) of *rac* **11** in CD_2Cl_2

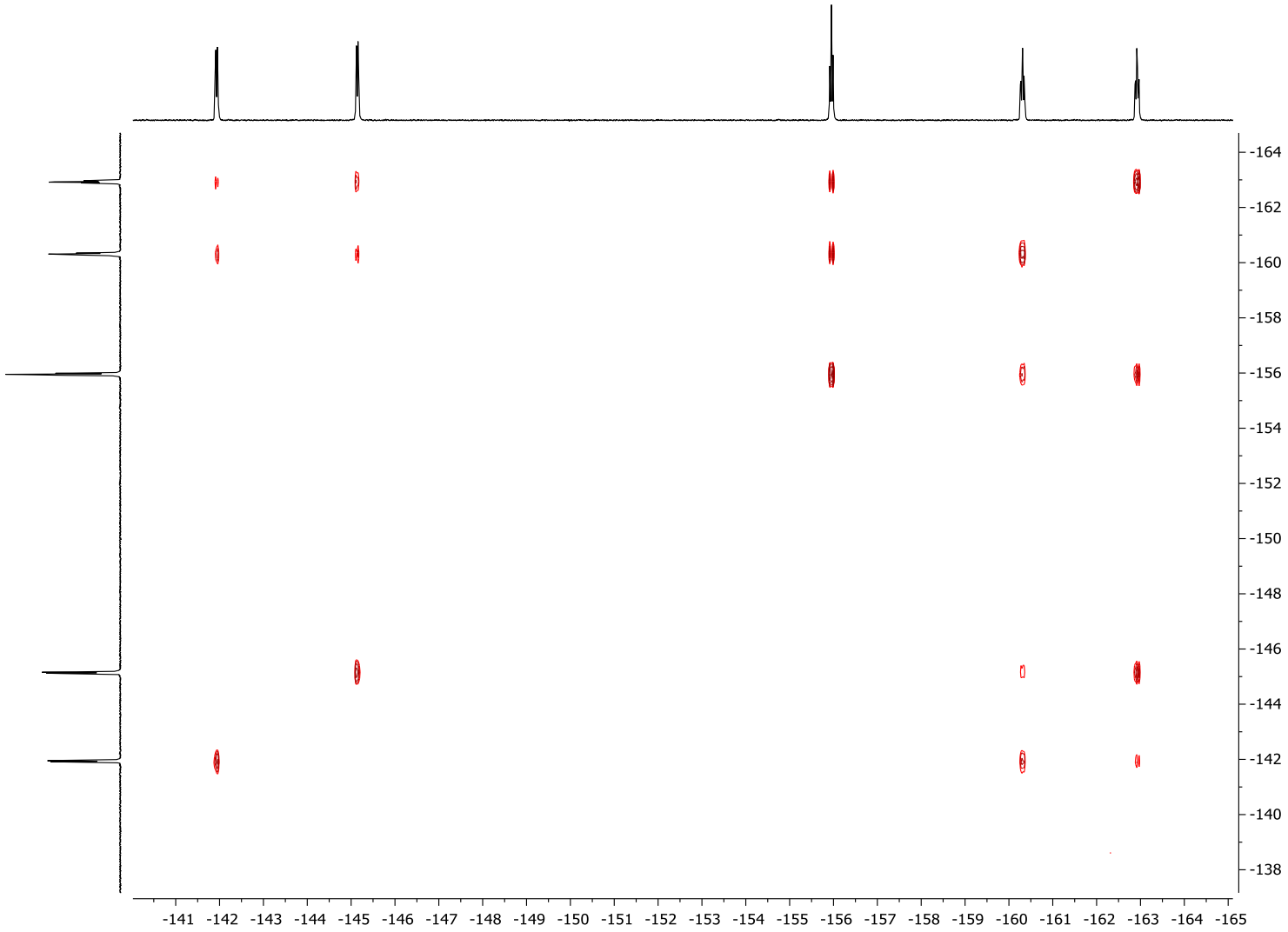

Figure S25. ^{19}F–^{19}F COSY NMR spectrum of *rac* **11** in CD_2Cl_2.

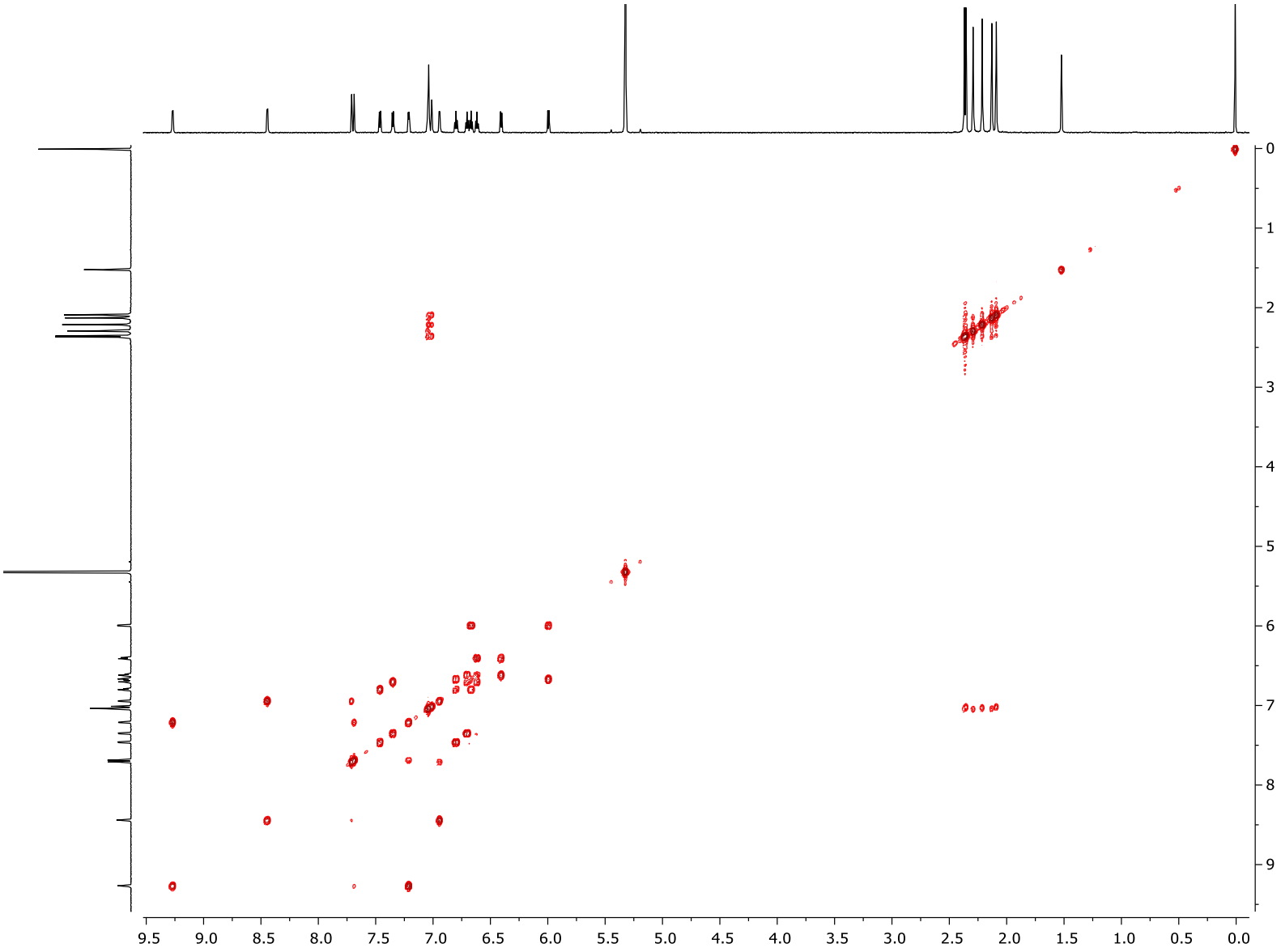

Figure S26. ^{1}H–^{1}H COSY NMR spectrum of *rac* **11** in CD_2Cl_2 (TMS).

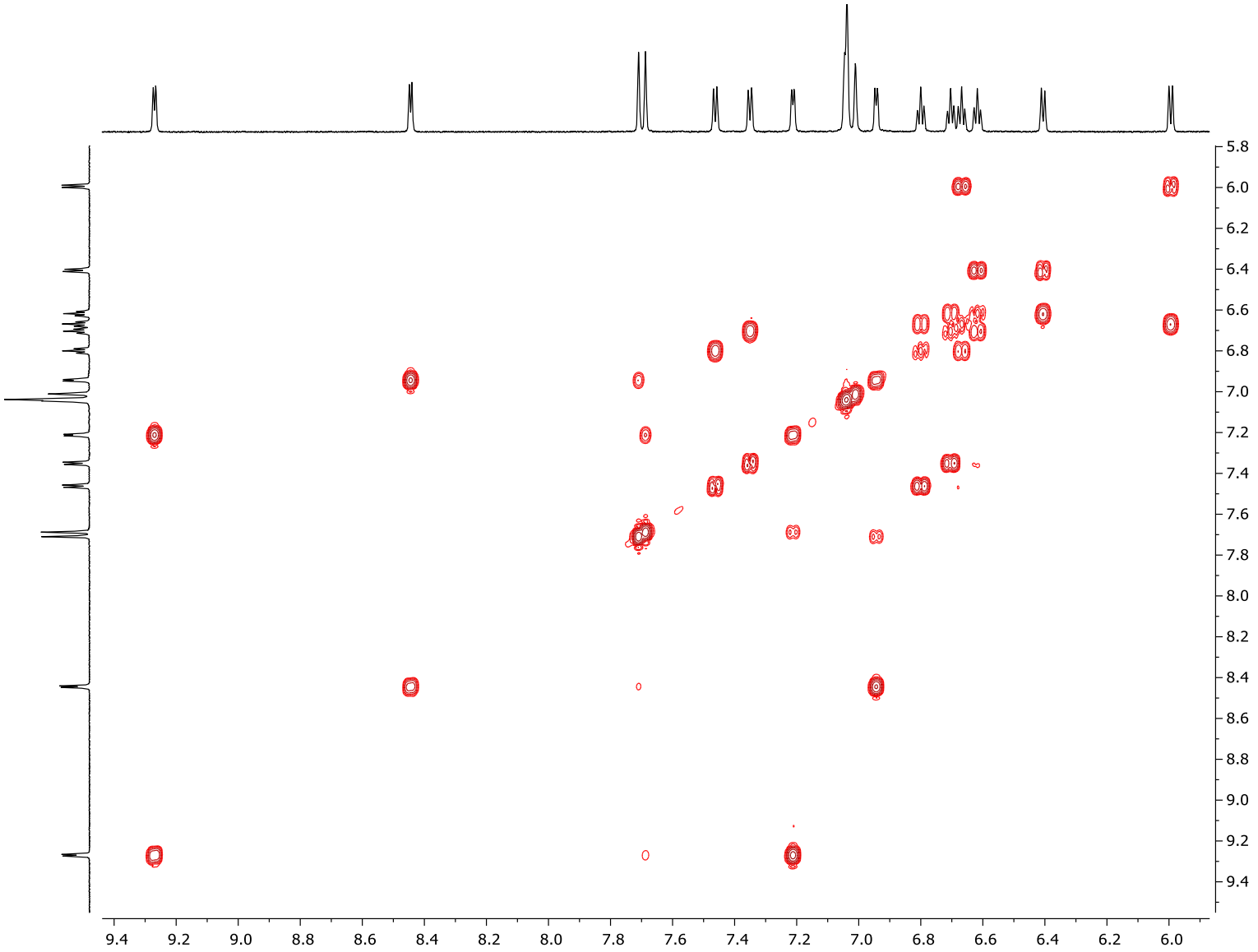

Figure S27. Expansion of the aromatic region of the ^{1}H–^{1}H COSY NMR spectrum of *rac* **11** in CD_2Cl_2 (TMS).

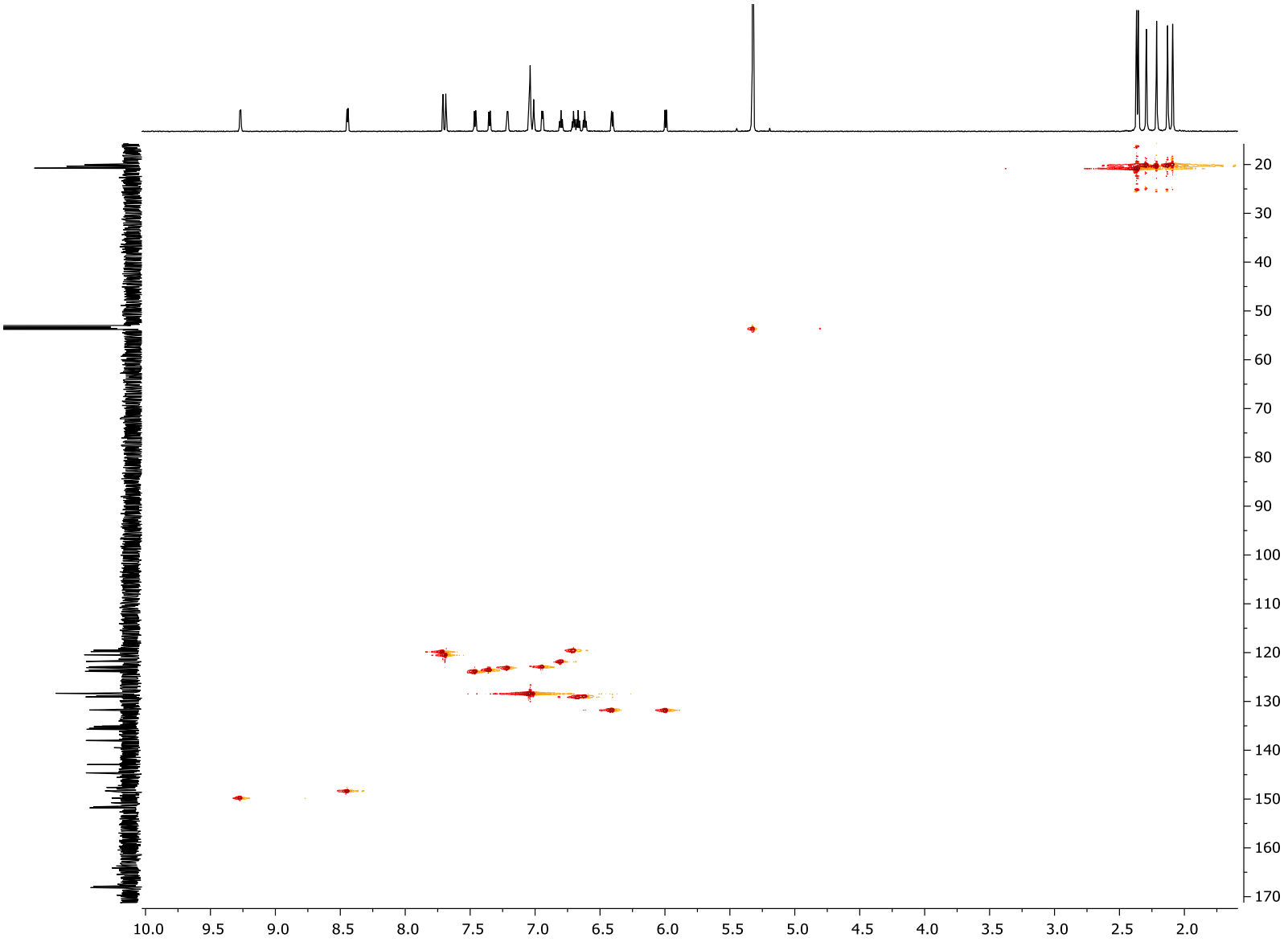

Figure S28. $^{1}H–^{13}C$ HSQC NMR spectrum of *rac* **11** in CD_2Cl_2 (TMS).

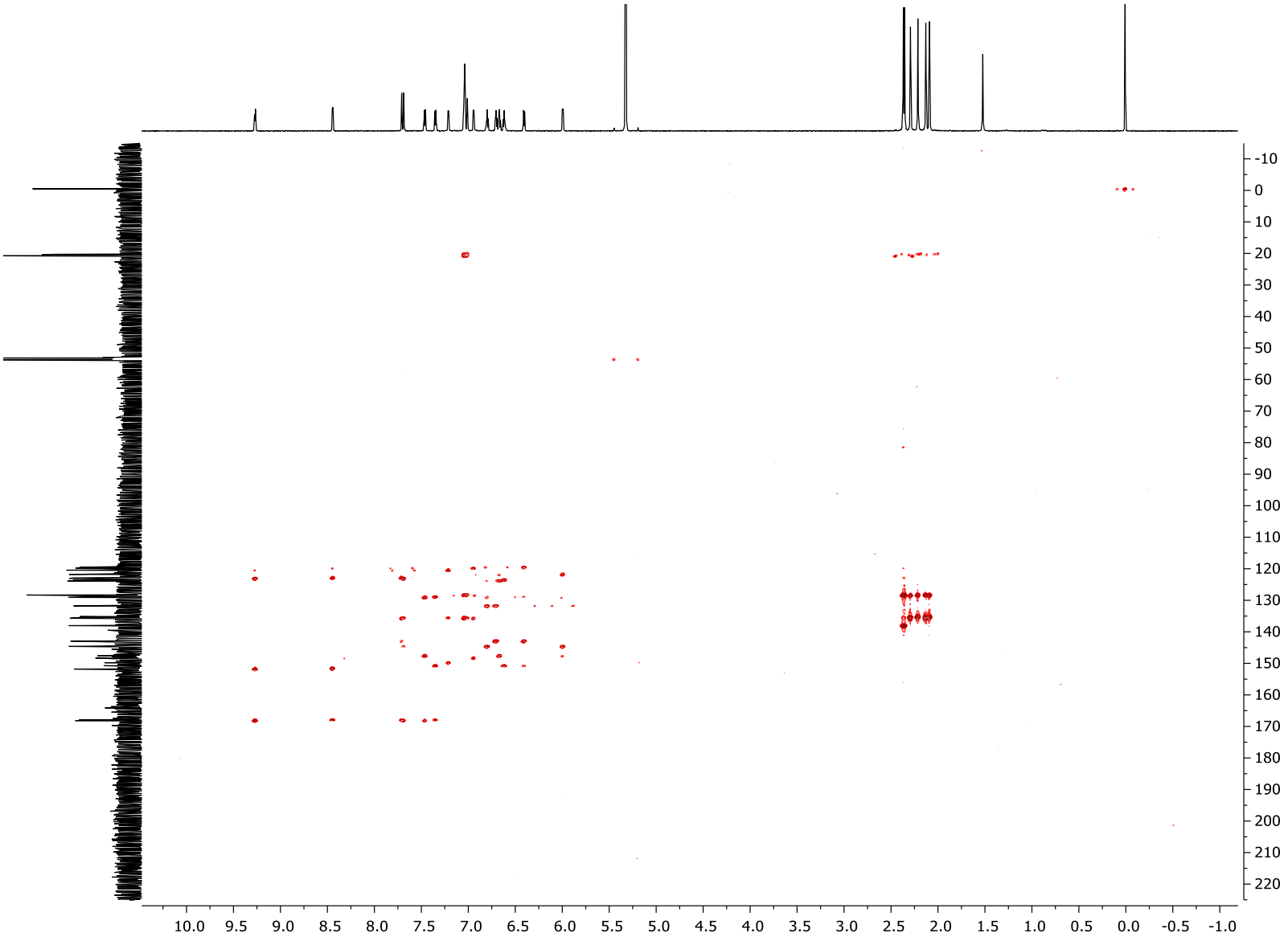

Figure S29. $^{1}H–^{13}C$ HMBC NMR spectrum of *rac* **11** in CD_2Cl_2 (TMS).

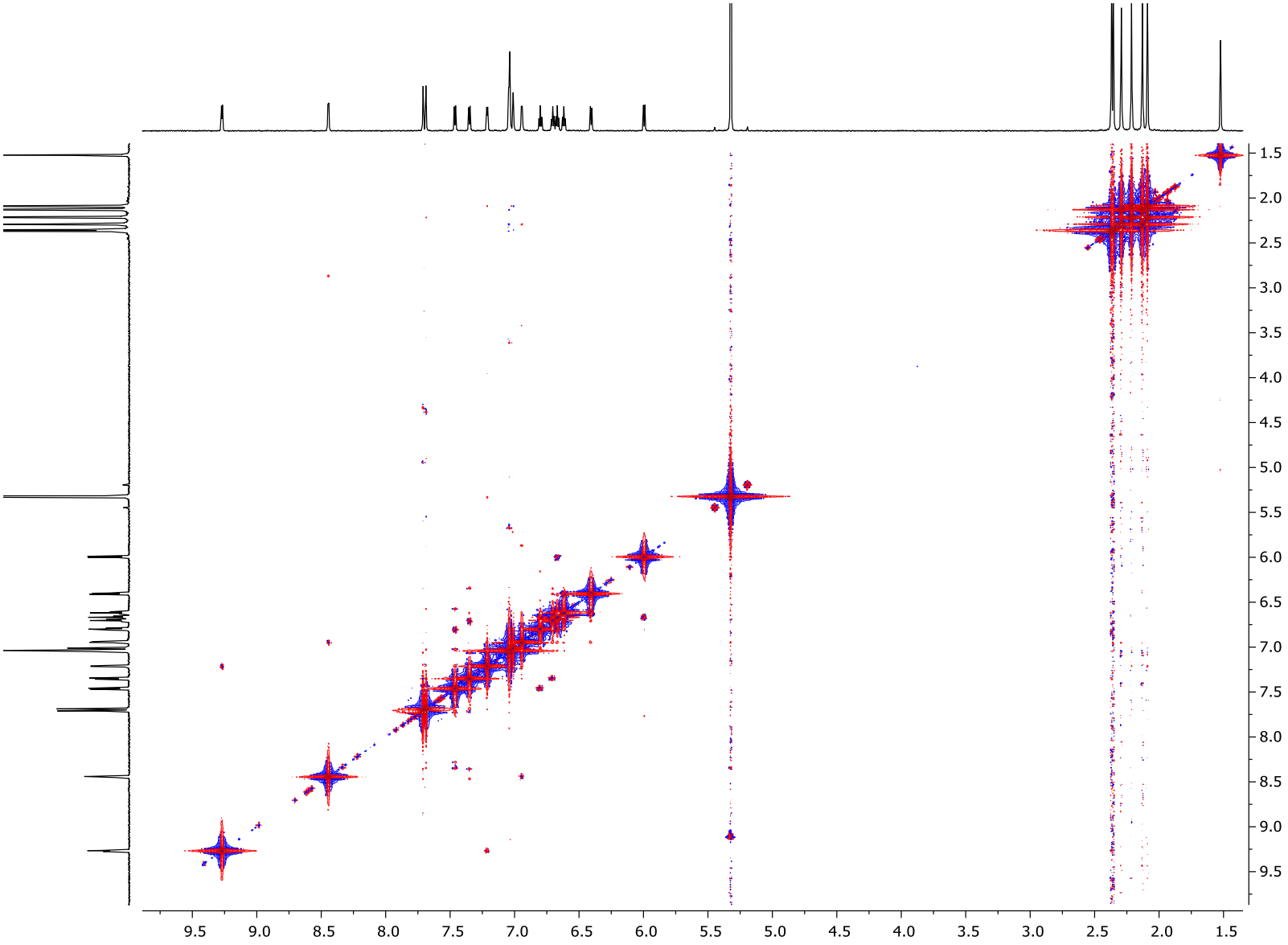

Figure S30. ^{1}H–^{1}H NOESY NMR spectrum of *rac* **11** in CD_2Cl_2 (TMS).

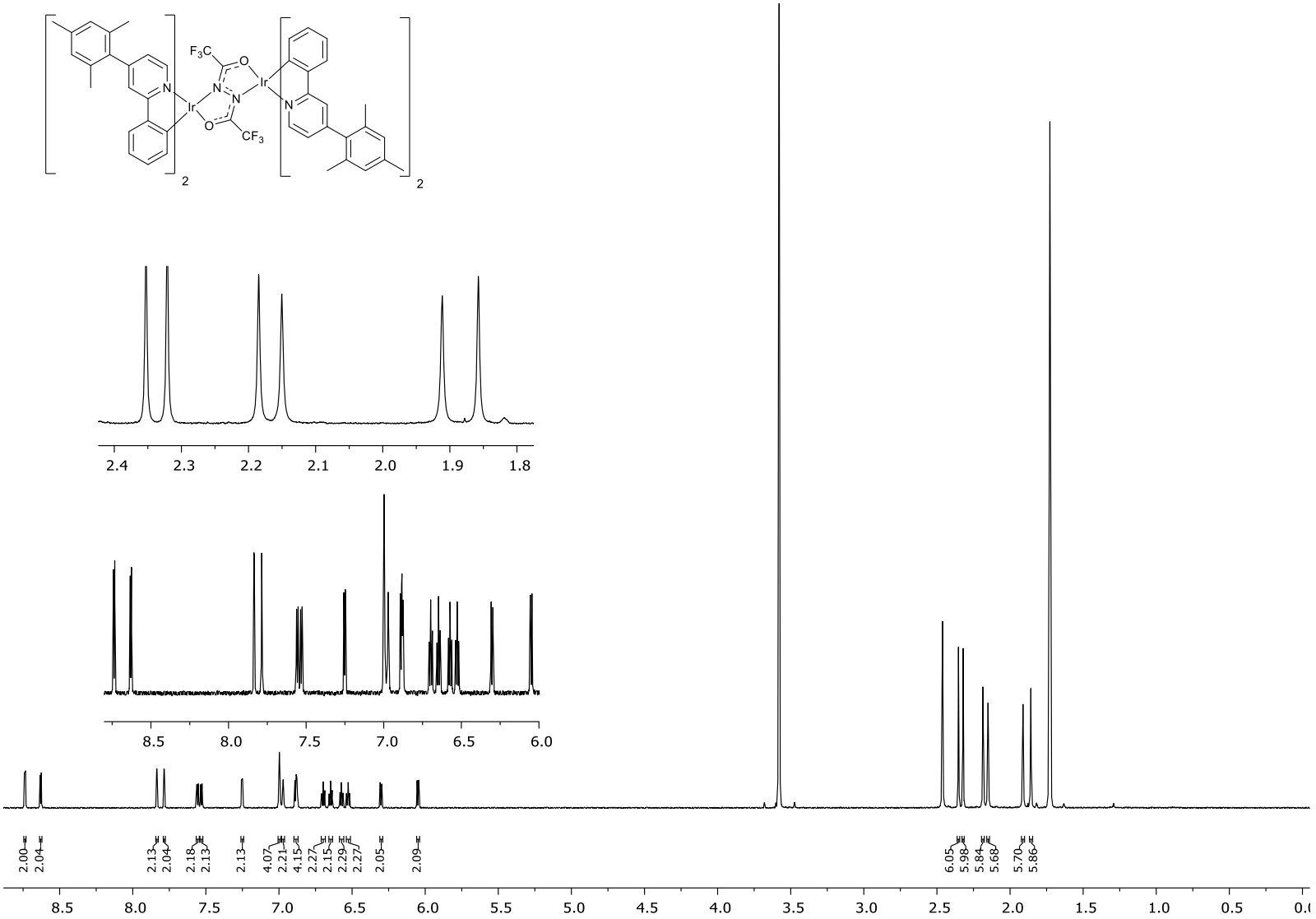

Figure S31. ^{1}H NMR spectrum (700 MHz) of *meso* **12** in THF-d_8.

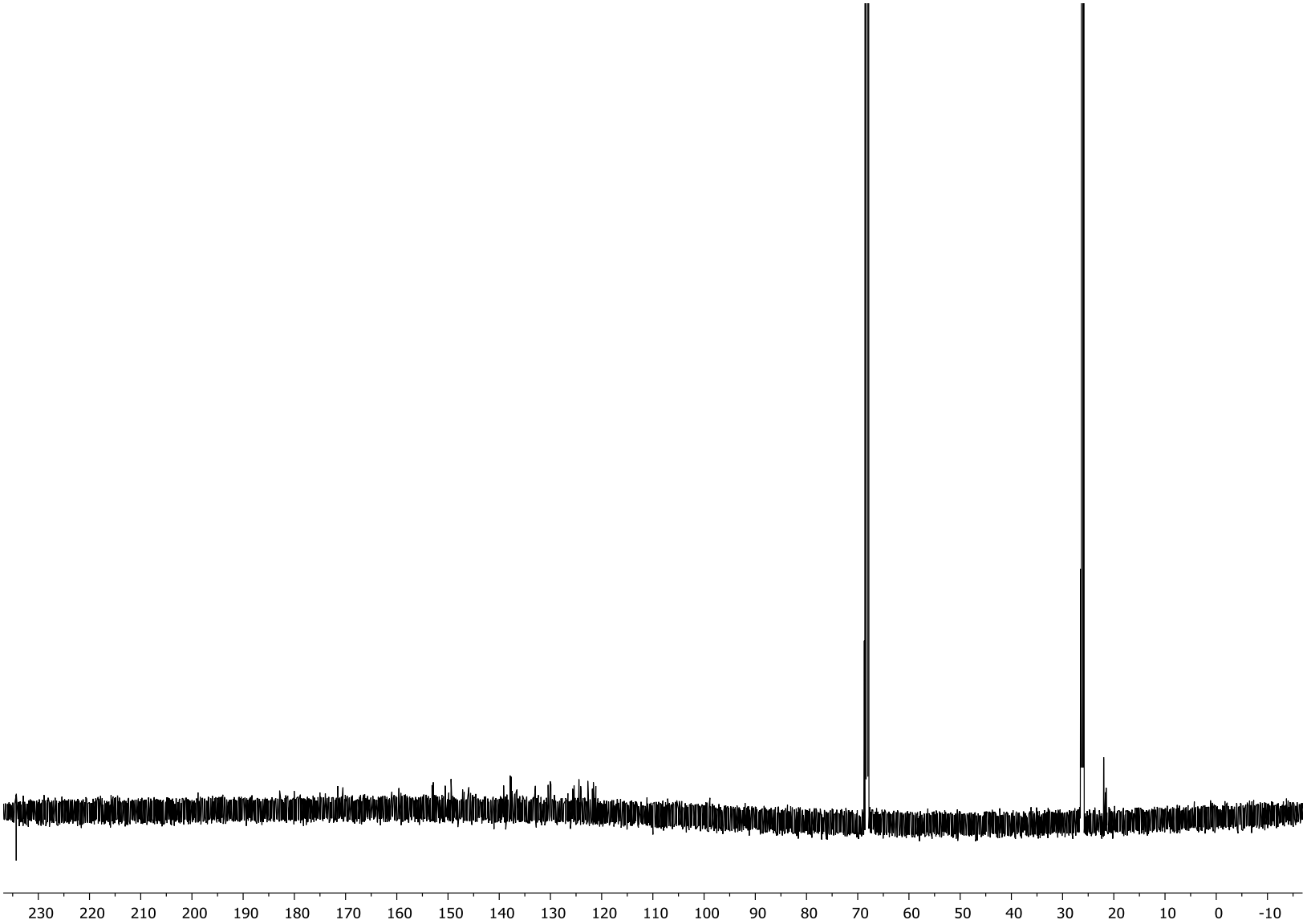

Figure S32. ^{13}C NMR spectrum (151 MHz) of *meso* **12** in THF-d_8.

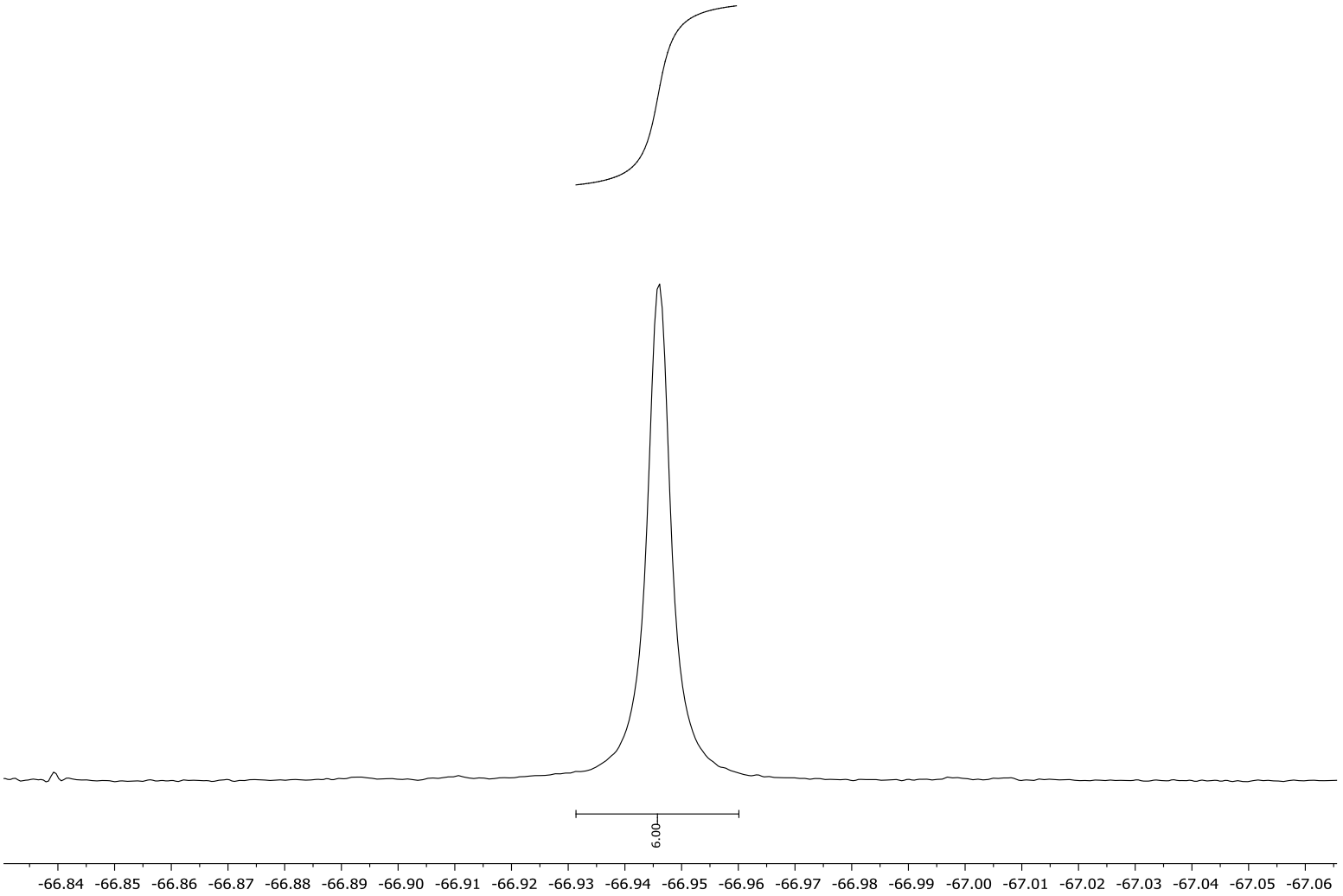

Figure S33. $^{19}F\{^{1}H\}$ NMR spectrum (376 MHz) of *meso* **12** in THF-d_8.

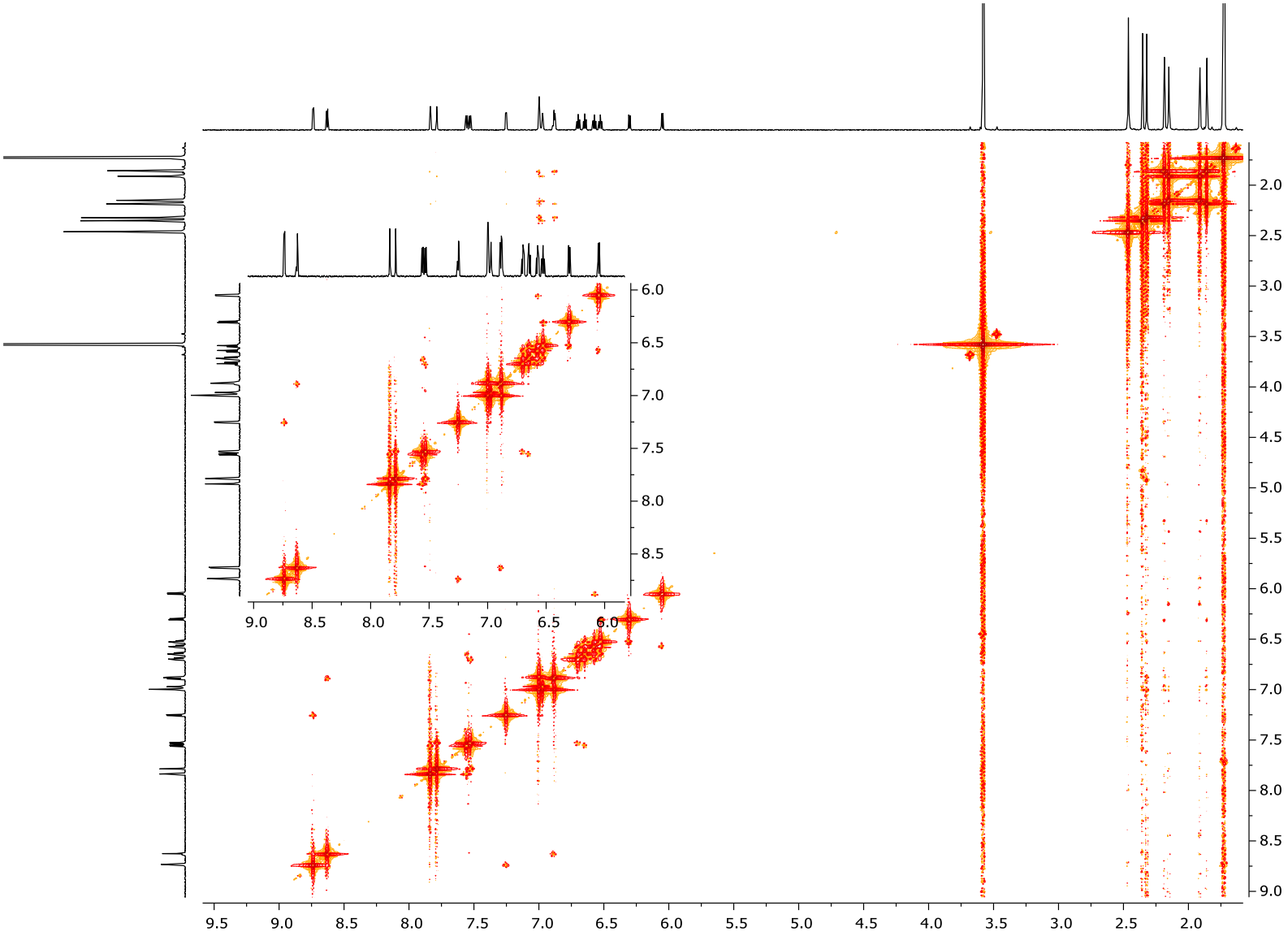

Figure S34. ^{1}H–^{1}H COSY NMR spectrum of *meso* **12** in THF-d_8.

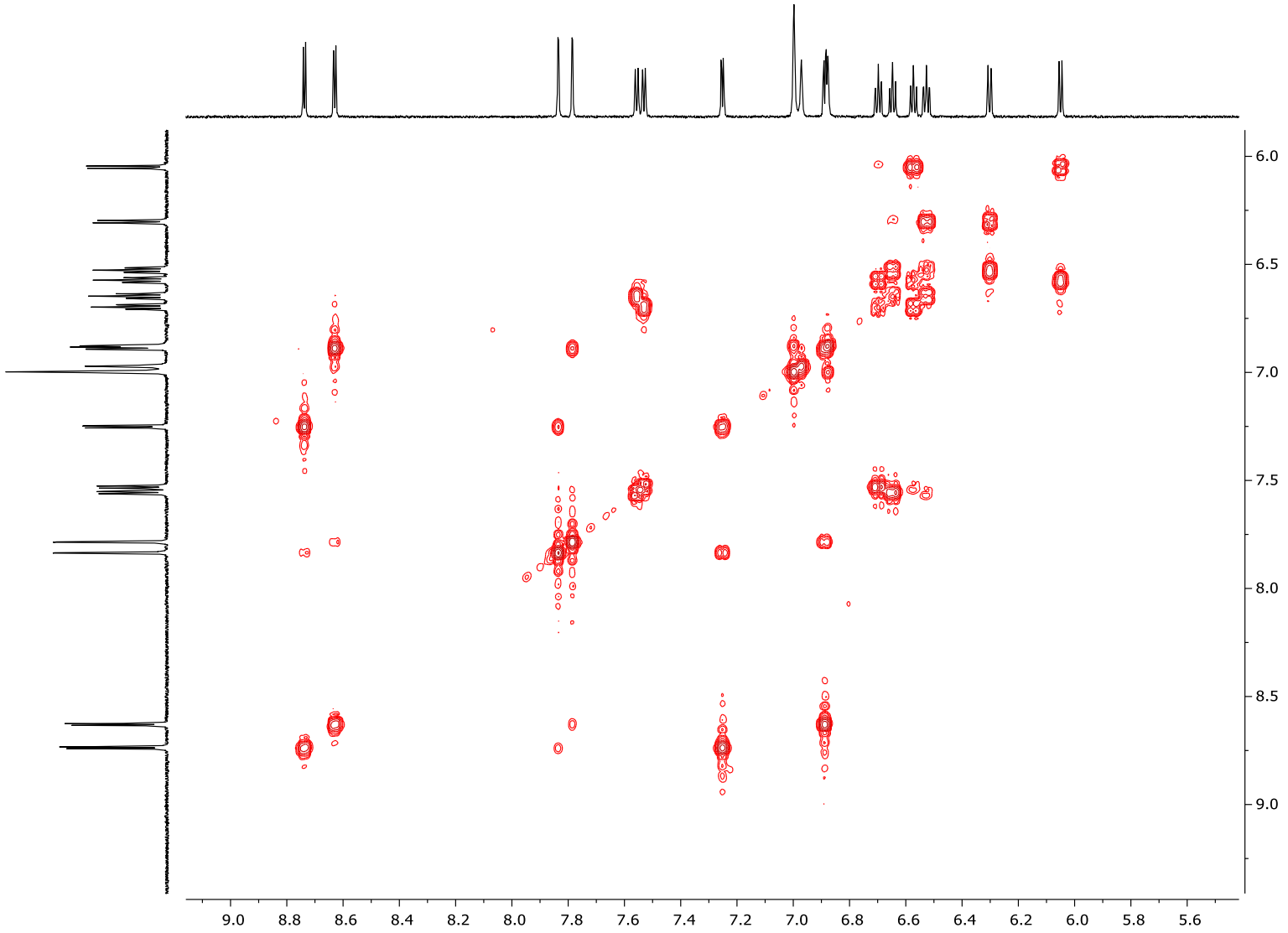

Figure S35. Expansion of the aromatic region of the ^{1}H–^{1}H COSY NMR spectrum of *meso* **12** in THF-d_8.

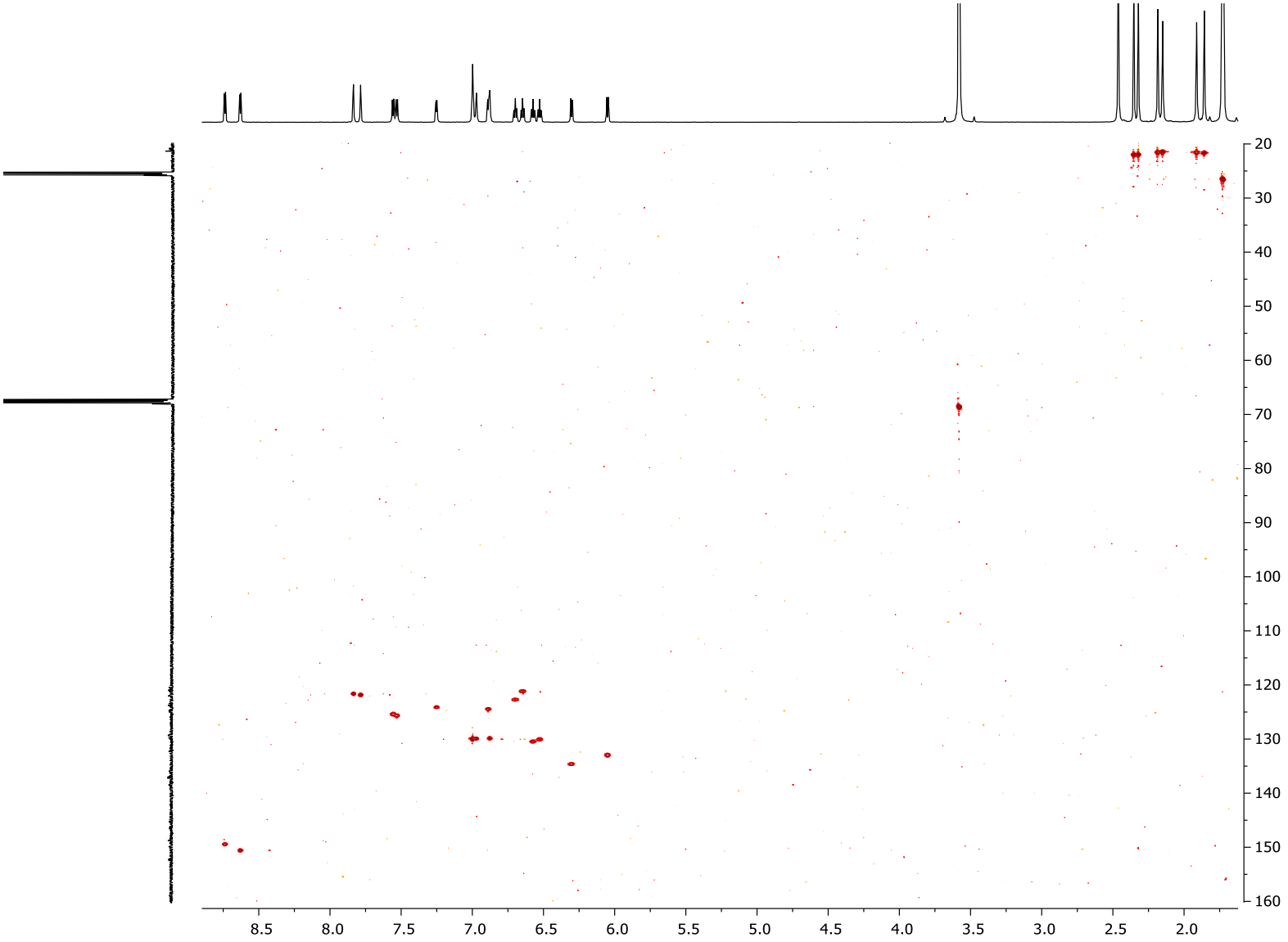

Figure S36. $^{1}H–^{13}C$ HSQC NMR spectrum of *meso* **12** in THF-d_8.

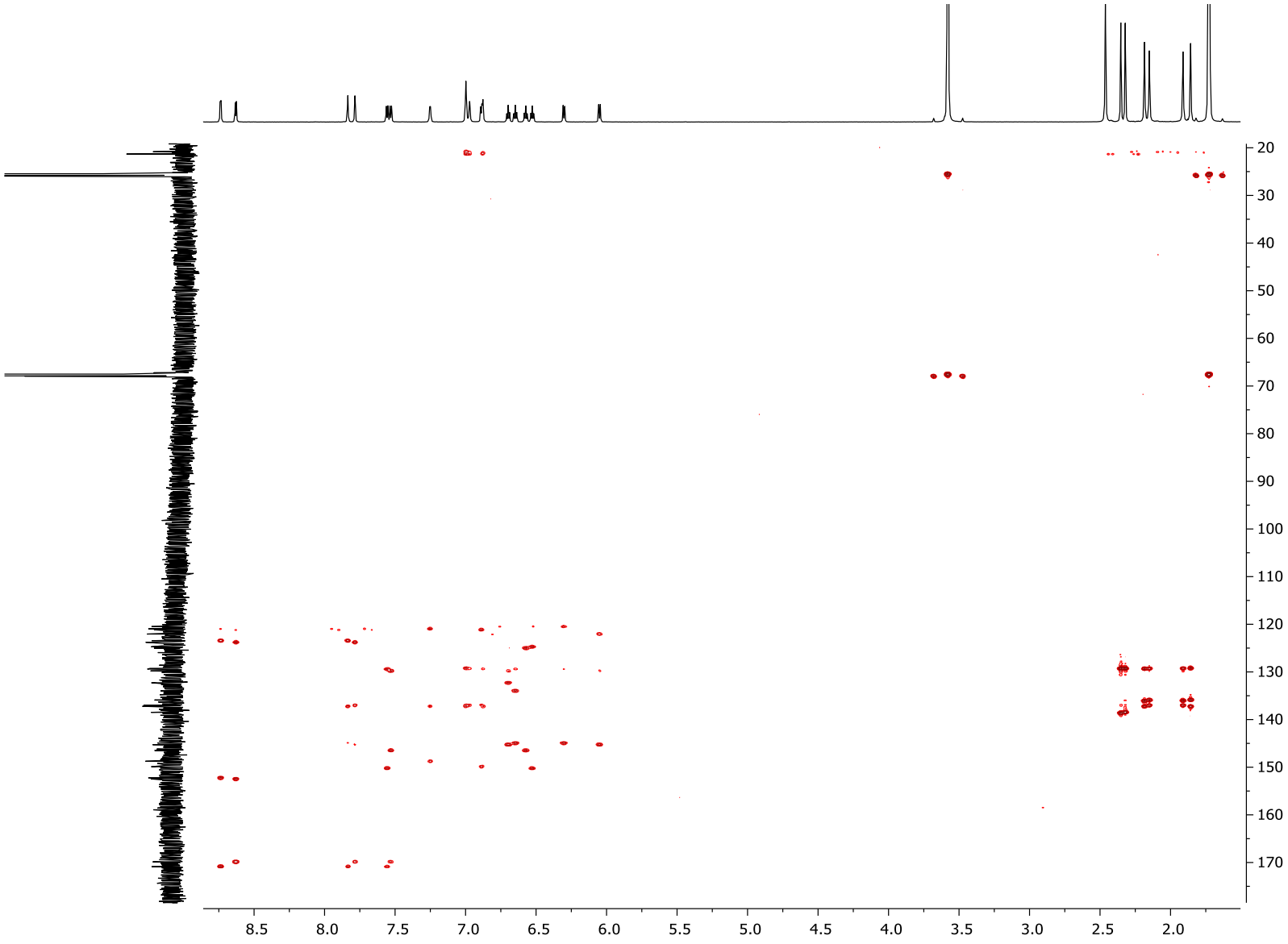

Figure S37. $^{1}H–^{13}C$ HMBC NMR spectrum of *meso* **12** in THF-d_8.

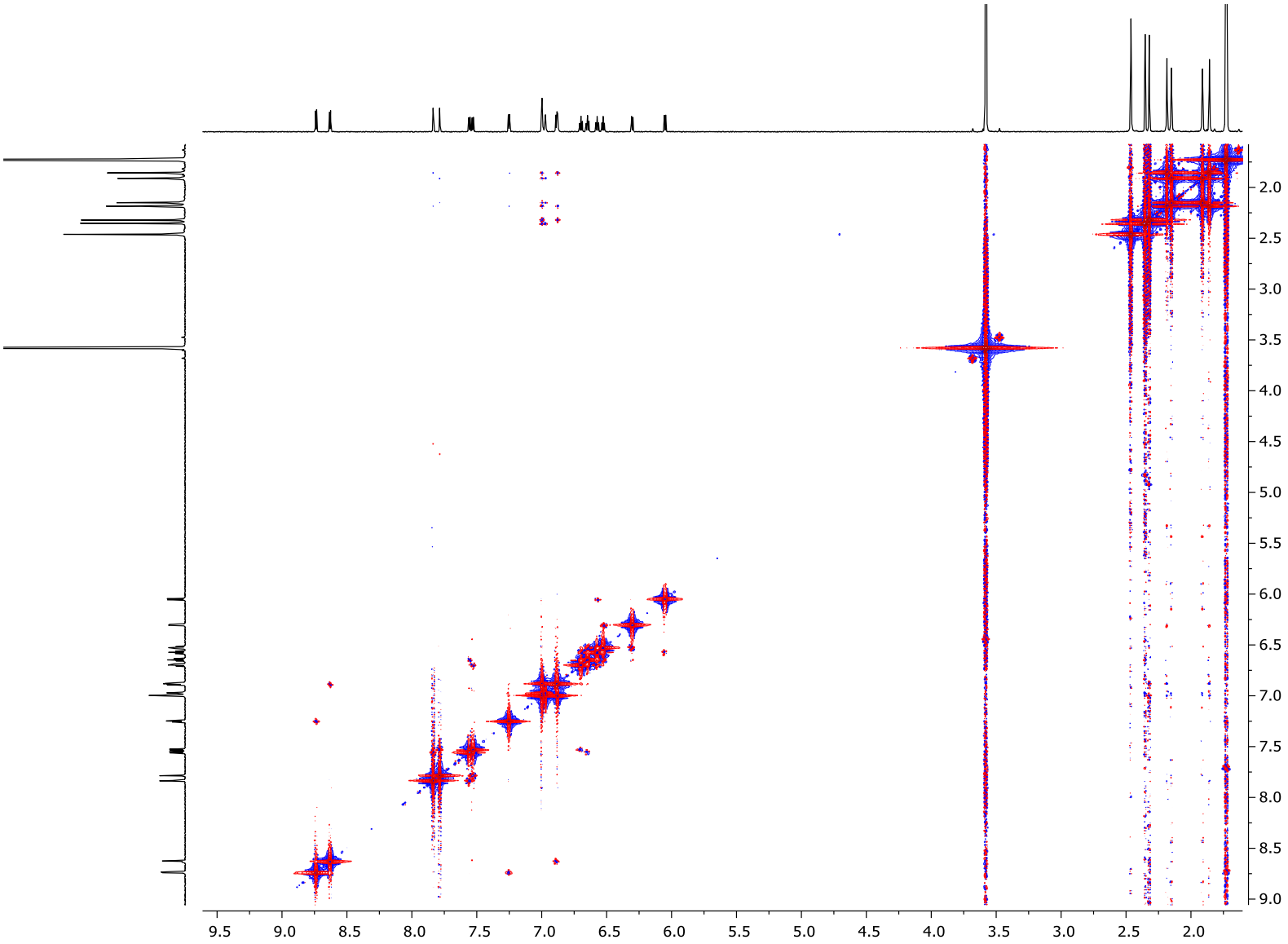

Figure S38. ^{1}H–^{1}H NOESY NMR spectrum of *meso* **12** in THF-d_8.

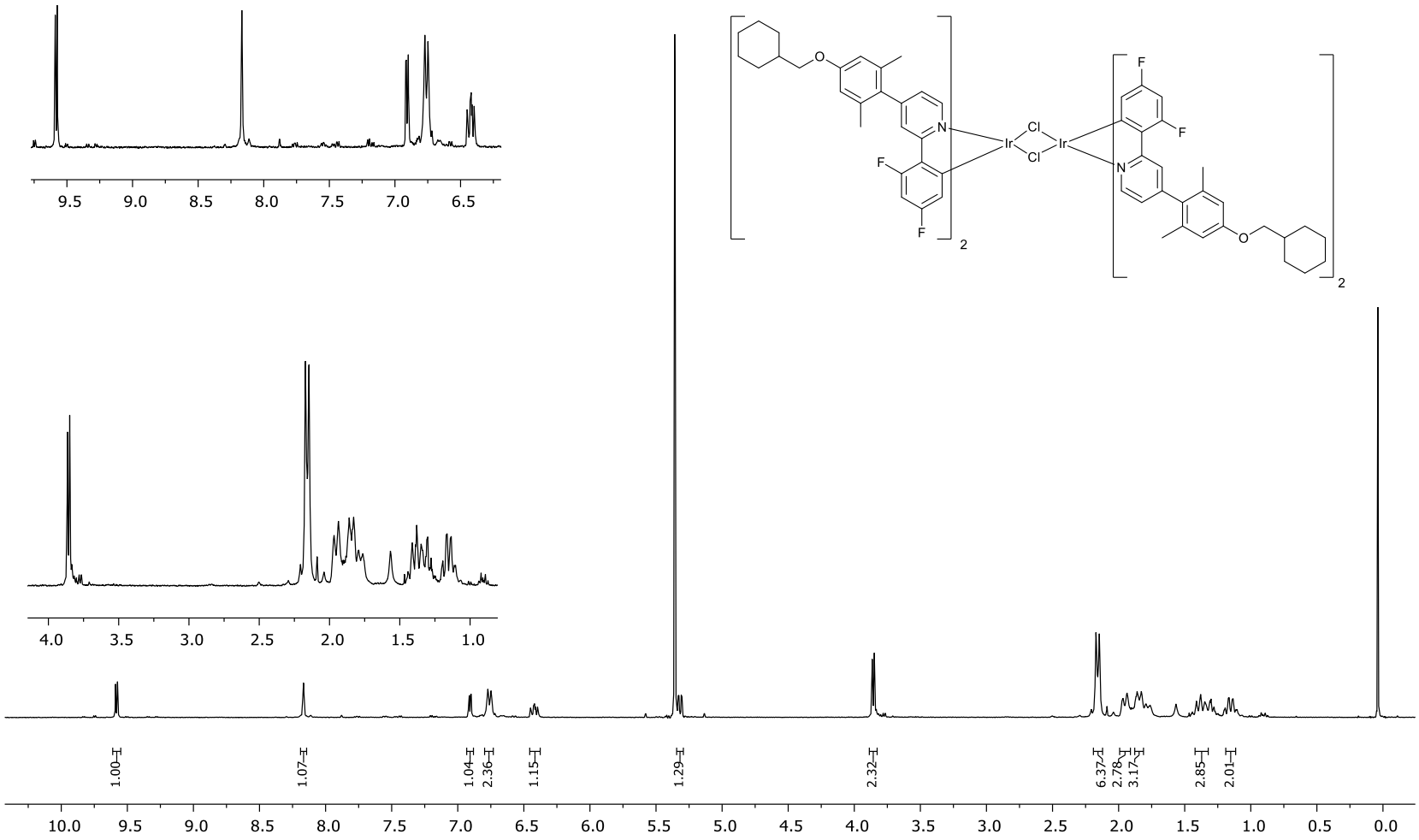

Figure S39. ^{1}H NMR spectrum (400 MHz) of the μ–dichloro dimer isolated as an intermediate in the synthesis of complex **13** in CD_2Cl_2 (TMS).

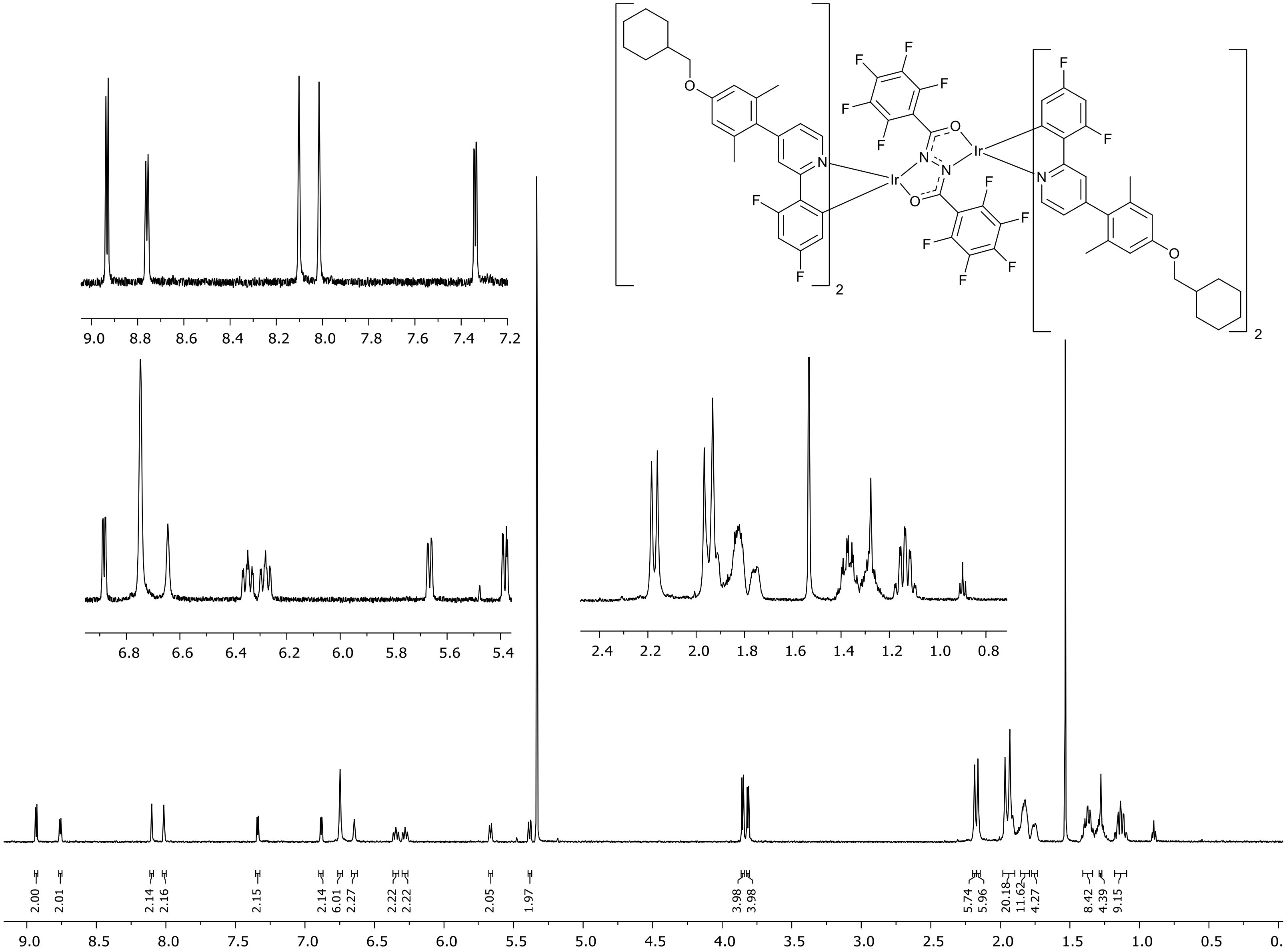

Figure S40. ^{1}H NMR spectrum (600 MHz) of *meso* **13** in CD_2Cl_2.

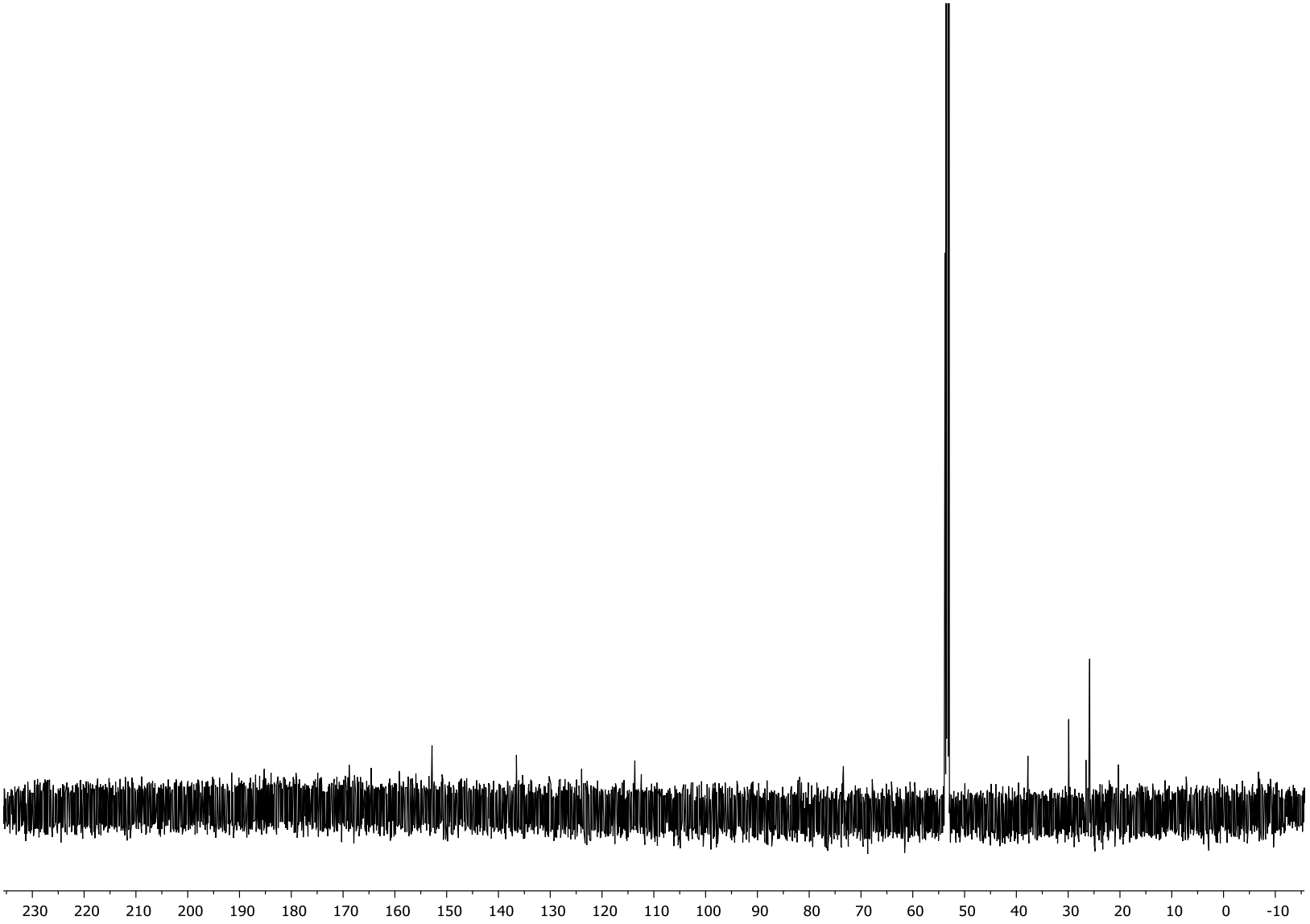

Figure S41. ^{13}C NMR spectrum (151 MHz) of *meso* **13** in CD_2Cl_2.

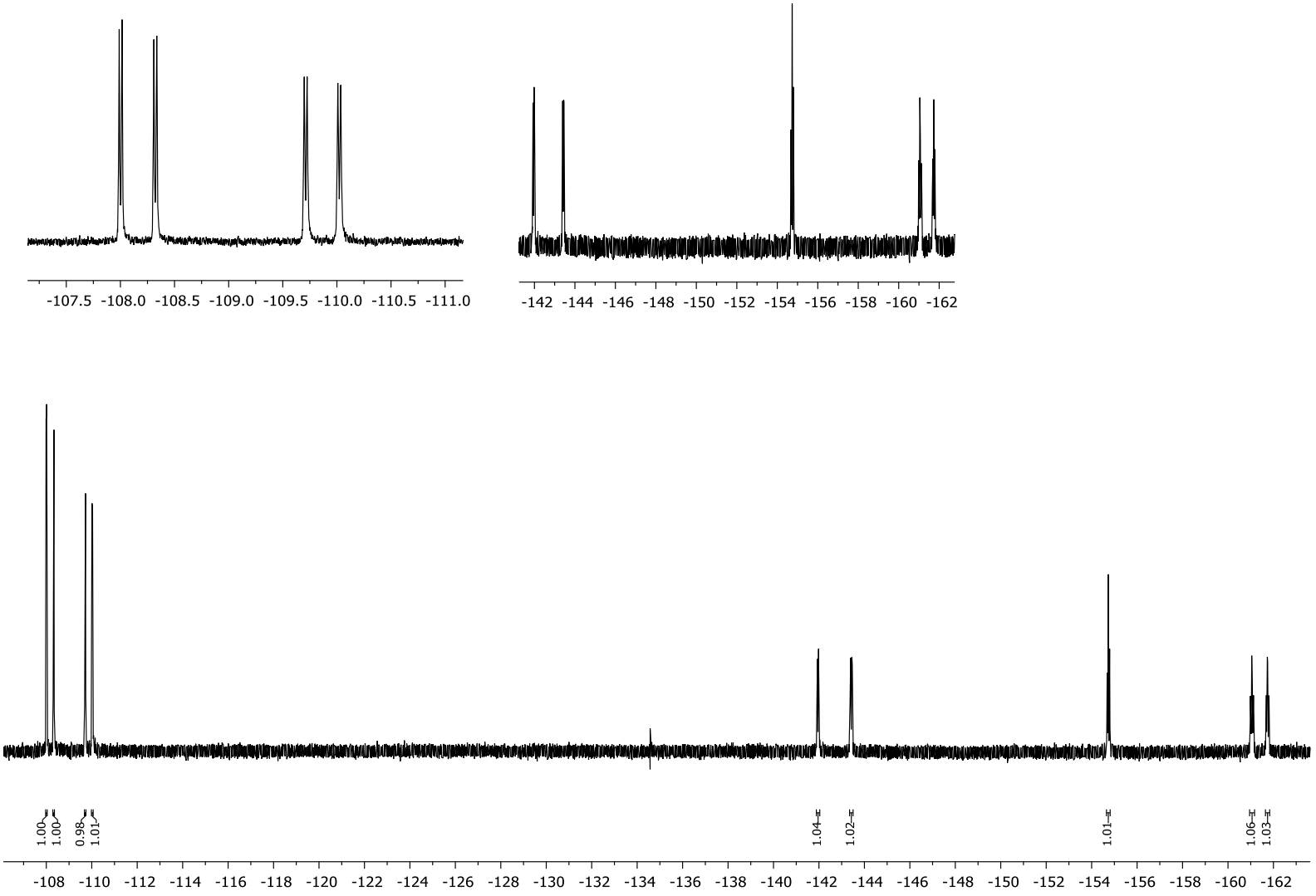

Figure S42. $^{19}F\{^{1}H\}$ NMR spectrum (376 MHz) of *meso* **13** in CD_2Cl_2**.**

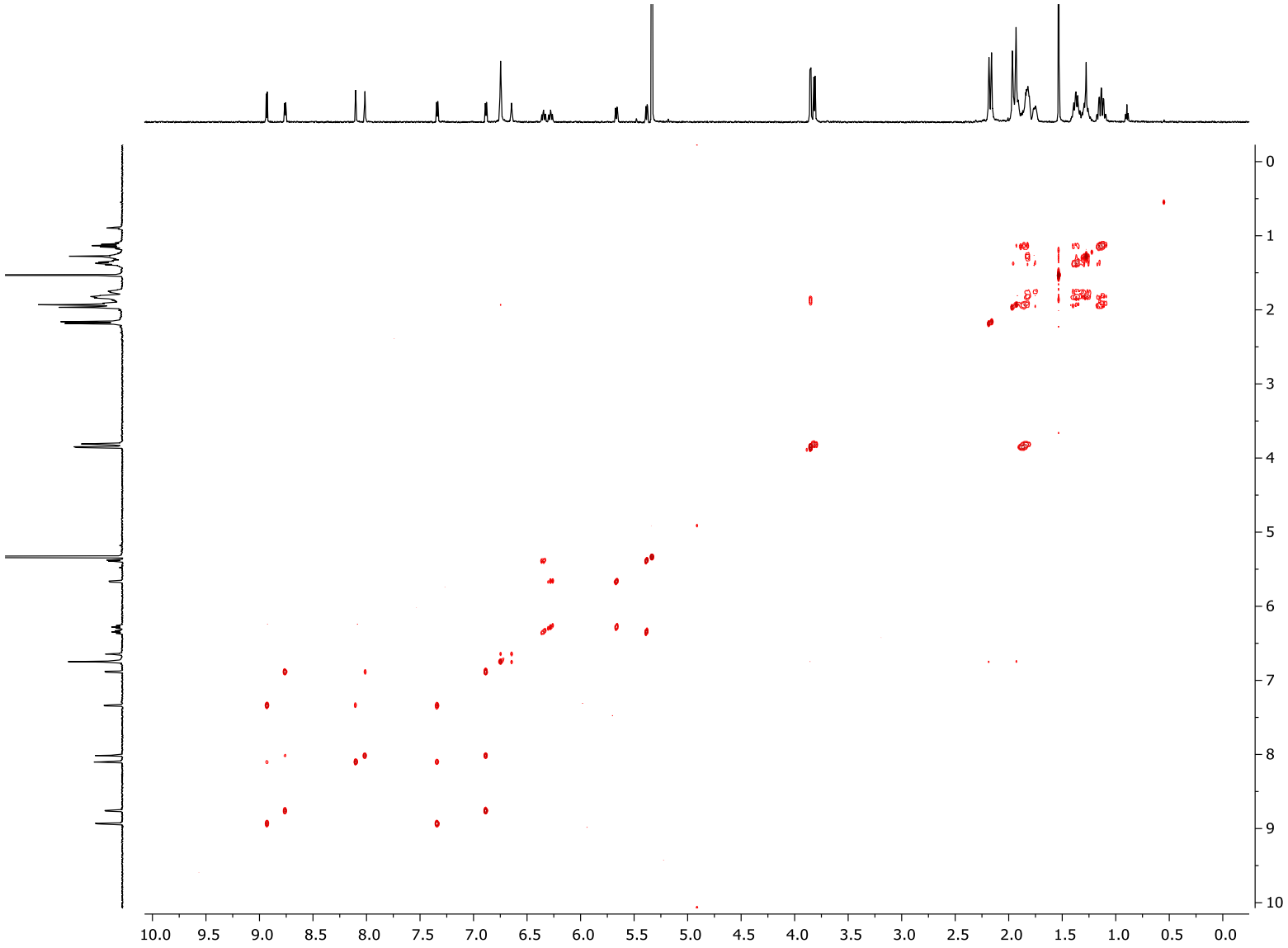

Figure S43. ^{1}H–^{1}H COSY NMR spectrum of *meso* **13** in CD_2Cl_2.

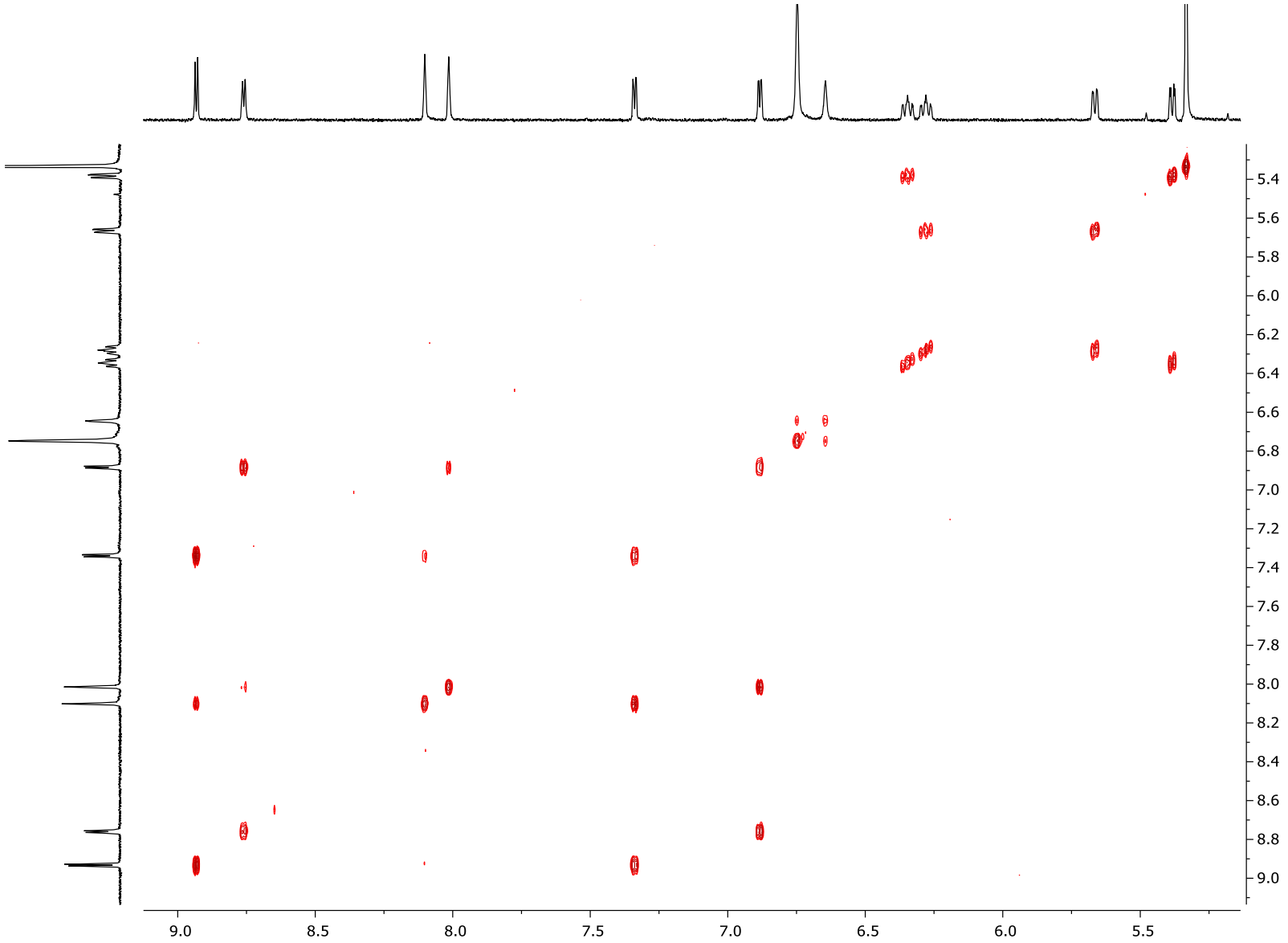

Figure S44. Expansion of the aromatic region of the ^{1}H–^{1}H COSY NMR spectrum of *meso* **13** in CD_2Cl_2.

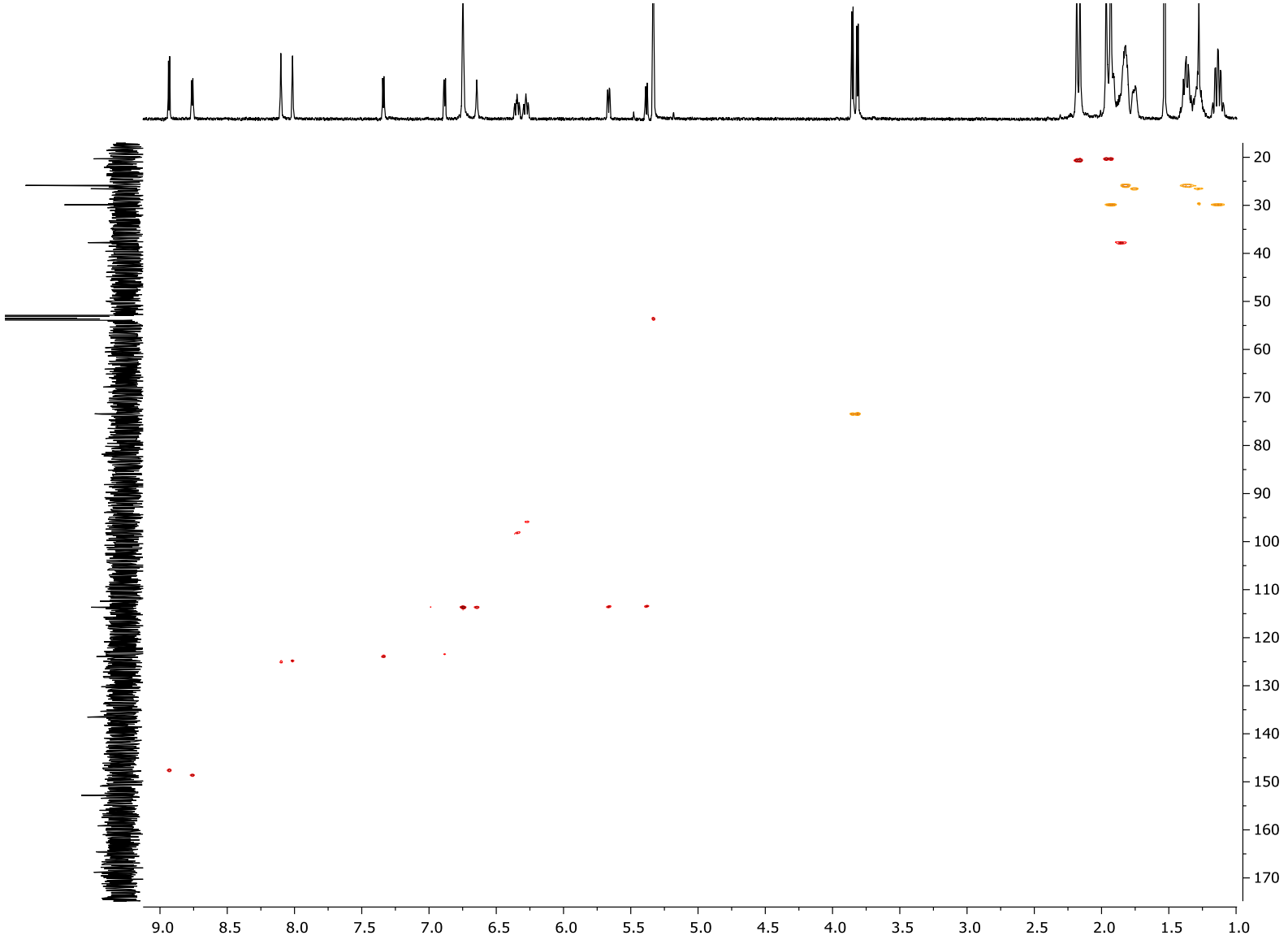

Figure S45. $^{1}H–^{13}C$ HSQC NMR spectrum of *meso* **13** in CD_2Cl_2.

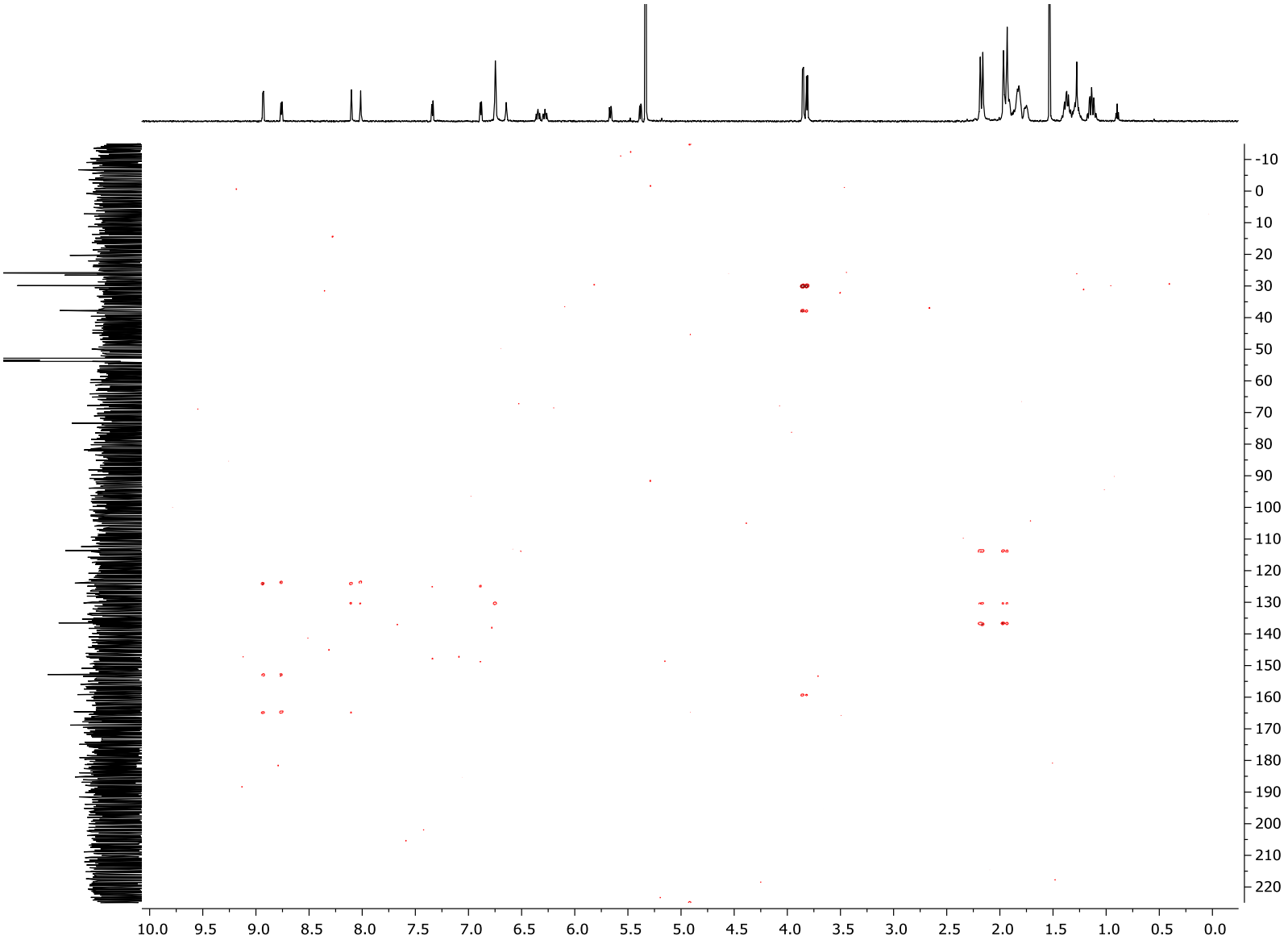

Figure S46. $^{1}H–^{13}C$ HMBC NMR spectrum of *meso* **13** in CD_2Cl_2.

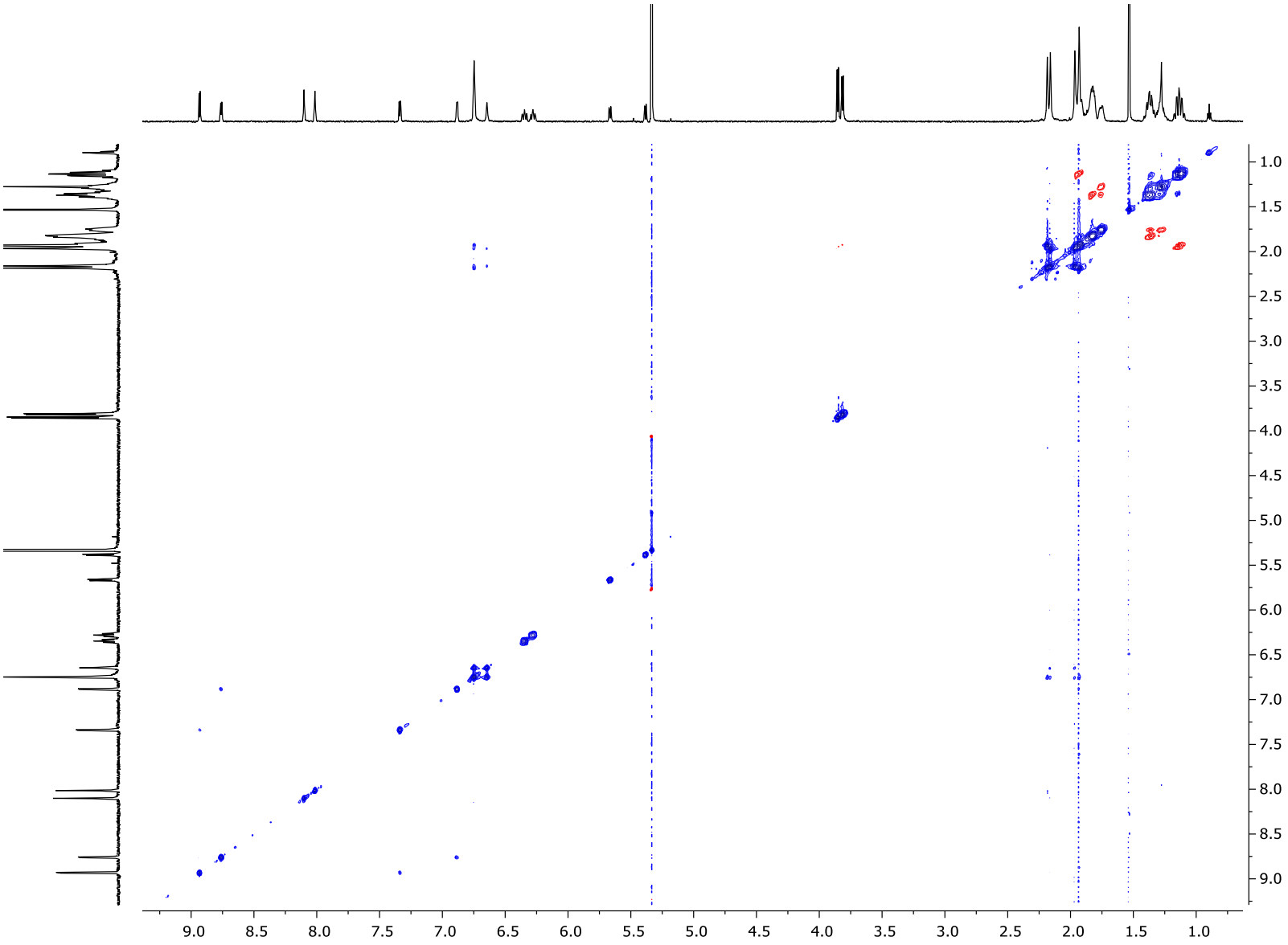

Figure S47. ^{1}H–^{1}H NOESY NMR spectrum of *meso* **13** in CD_2Cl_2.

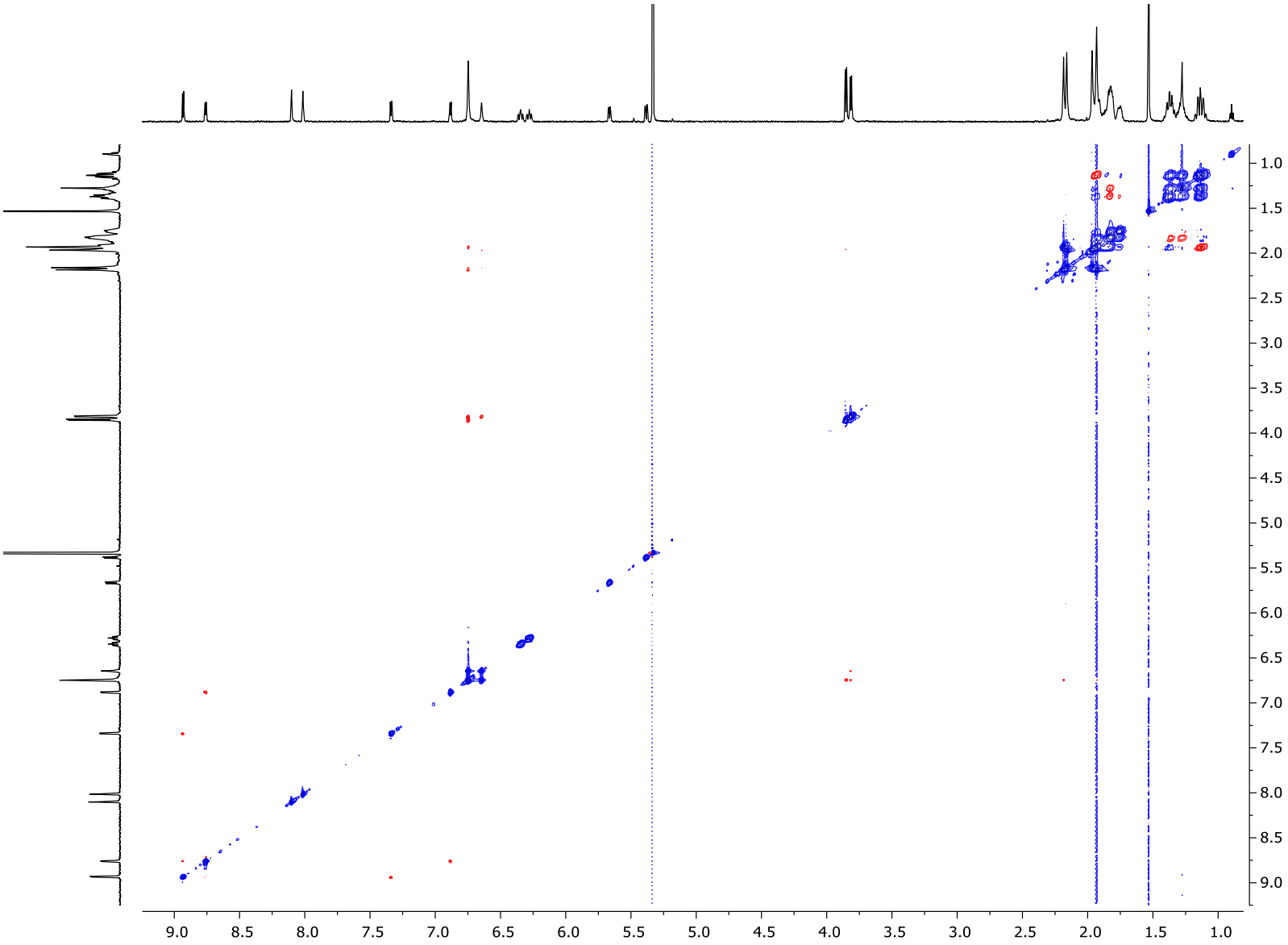

Figure S48. ^{1}H–^{1}H ROESY NMR spectrum of *meso* **13** in CD_2Cl_2.

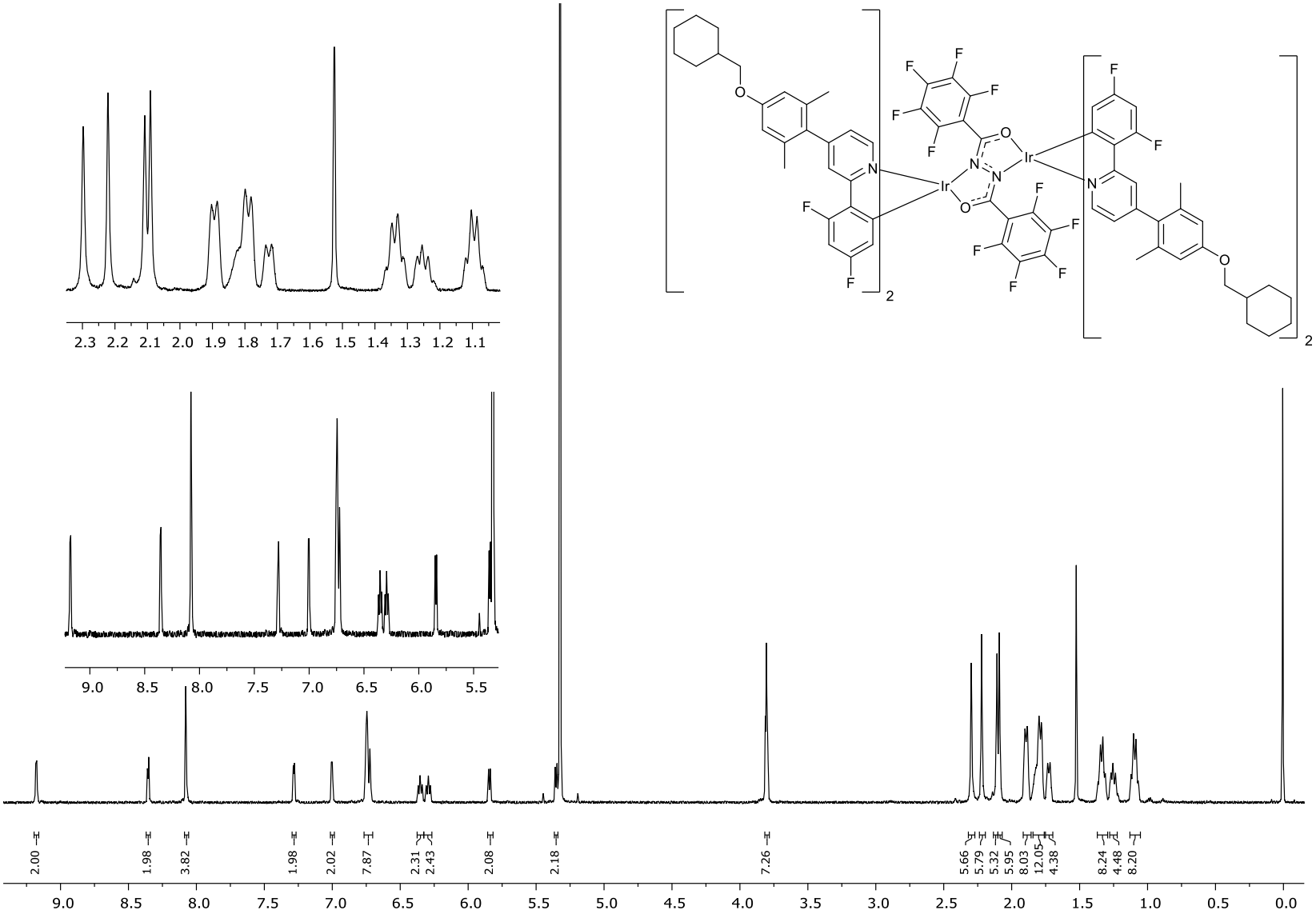

Figure S49. ^{1}H NMR spectrum (700 MHz) of *rac* **13** in CD_2Cl_2 (TMS).

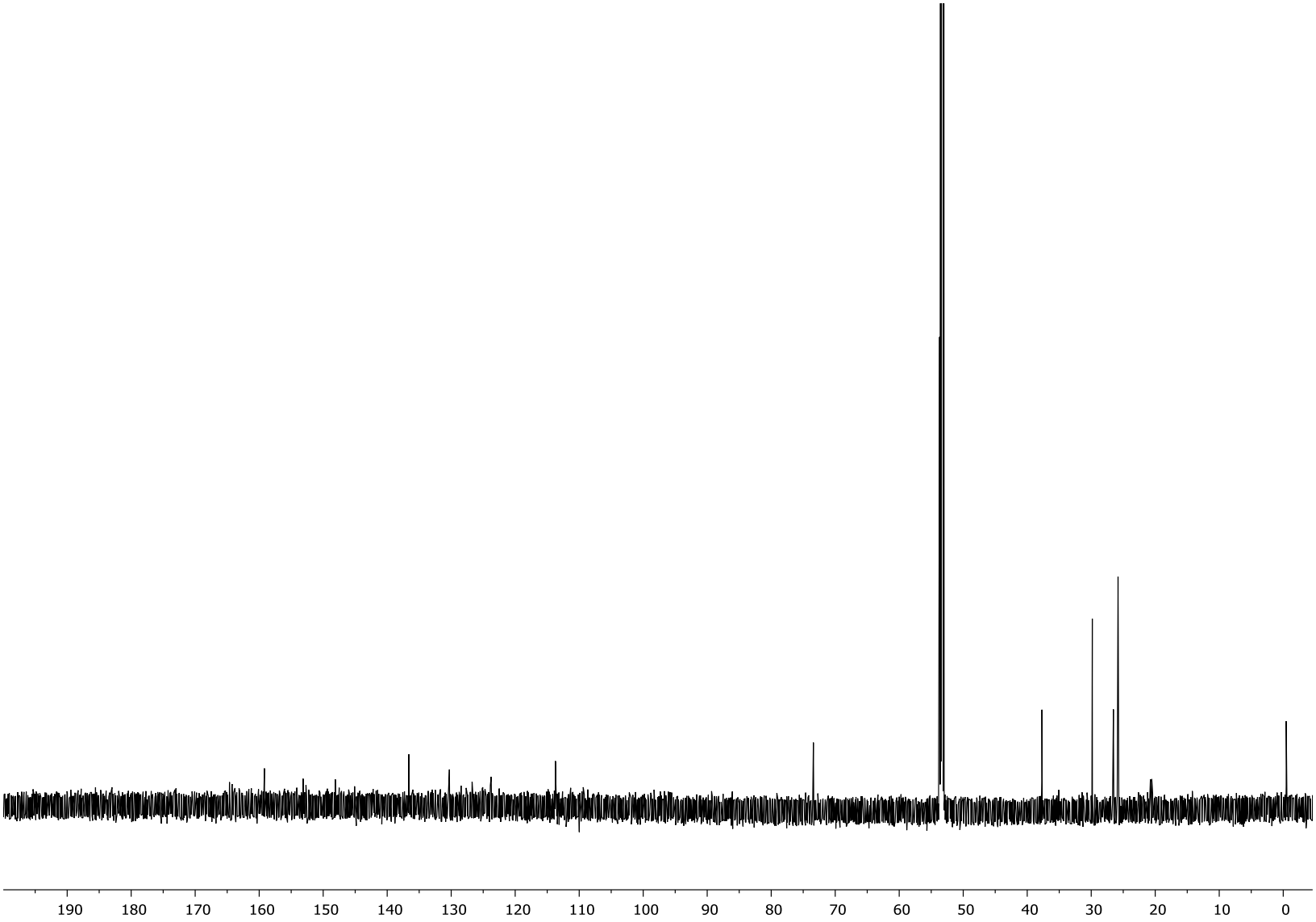

Figure S50. ^{13}C NMR spectrum (151 MHz) of *rac* **13** in CD_2Cl_2 (TMS).

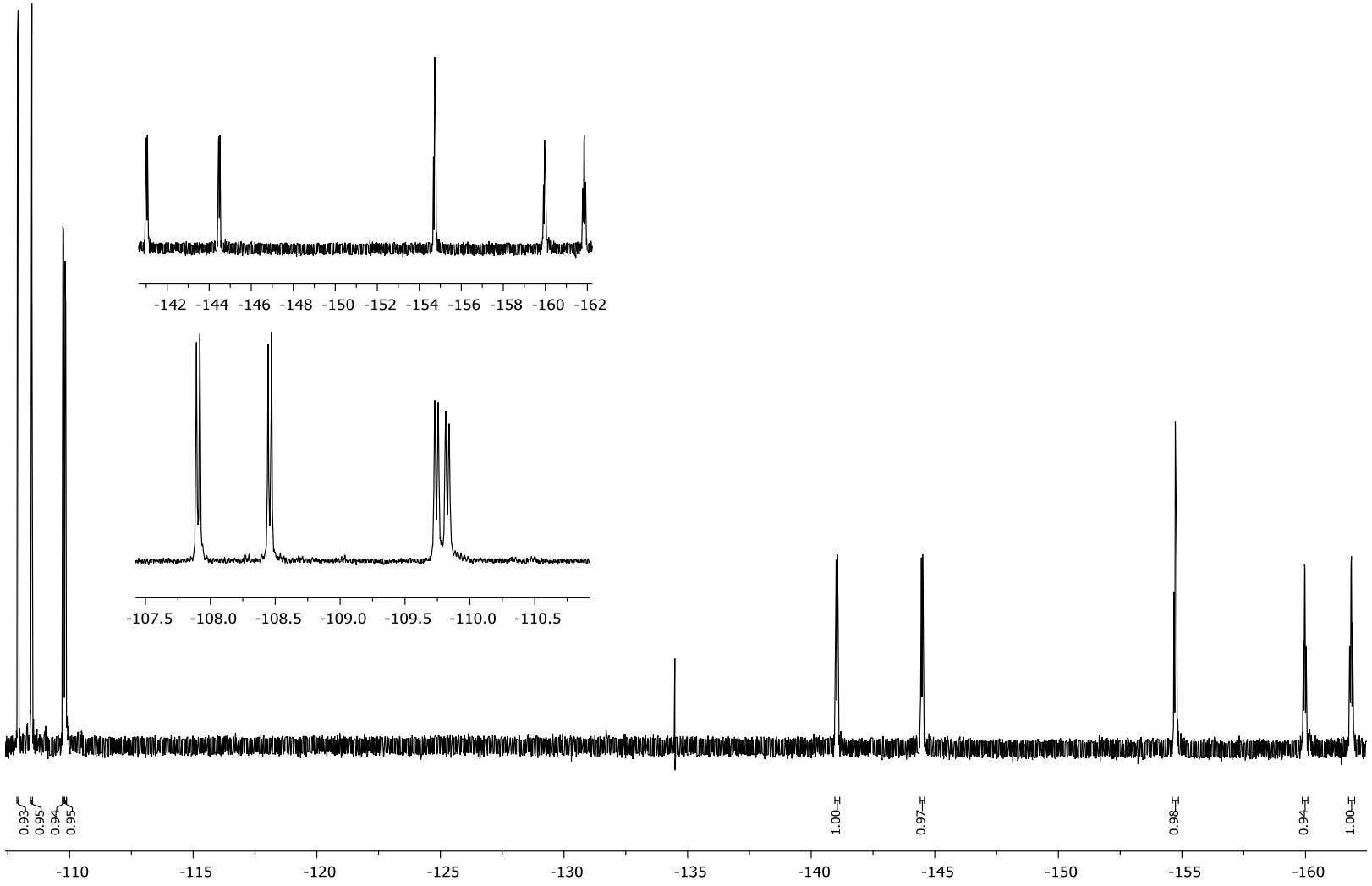

Figure S51. $^{19}F\{^{1}H\}$ NMR spectrum (376 MHz) of *rac* **13** in CD_2Cl_2**.**

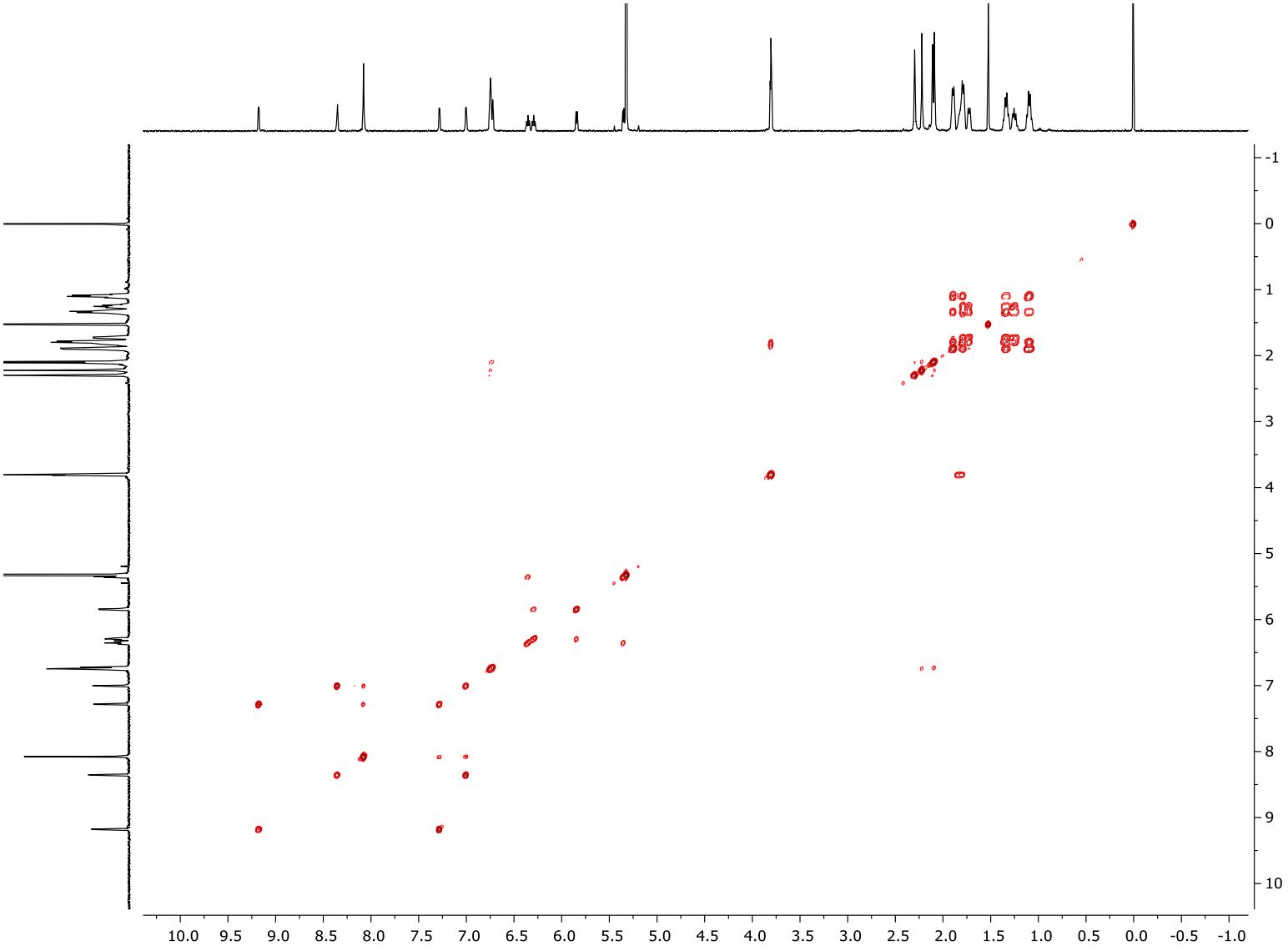

Figure S52. ^{1}H–^{1}H COSY NMR spectrum of *rac* **13** in CD_2Cl_2 (TMS).

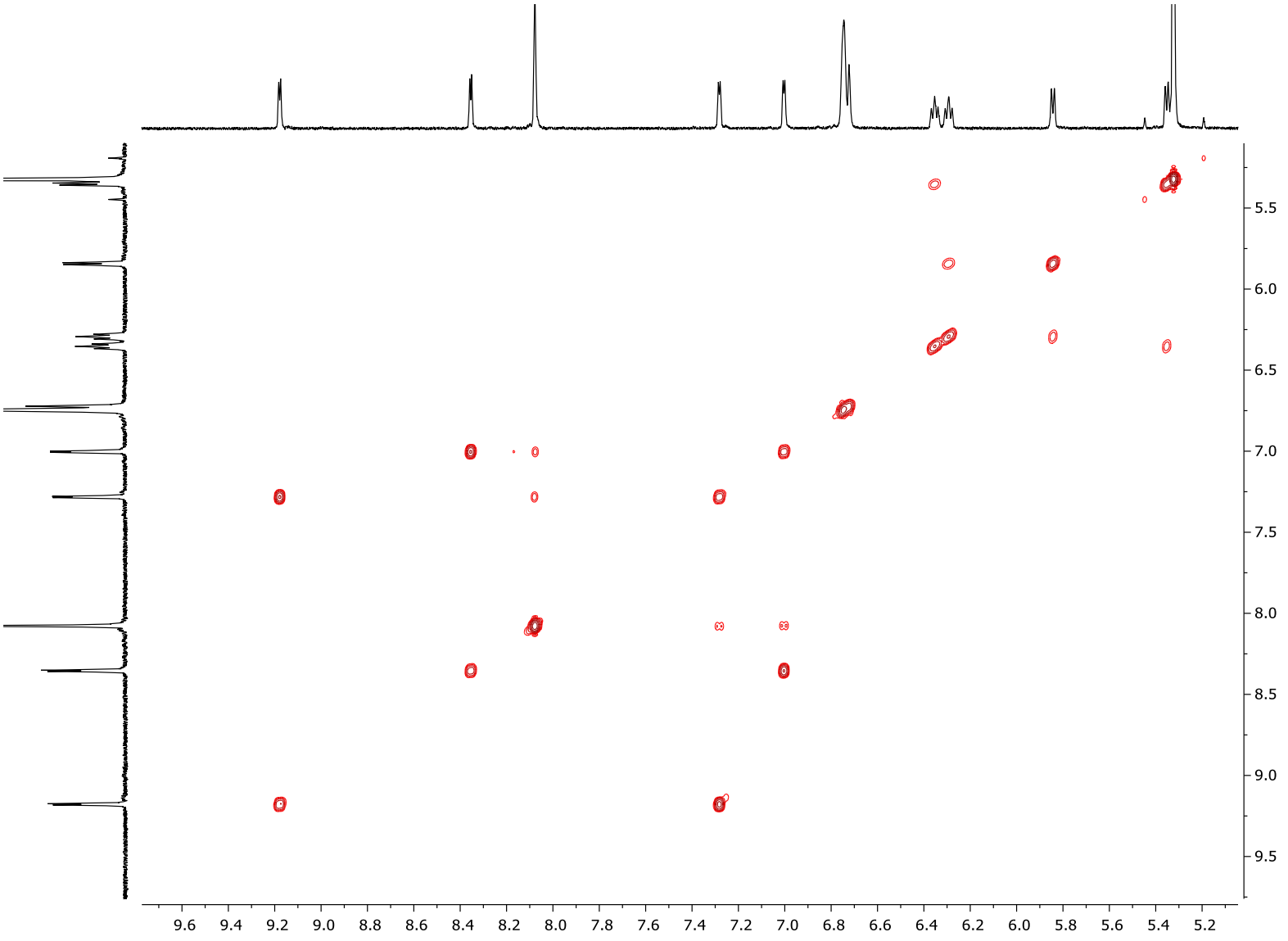

Figure S53. Expansion of the aromatic region of the ^{1}H–^{1}H COSY NMR spectrum of *rac* **13** in CD_2Cl_2 (TMS).

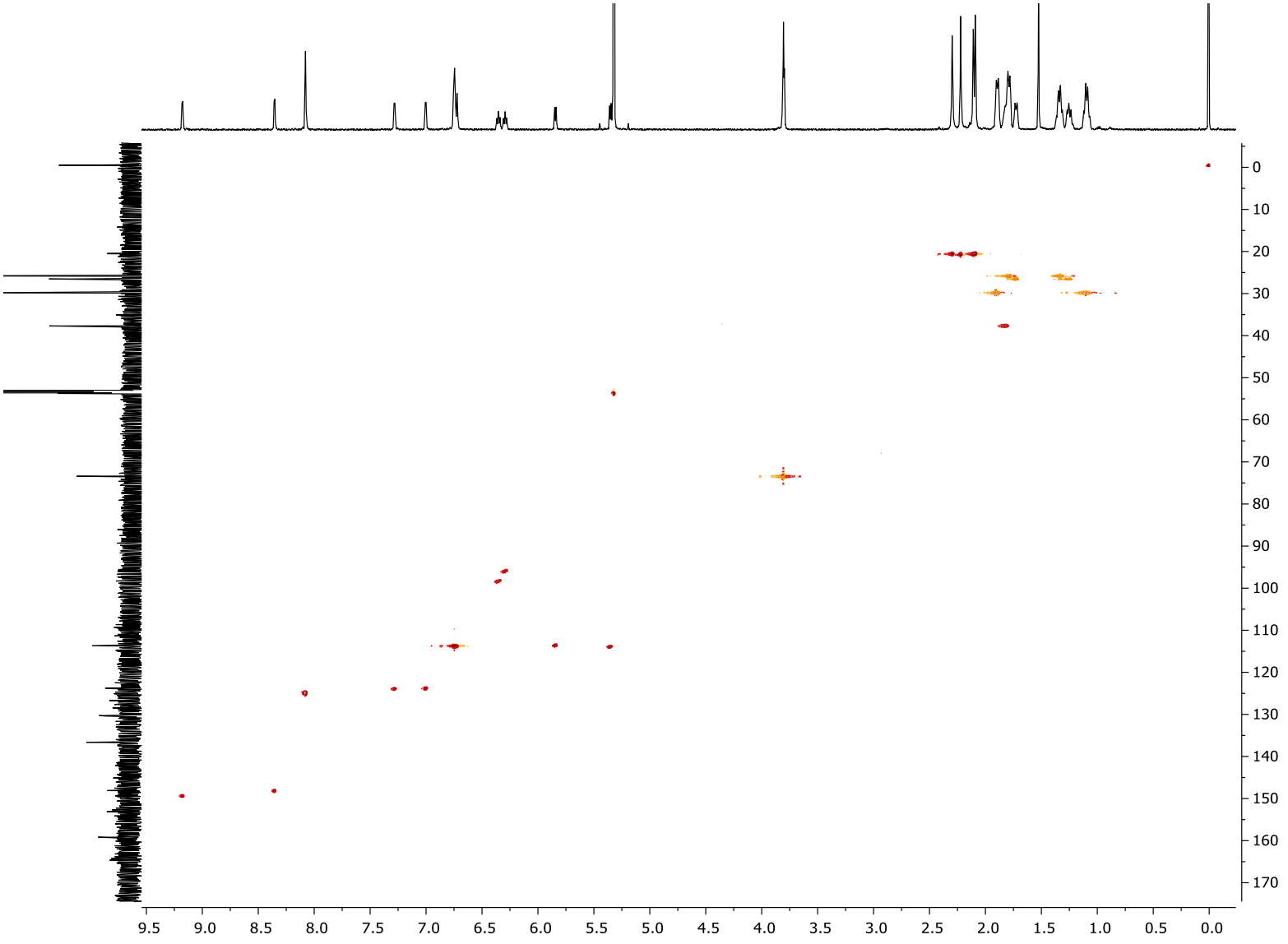

Figure S54. $^{1}H–^{13}C$ HSQC NMR spectrum of *rac* **13** in CD_2Cl_2 (TMS).

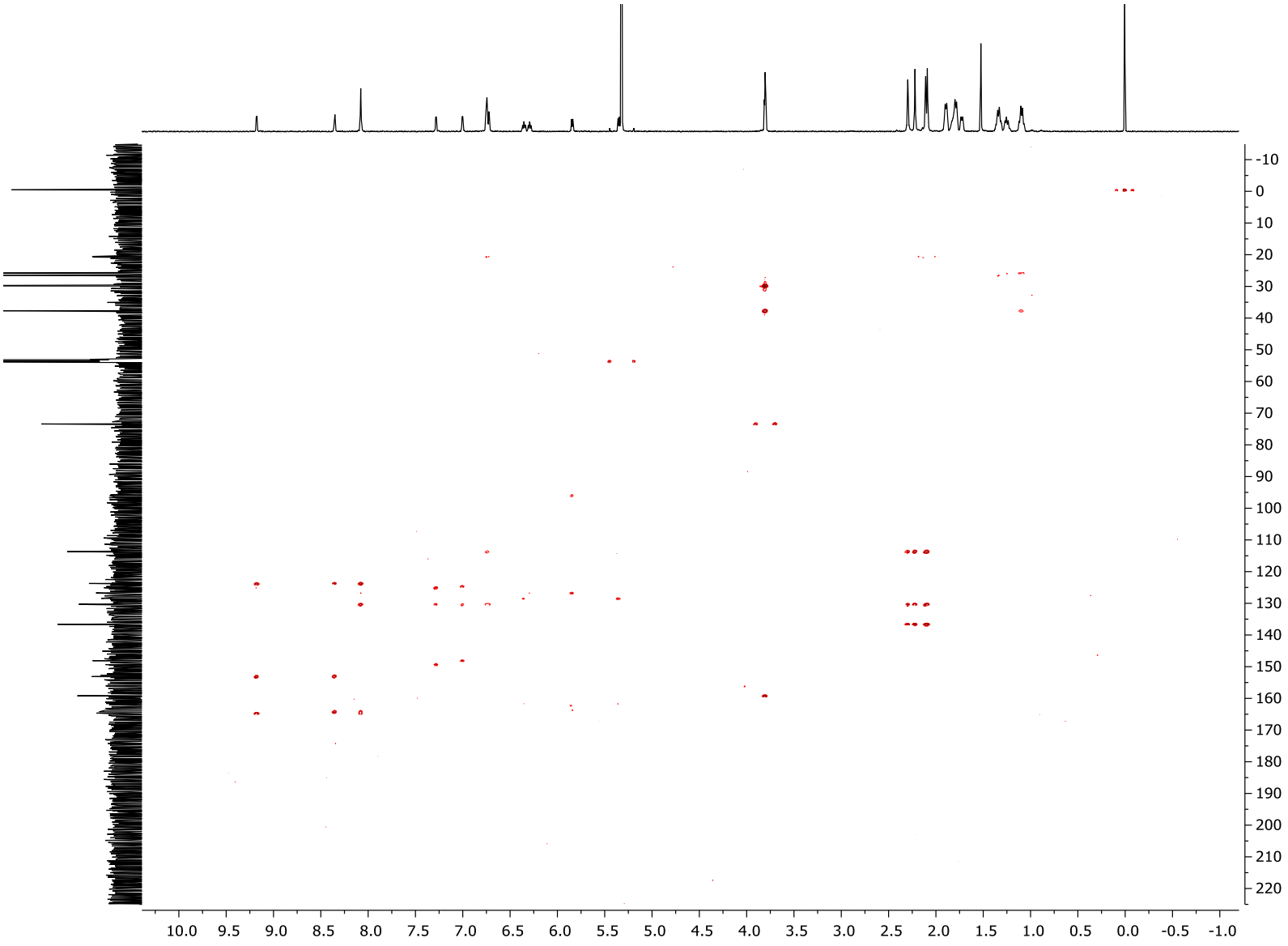

Figure S55. ^{1}H–^{13}C HMBC NMR spectrum of *rac* **13** in CD_2Cl_2 (TMS).

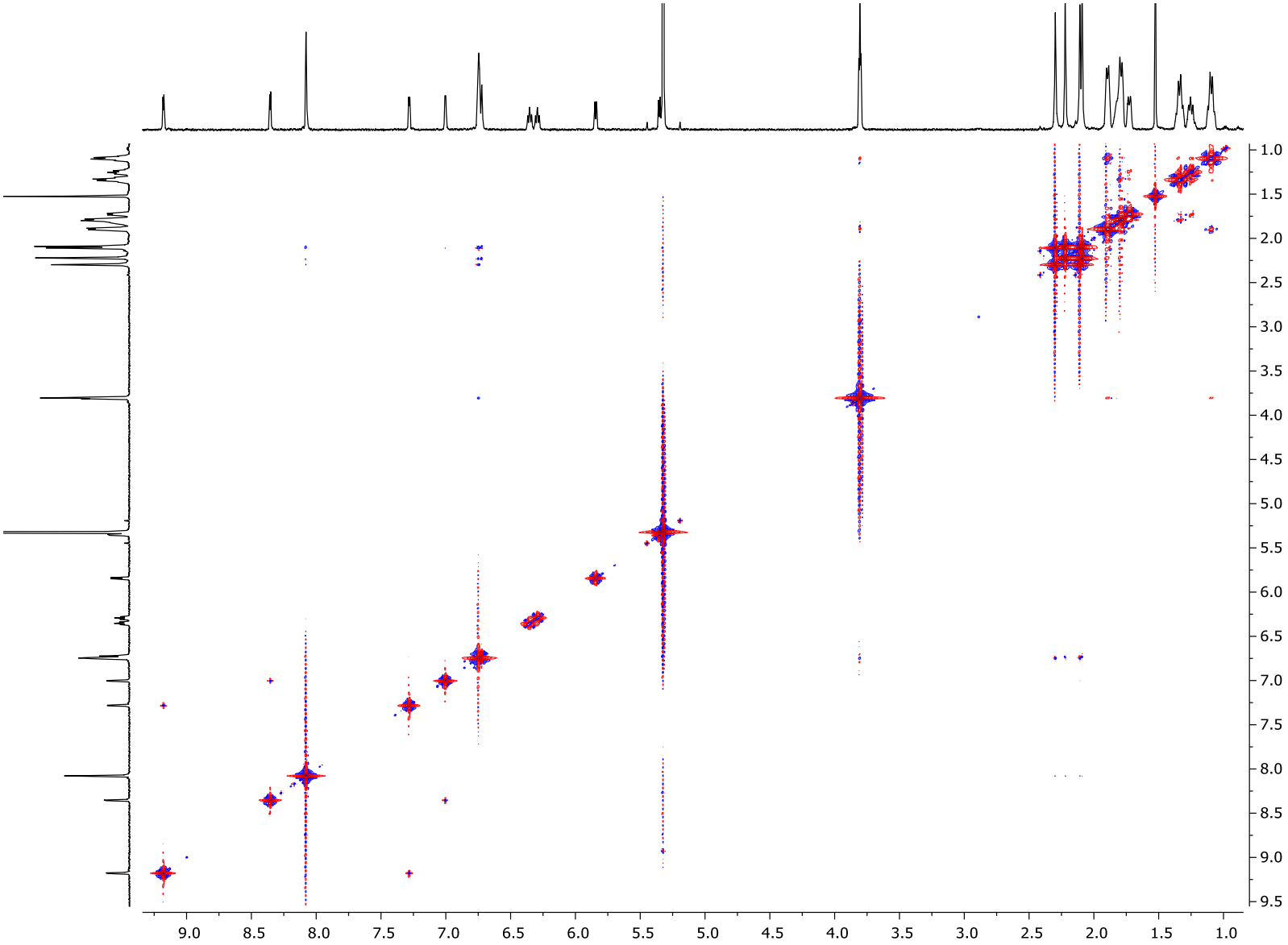

Figure S56. ^{1}H–^{1}H NOESY NMR spectrum of *rac* **13** in CD_2Cl_2 (TMS).

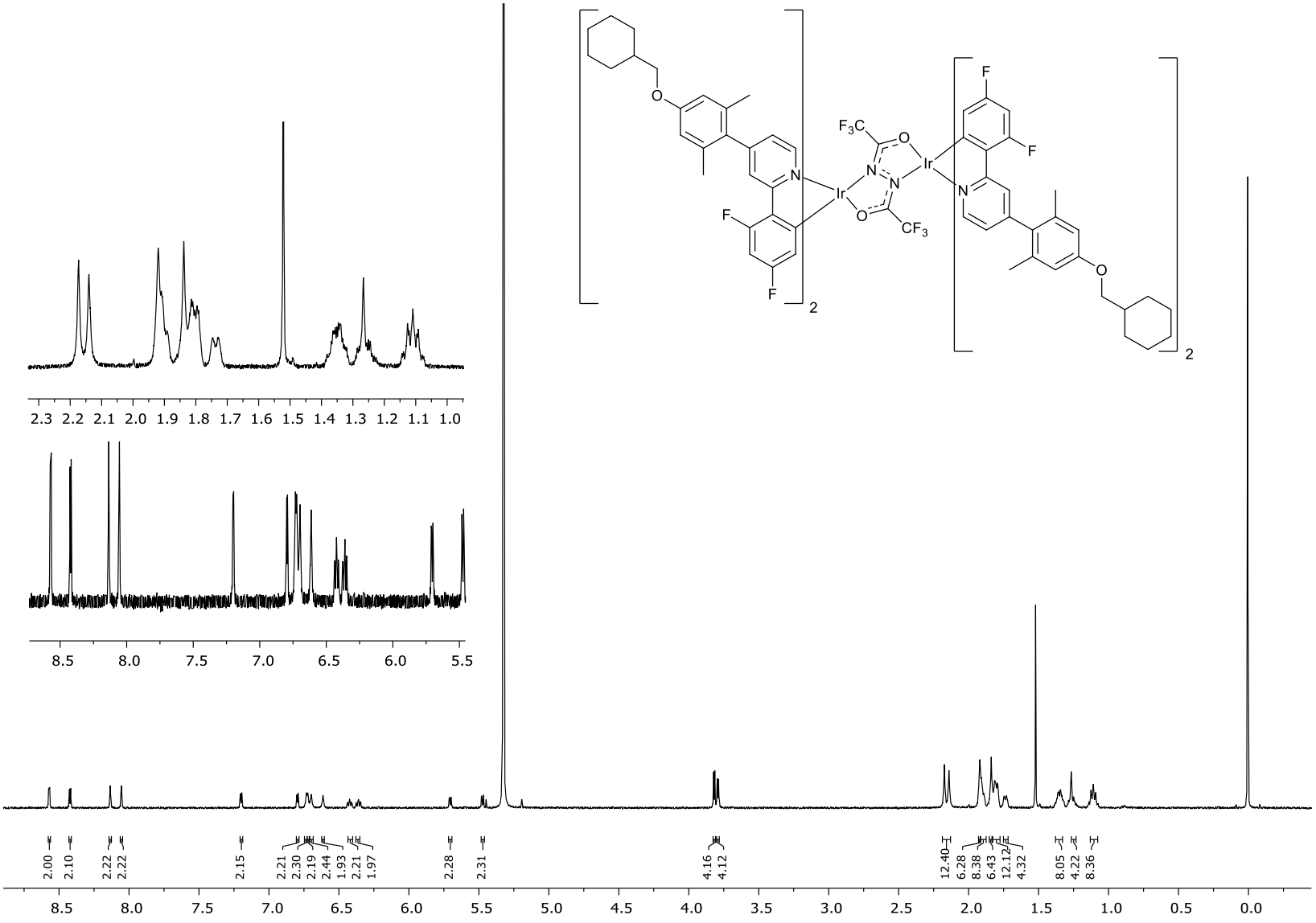

Figure S57. ^{1}H NMR spectrum (700 MHz) of **14** in CD_2Cl_2 (TMS).

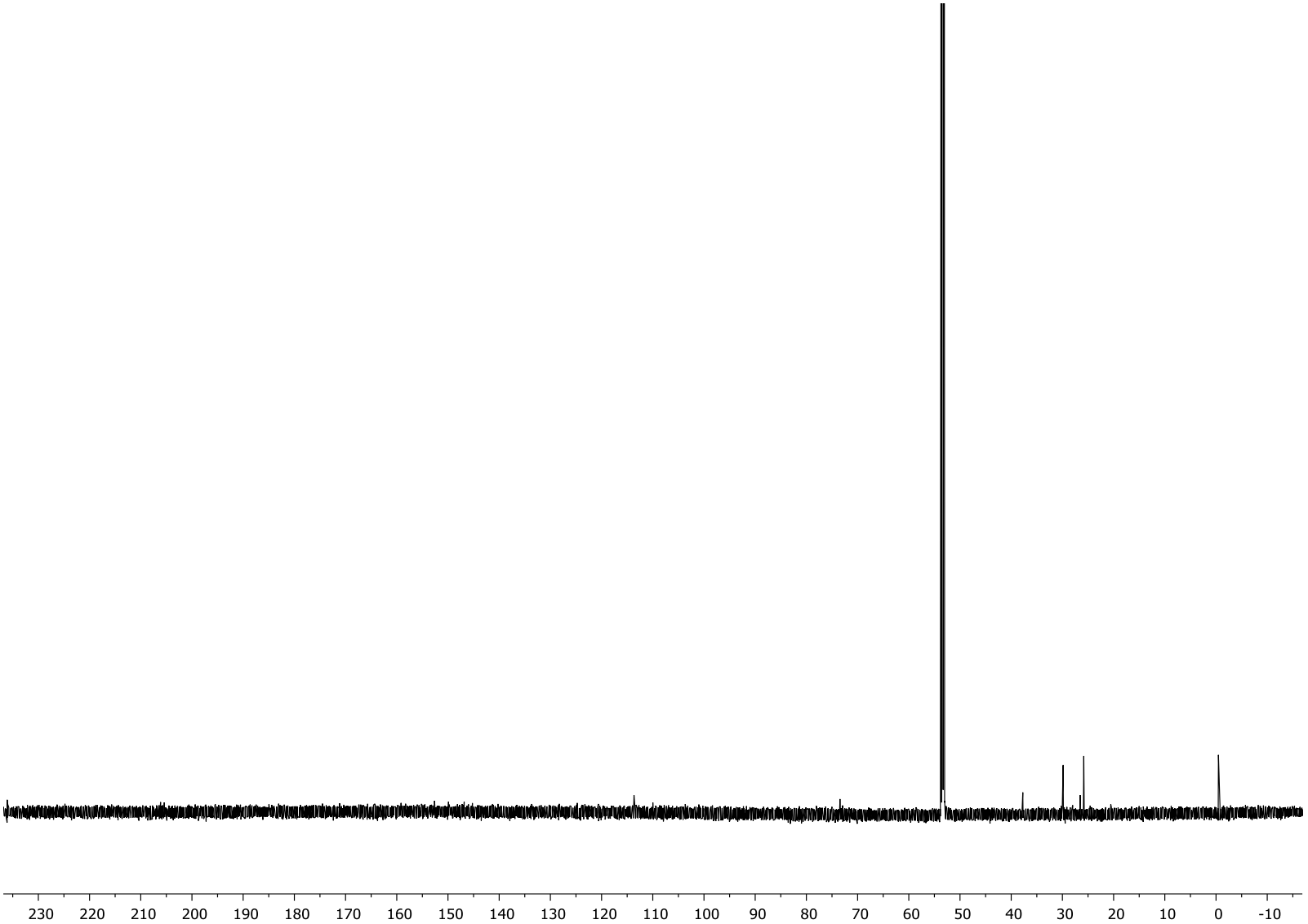

Figure S58. ^{13}C NMR spectrum (151 MHz) of **14** in CD_2Cl_2 (TMS).

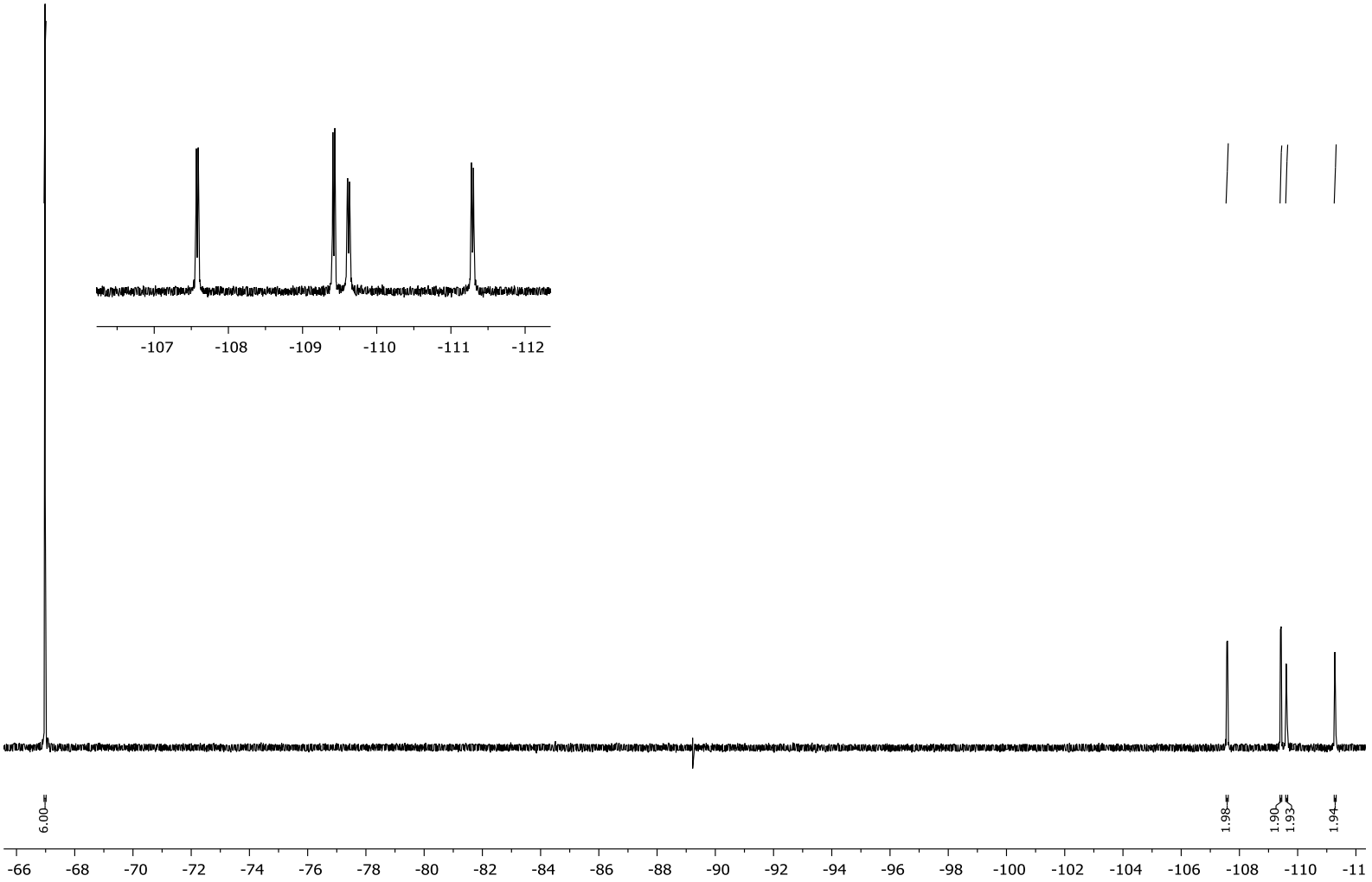

Figure S59. $^{19}F\{^{1}H\}$ NMR spectrum (376 MHz) of **14** in CD_2Cl_2.

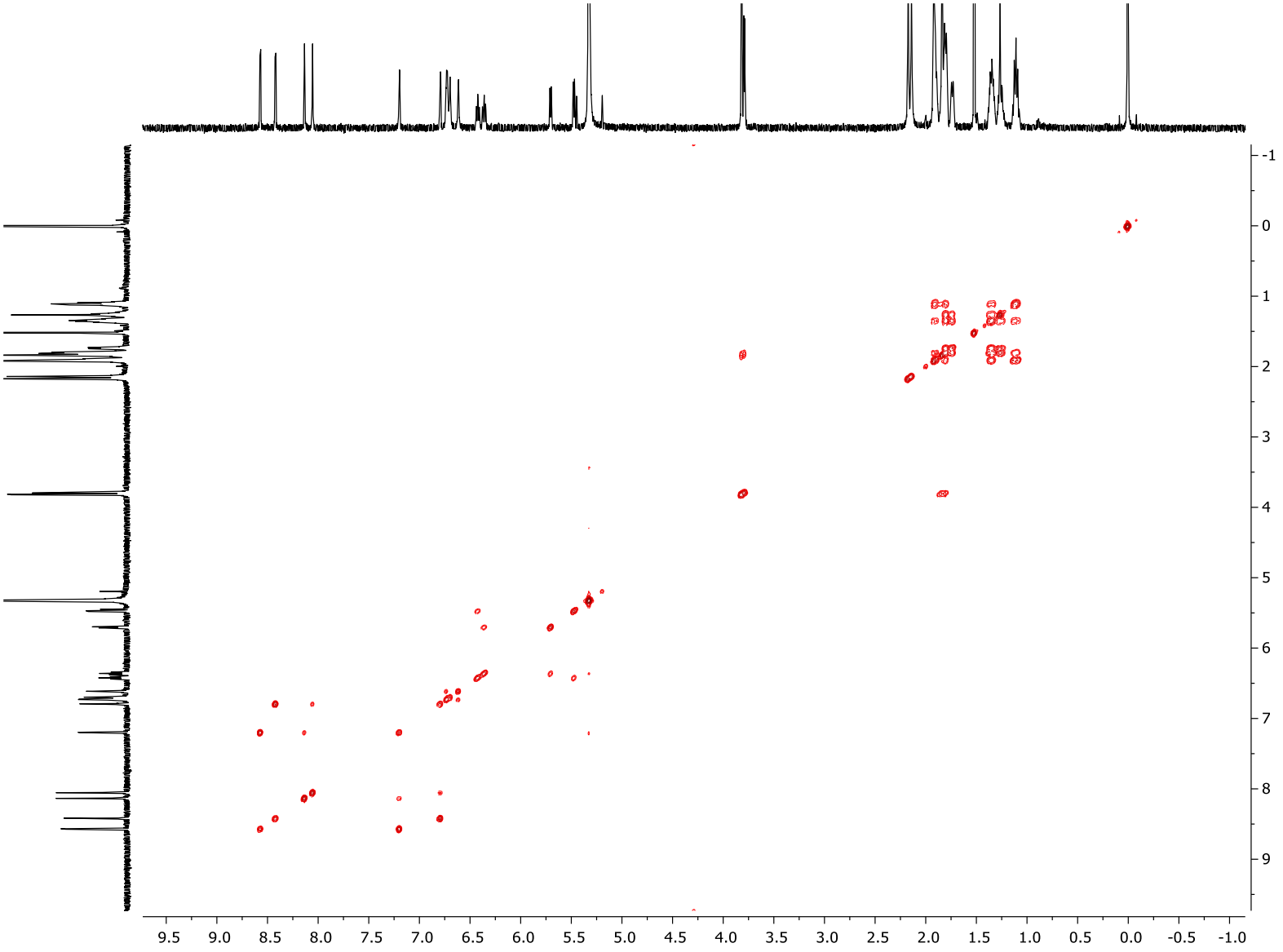

Figure S60. ^{1}H–^{1}H COSY NMR spectrum of **14** in CD_2Cl_2 (TMS).

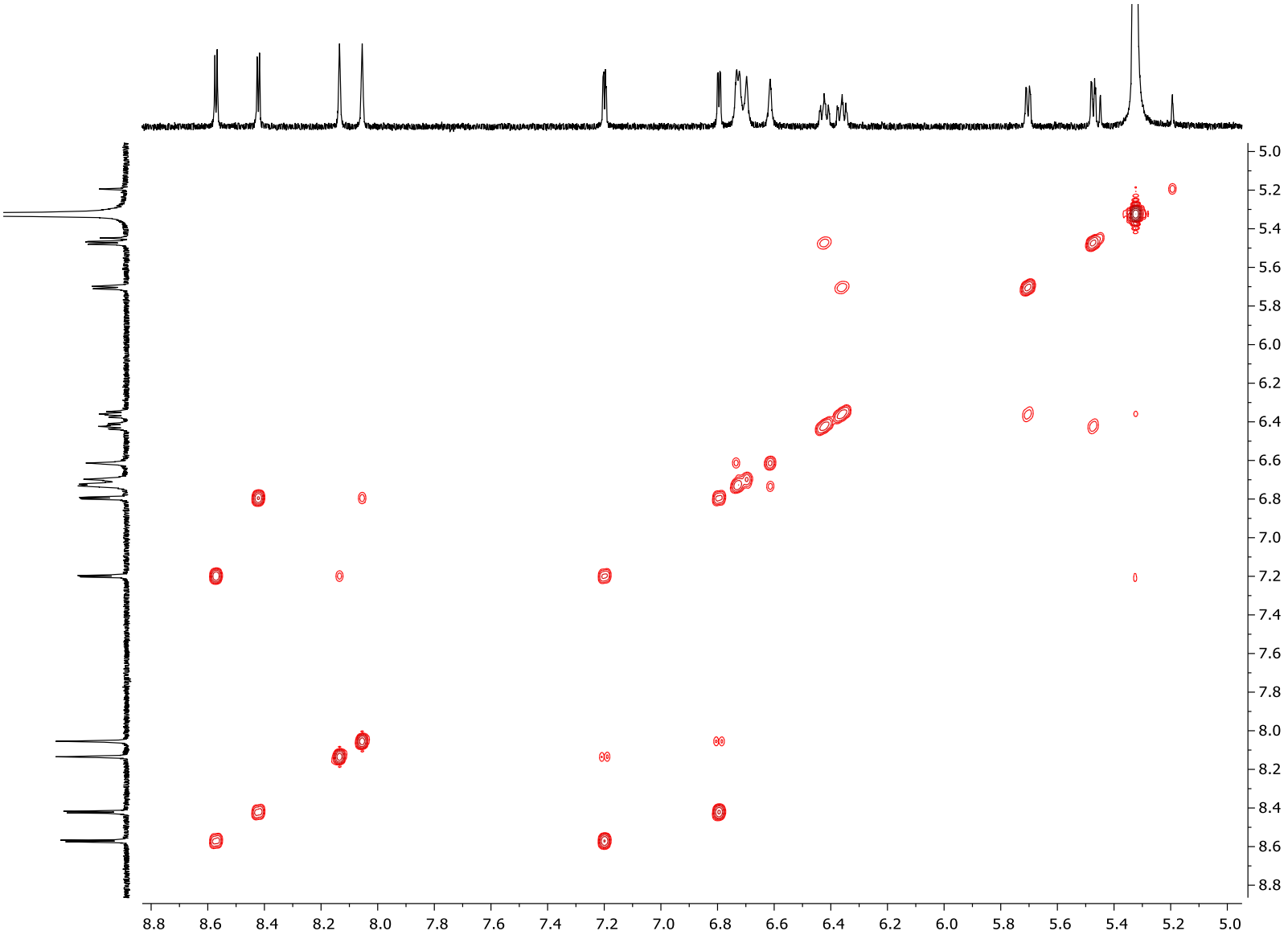

Figure S61. Expansion of the aromatic region of the ^{1}H–^{1}H COSY NMR spectrum of **14** in CD_2Cl_2 (TMS).

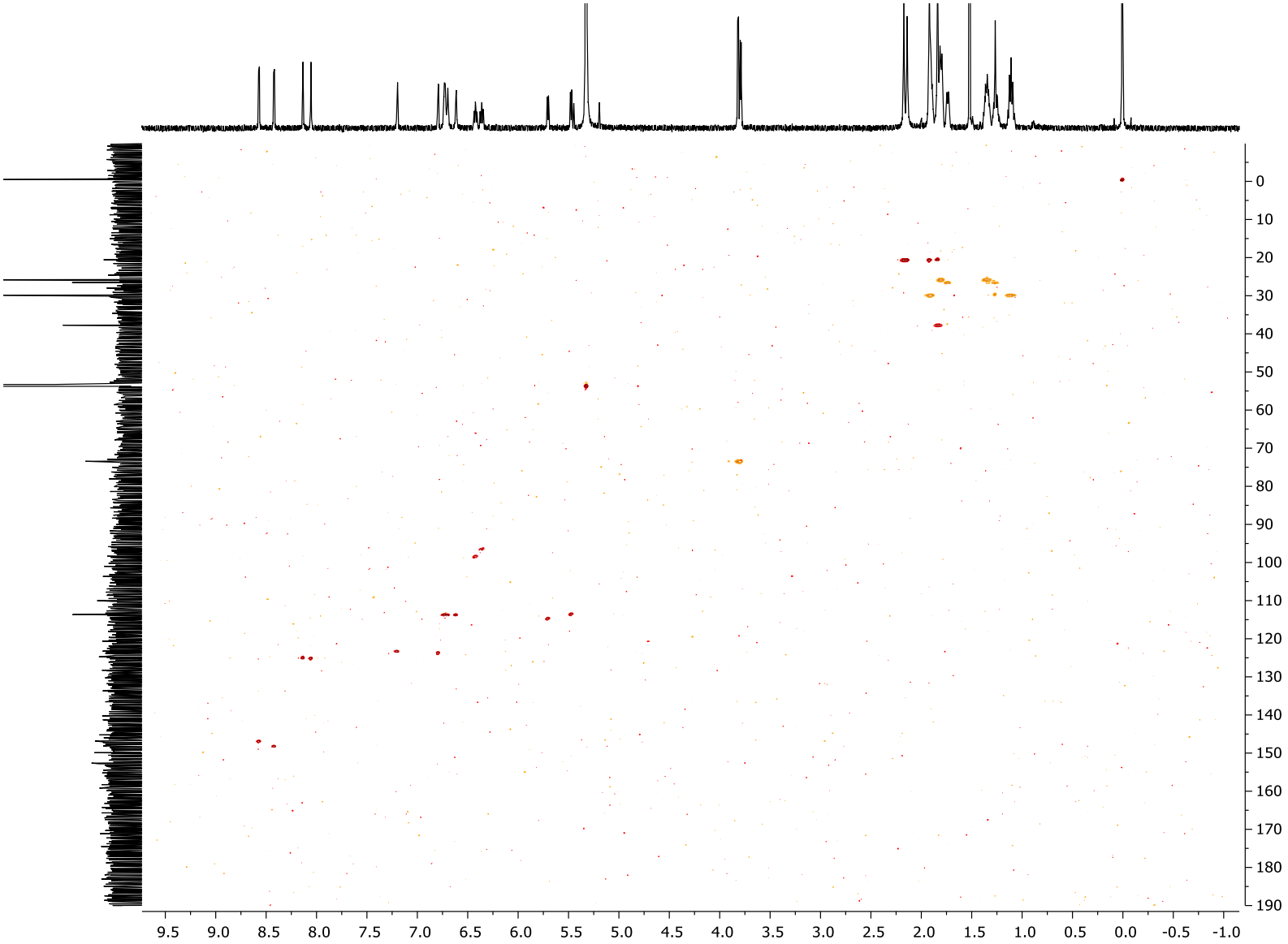

Figure S62. $^{1}H–^{13}C$ HSQC NMR spectrum of **14** in CD_2Cl_2 (TMS).

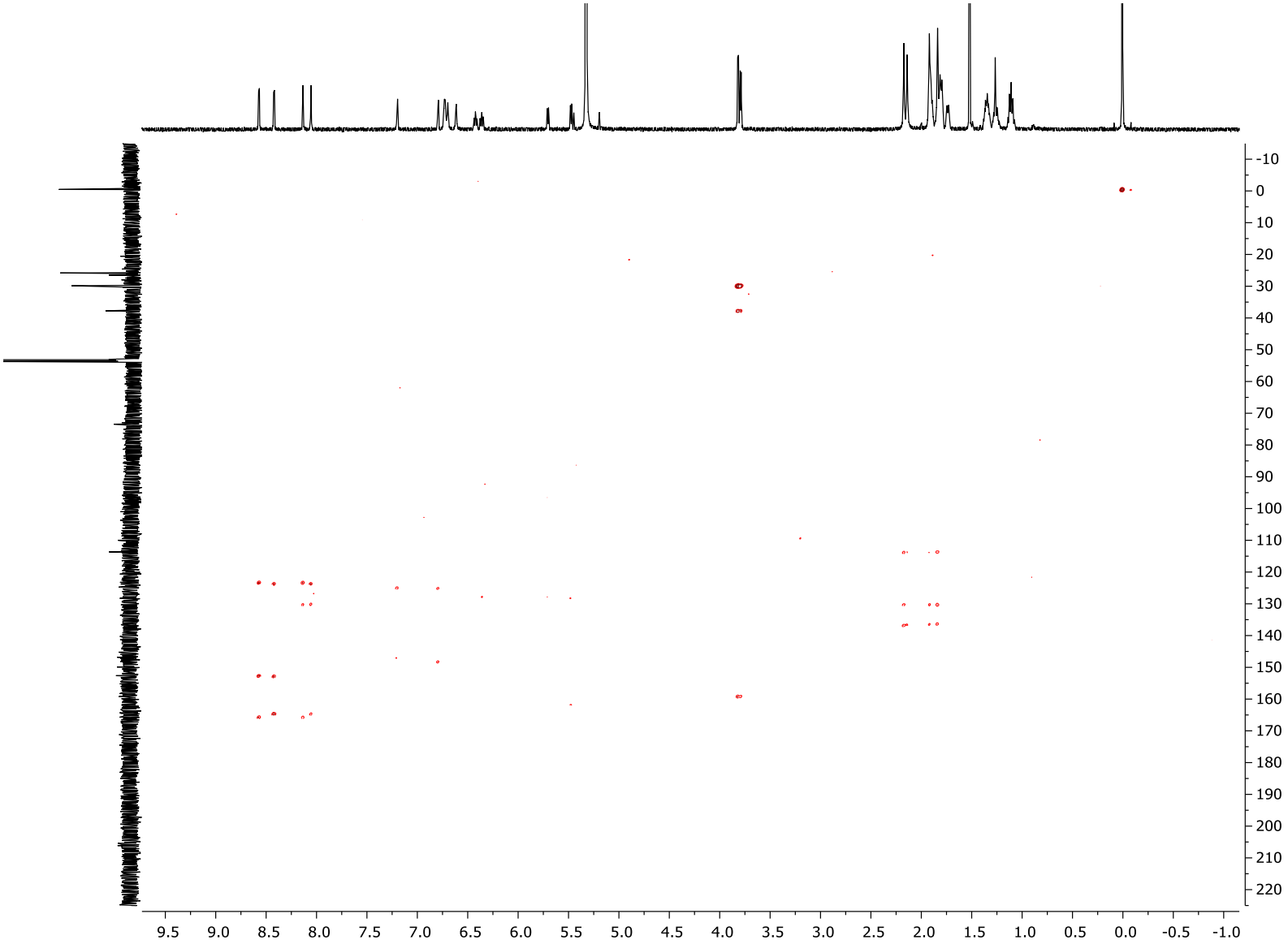

Figure S63. $^{1}H–^{13}C$ HMBC NMR spectrum of **14** in CD_2Cl_2 (TMS).

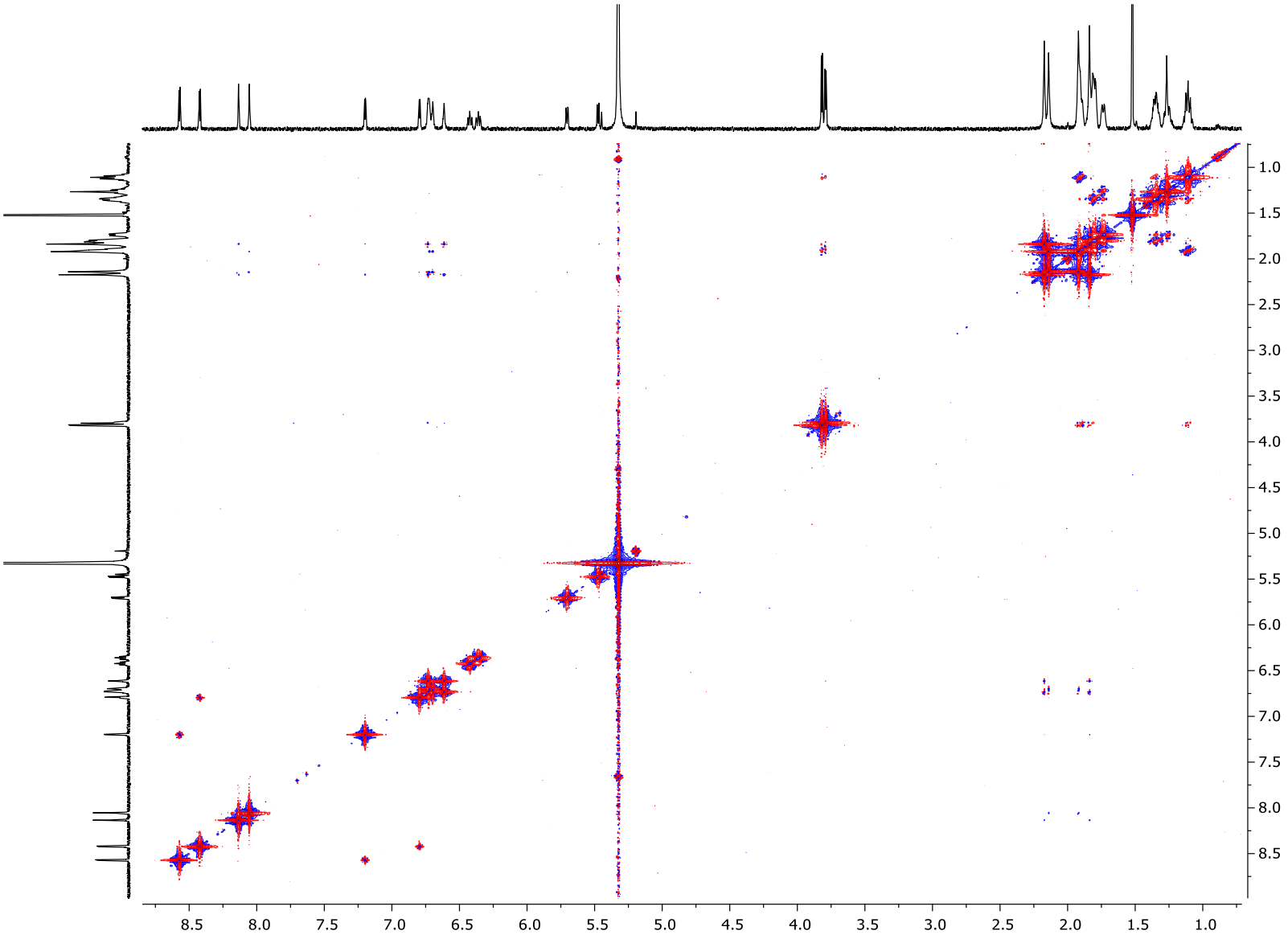

Figure S64. ^{1}H–^{1}H NOESY NMR spectrum of **14** in CD_2Cl_2 (TMS).

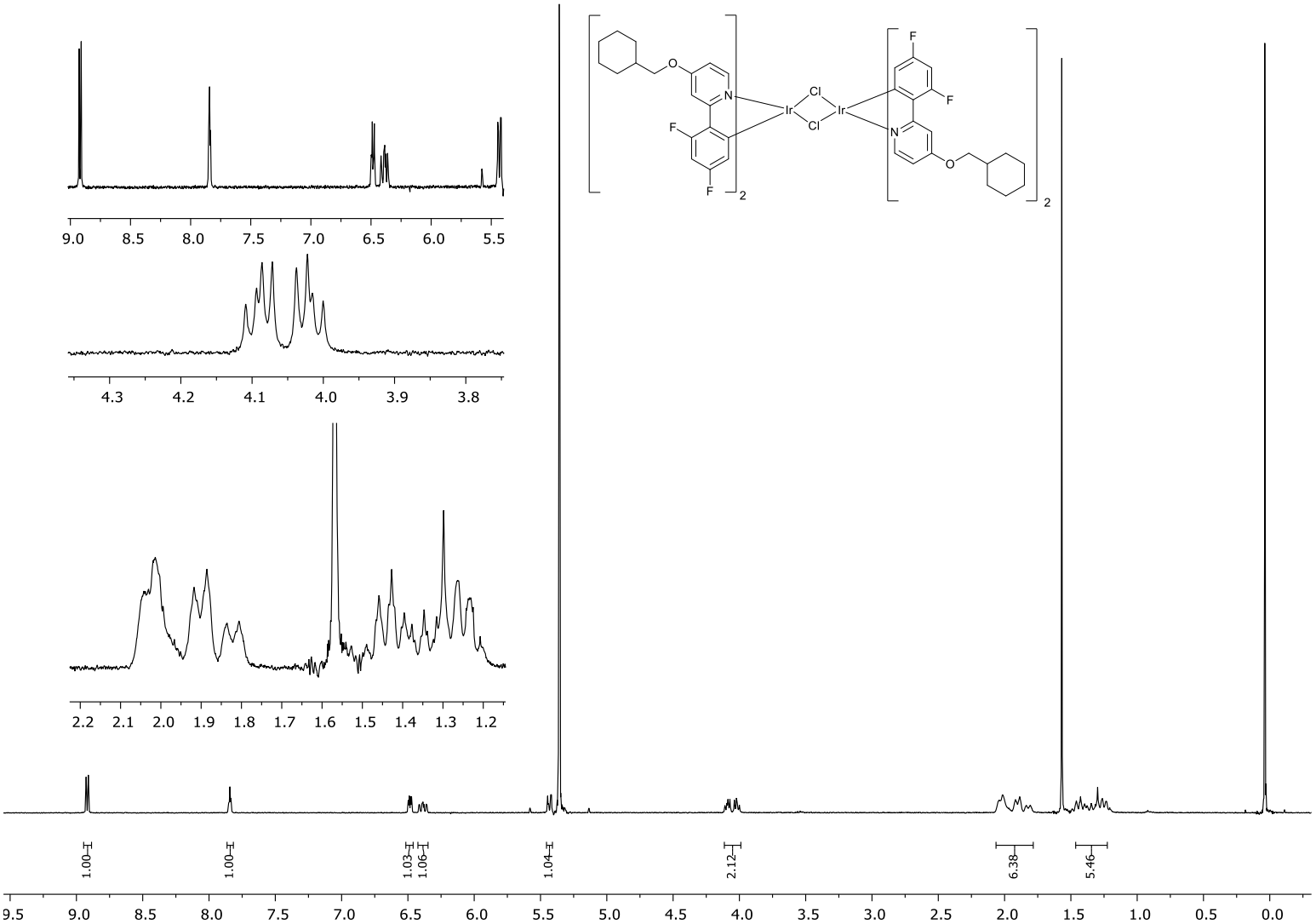

Figure S65. ^{1}H NMR spectrum (400 MHz) of the μ–dichloro dimer isolated as an intermediate in the synthesis of complex **15** in CD_2Cl_2 (TMS).

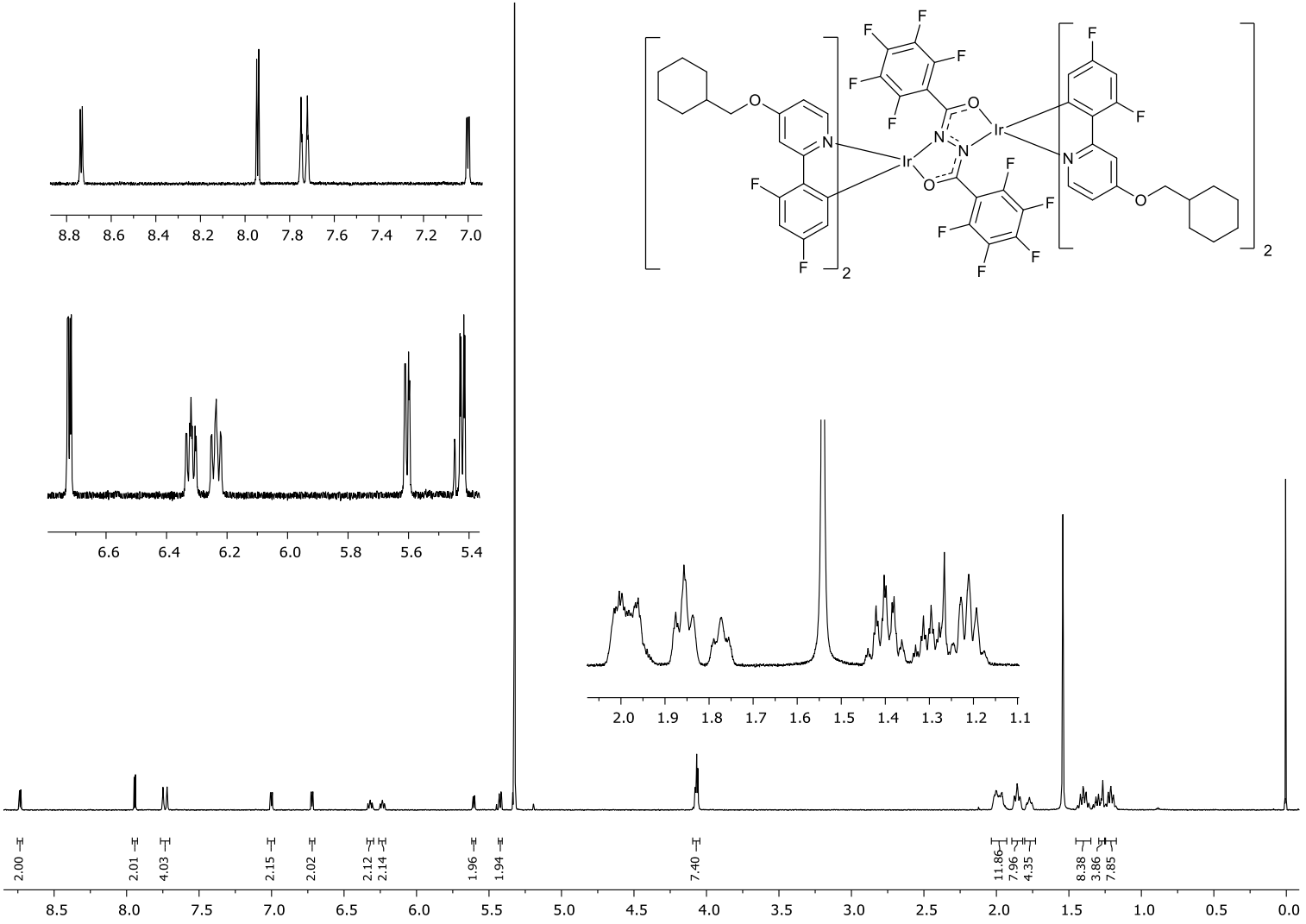

Figure S66. ^{1}H NMR spectrum (700 MHz) of **15** in CD_2Cl_2 (TMS).

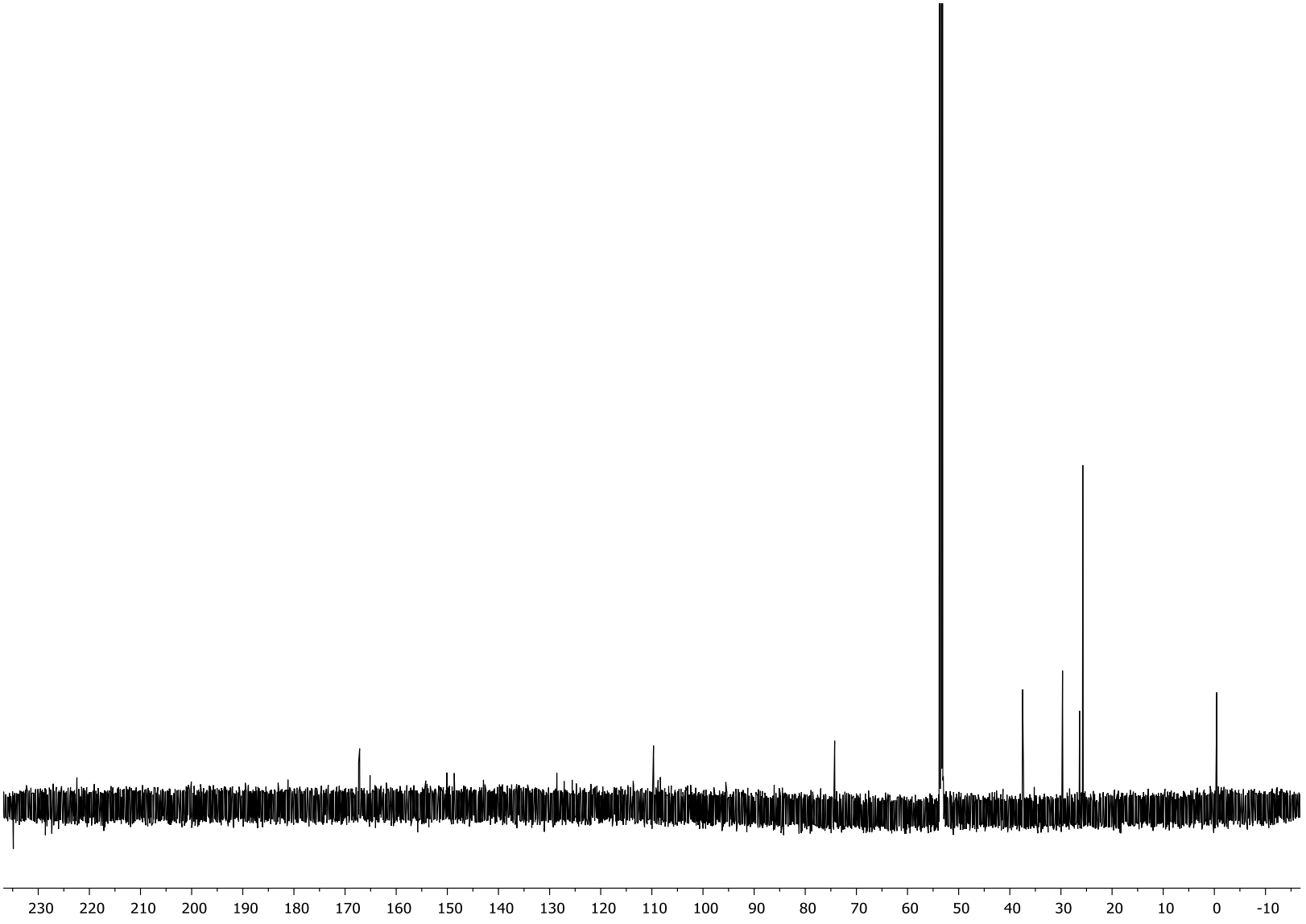

Figure S67. ^{13}C NMR spectrum (151 MHz) of **15** in CD_2Cl_2 (TMS).

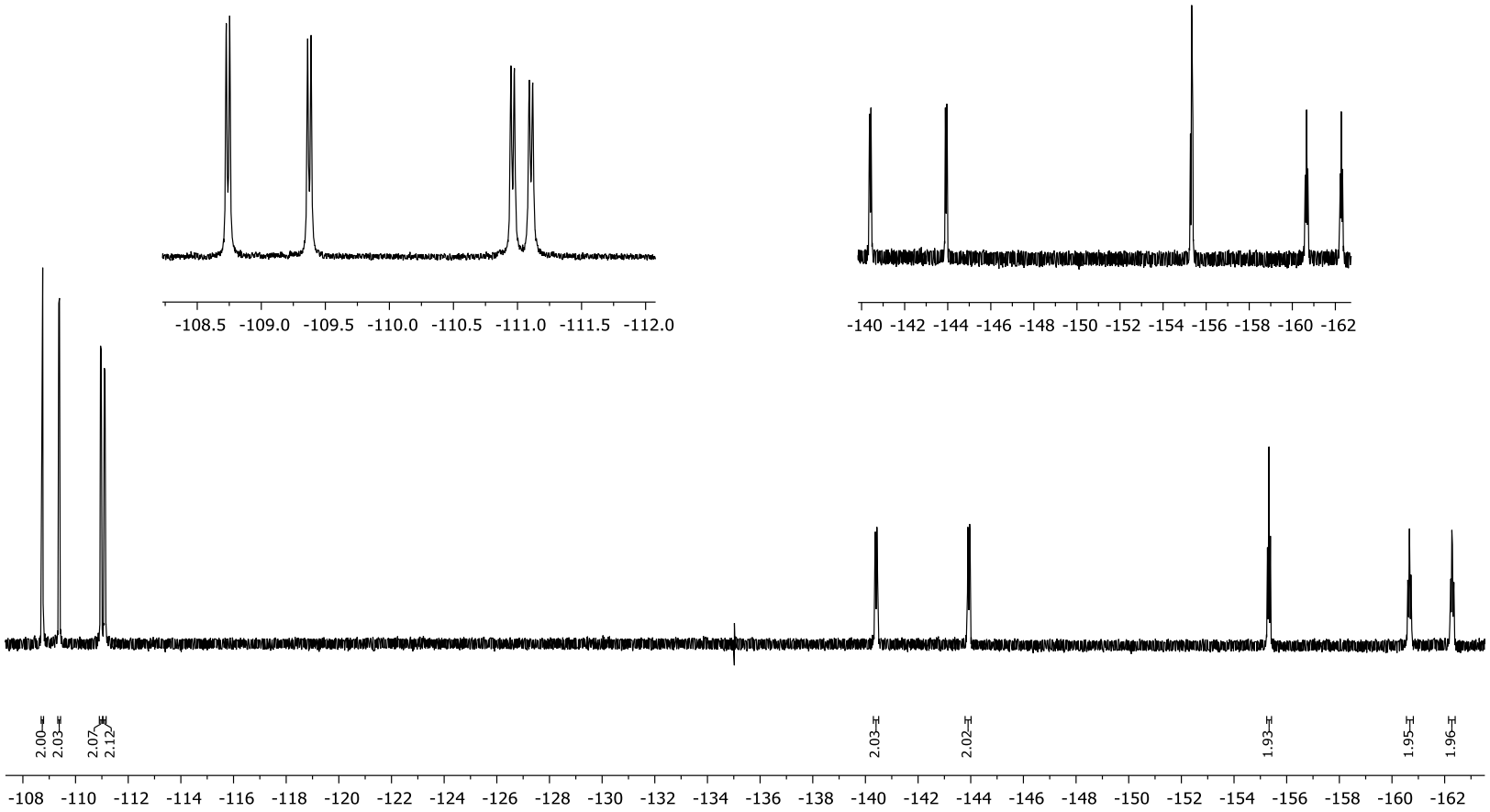

Figure S68. $^{19}F\{^{1}H\}$ NMR spectrum (376 MHz) of **15** in CD_2Cl_2.

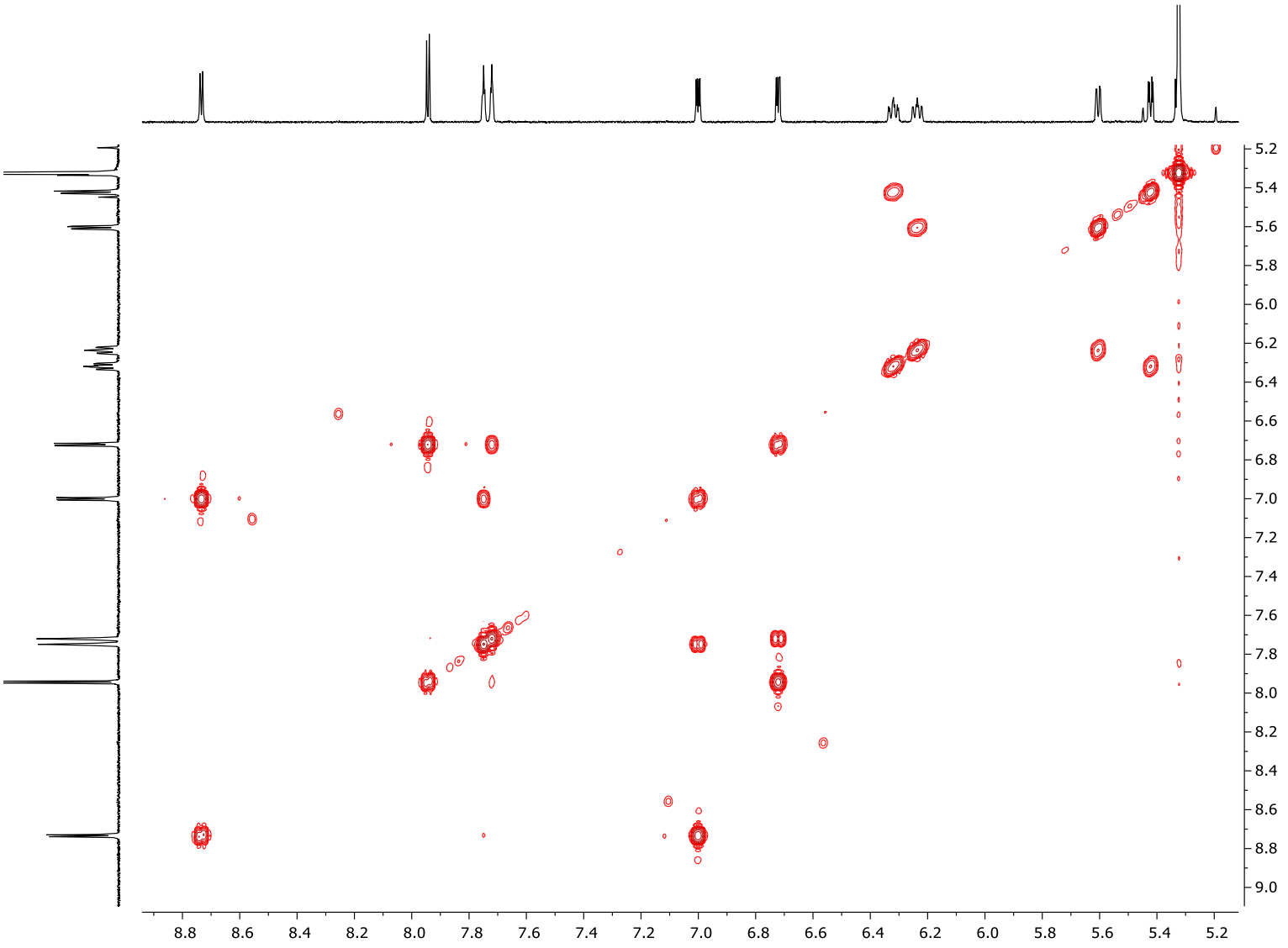

Figure S69. Expansion of the aromatic region of the ^{1}H–^{1}H COSY NMR spectrum of **15** in CD_2Cl_2 (TMS).

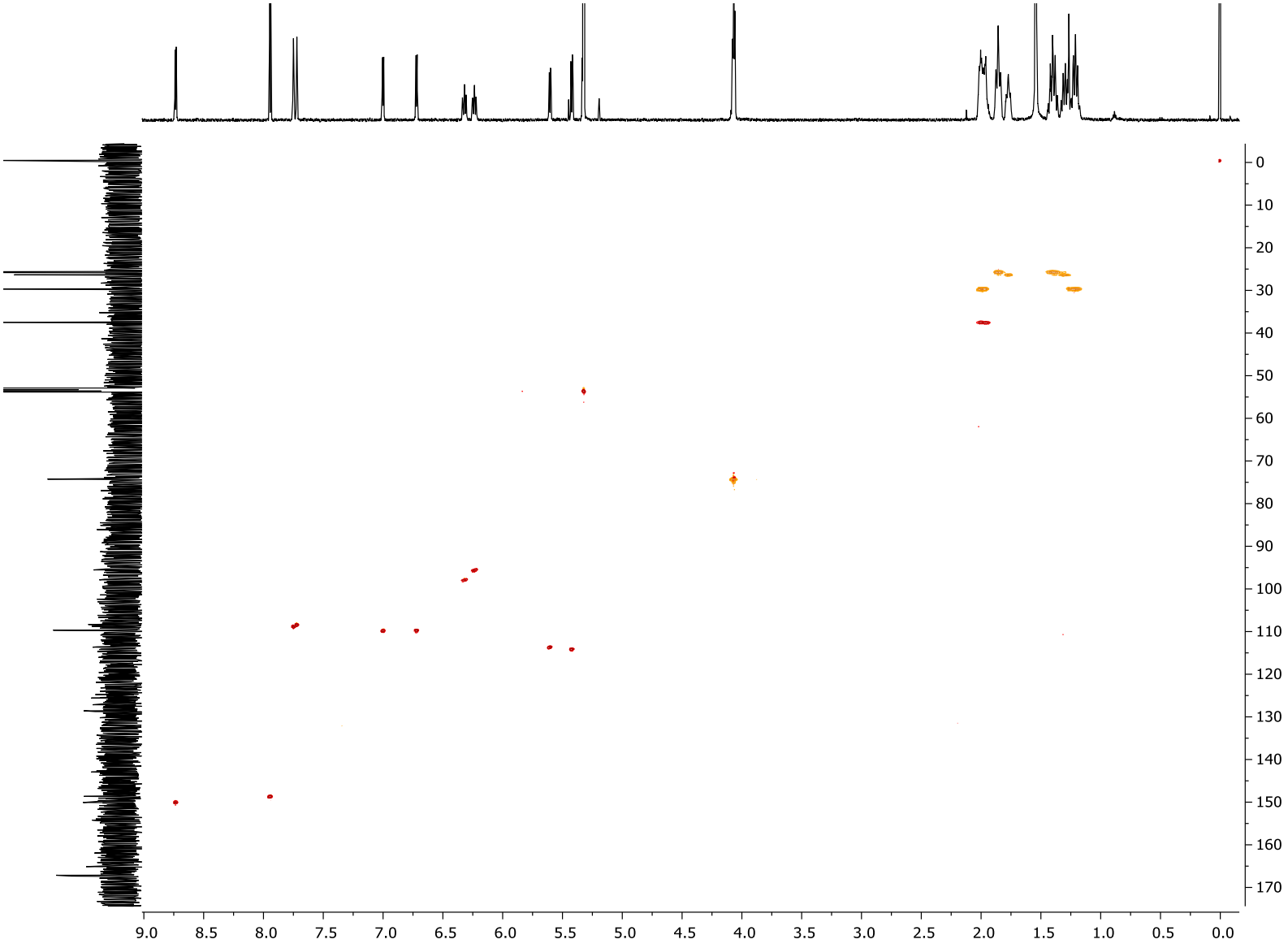

Figure S70. $^{1}H–^{13}C$ HSQC NMR spectrum of **15** in CD_2Cl_2 (TMS).

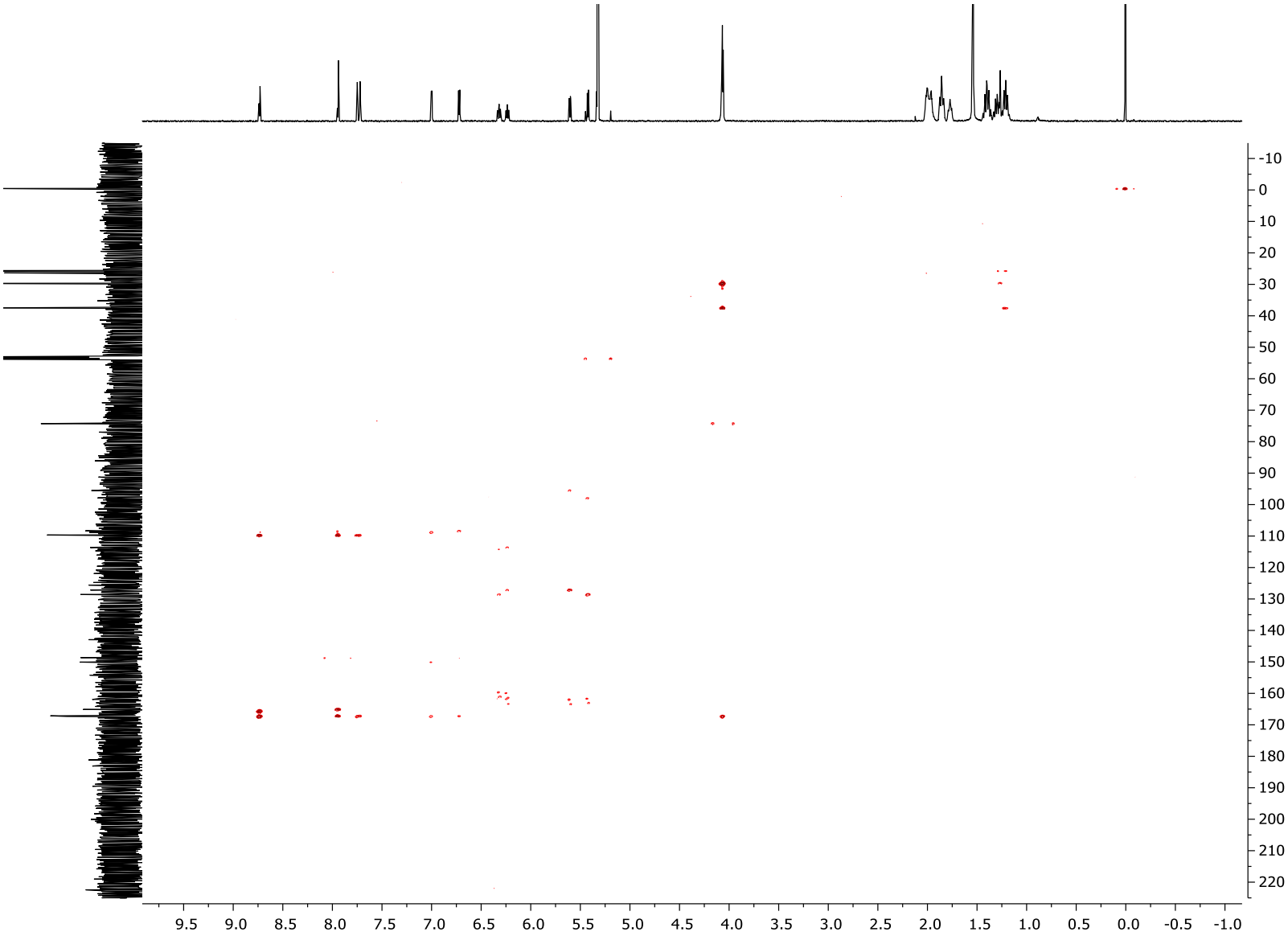

Figure S71. $^{1}H–^{13}C$ HMBC NMR spectrum of **15** in CD_2Cl_2 (TMS).

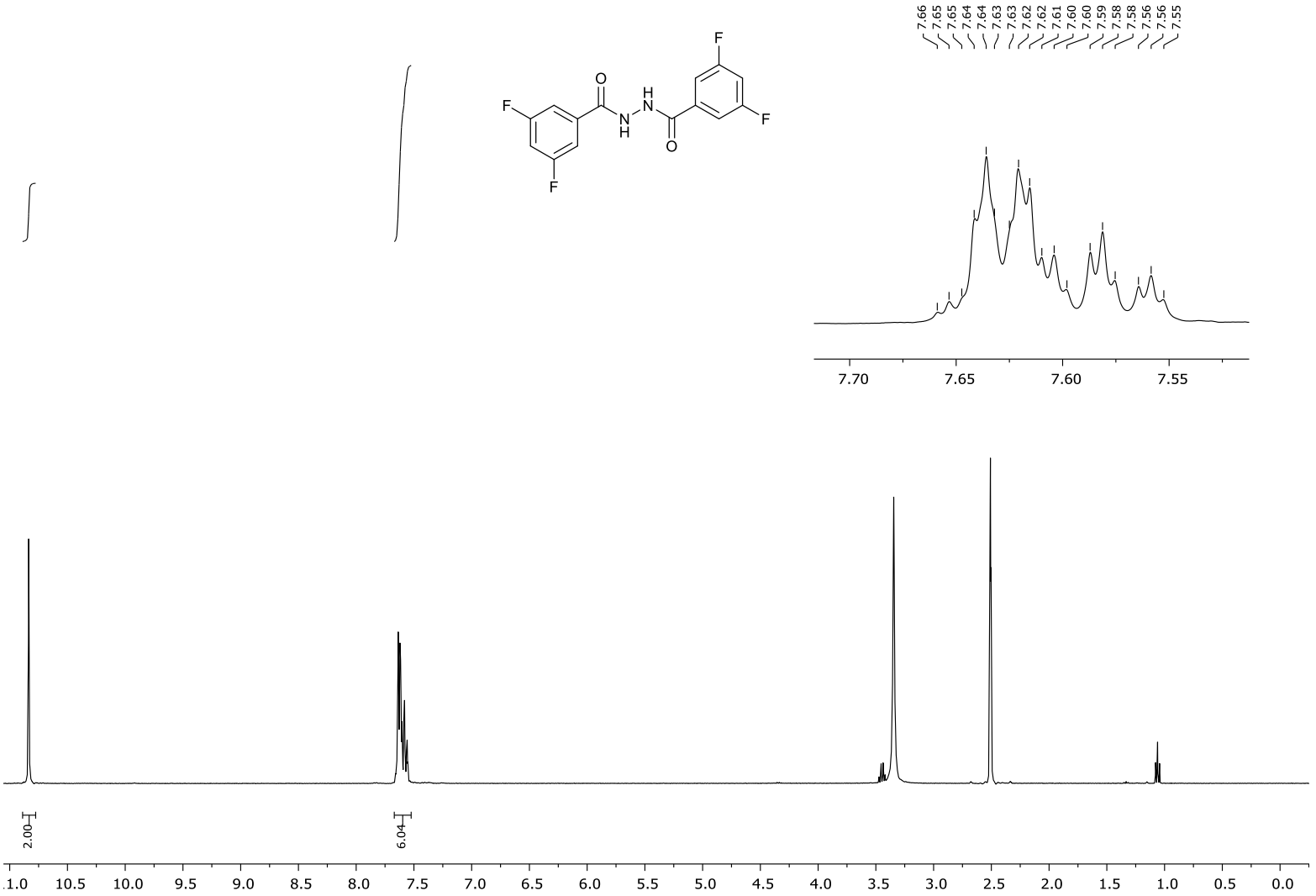

Figure S72. ^{1}H NMR spectrum (400 MHz) of **17a** in DMSO-d_6.

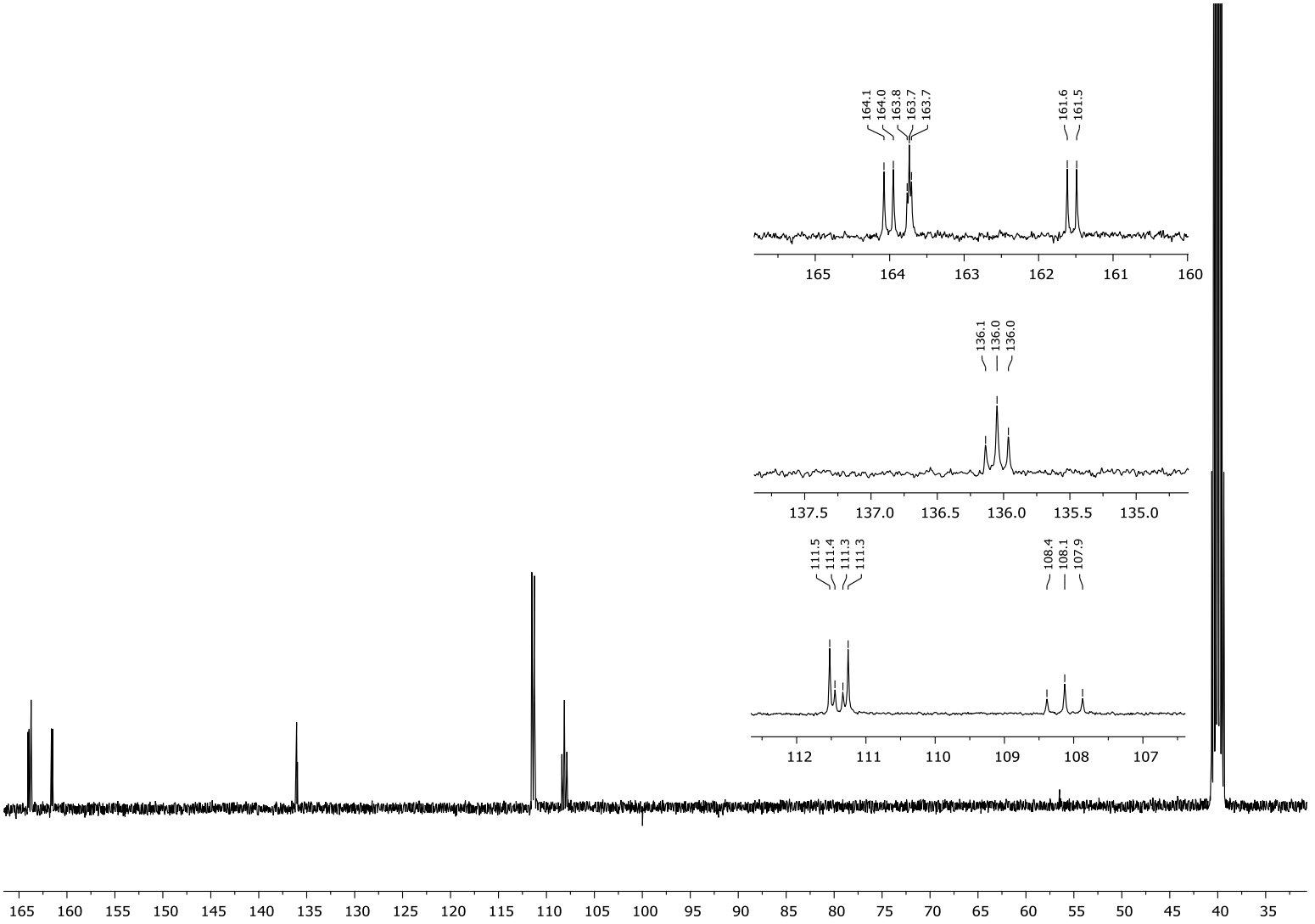

Figure S73. ^{13}C NMR spectrum (101 MHz) of **17a** in DMSO-d_6.

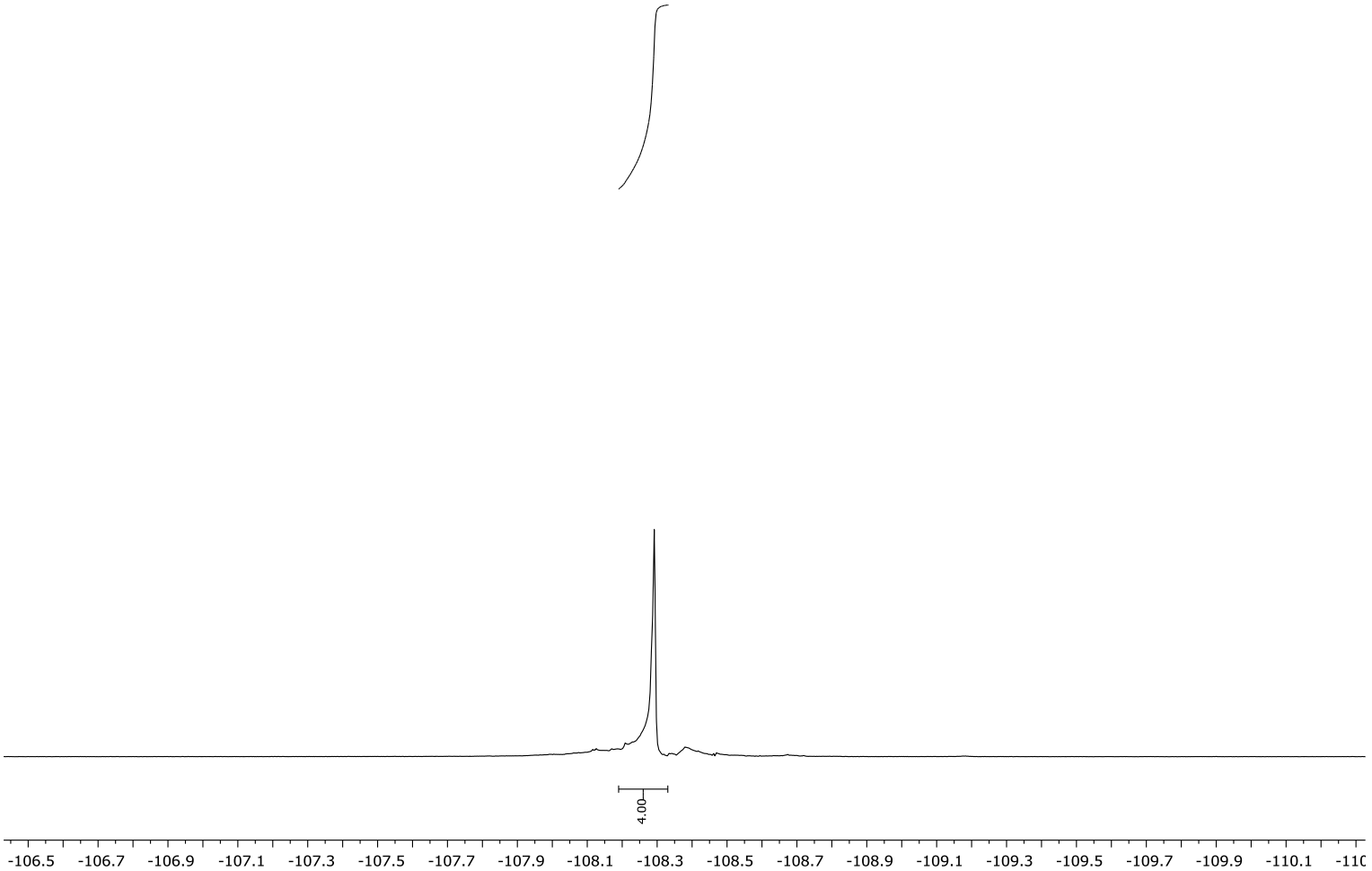

Figure S74. $^{19}F\{^{1}H\}$ NMR spectrum (376 MHz) of **17a** in DMSO-d_6.

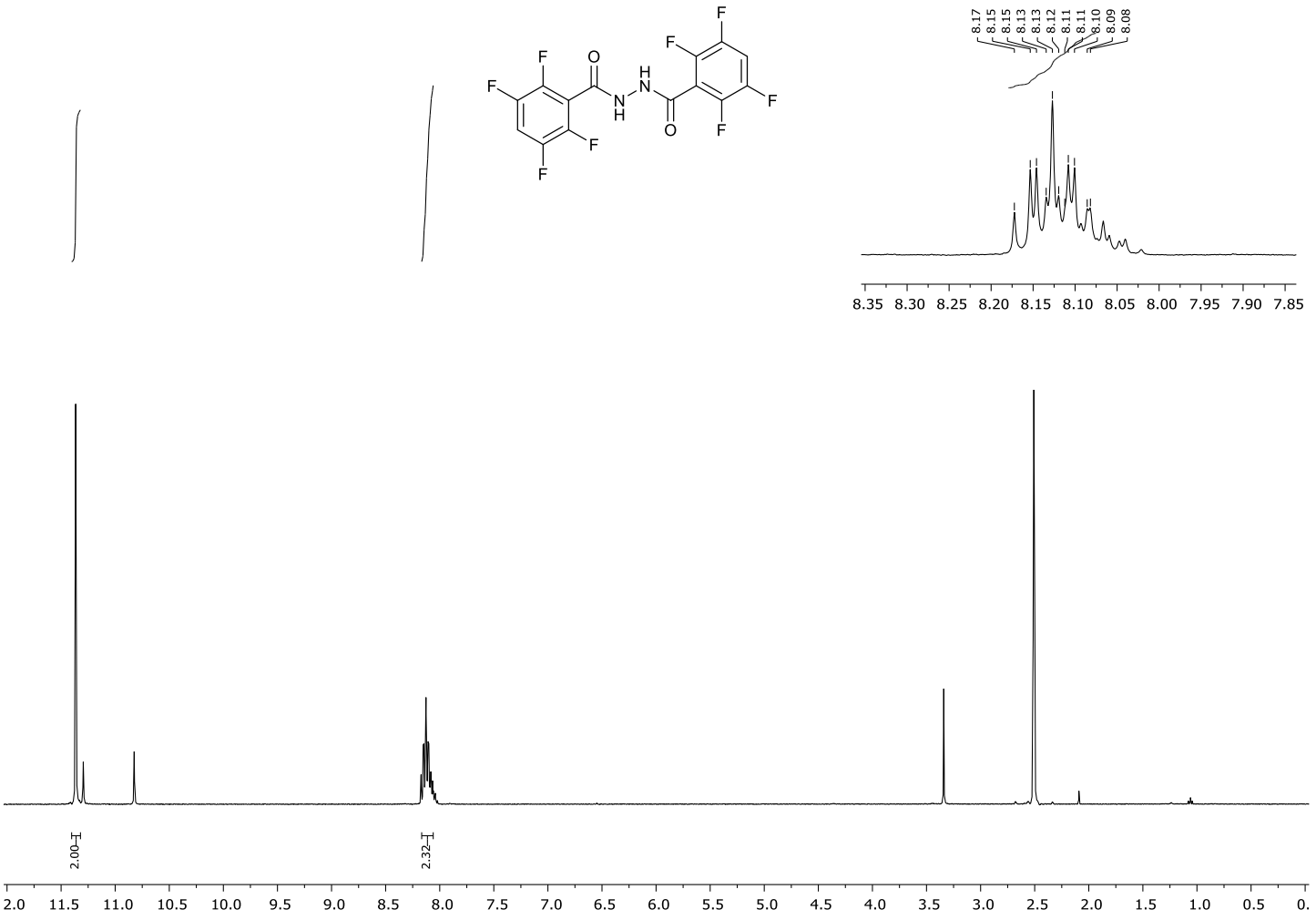

Figure S75. ^{1}H NMR spectrum (400 MHz) of **17b** in DMSO-d_6.

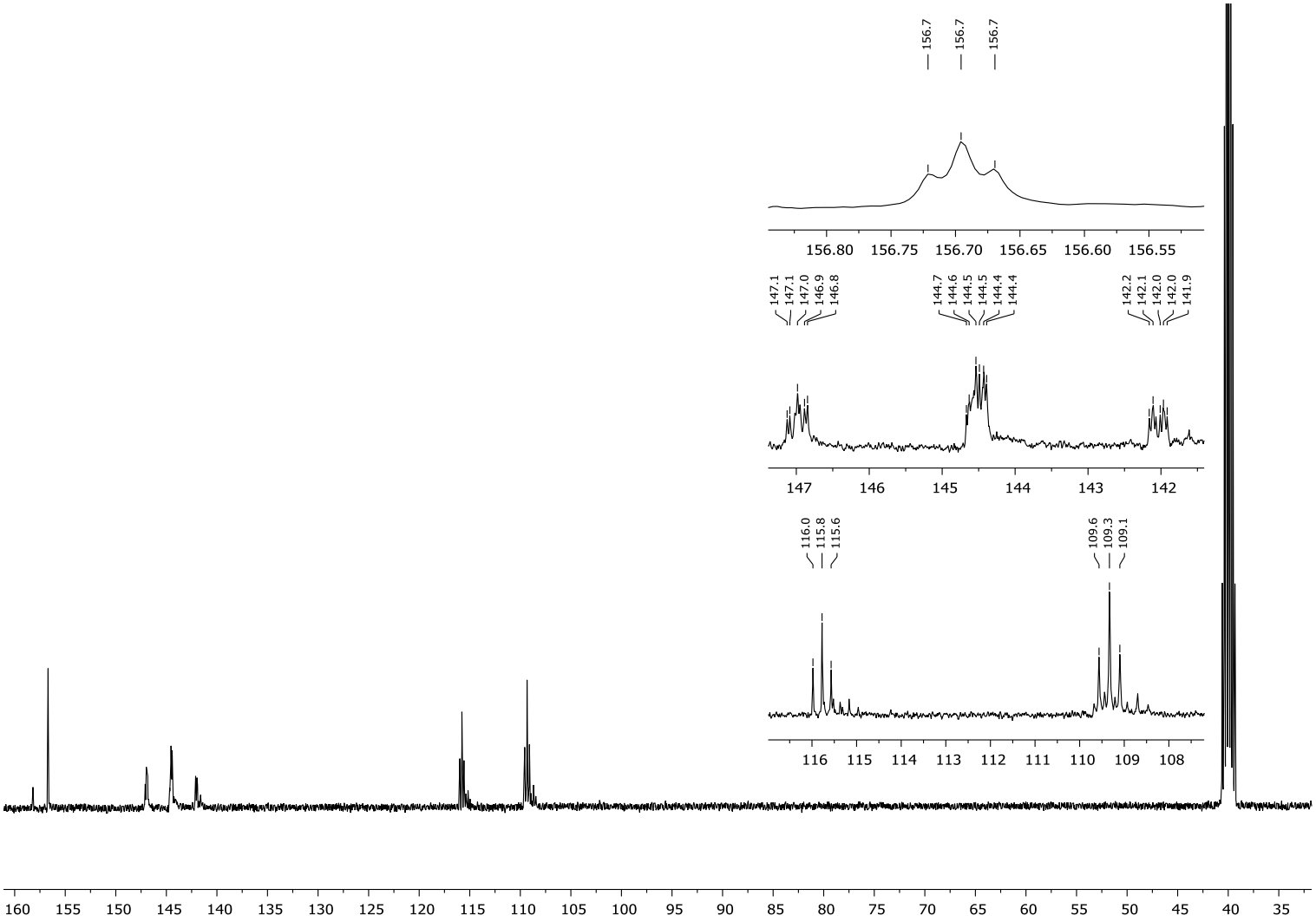

Figure S76. ^{13}C NMR spectrum (101 MHz) of **17b** in DMSO-d_6.

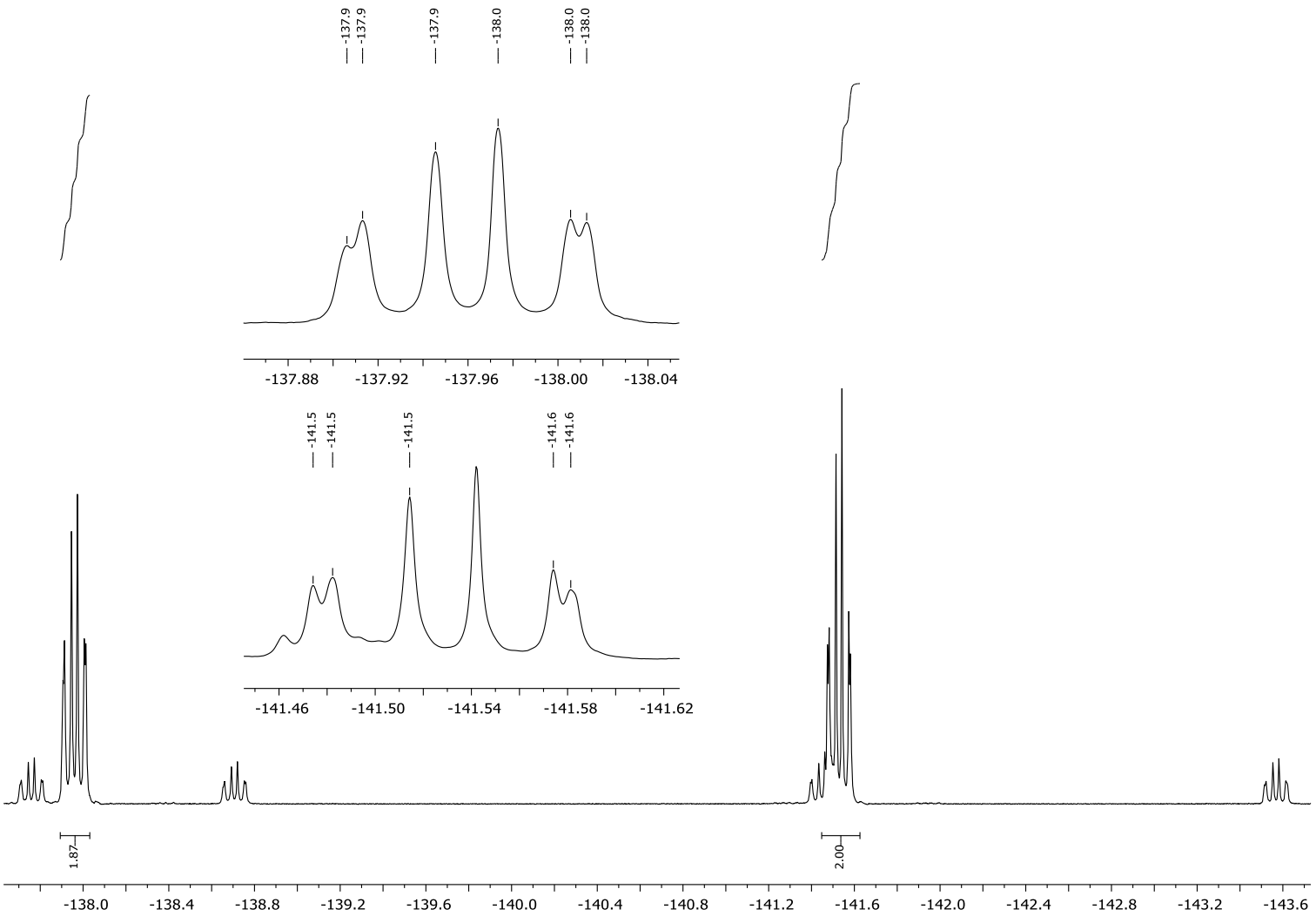

Figure S77. $^{19}F\{^{1}H\}$ NMR spectrum (376 MHz) of **17b** in DMSO-d_6.

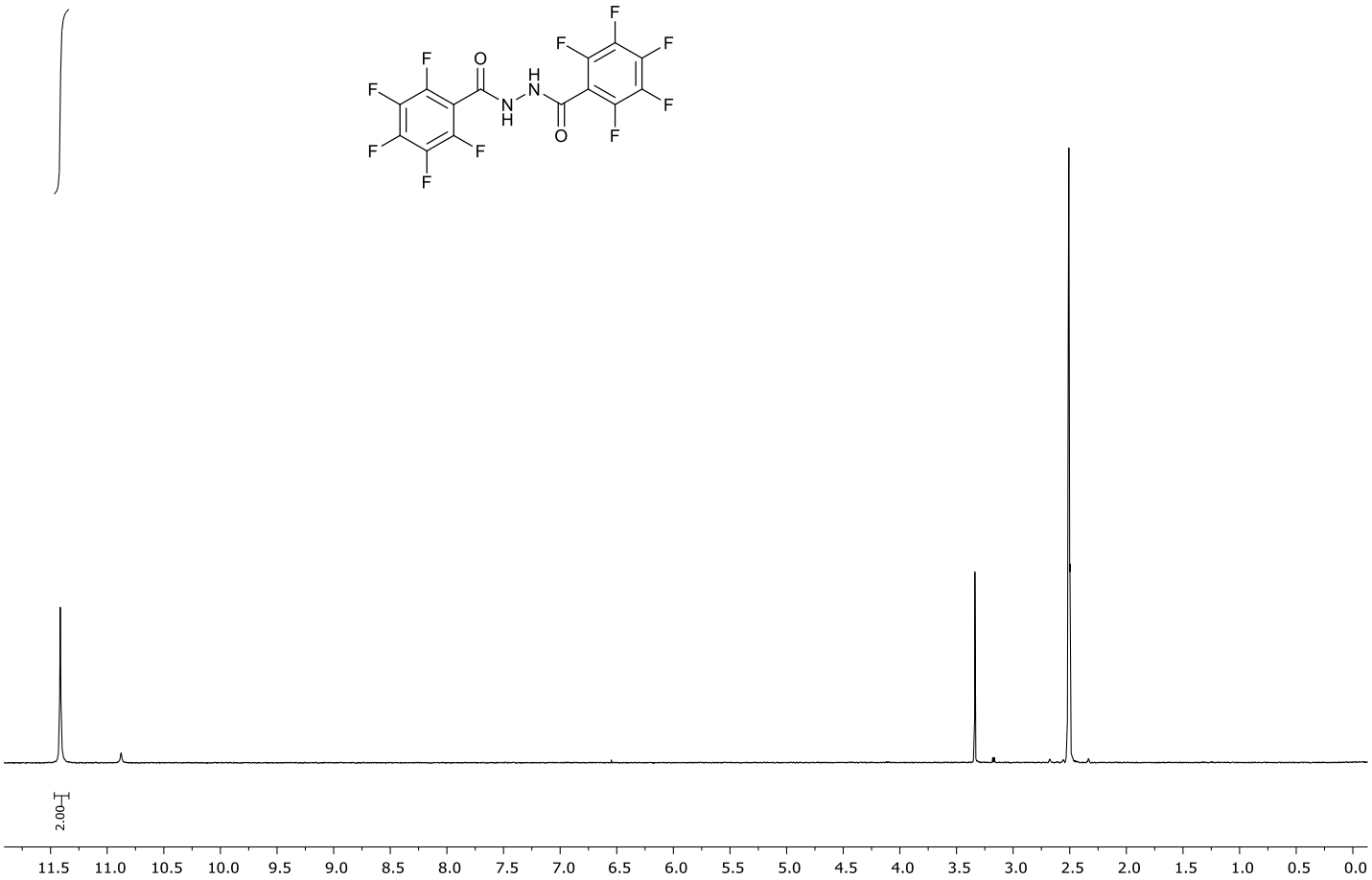

Figure S78. ^{1}H NMR spectrum (400 MHz) of **17c** in DMSO-d_6.

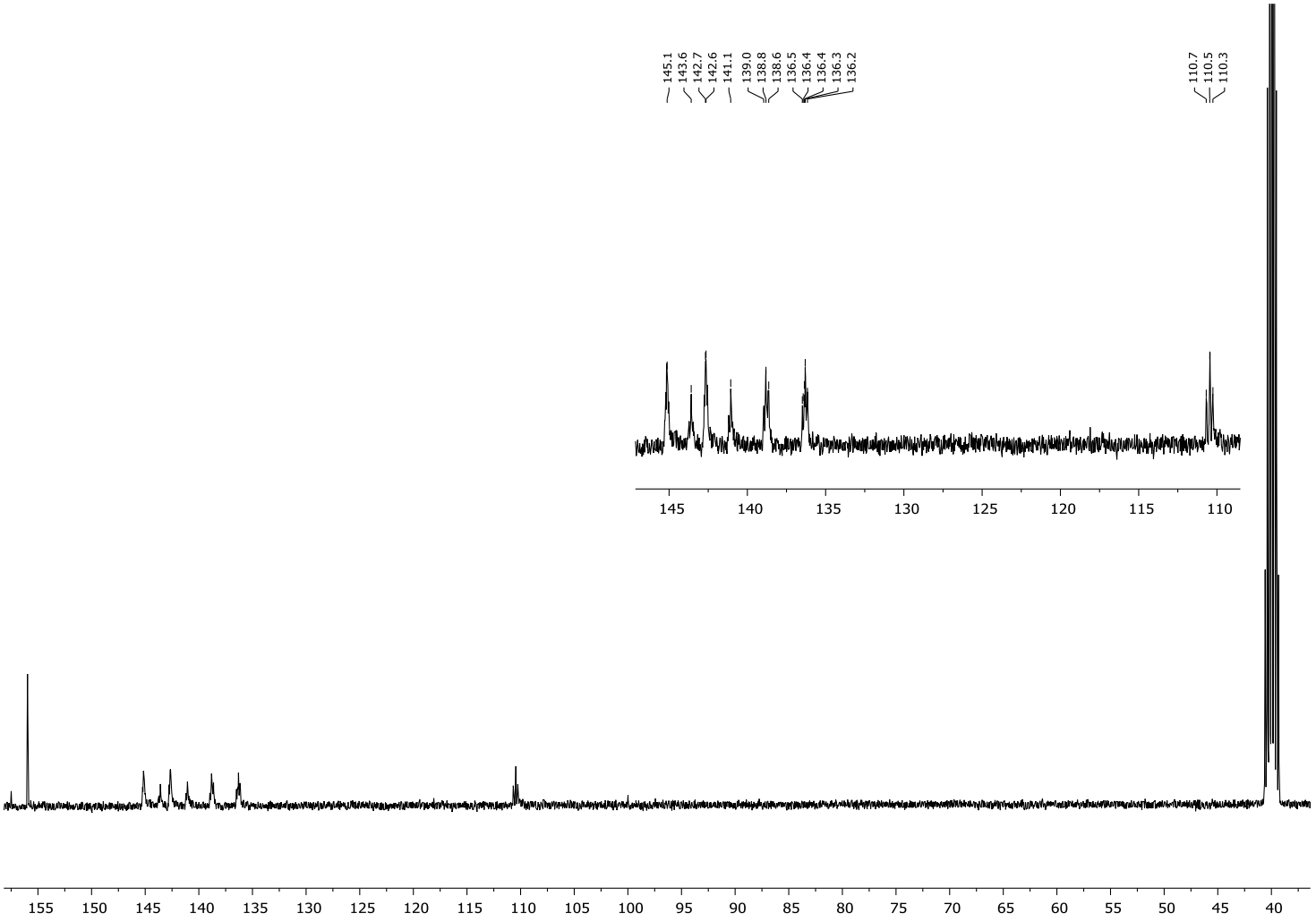

Figure S79. ^{13}C NMR spectrum (101 MHz) of **17c** in DMSO-d_6.

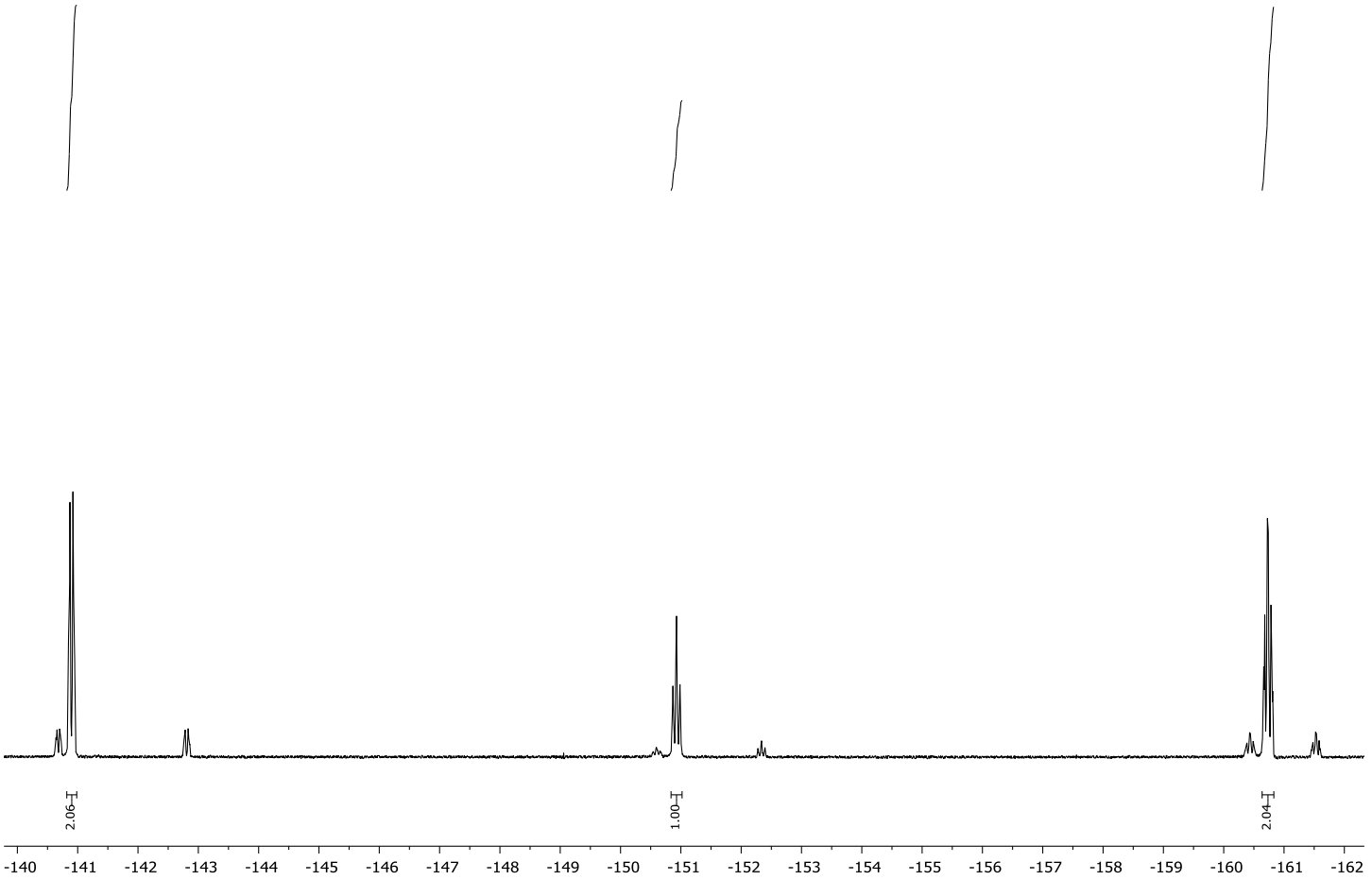

Figure S80. $^{19}F\{^{1}H\}$ NMR spectrum (376 MHz) of **17c** in DMSO-d_6.

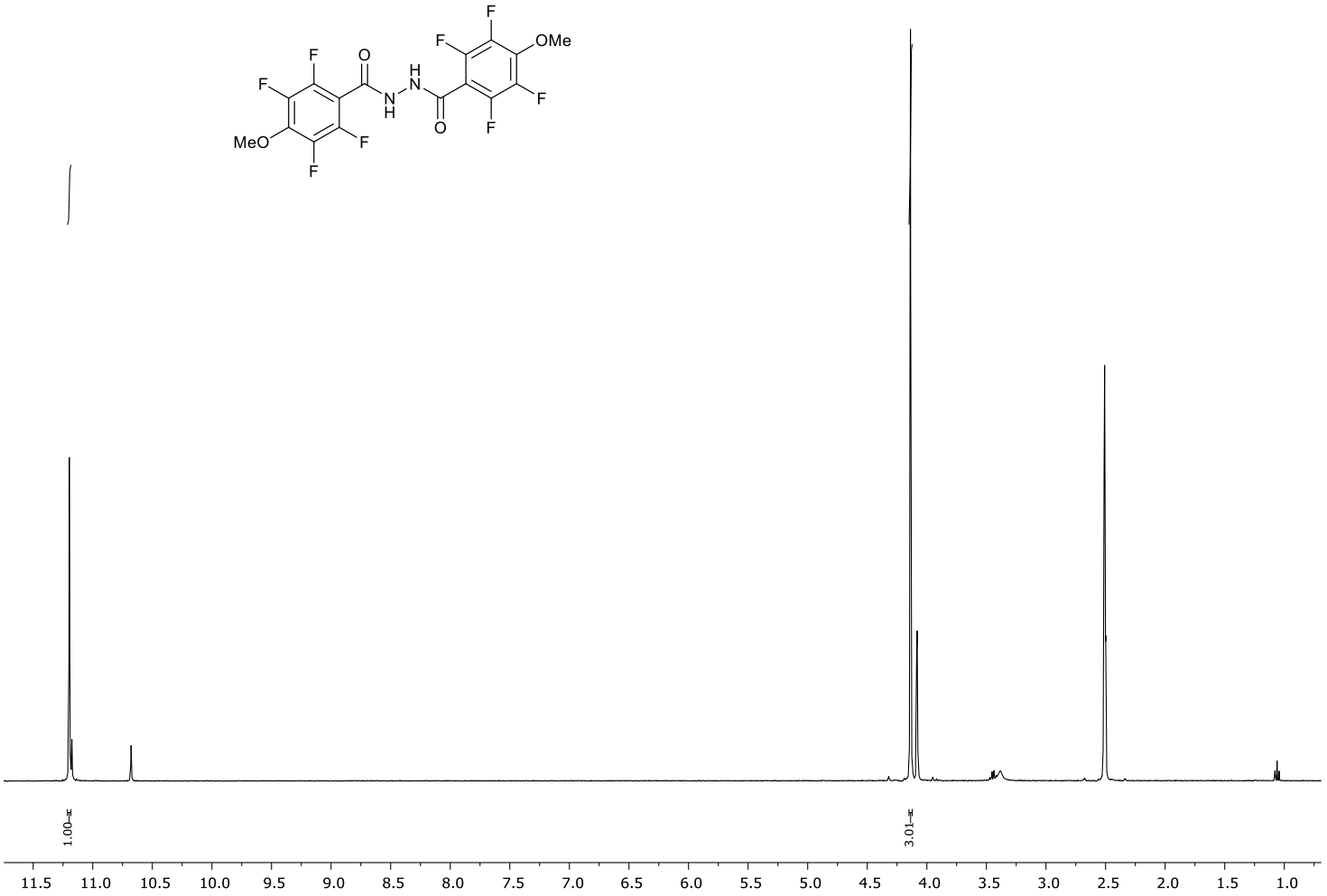

Figure S81. ^{1}H NMR spectrum (400 MHz) of **17d** in DMSO-d_6.

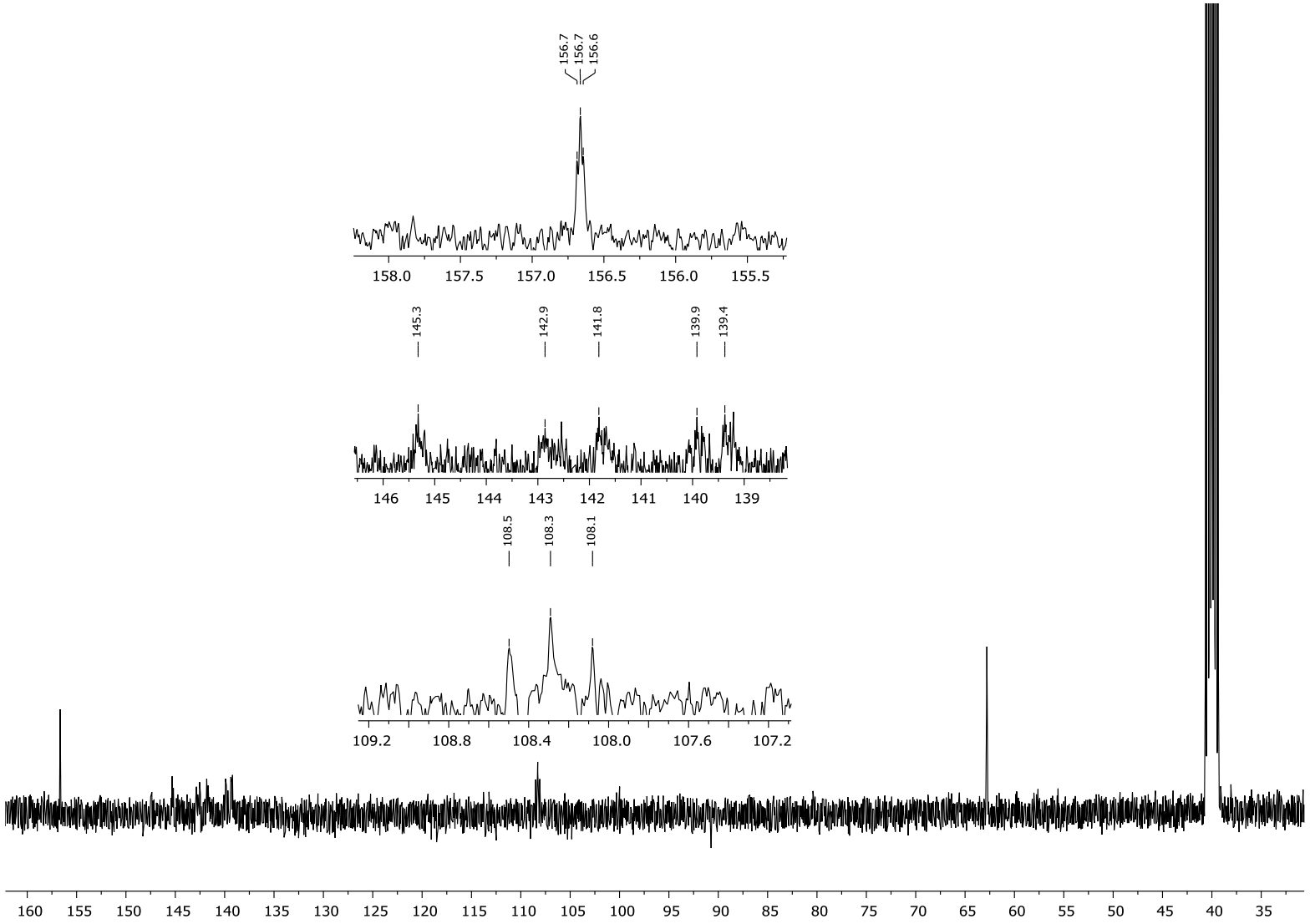

Figure S82. ^{13}C NMR spectrum (101 MHz) of **17d** in DMSO-d_6.

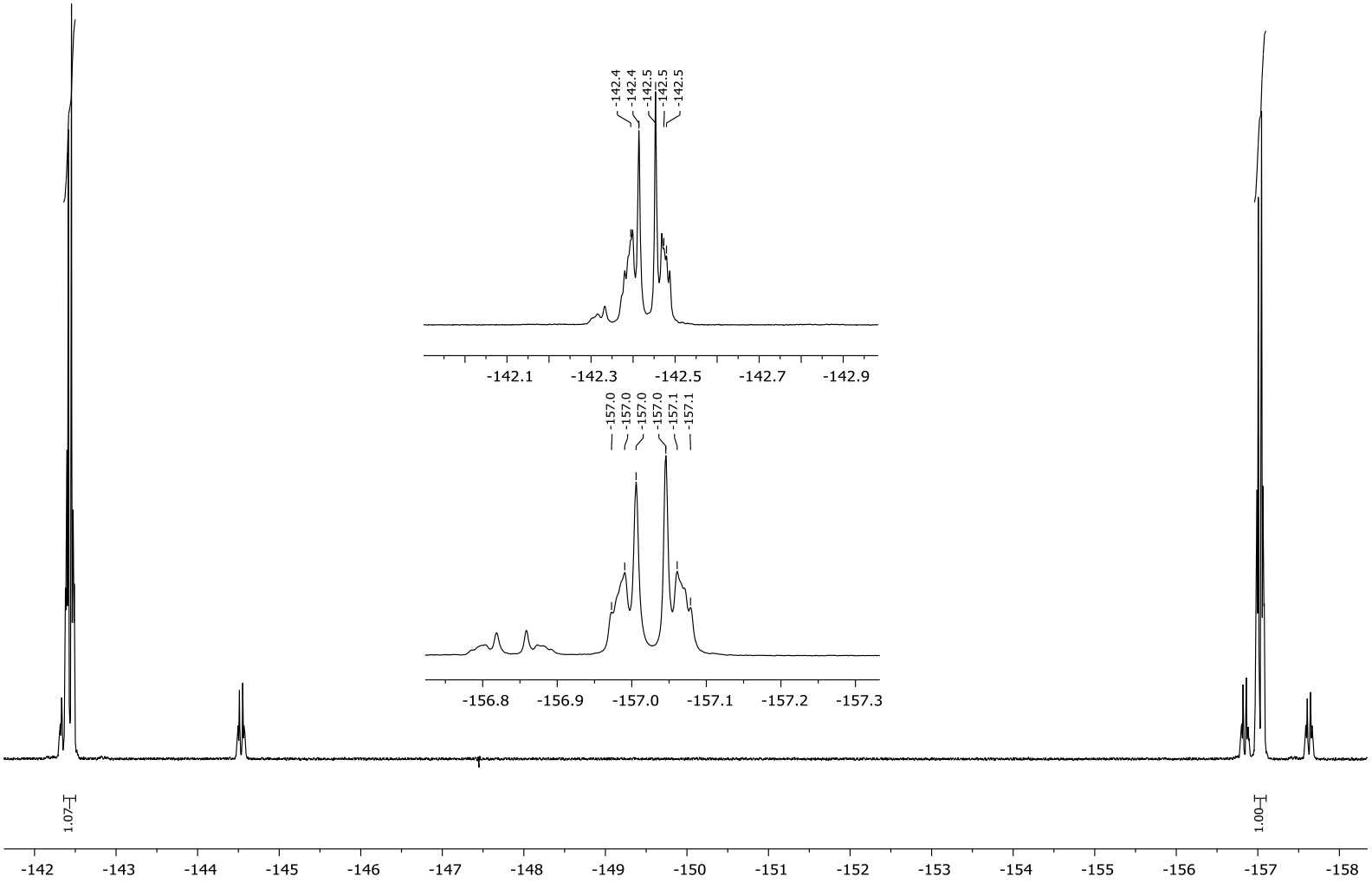

Figure S83. $^{19}F\{^{1}H\}$ NMR spectrum (376 MHz) of **17d** in DMSO-d_6.

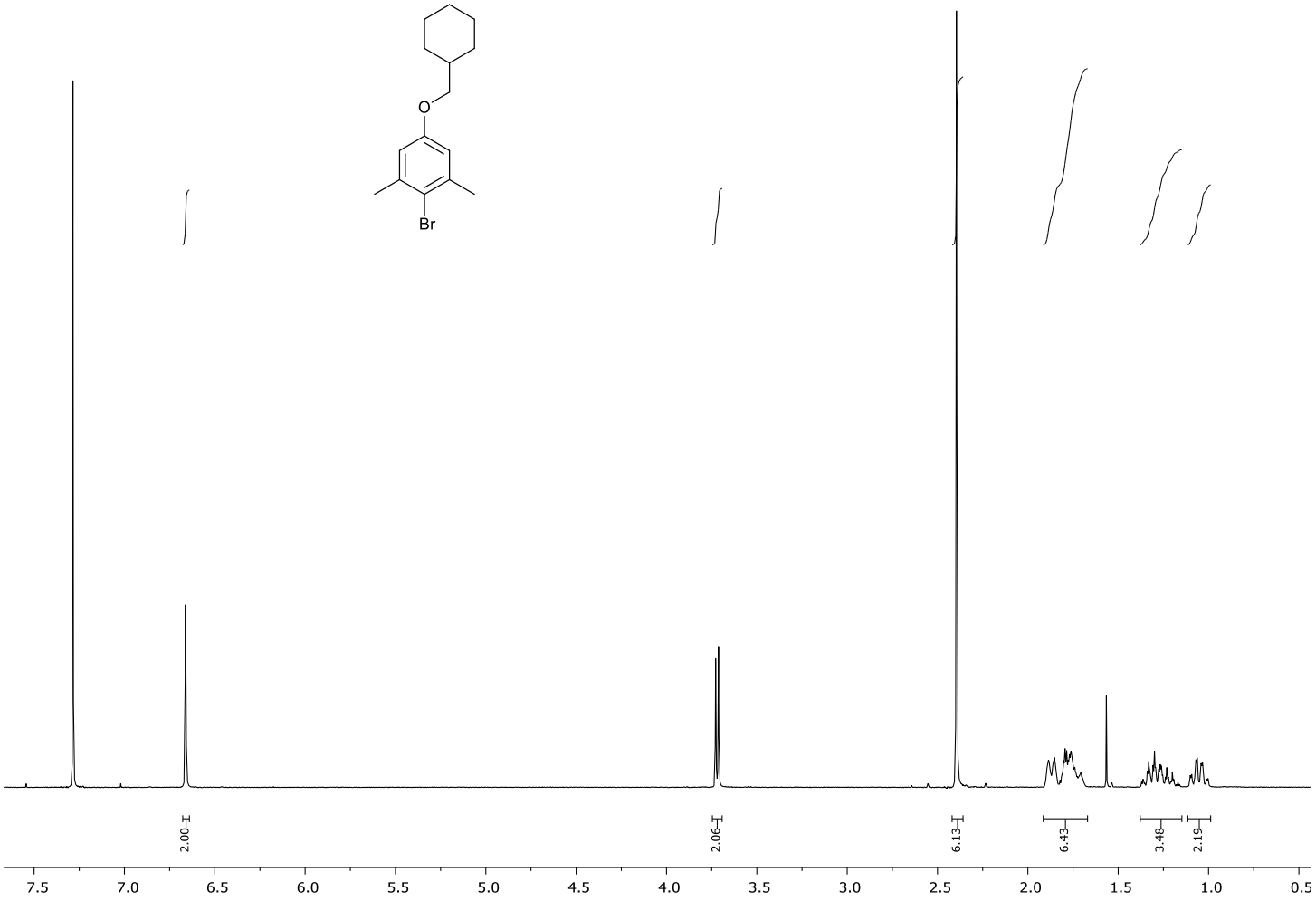

Figure S84. ^{1}H NMR spectrum (400 MHz) of **24** in $CDCl_3$.

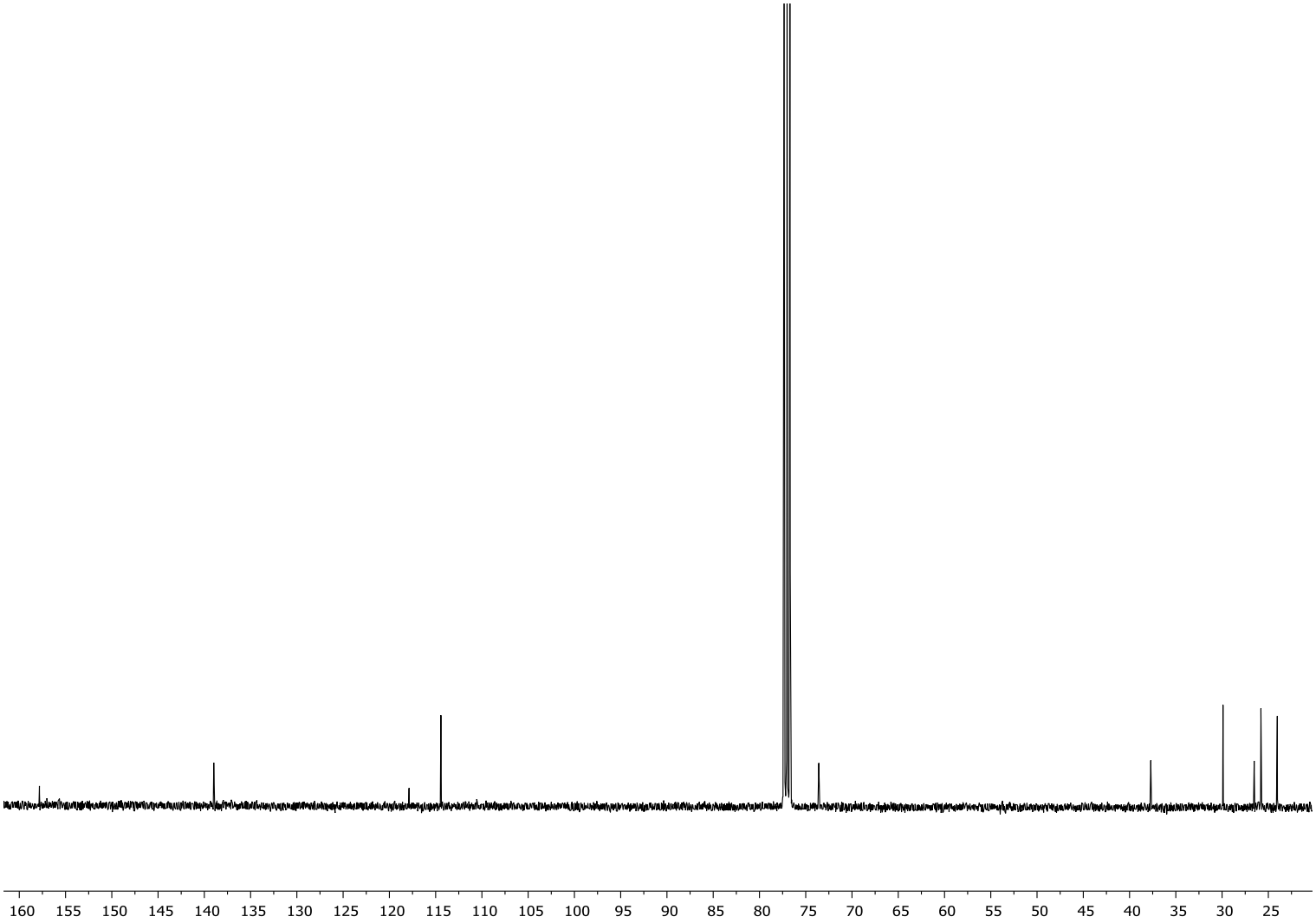

Figure S85. ^{13}C NMR spectrum (101 MHz) of **24** in $CDCl_3$.

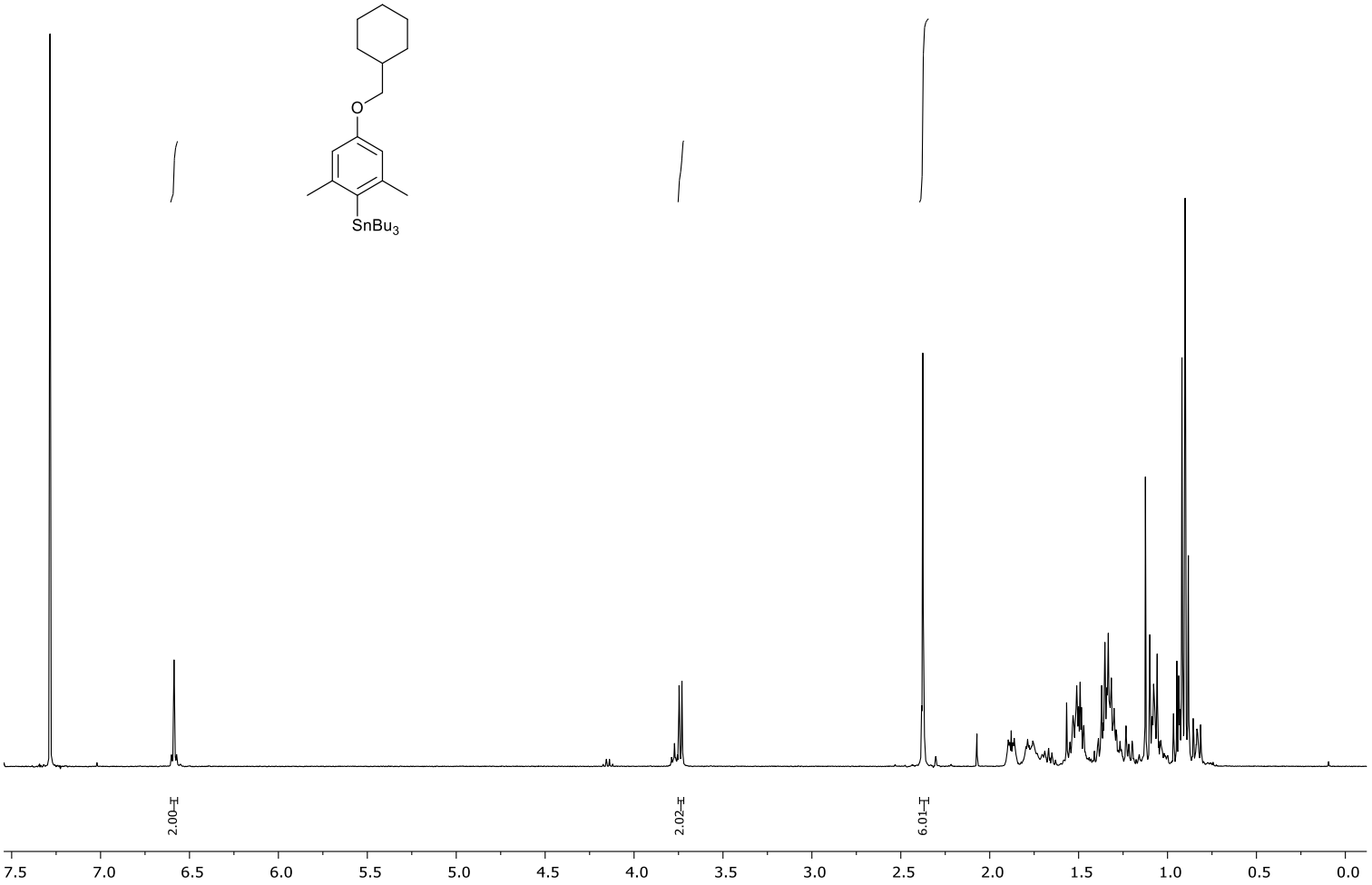

Figure S86. ^{1}H NMR spectrum (400 MHz) of **25** in $CDCl_3$.

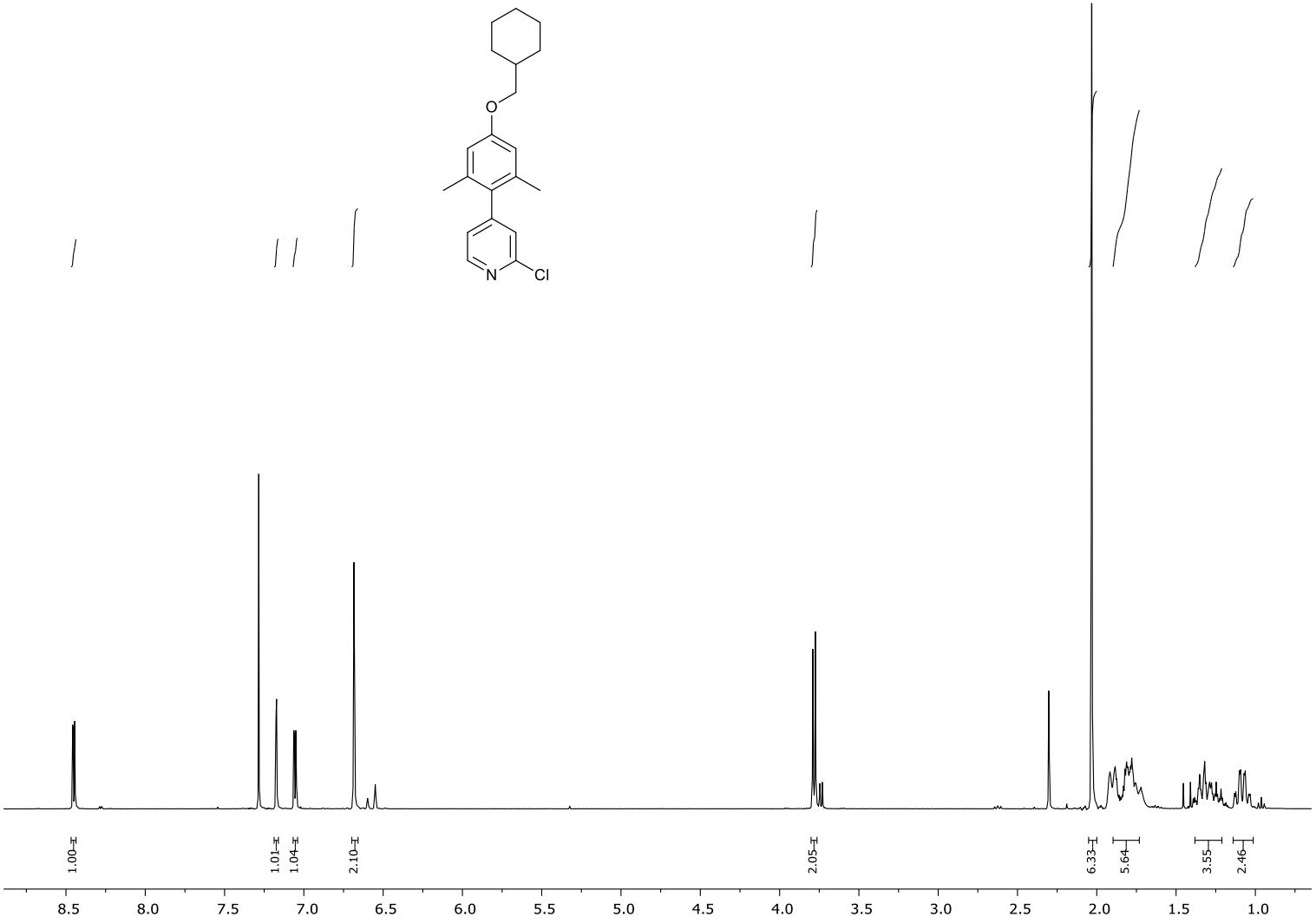

Figure S87. ^{1}H NMR spectrum (400 MHz) of **26** in $CDCl_3$.

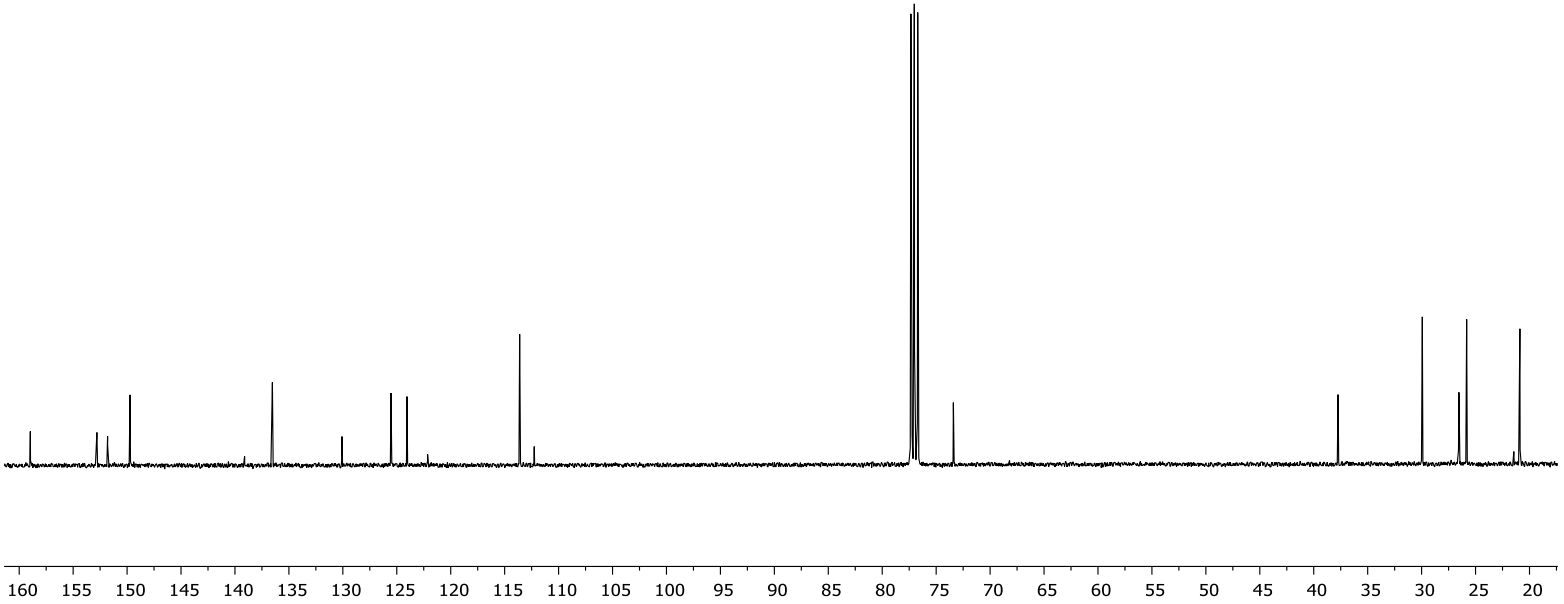

Figure S88. ^{13}C NMR spectrum (101 MHz) of **26** in $CDCl_3$.

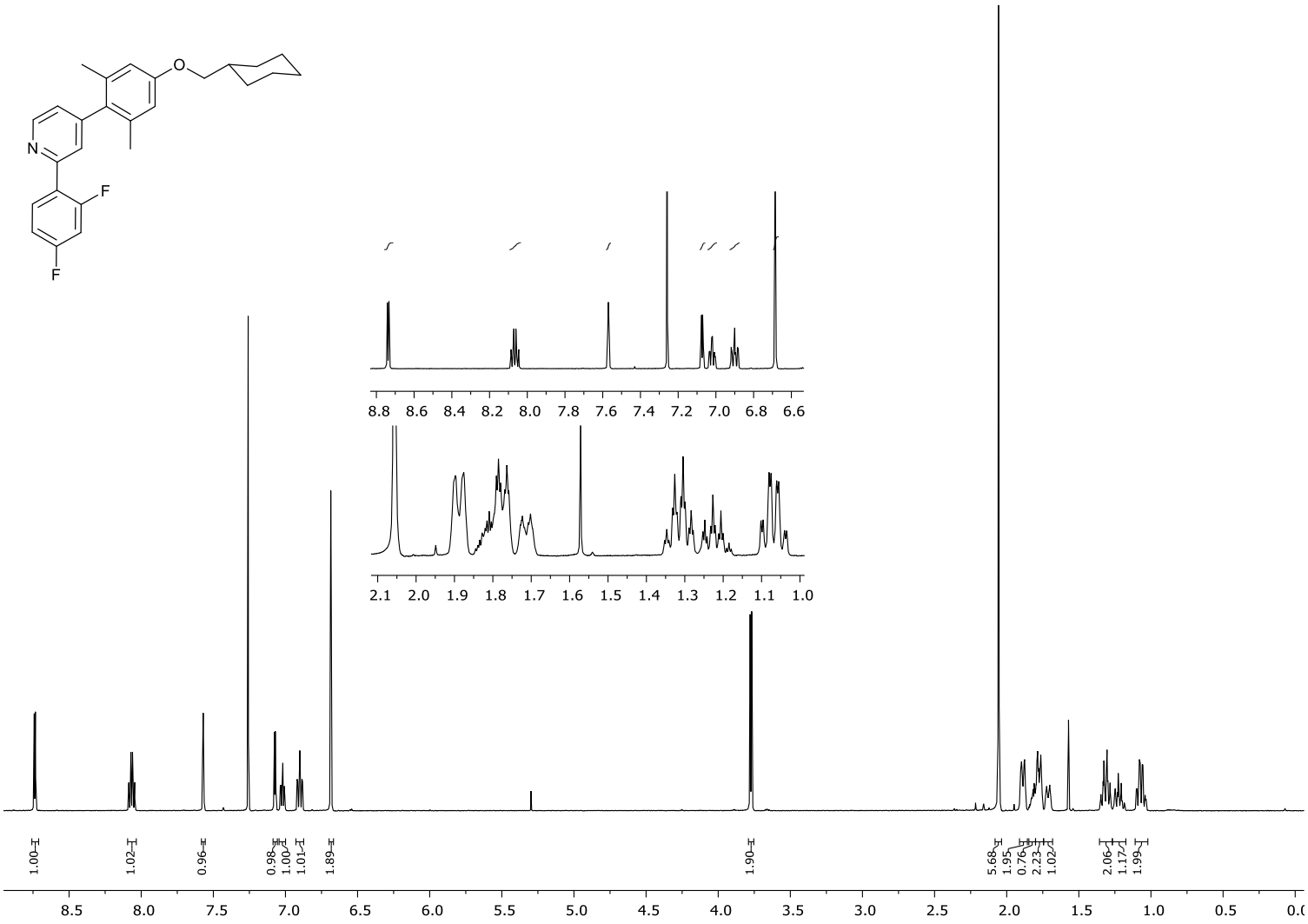

Figure S89. ^{1}H NMR spectrum (600 MHz) of **21** in $CDCl_3$.

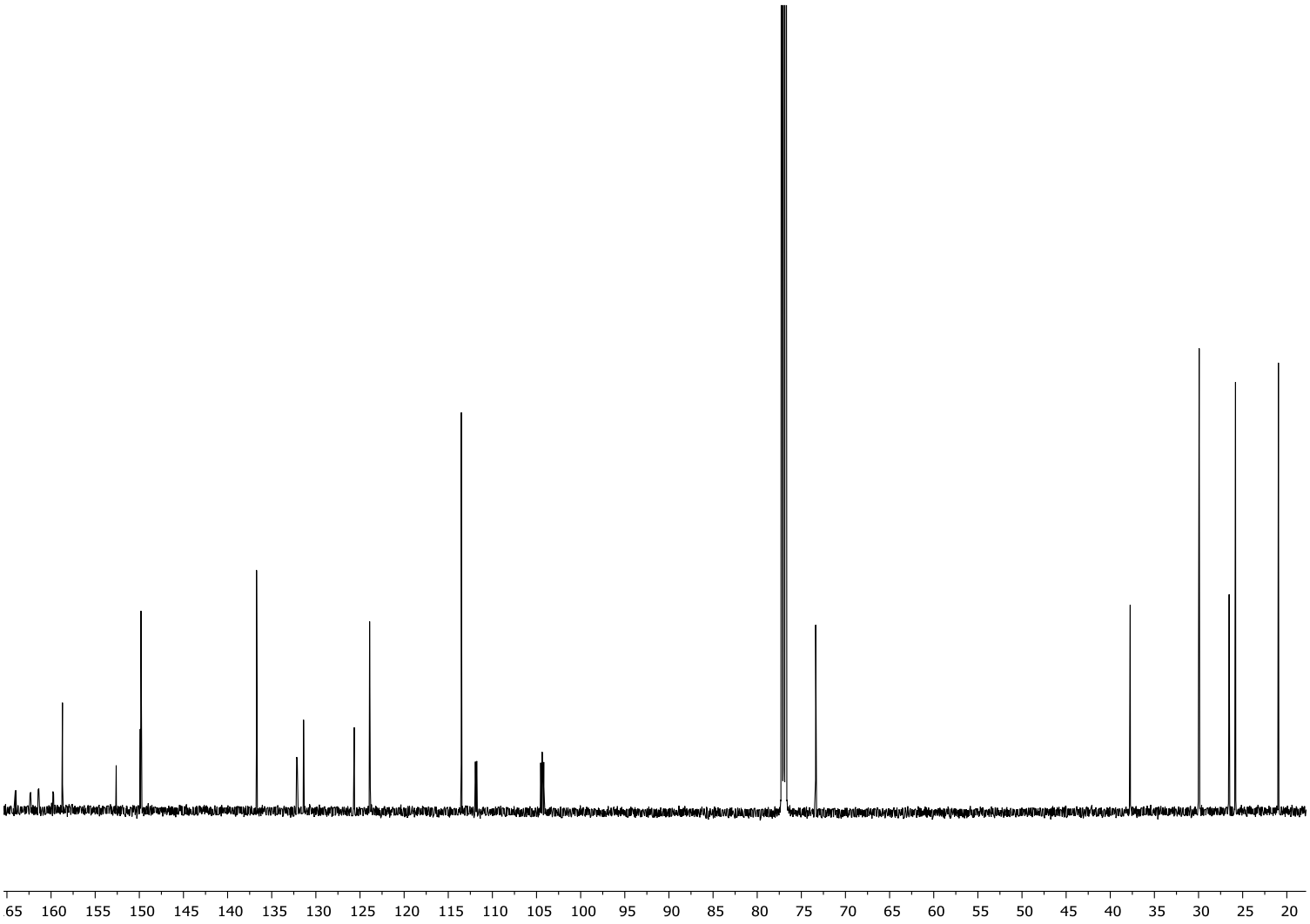

Figure S90. ^{13}C NMR spectrum (151 MHz) of **21** in $CDCl_3$.

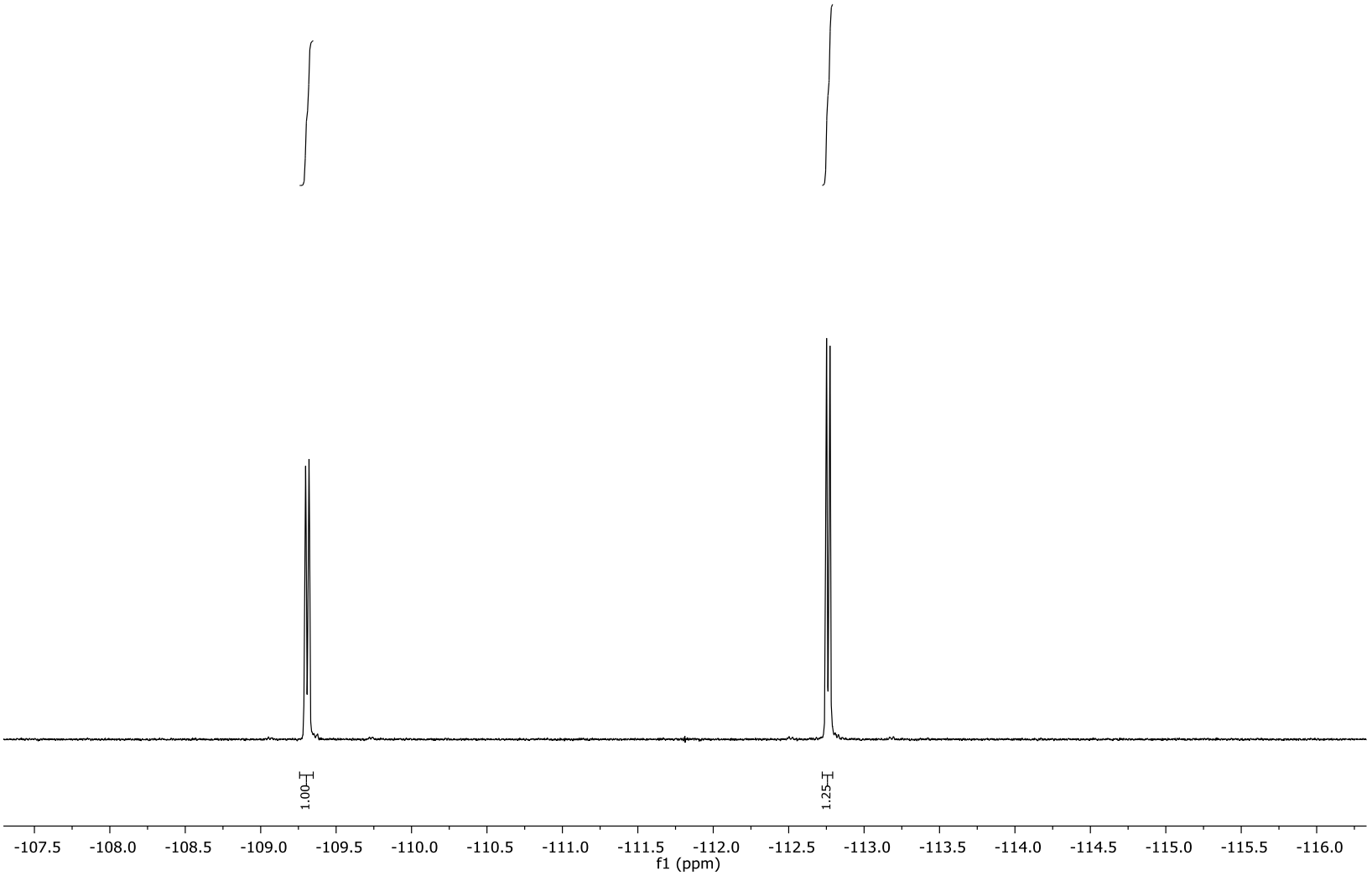

Figure S91. $^{19}F\{^{1}H\}$ NMR spectrum (376 MHz) of **22** in $CDCl_3$.

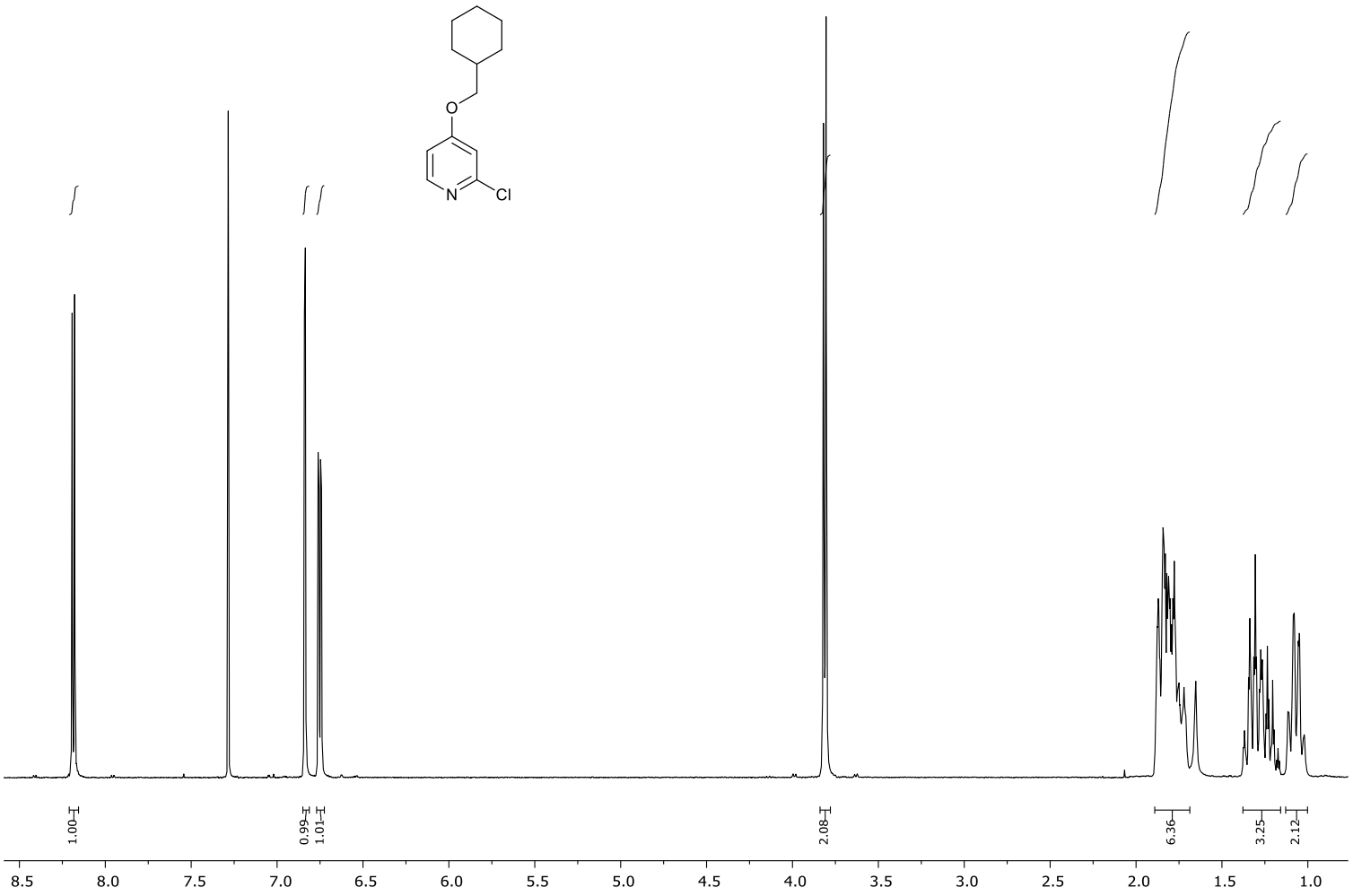

Figure S92. ^{1}H NMR spectrum (400 MHz) of **28** in $CDCl_3$.

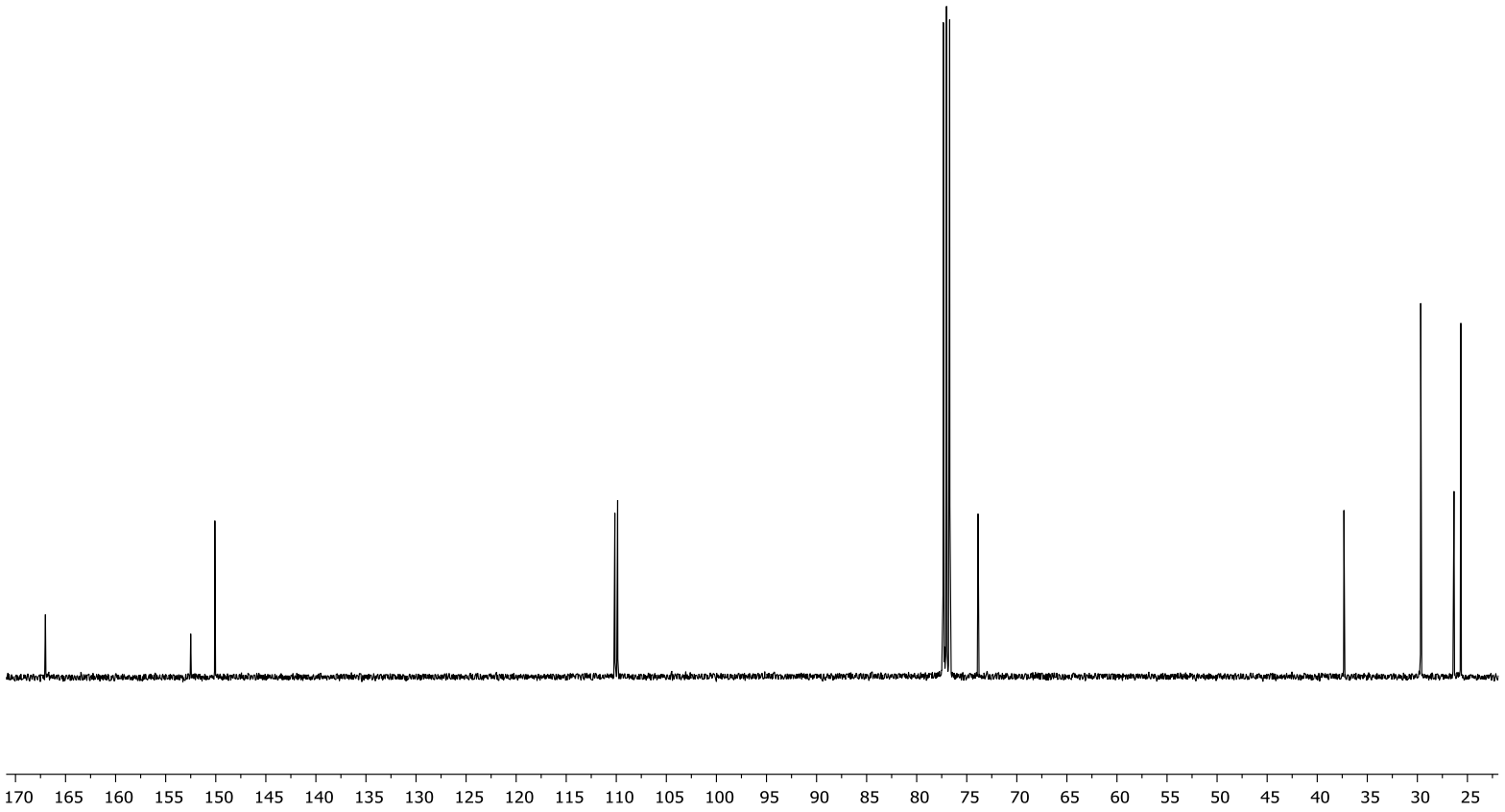

Figure S93. ^{13}C NMR spectrum (101 MHz) of **28** in $CDCl_3$.

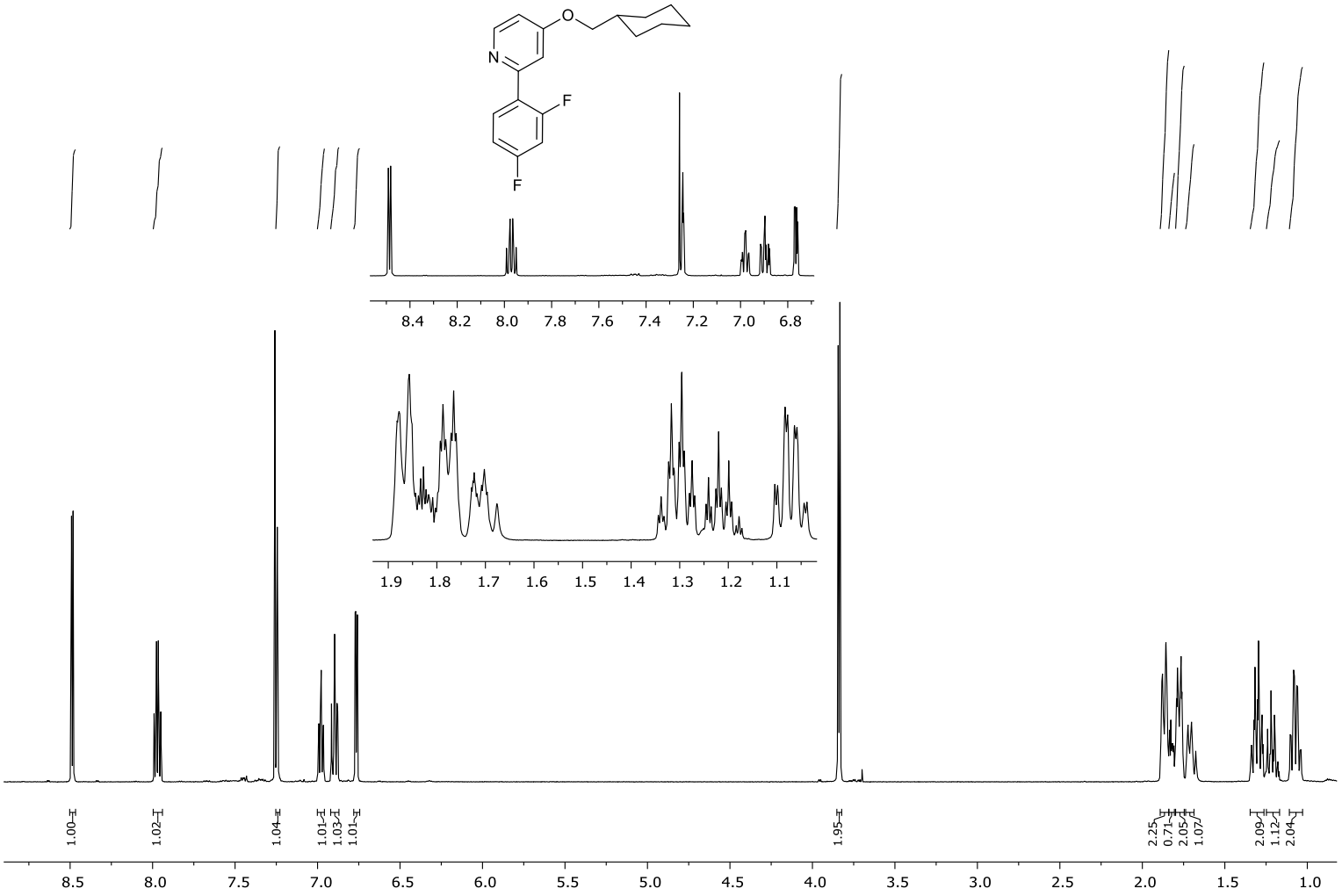

Figure S94. ^{1}H NMR spectrum (600 MHz) of **22** in $CDCl_3$.

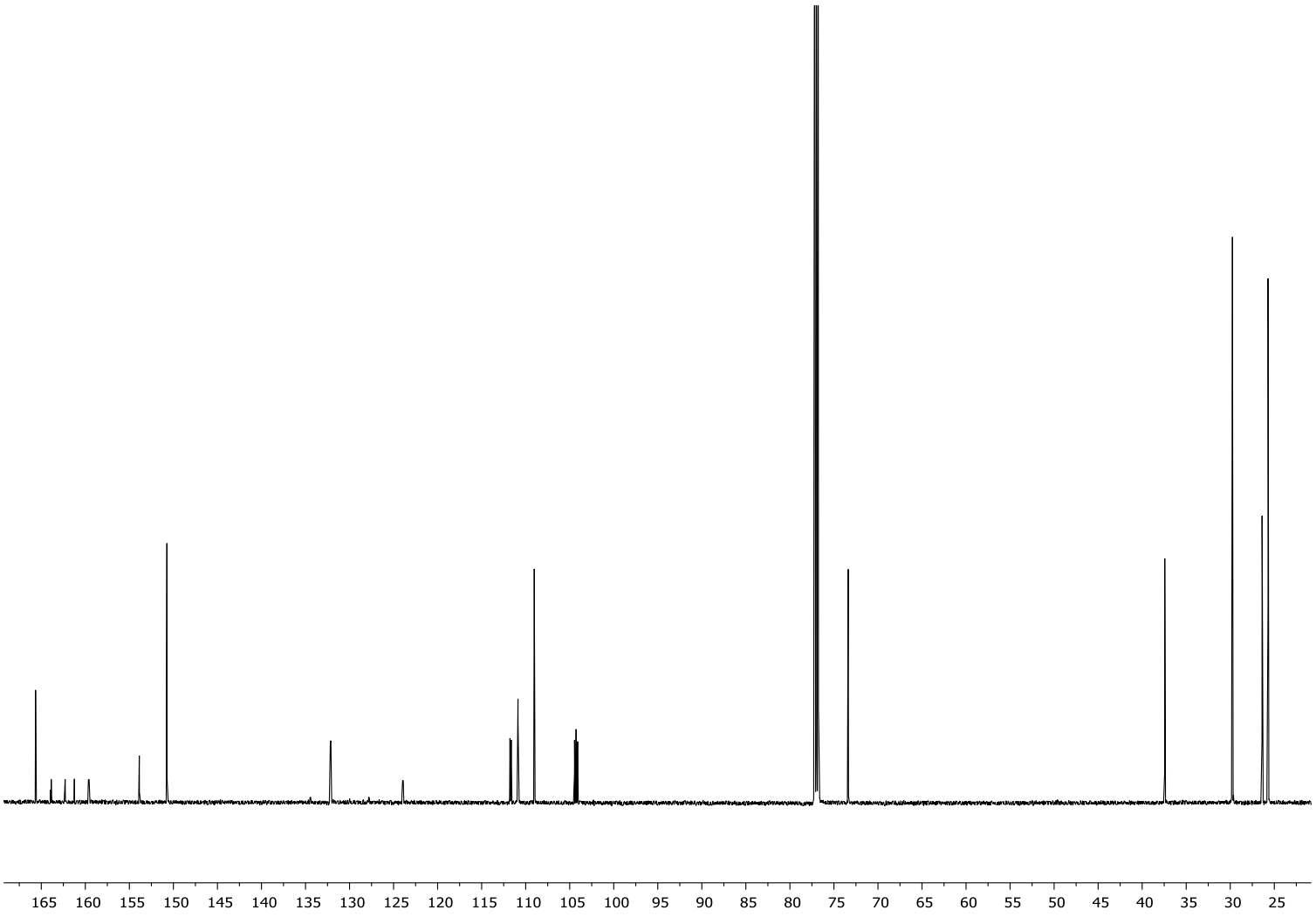

Figure S95. ^{13}C NMR spectrum (151 MHz) of **22** in $CDCl_3$.

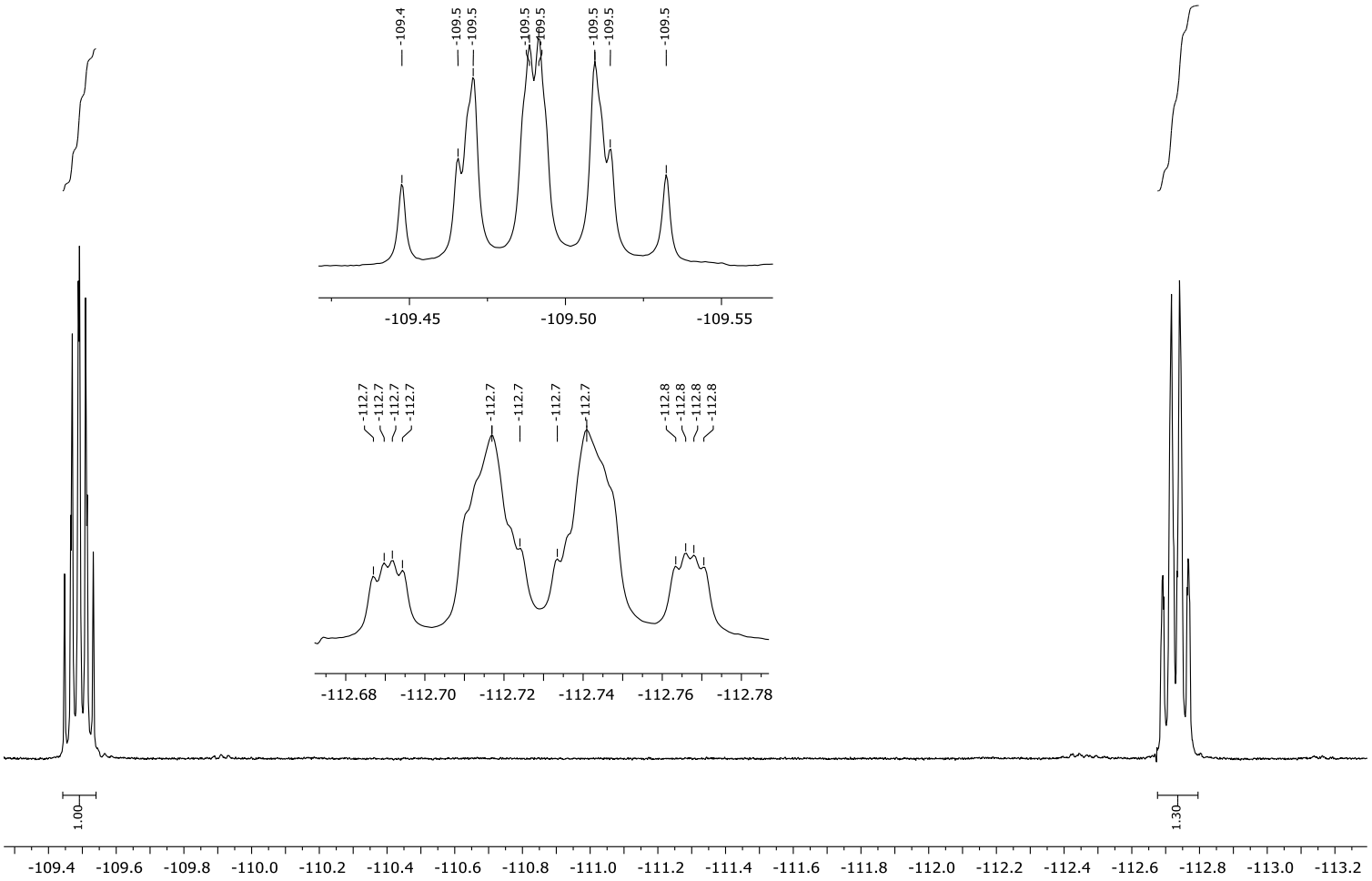

Figure S96. $^{19}F\{^{1}H\}$ NMR spectrum (376 MHz) of **22** in $CDCl_3$

X–ray Crystallography

Table S1. Selected geometrical parameters of diiridium complexes (bond distances averaged, in Å).

CCDC numbers are as follows: **7** $3CH_2Cl_2$ = 1576081, **9** = 1576082, α-**10** = 1576083, β-**10** = 1576084, **11** $2CH_2Cl_2$ = 1576093, **12** $5CH_2Cl_2$ = 1576094, **13** $2.25CD_2Cl_2$ = 1576095**.**

	7 $3CH_2Cl_2$	**9**	α-**10**	β-**10**	**11** $2CH_2Cl_2$	**12** $5CH_2Cl_2$[a]	**13** $2.25CD_2Cl_2$
Space group	$P\bar{1}$	$I4_1/a$	$C2/c$	$P2_1/n$	$P\bar{1}$	$P\bar{1}$	$P\bar{1}$
Molec. symm	C_i	C_i	C_2	--	--	C_i	--
Ir centres	ΔΛ	ΔΛ	ΔΔ, ΛΛ	ΔΔ, ΛΛ	ΔΔ, ΛΛ	ΔΛ	ΔΔ, ΛΛ
Ir…Ir, Å	5.091	5.089	5.117	5.062	5.082	5.147, 5.152	5.070
Ir-C (*trans*-O)	1.998(2)	2.006(6)	2.001(2)	1.994(4)	1.992(7)	1.994(3)	1.988(4)
Ir-C (*trans*-N)	2.001(2)	1.994(6)	1.997(2)	2.002(4)	2.000(7)	1.992(3)	1.996(4)
Ir-N, stacked	2.032(2)	2.005(6)	2.040(1)	2.033(3)	2.033(5)	2.029(3)	2.035(3)
Ir-N, non-stacked	2.042(2)	1.973(6)	2.044(1)	2.031(3)	2.037(5)	2.042(3)	2.031(3)
OCNNCO folding, °	planar	planar	6.8	24.3	14.3	planar	17.9
Ir displacement, Å	0.01	0.23	0.06	0.28, 0.39	0.26, 0.20	0.52, 0.00	0.17, 0.24
Ir-O	2.152(2)	2.161(2)	2.156(1)	2.147(3)	2.142(5)	2.144(2)	2.127(3)
Ir-N	2.171(2)	2.170(3)	2.180(1)	2.164(3)	2.169(5)	2.214(2)	2.175(3)
N-N	1.438(3)	1.435(5)	1.439(2)	1.443(4)	1.448(6)	1.445(2)	1.436(4)
N-C	1.312(3)	1.308(4)	1.314(2)	1.307(5)	1.305(8)	1.310(4)	1.301(5)
C-O	1.286(2)	1.279(4)	1.283(2)	1.275(4)	1.279(8)	1.268(4)	1.278(4)
Θ, °[b]	8.5	5.9	13.5	6.9, 8.7	4.6, 6.0	--	6.2, 3.4
D, Å[c]	3.32	3.24	3.42	3.39, 3.35	3.33, 3.30	--	3.27, 3.19

[a] contains two crystallographically non-equivalent centrosymmetric dimers; [b] interplanar angle between ring *A* of the bridging ligand and ring *B* of the cyclometalating ligand (see Figure 4); [c] distance between the plane of ring *B* and the centroid of ring *A*.

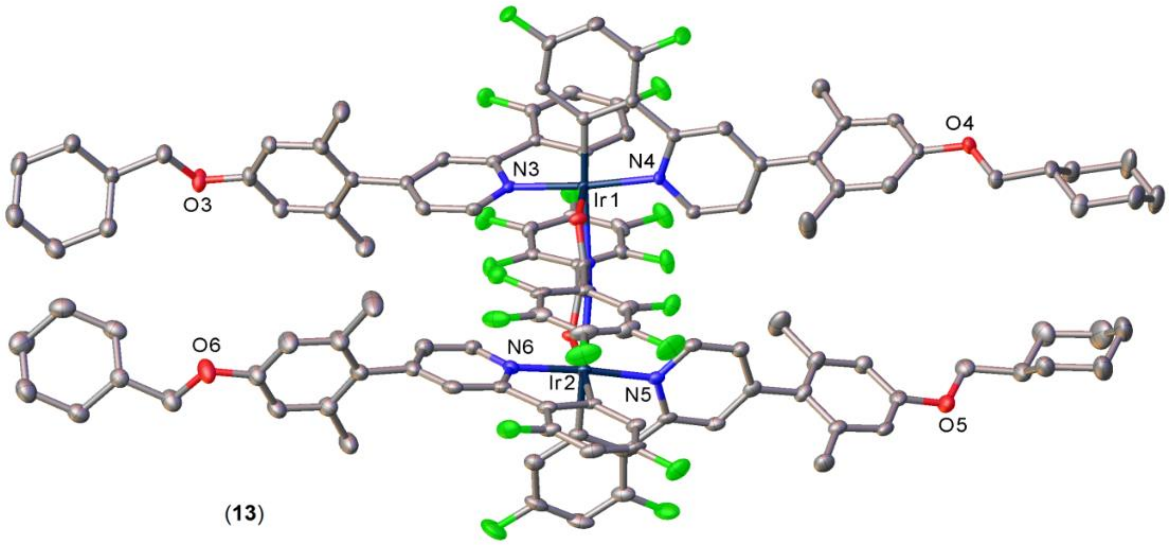

Figure S97. X-ray molecular structure of *rac* **13**. Thermal ellipsoids are drawn at 50% probability level. H atoms are omitted for clarity.

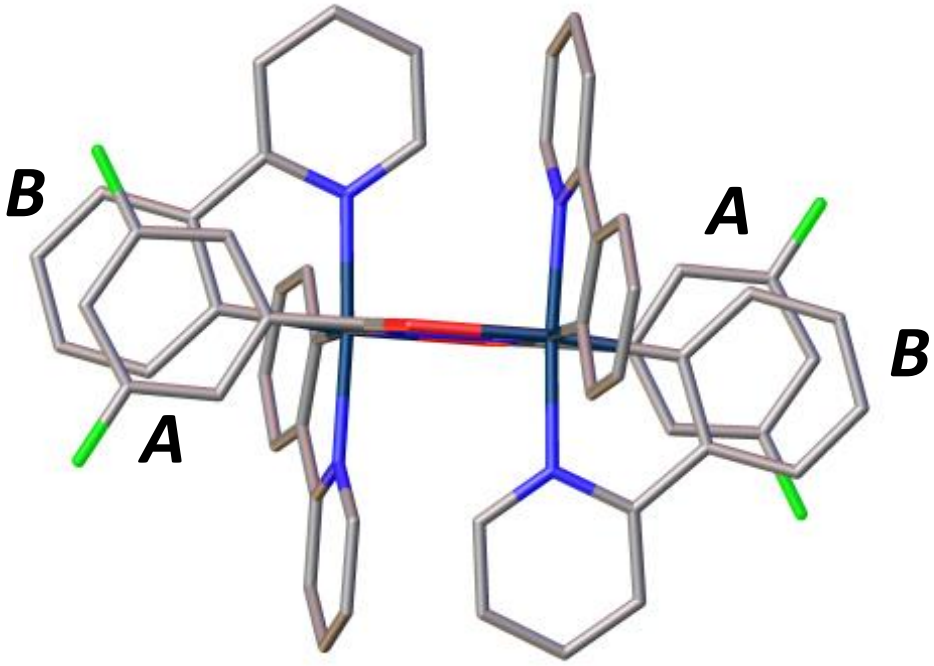

Figure S98. Molecular structure of *meso* **7** viewed perpendicular to the plane of the cyclometalating phenyl moieties to highlight intramolecular π–π interactions. The bridge (*A*) and cyclometalating ligand (*B*) phenyl groups that are engaged in intramolecular π–π stacking are labelled (see Table S1).

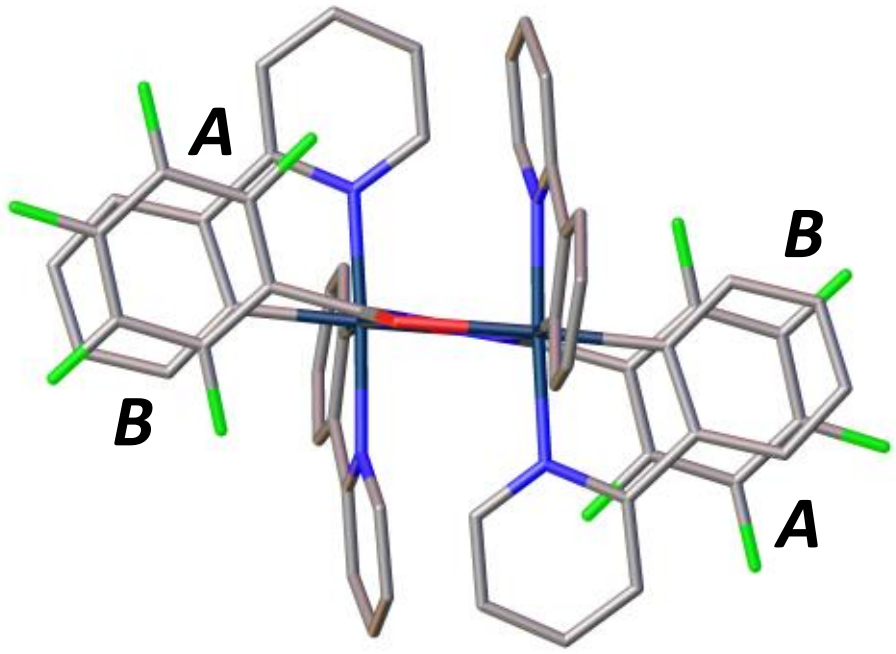

Figure S99. Molecular structure of *meso* **9** viewed perpendicular to the plane of the cyclometalating phenyl moieties to highlight intramolecular π–π interactions. The bridge (*A*) and cyclometalating ligand (*B*) phenyl groups that are engaged in intramolecular π–π stacking are labelled (see Table S1).

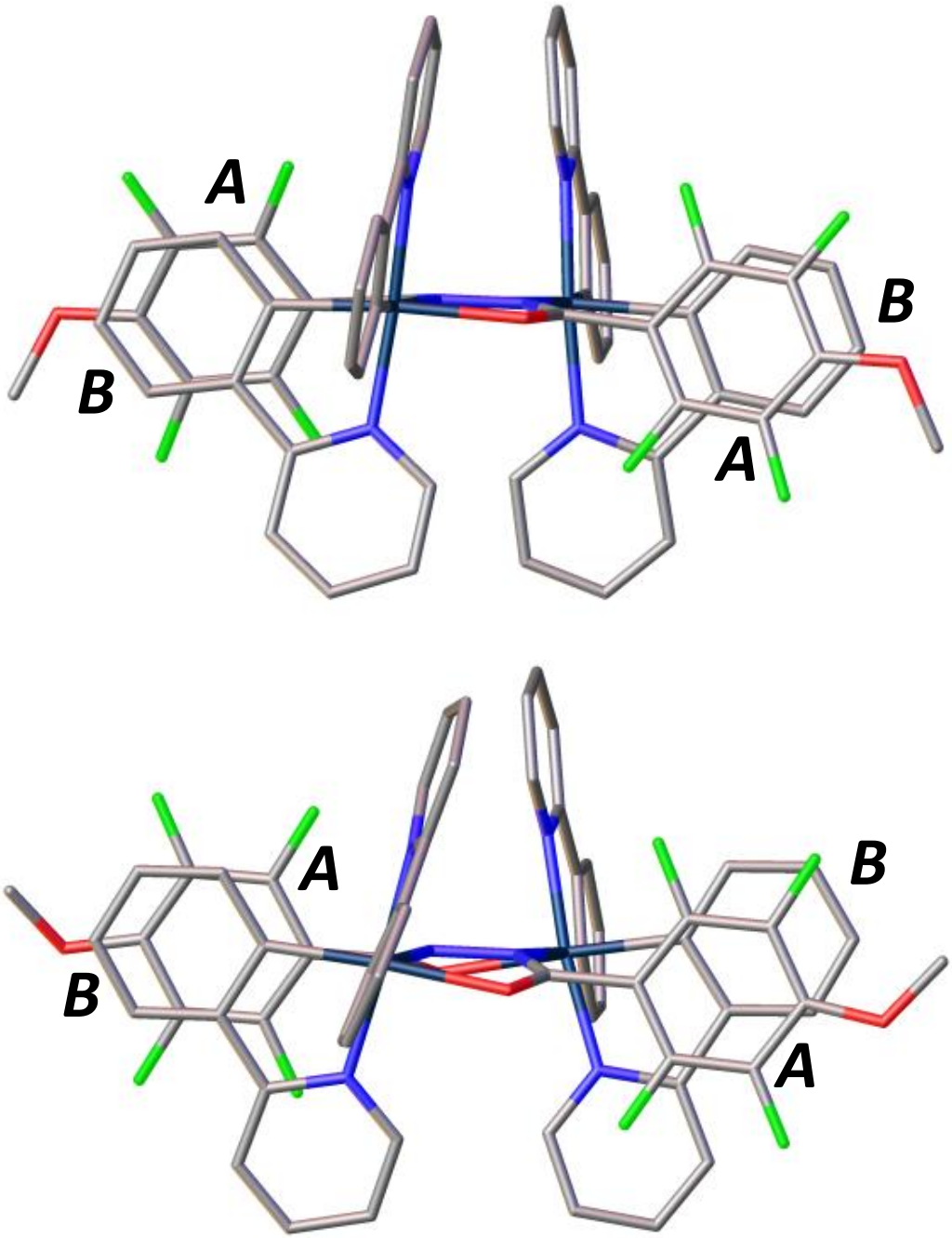

Figure S100. Molecular structures of α-ΔΔ **10** (top) and β-ΔΔ **10** (bottom) viewed perpendicular to the plane of the cyclometalating phenyl moieties to highlight intramolecular π–π interactions. The bridge (*A*) and cyclometalating ligand (*B*) phenyl groups that are engaged in intramolecular π–π stacking are labelled (see Table S1).

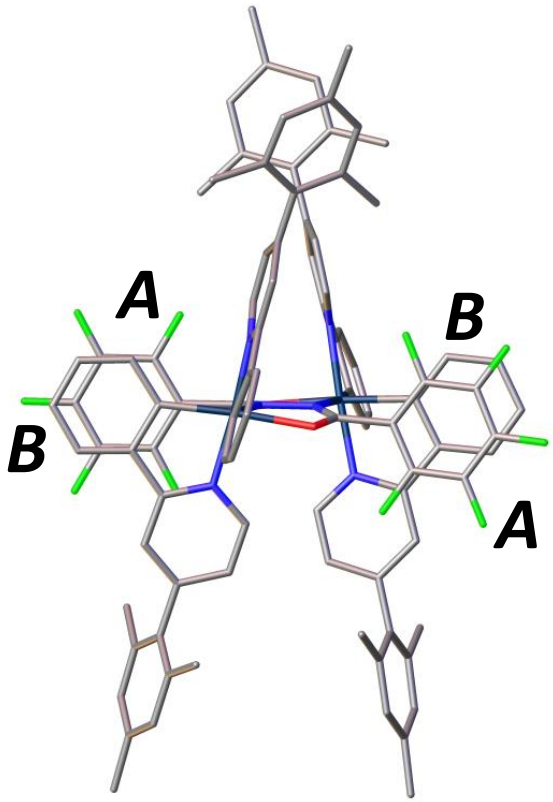

Figure S101. Molecular structure of ΔΔ **11** viewed perpendicular to the plane of the cyclometalating phenyl moieties to highlight intramolecular π–π interactions. The bridge (*A*) and cyclometalating ligand (*B*) phenyl groups that are engaged in intramolecular π–π stacking are labelled (see Table S1).

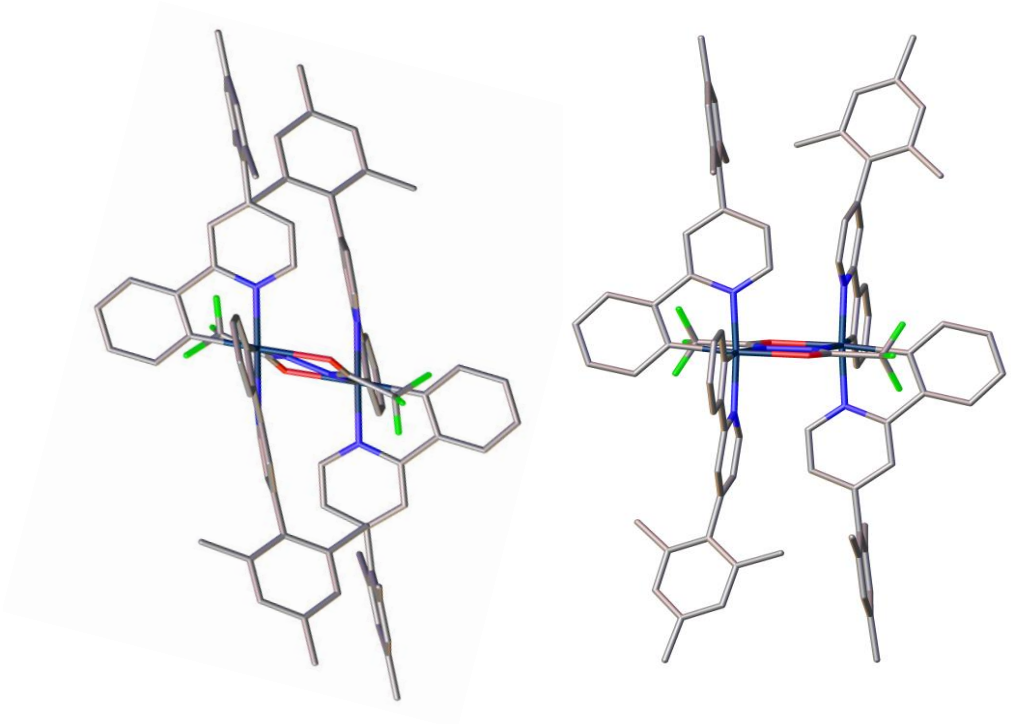

Figure S102. Molecular structures of molecule A (left) and molecule B (right) of *meso* **12** viewed perpendicular to the plane of the cyclometalating phenyl moieties.

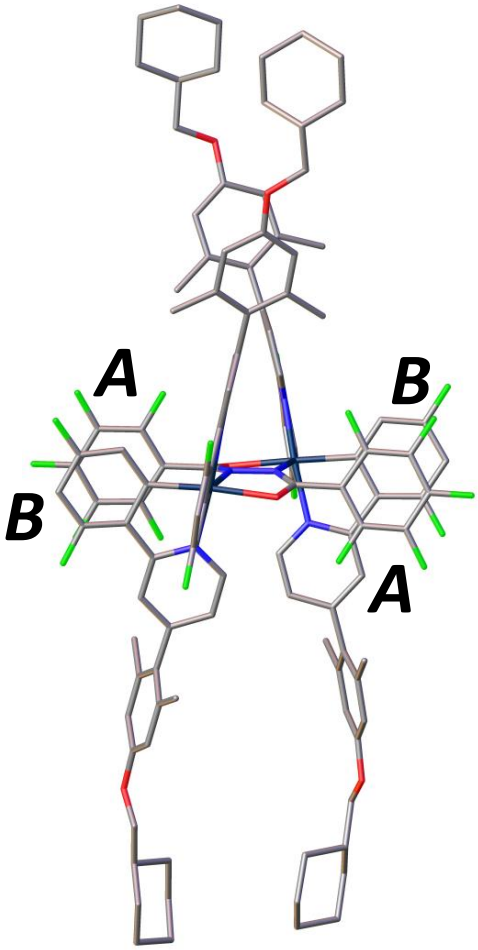

Figure S103. Molecular structure of **ΔΔ 13** viewed perpendicular to the plane of the cyclometalating phenyl moieties to highlight intramolecular π–π interactions. The bridge (*A*) and cyclometalating ligand (*B*) phenyl groups that are engaged in intramolecular π–π stacking are labelled (see Table S1).

Electrochemistry

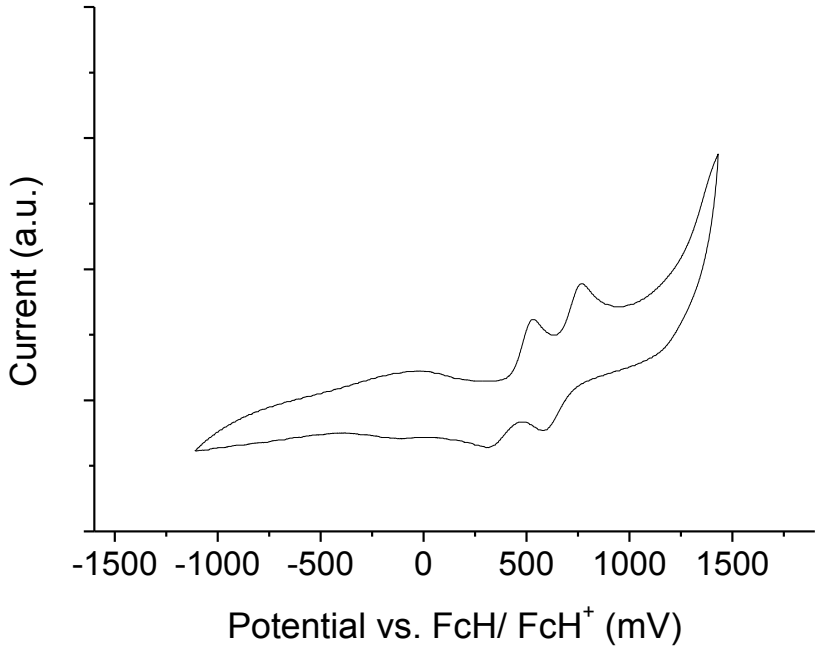

Figure S104. Cyclic voltammogram in 0.1 M *n*-Bu_4PF_6/ DCM showing the oxidation processes for complex **7**.

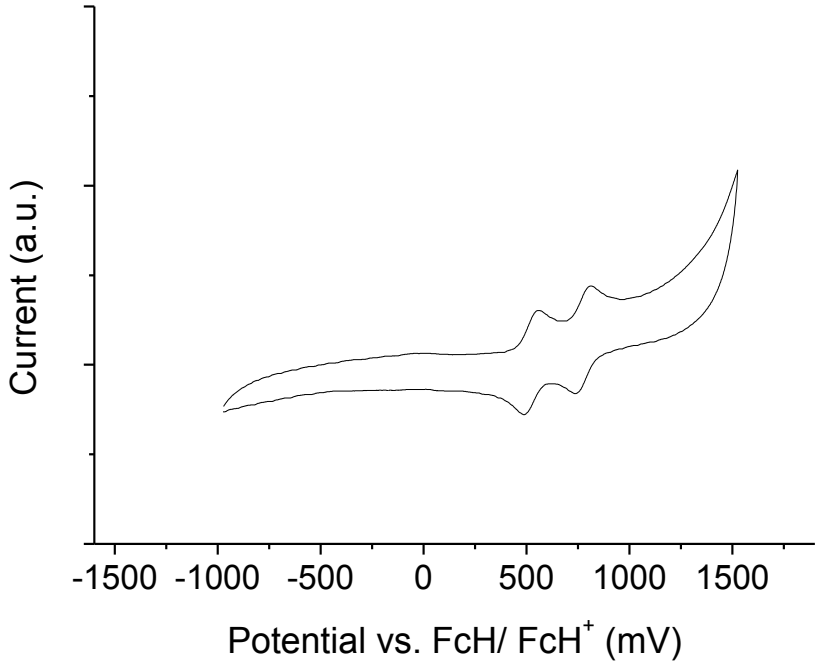

Figure S105. Cyclic voltammogram in 0.1 M *n*-Bu_4PF_6/ DCM showing the oxidation processes for complex **8**.

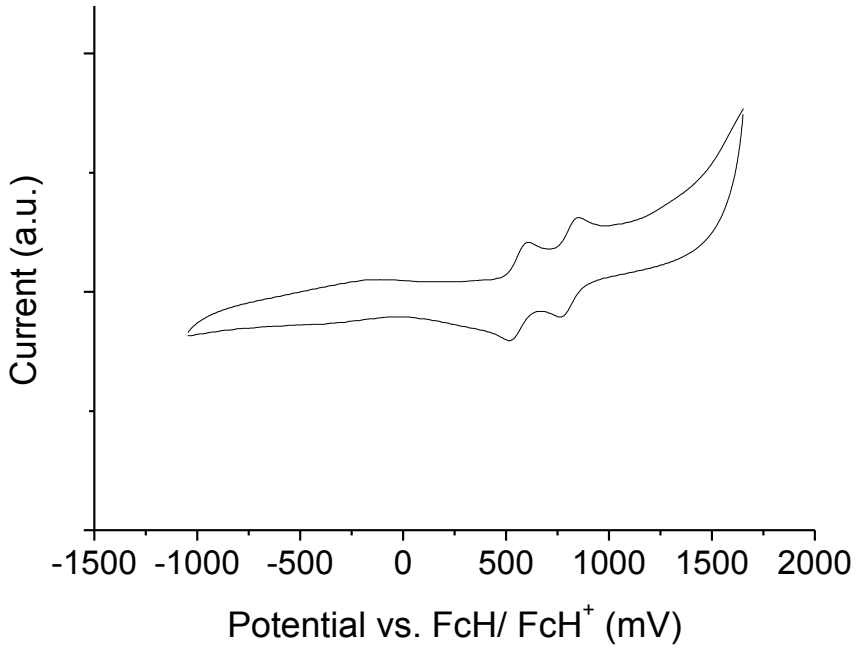

Figure S106. Cyclic voltammogram in 0.1 M *n*-Bu_4PF_6/ DCM showing the oxidation processes for complex **9**.

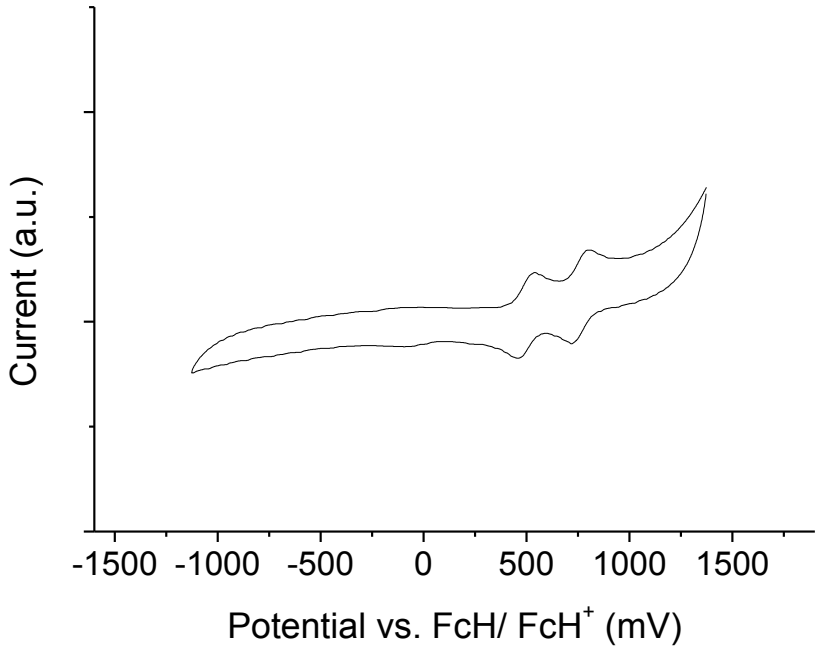

Figure S107. Cyclic voltammogram in 0.1 M *n*-Bu_4PF_6/ DCM showing the oxidation processes for complex **10**.

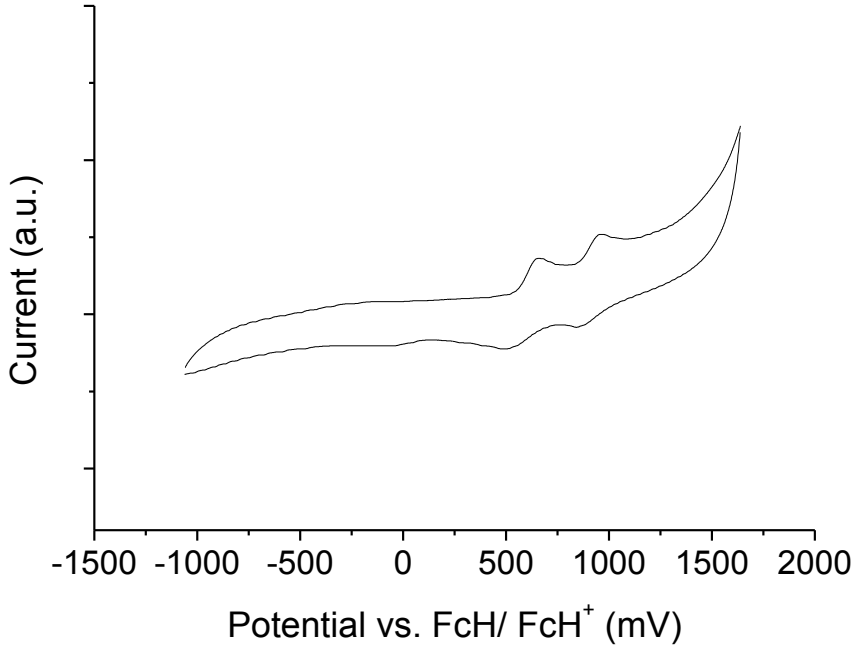

Figure S108. Cyclic voltammogram in 0.1 M *n*-Bu_4PF_6/ DCM showing the oxidation processes for complex **11**.

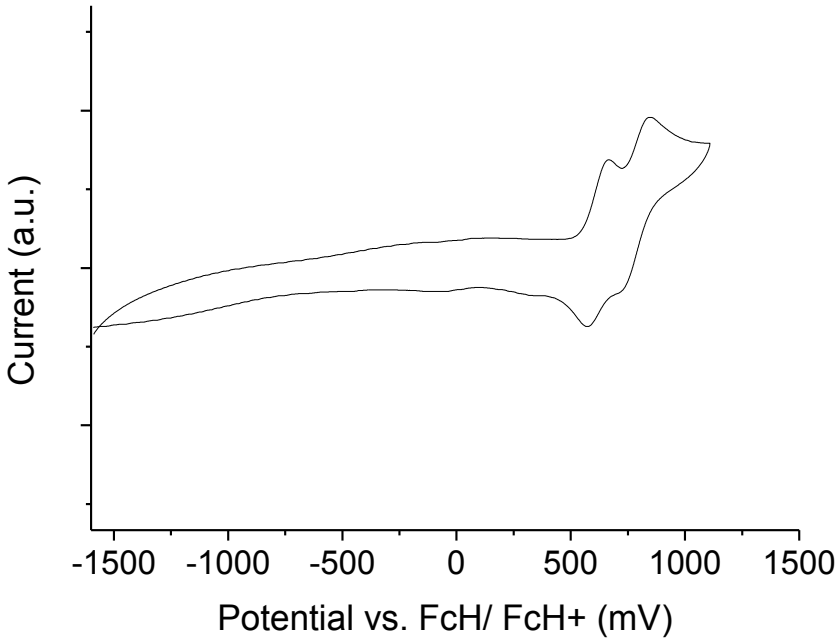

Figure S109. Cyclic voltammogram in 0.1 M *n*-Bu_4PF_6/ DCM showing the oxidation processes for complex **12**.

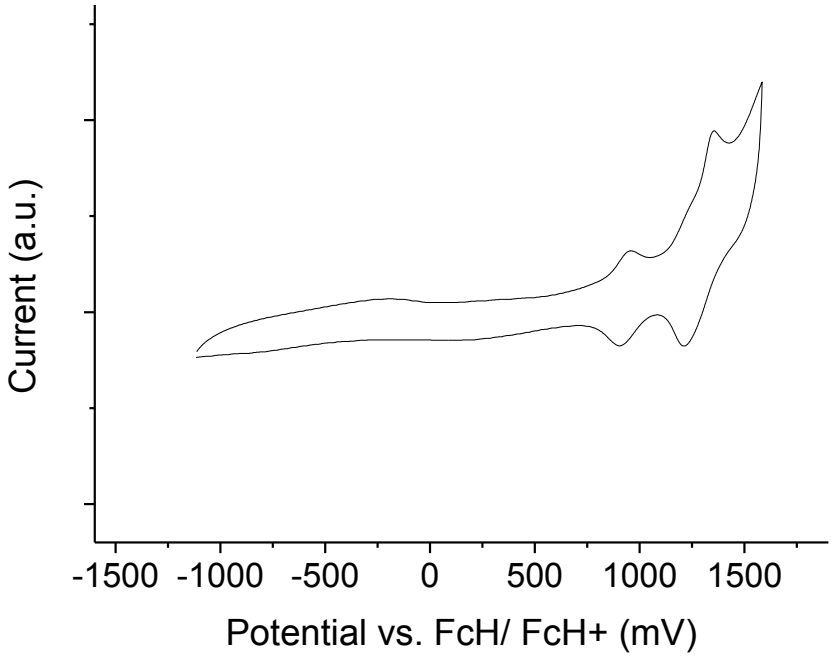

Figure S110. Cyclic voltammogram in 0.1 M *n*-Bu_4PF_6/ DCM showing the oxidation processes for complex *meso* **13**.

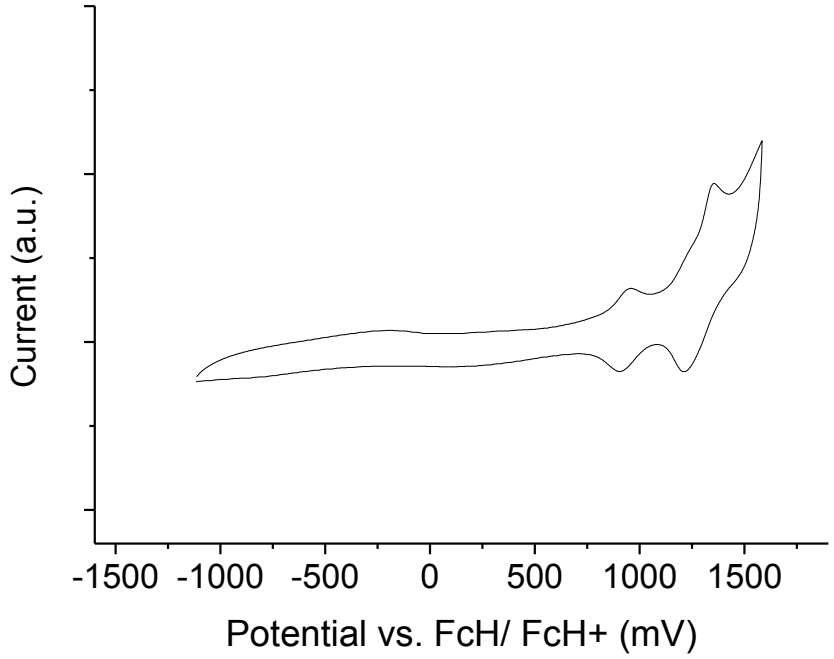

Figure S111. Cyclic voltammogram in 0.1 M *n*-Bu_4PF_6/ DCM showing the oxidation processes for complex *rac* **13**.

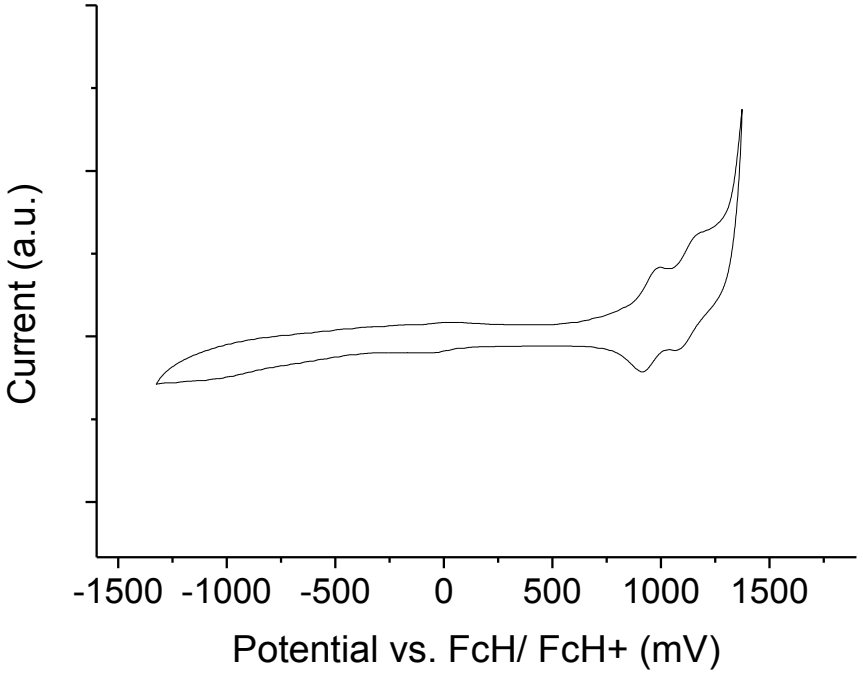

Figure S112. Cyclic voltammogram in 0.1 M *n*-Bu_4PF_6/ DCM showing the oxidation processes for complex **14**.

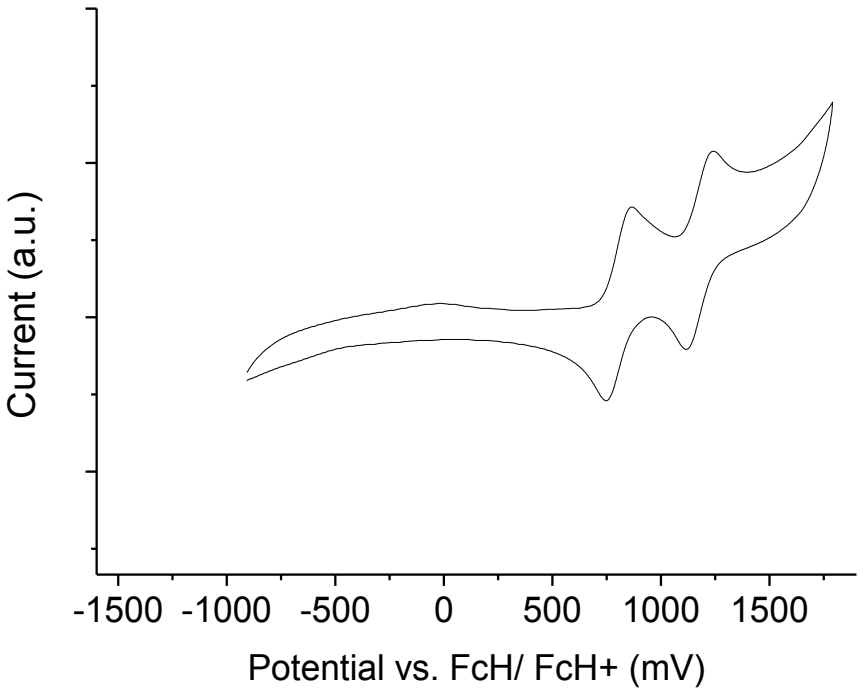

Figure S113. Cyclic voltammogram in 0.1 M *n*-Bu_4PF_6/ DCM showing the oxidation processes for complex **15**.

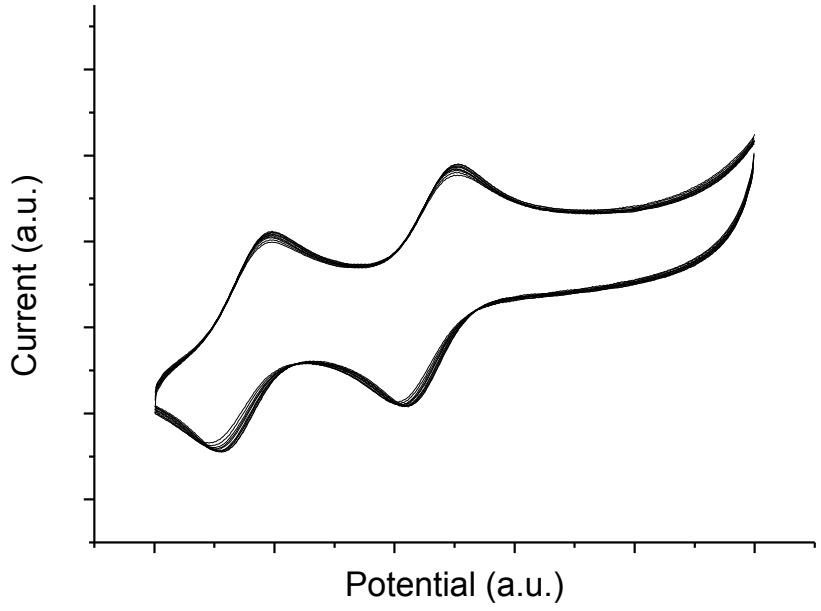

Figure S114. Cyclic voltammograms in 0.1 M *n*-Bu_4PF_6/ DCM showing the oxidation processes for complex **11** over 10 consecutive scans. The potential axis is arbitrary due to the absence of internal ferrocene. The oxidation potentials slightly drift due to the use of a quasireference electrode.

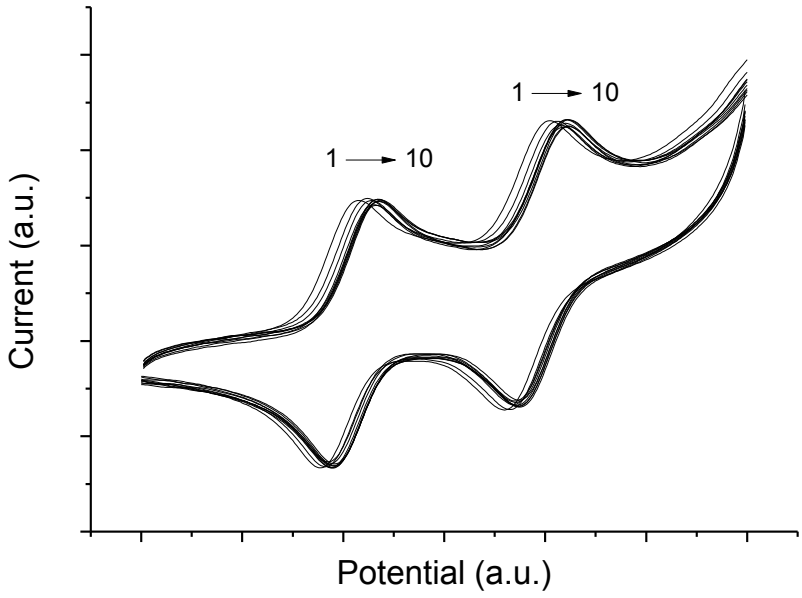

Figure S115. Cyclic voltammograms in 0.1 M *n*-Bu_4PF_6/ DCM showing the oxidation processes for complex **15** over 10 consecutive scans. The potential axis is arbitrary due to the absence of internal ferrocene. The oxidation potentials slightly drift due to the use of a quasireference electrode.

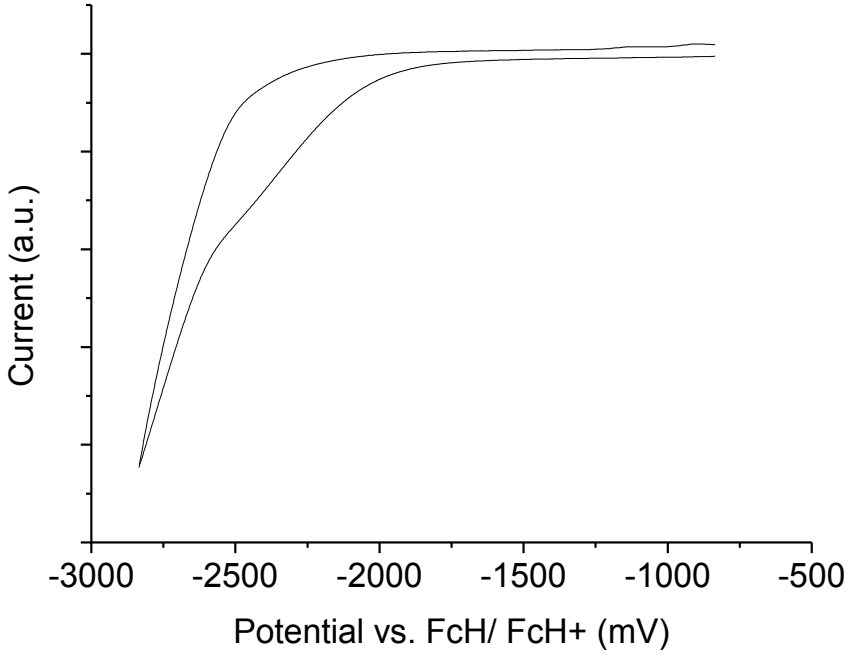

Figure S116. Cyclic voltammogram in 0.1 M *n*-Bu_4PF_6/ THF showing the reduction process for complex **7**.

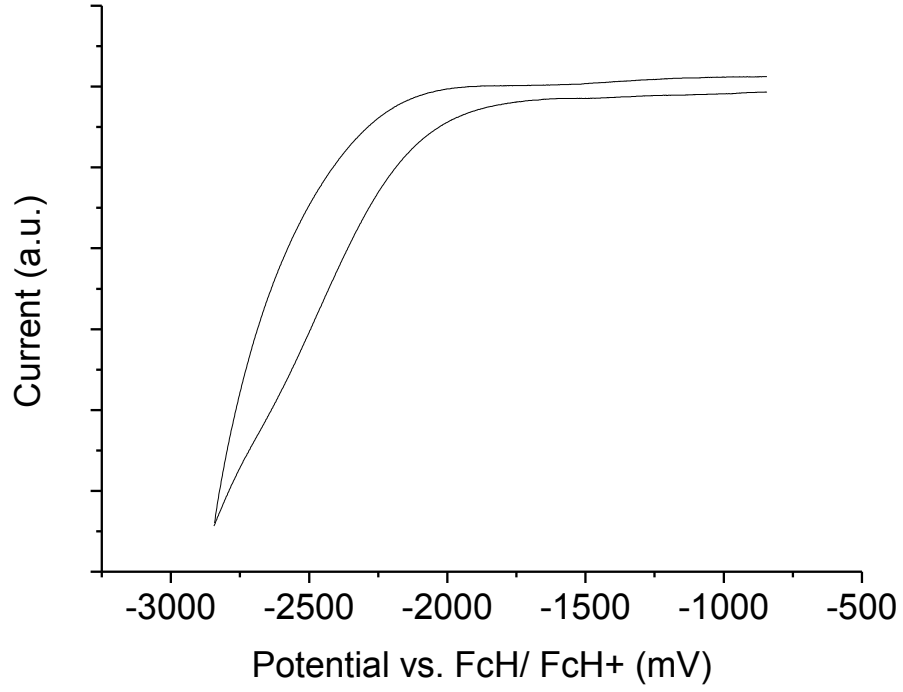

Figure S117. Cyclic voltammogram in 0.1 M *n*-Bu_4PF_6/ THF showing the reduction process for complex **8**.

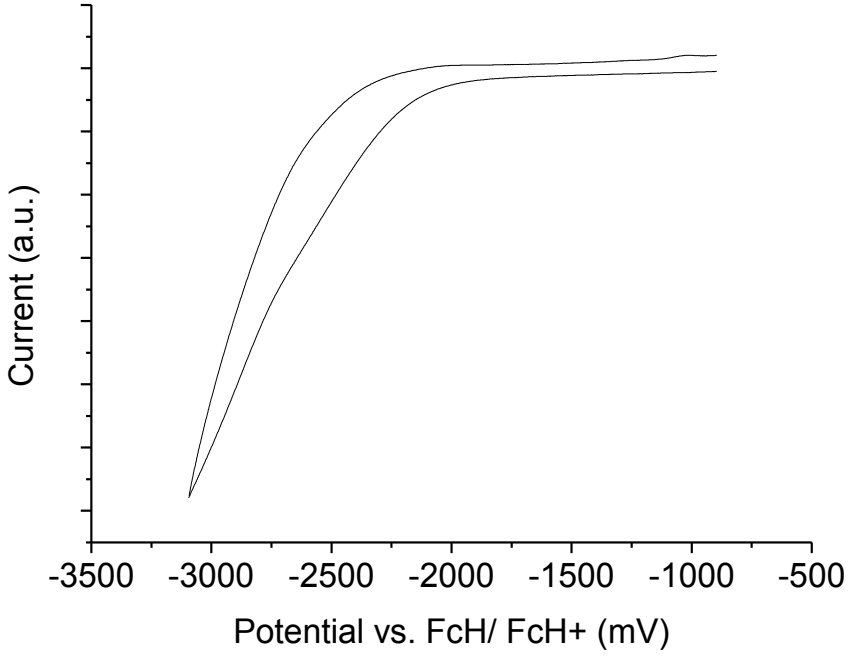

Figure S118. Cyclic voltammogram in 0.1 M *n*-Bu_4PF_6/ THF showing the reduction process for complex **9**.

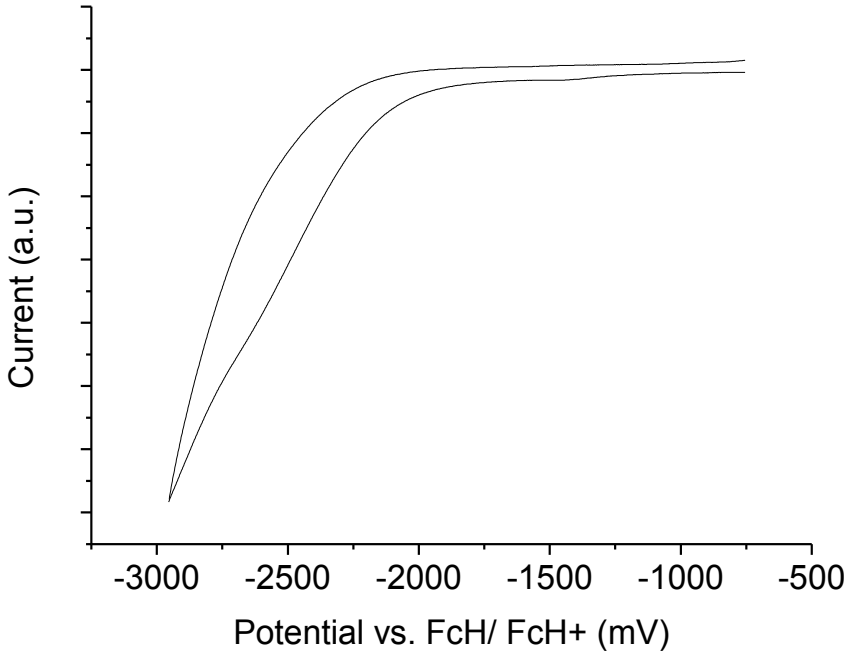

Figure S119. Cyclic voltammogram in 0.1 M *n*-Bu_4PF_6/ THF showing the reduction process for complex **10**.

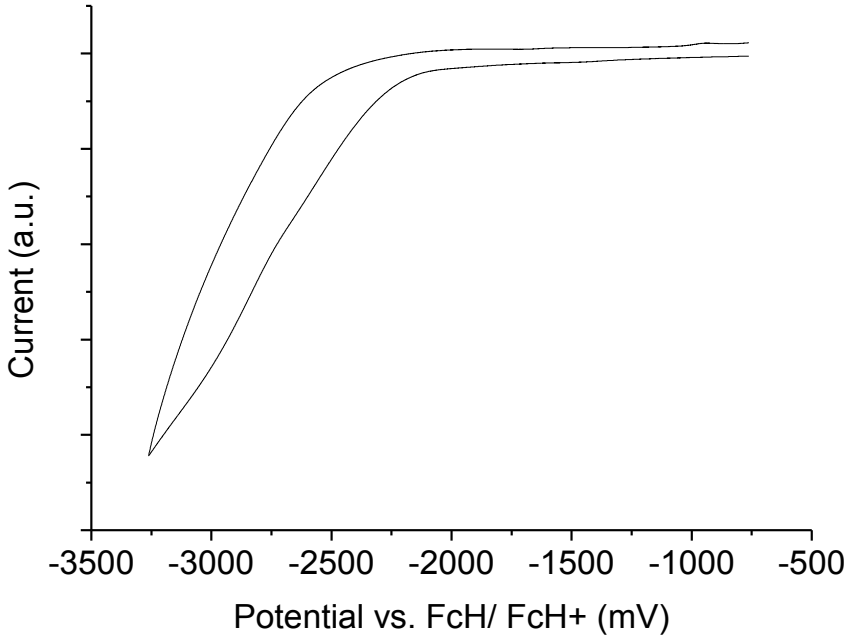

Figure S120. Cyclic voltammogram in 0.1 M *n*-Bu_4PF_6/ THF showing the reduction process for complex *rac* **11**.

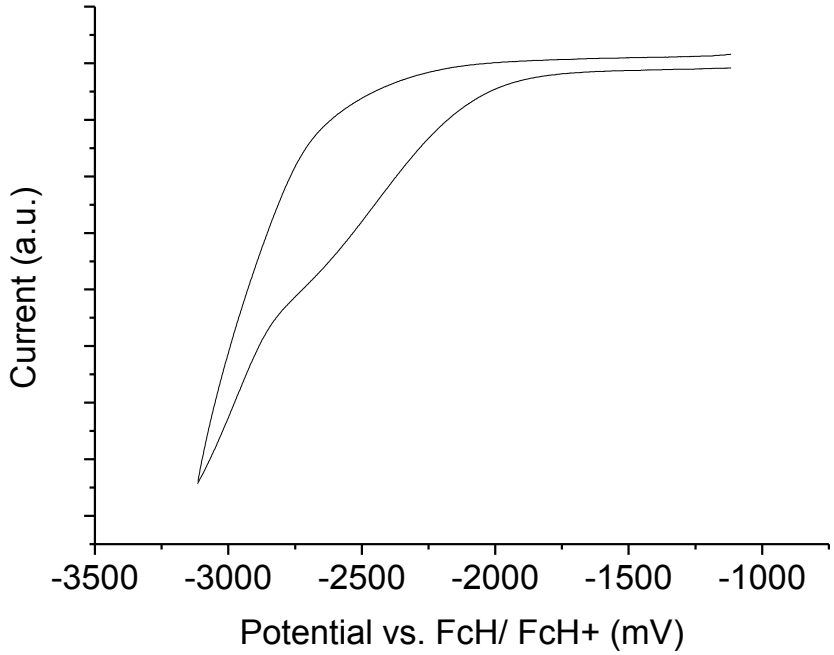

Figure S121. Cyclic voltammogram in 0.1 M *n*-Bu_4PF_6/ THF showing the reduction process for complex *meso* **12**.

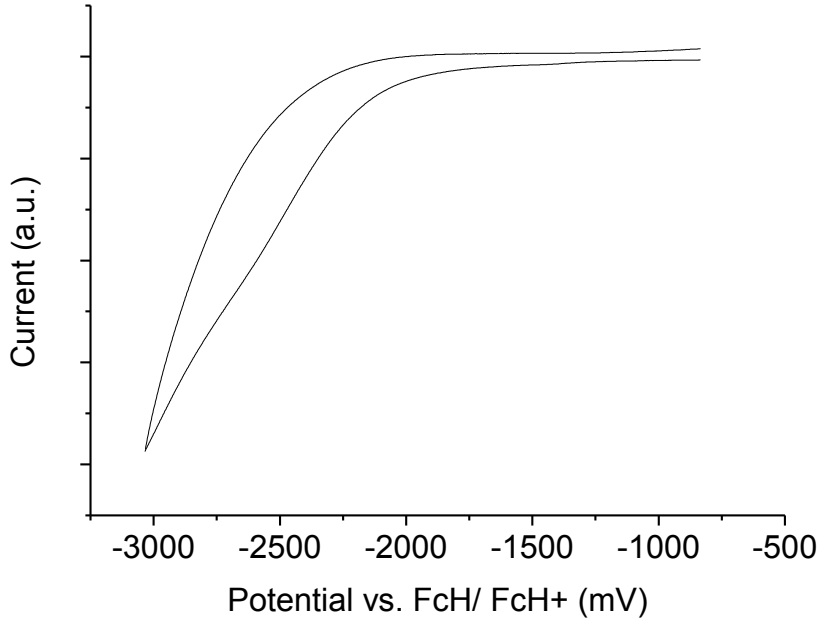

Figure S122. Cyclic voltammogram in 0.1 M *n*-Bu_4PF_6/ THF showing the reduction process for complex *meso* **13**.

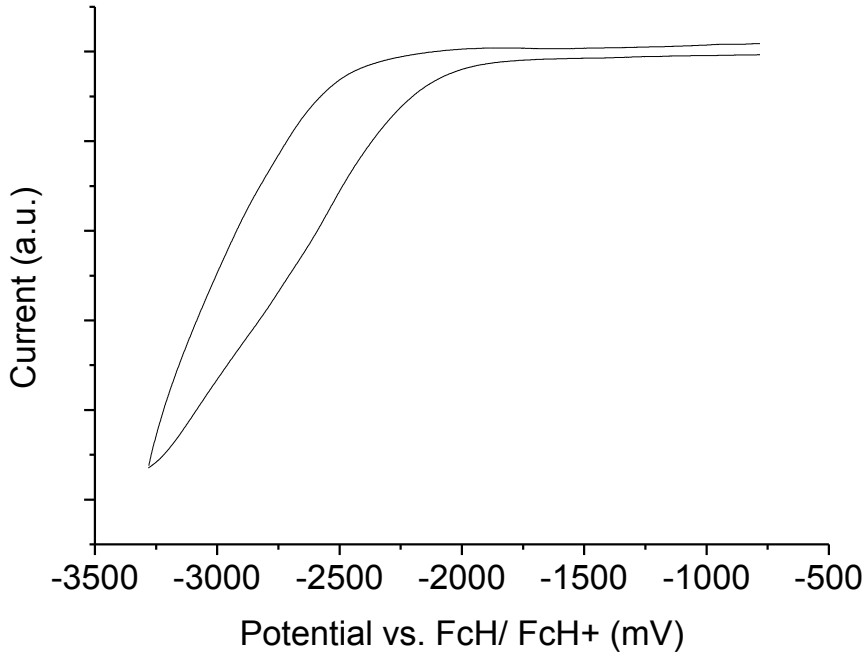

Figure S123. Cyclic voltammogram in 0.1 M *n*-Bu_4PF_6/ THF showing the reduction process for complex *rac* **13**.

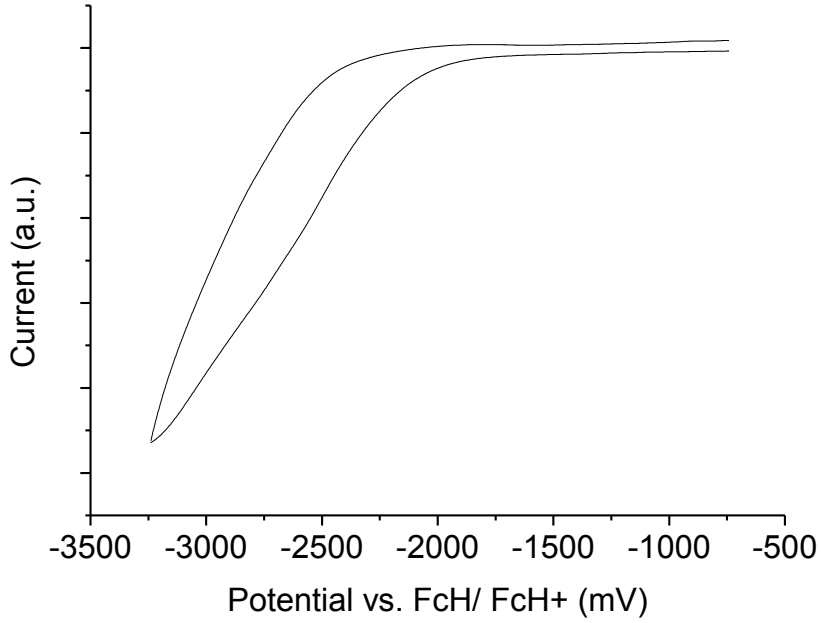

Figure S124. Cyclic voltammogram in 0.1 M *n*-Bu_4PF_6/ THF showing the reduction process for complex **14**.

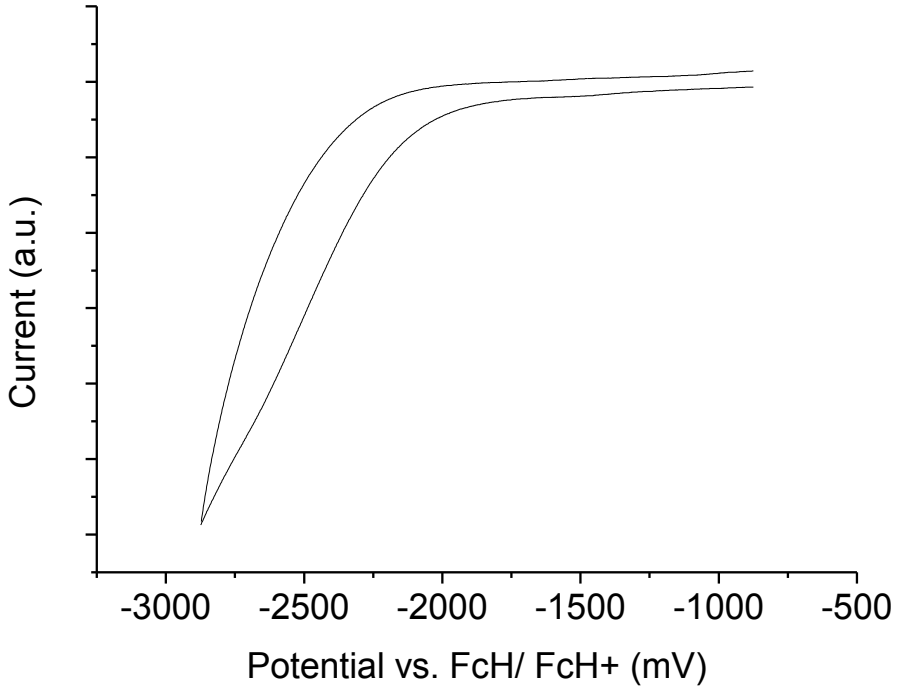

Figure S125. Cyclic voltammogram in 0.1 M *n*-Bu_4PF_6/ THF showing the reduction process for complex **15**.

Computations

Table S2 Summary of the HOMO compositions for the most stable minima of the *rac* and *meso* diastereomers of the complexes.

Complex	Isomer	Ir	Bridge centre	Bridge aryl	Ph[a]	Py[b]
7	*meso*	42	28	1	23	6
	rac	38	41	2	14	5
8	*meso*	45	18	1	31	5
	rac	48	4	0	42	6
9	*meso*	45	16	1	33	5
	rac	48	4	0	42	6
10	*meso*	45	20	1	29	5
	rac	40	44	2	9	5
11	*meso*	44	22	1	28	6
	rac	47	4	0	42	6
12	*meso*	45	4	-	46	6
	rac	45	3	-	46	6
13	*meso*	42	35	1	15	5
	rac	40	44	2	8	6
14	*meso*	45	4	-	44	7
	rac	45	4	-	44	7
15	*meso*	42	42	1	9	6
	rac	42	46	1	4	7

The atom/ group contributions are stated as percentages. [a]Phenyl moieties of the cyclometalating ligands [b]Pyridyl moieties of the cyclometalating ligands.

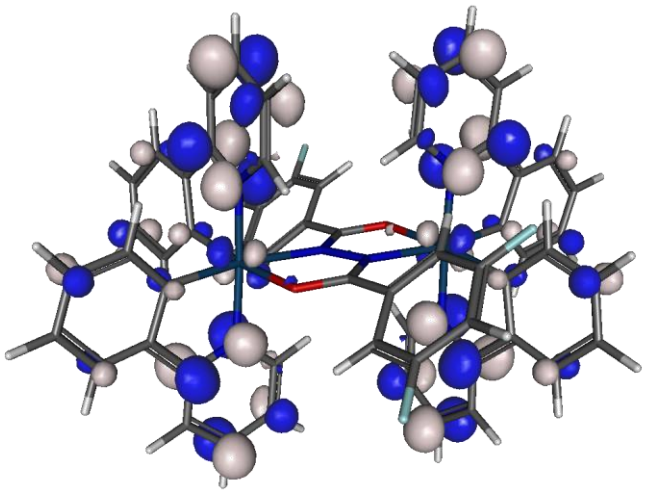

LUMO

–1.50 eV

Ir : Bridge : F_2 : Ph : Py

5 : 2 : 1 : 21 : 72

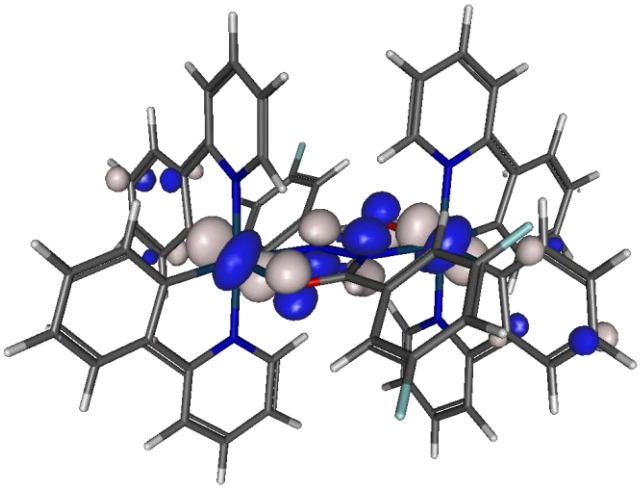

HOMO

–4.95 eV

Ir : Bridge : F_2: Ph : Py

42 : 28 : 1 : 23 : 6

Figure S126. Frontier molecular orbitals for the most stable minimum of *meso* **7**

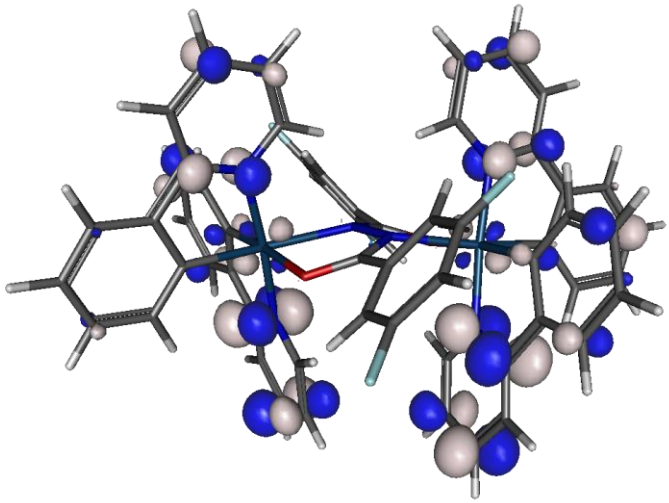

LUMO

–1.47 eV

Ir : Bridge : F_2: Ph : Py

5 : 1 : 1 : 22 : 70

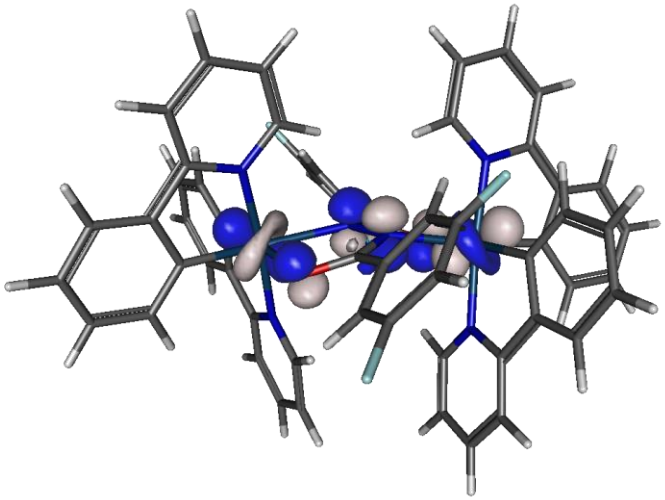

HOMO

–4.92 eV

Ir : Bridge : F_2 : Ph : Py

38 : 41 : 2 : 14 : 5

Figure S127. Frontier molecular orbitals for the most stable minimum of *rac* **7**

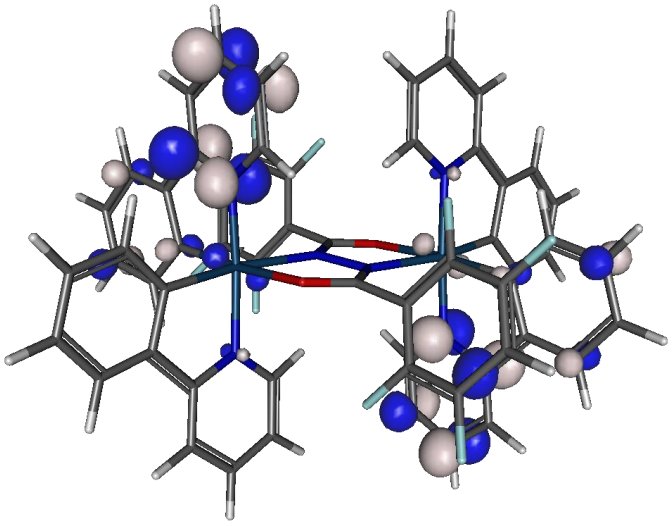

LUMO

–1.46 eV

Ir : Bridge : F_4 : Ph : Py

5 : 1 : 1 : 23 : 71

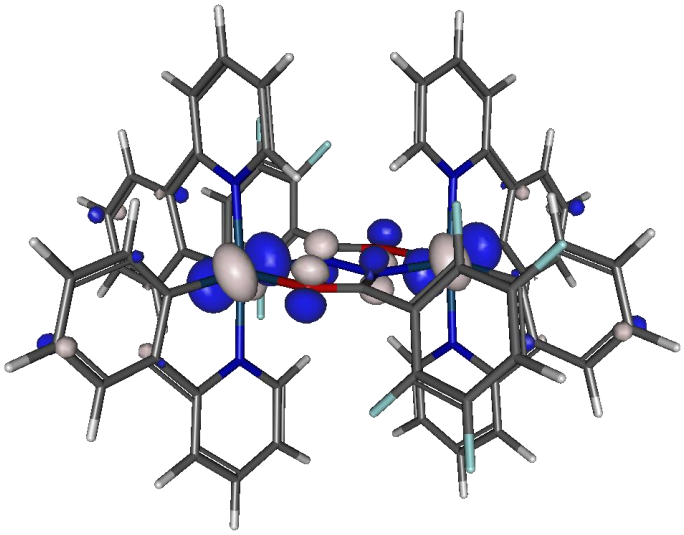

HOMO

–4.95 eV

Ir : Bridge : F_4 : Ph : Py

45 : 18 : 1 : 31 : 5

Figure S128. Frontier molecular orbitals for the most stable minimum of *meso* **8**

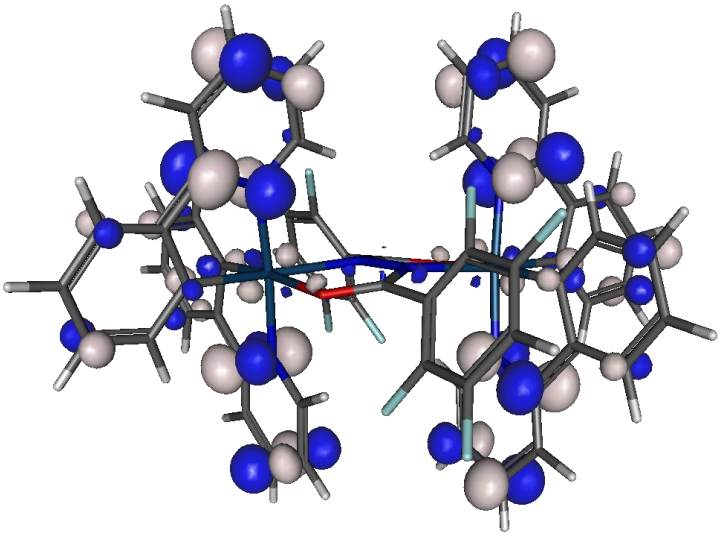

LUMO

–1.43 eV

Ir : Bridge : F_4 : Ph : Py

4 : 2 : 4 : 22 : 68

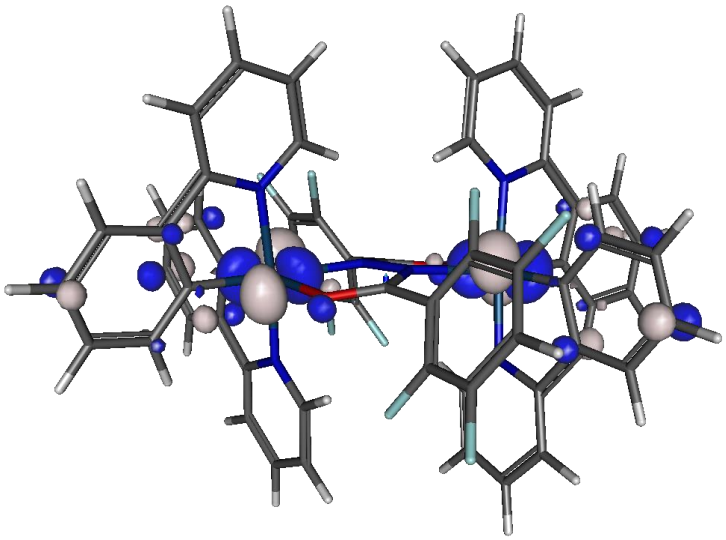

HOMO

–4.97 eV

Ir : Bridge : F_4 : Ph : Py

48 : 4 : 0 : 42 : 6

Figure S129. Frontier molecular orbitals for the most stable minimum of *rac* **8**

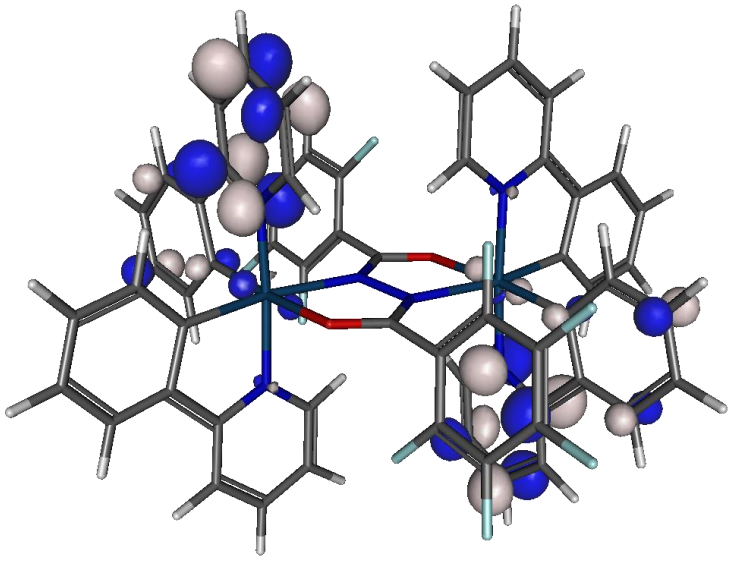

LUMO

–1.56 eV

Ir : Bridge : F_5 : Ph : Py

5 : 1 : 1 : 23 : 70

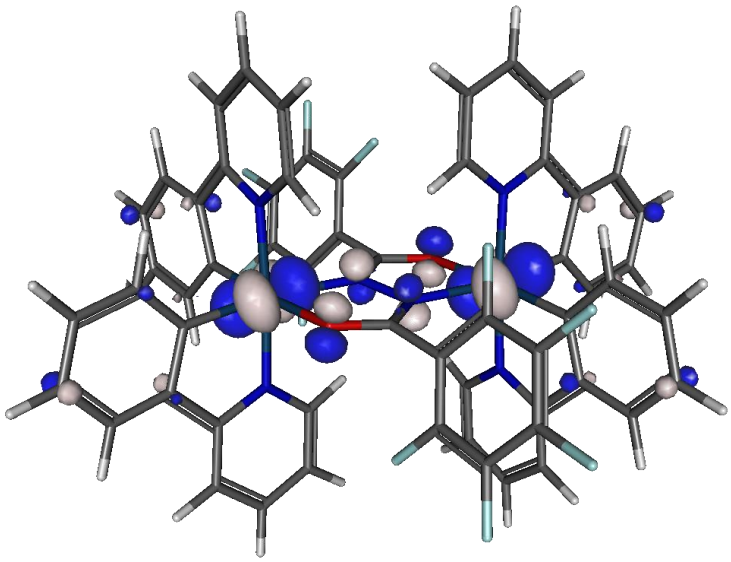

HOMO

–5.06 eV

Ir : Bridge : F_5 : Ph : Py

45 : 16 : 1 : 33 : 5

Figure S130. Frontier molecular orbitals for the most stable minimum of *meso* **9**

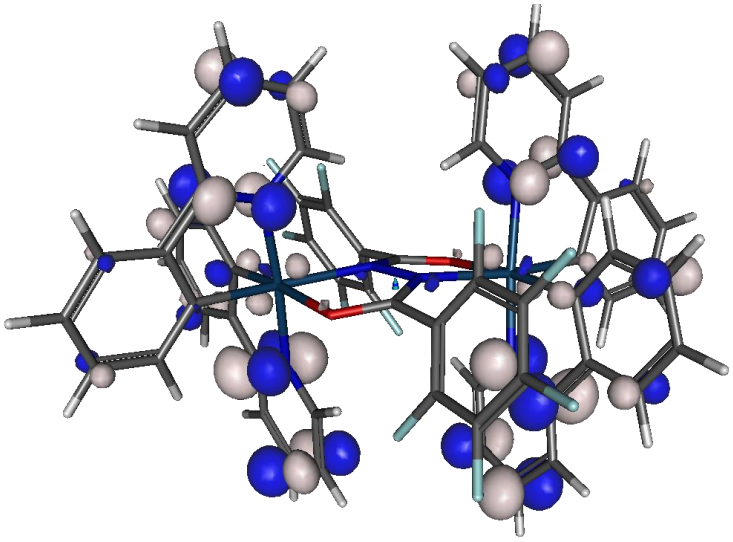

LUMO

–1.53 eV

Ir : Bridge : F_5 : Ph : Py

4 : 2 : 3 : 22 : 68

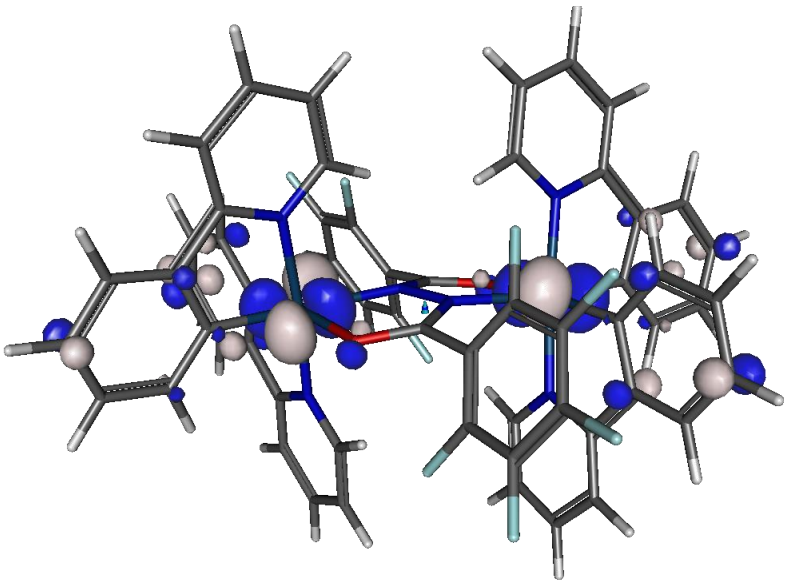

HOMO

–5.07 eV

Ir : Bridge : F_5 : Ph : Py

48 : 4 : 0 : 42 : 6

Figure S131. Frontier molecular orbitals for the most stable minimum of *rac* **9**

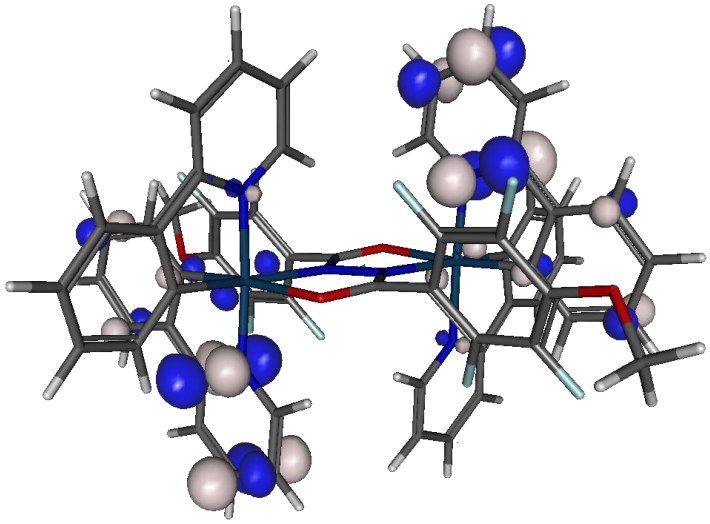

LUMO

–1.39 eV

Ir : Bridge : F_4 : Ph : Py

5 : 1 : 1 : 22 : 71

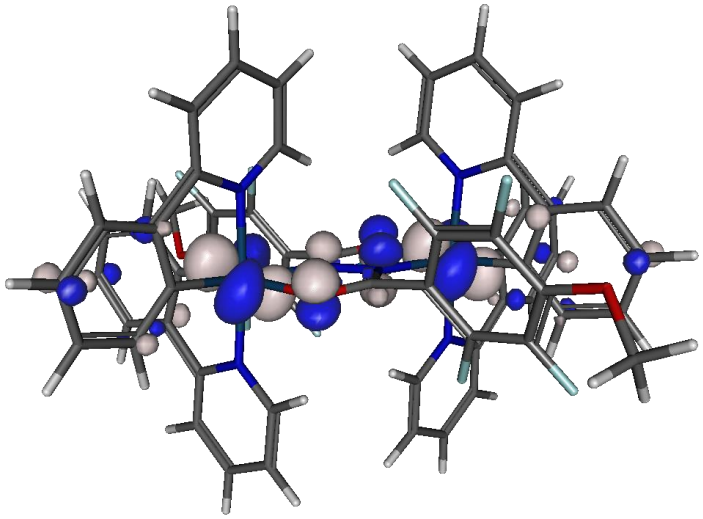

HOMO

–4.88 eV

Ir : Bridge : F_4 : Ph : Py

45 : 20 : 1 : 29 : 5

Figure S132. Frontier molecular orbitals for the most stable minimum of *meso* **10**

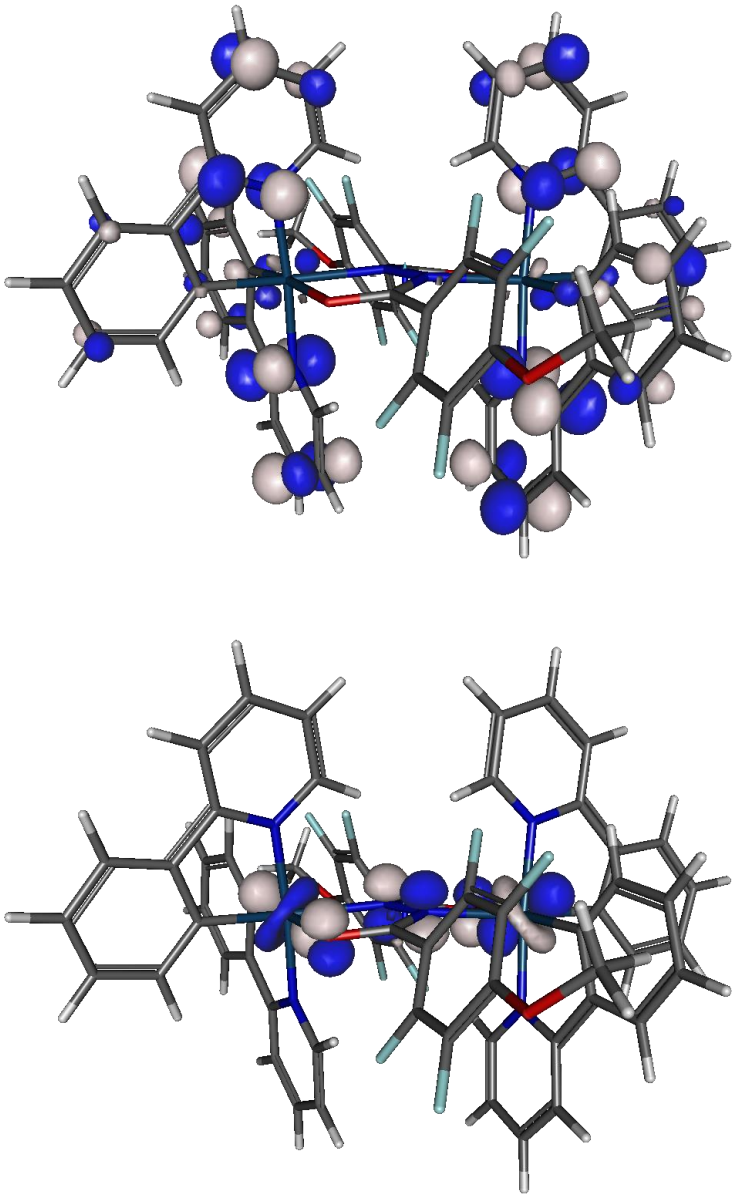

LUMO

–1.38 eV

Ir : Bridge : F_4 : Ph : Py

4 : 1 : 1 : 24 : 70

HOMO

–4.91 eV

Ir : Bridge : F_4 : Ph : Py

40 : 44 : 2 : 9 : 5

Figure S133. Frontier molecular orbitals for the most stable minimum of *rac* **10**

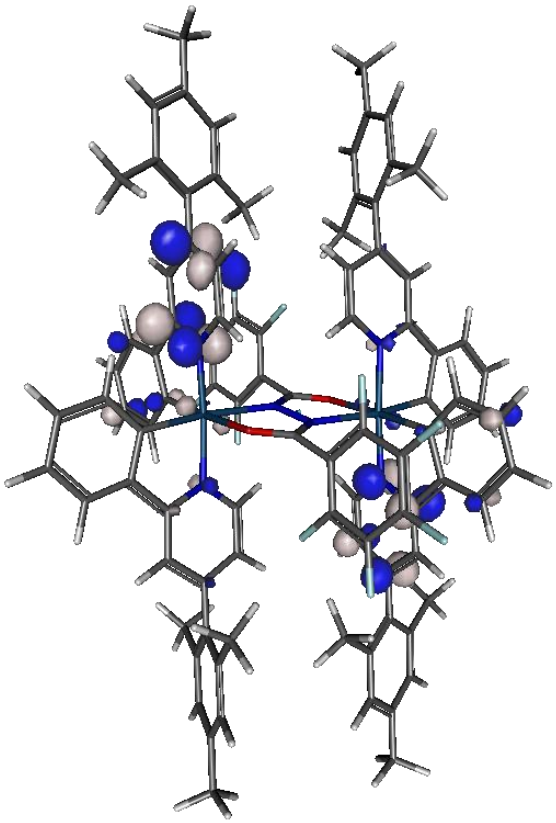

LUMO

–1.48 eV

Ir : Bridge : F_5 : Ph : Py

5 : 1 : 1 : 22 : 67

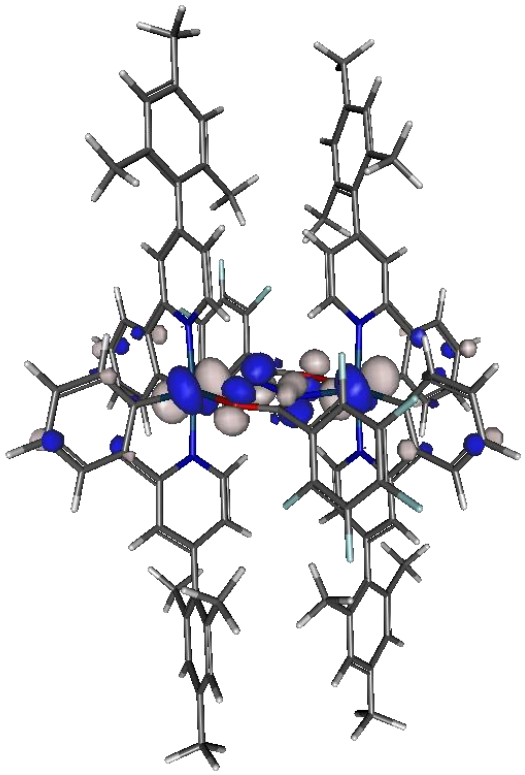

HOMO

–4.96 eV

Ir : Bridge : F_5 : Ph : Py

44 : 22 : 1 : 28 : 6

Figure S134. Frontier molecular orbitals for the most stable minimum of *meso* **11**

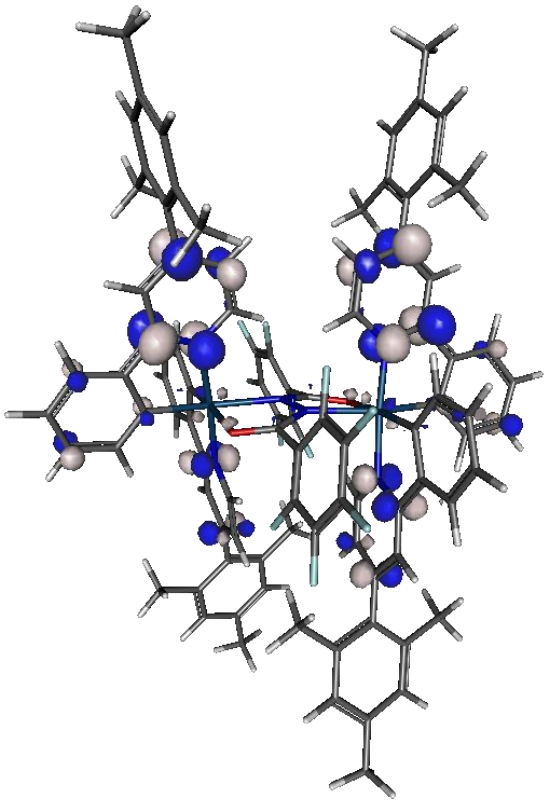

LUMO

–1.46 eV

Ir : Bridge : F_5 : Ph : Py

4 : 3 : 6 : 21 : 64

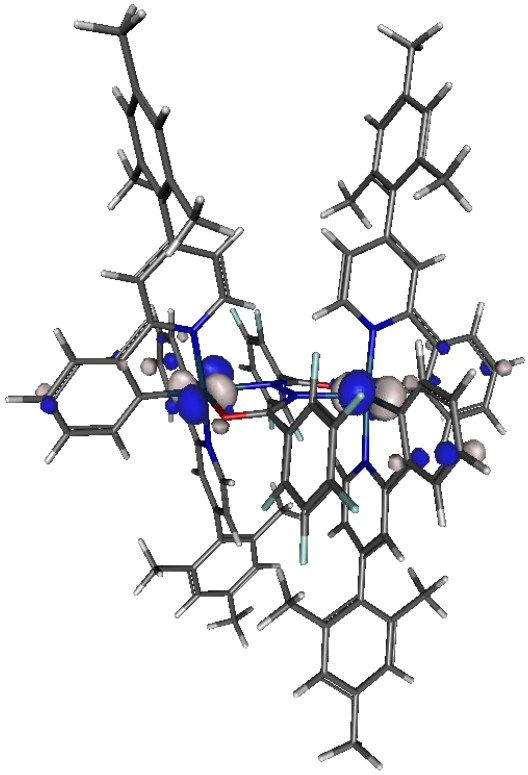

HOMO

–5.02 eV

Ir : Bridge : F_5: Ph : Py

47 : 4 : 0 : 42 : 6

Figure S135. Frontier molecular orbitals for the most stable minimum of *rac* **11**

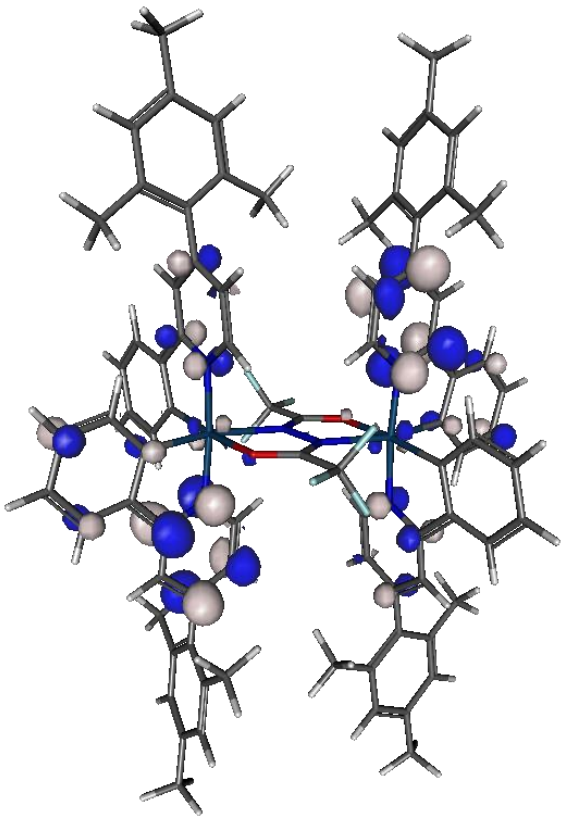

LUMO

–1.42 eV

Ir : Bridge : Ph : Py

4 : 2 : 21 : 69

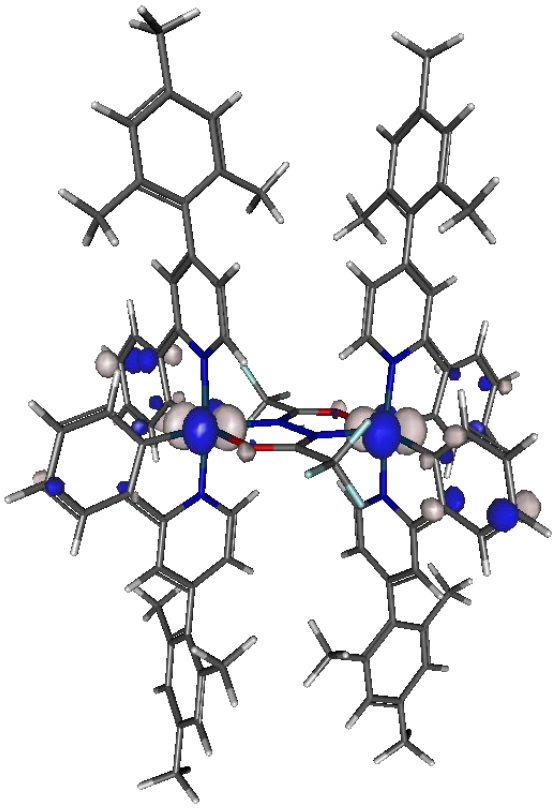

HOMO

–4.98 eV

Ir : Bridge : Ph : Py

45 : 4 : 46 : 6

Figure S136. Frontier molecular orbitals for the most stable minimum of *meso* **12**

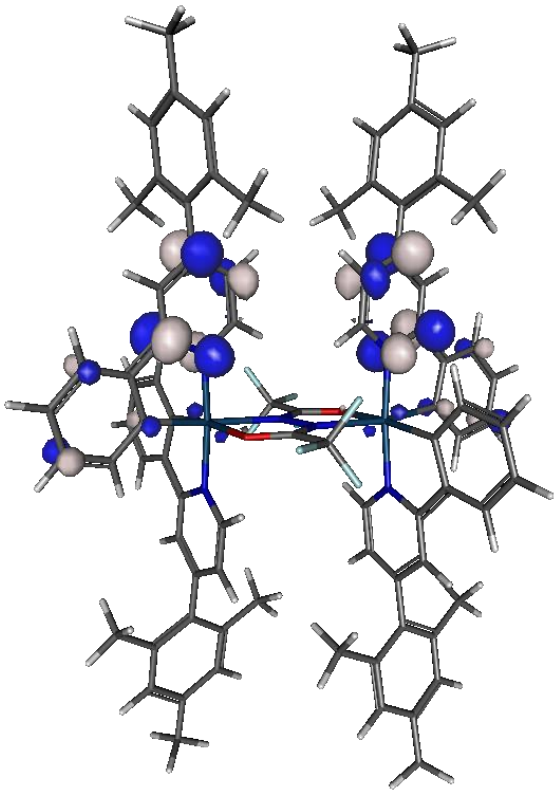

LUMO

–1.44 eV

Ir : Bridge : Ph : Py

4 : 2 : 21 : 71

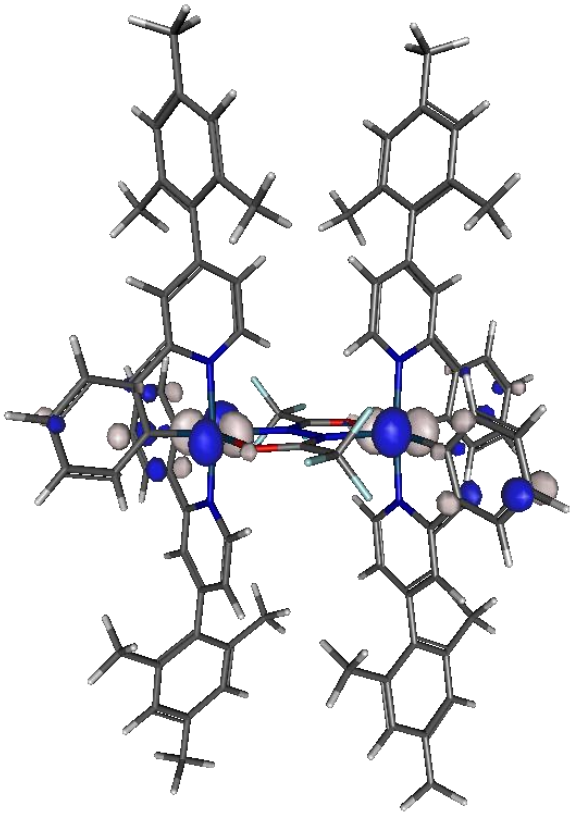

HOMO

–4.97 eV

Ir : Bridge : Ph : Py

45 : 3 : 46 : 6

Figure S137. Frontier molecular orbitals for the most stable minimum of *rac* **12**

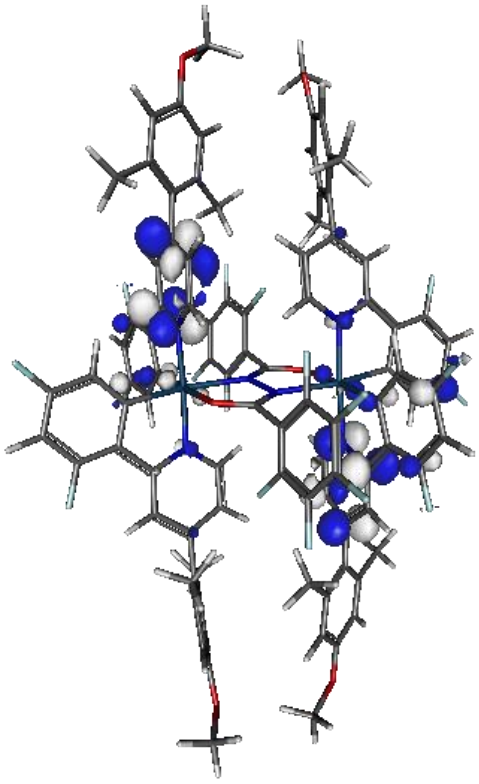

LUMO

–1.73 eV

Ir : Bridge : F_5 : Ph : Py

5 : 1 : 2 : 20 : 66

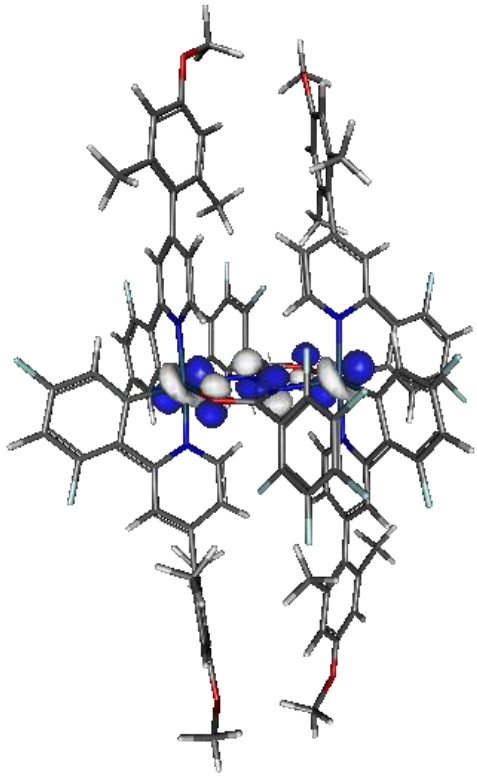

HOMO

–5.44 eV

Ir : Bridge : F_5 : Ph : Py

42 : 35 : 1 : 15 : 5

Figure S138. Frontier molecular orbitals for the most stable minimum of *meso* **13**

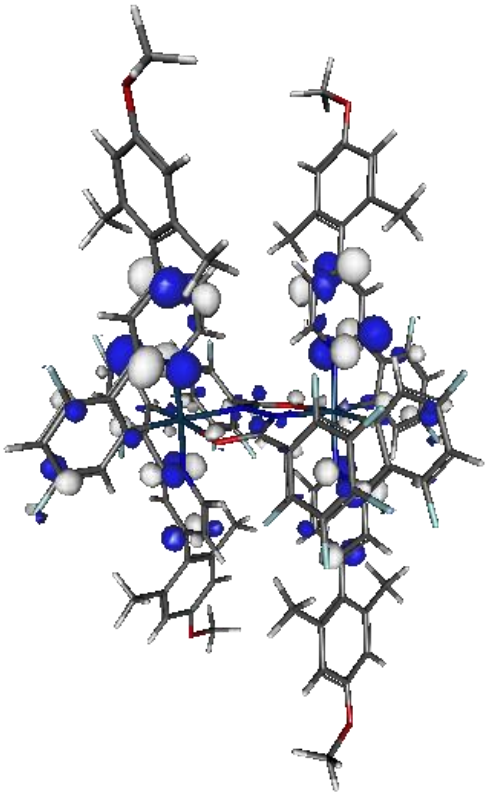

LUMO

–1.73 eV

Ir : Bridge : F_5 : Ph : Py

4 : 4 : 9 : 21 : 61

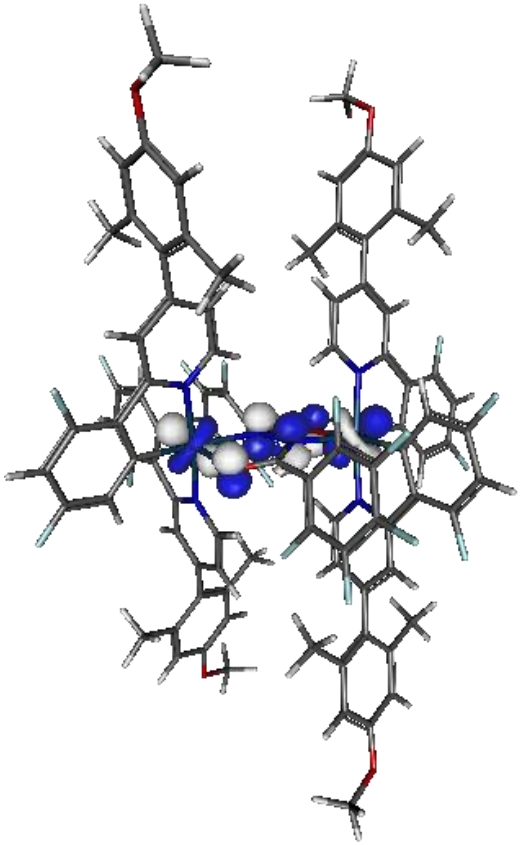

HOMO

–5.47 eV

Ir : Bridge : F_5 : Ph : Py

40 : 44 : 2 : 82 : 6

Figure S139. Frontier molecular orbitals for the most stable minimum of *rac* **13**

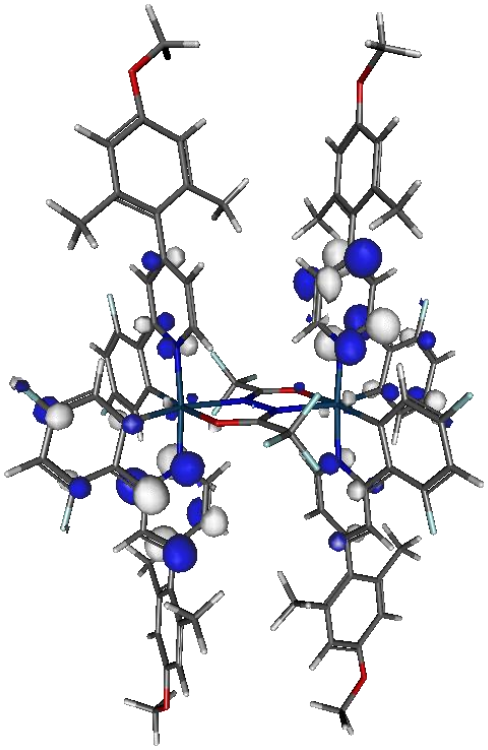

LUMO

–1.71 eV

Ir : Bridge : Ph : Py

4 : 2 : 22 : 68

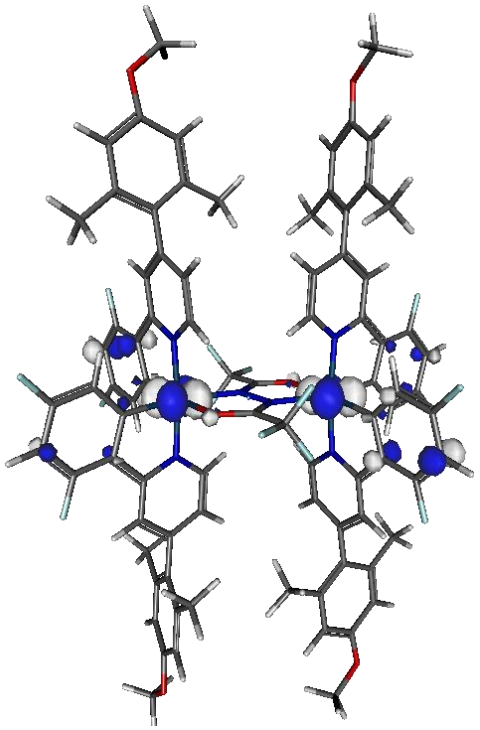

HOMO

–5.53 eV

Ir : Bridge : Ph : Py

45 : 4 : 44 : 7

Figure S140. Frontier molecular orbitals for the most stable minimum of *meso* **14**

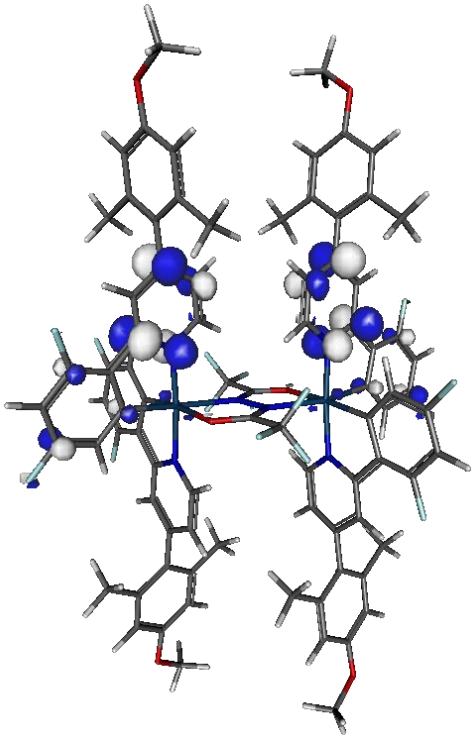

LUMO

–1.72 eV

Ir : Bridge : Ph : Py

4 : 2 : 22 : 70

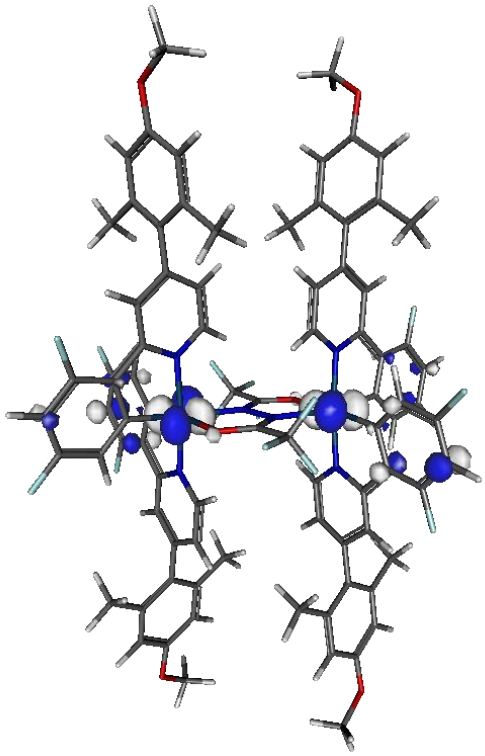

HOMO

–5.53 eV

Ir : Bridge : Ph : Py

45 : 4 : 44 : 7

Figure S141. Frontier molecular orbitals for the most stable minimum of *rac* **14**

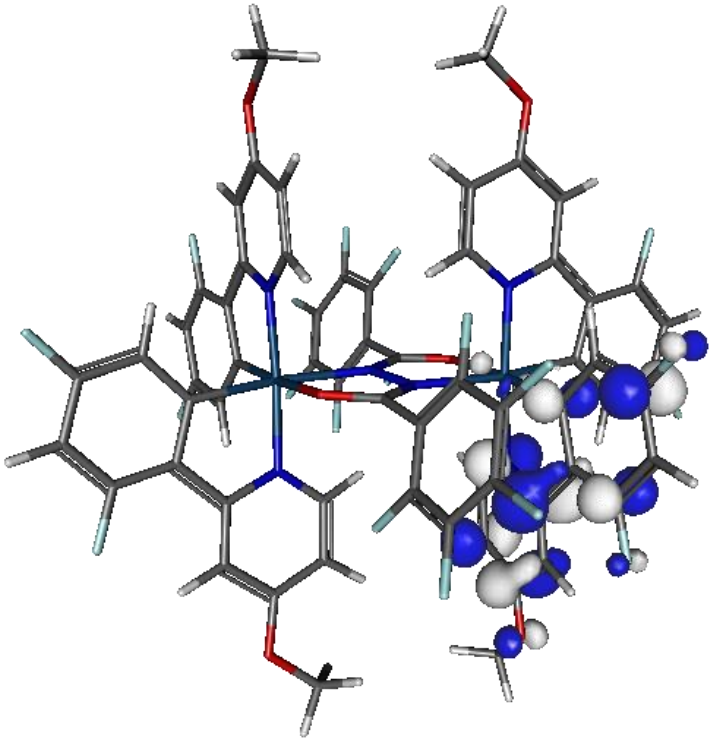

LUMO

–1.55 eV

Ir : Bridge : F_5 : Ph : Py

4 : 1 : 2 : 31 : 63

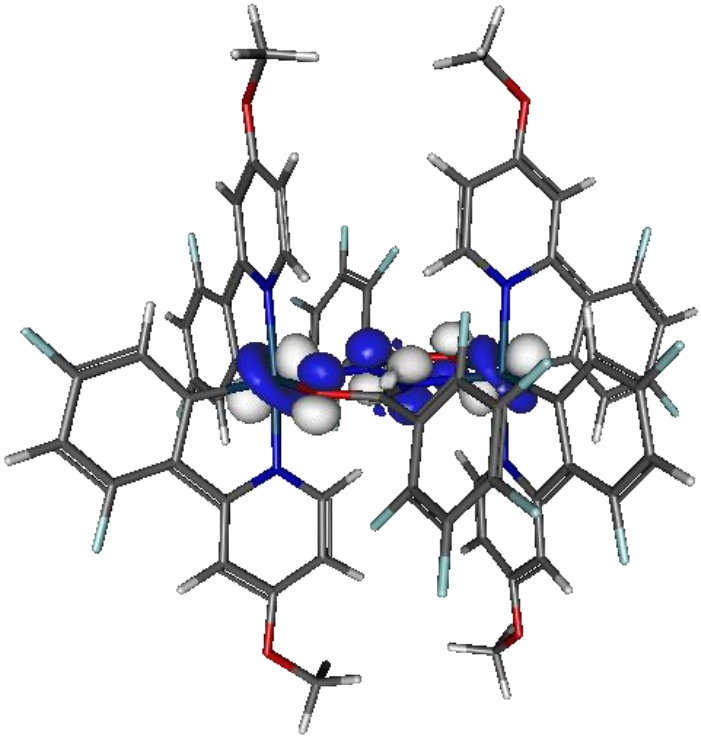

HOMO

–5.36 eV

Ir : Bridge : F_5 : Ph : Py

42 : 42 : 1 : 6 : 6

Figure S142. Frontier molecular orbitals for the most stable minimum of *meso* **15**

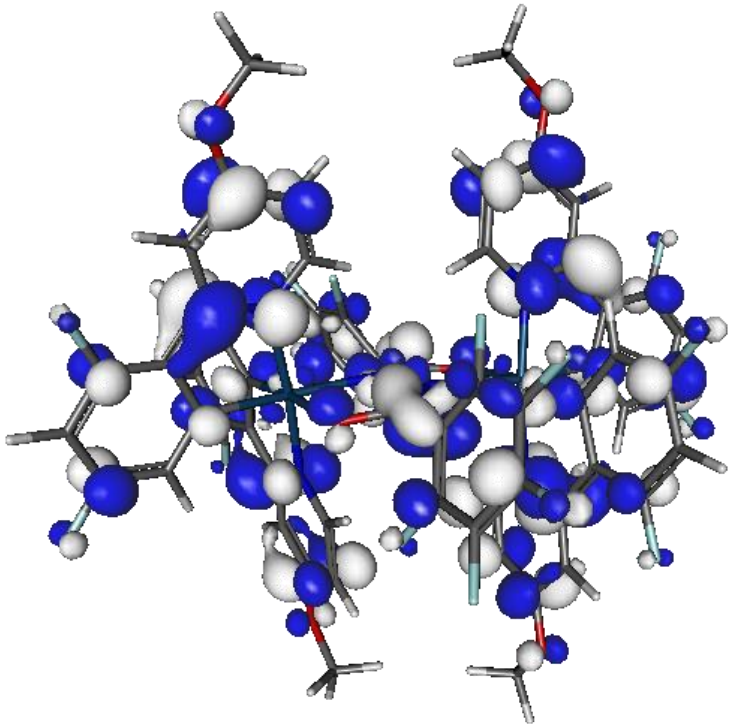

LUMO

–1.50 eV

Ir : Bridge : F_5 : Ph : Py

3 : 8 : 17 : 23 : 48

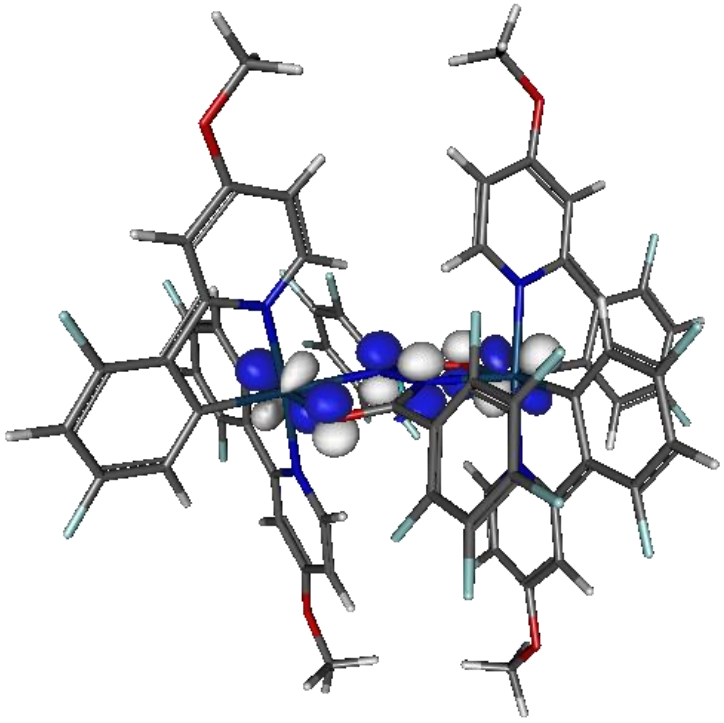

HOMO

–5.34 eV

Ir : Bridge : F_5 : Ph : Py

42 : 46 : 1 : 45 : 7

Figure S143. Frontier molecular orbitals for the most stable minimum of *rac* **15**

Thermal analysis

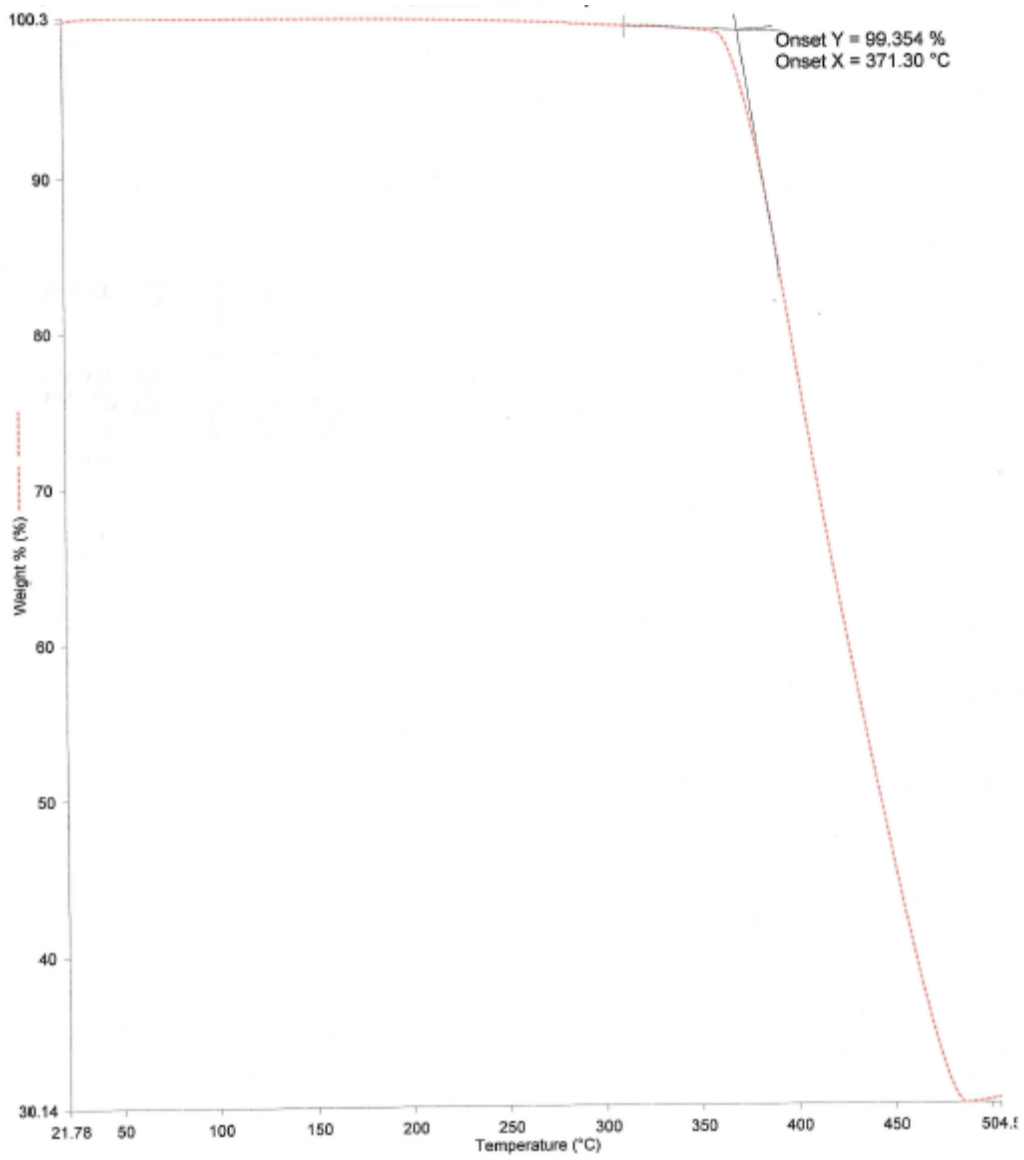

Figure S144. TGA trace of complex **7**. Onset = 371 °C.

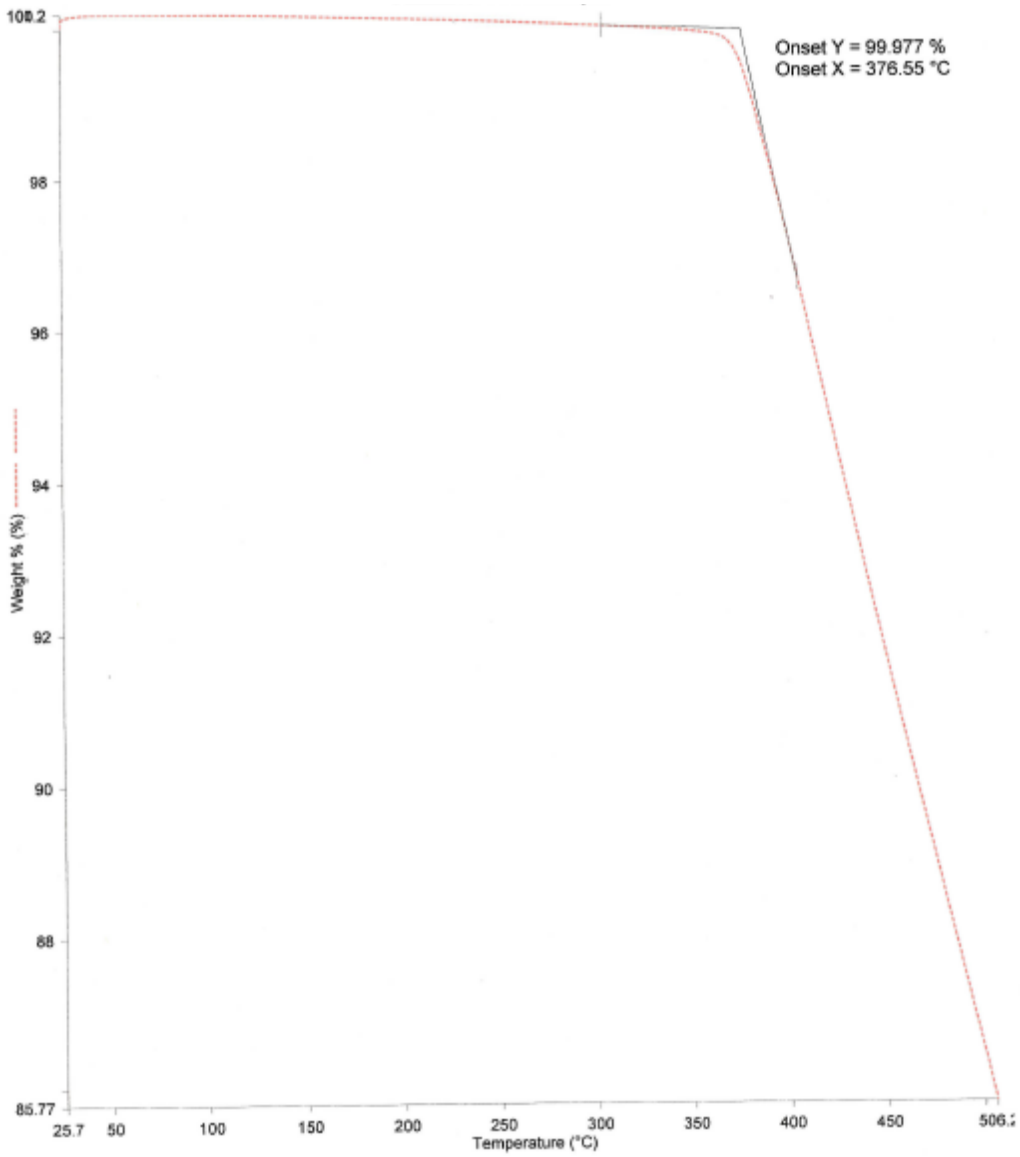

Figure S145. TGA trace of complex **8**. Onset = 377 °C.

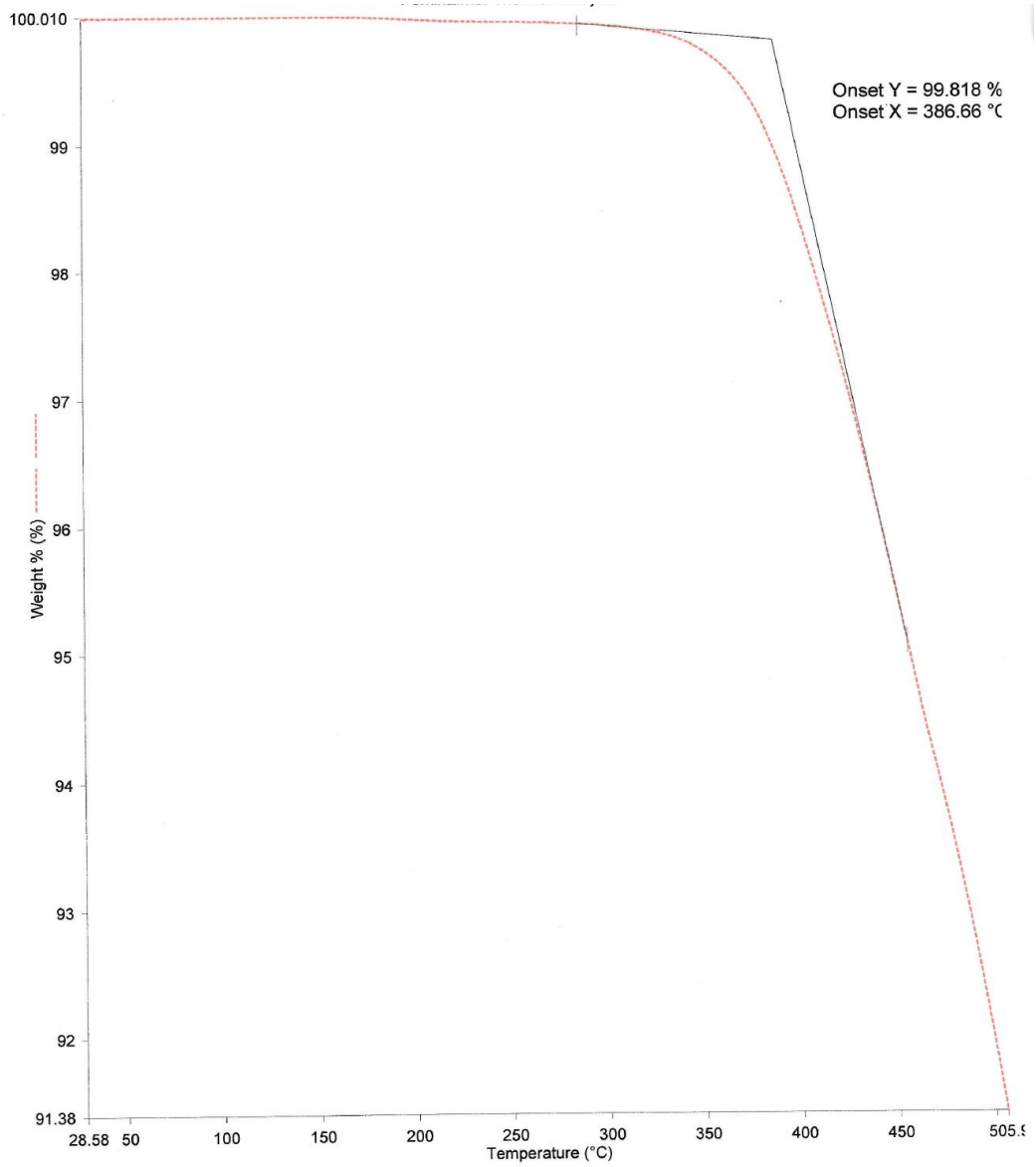

Figure S146. TGA trace of complex **9**. Onset = 387 °C.

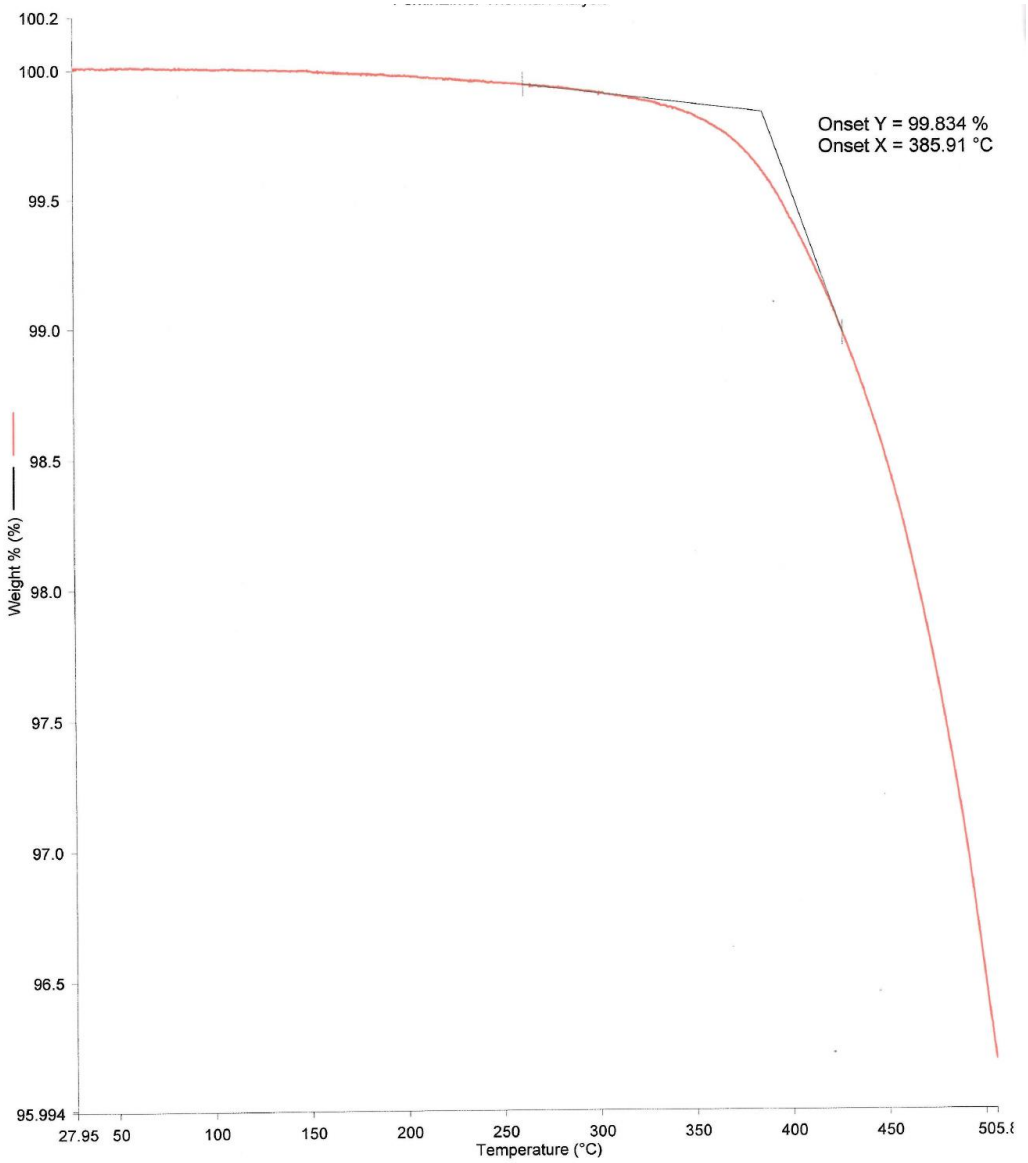

Figure S147. TGA trace of complex **10**. Onset = 386 °C.

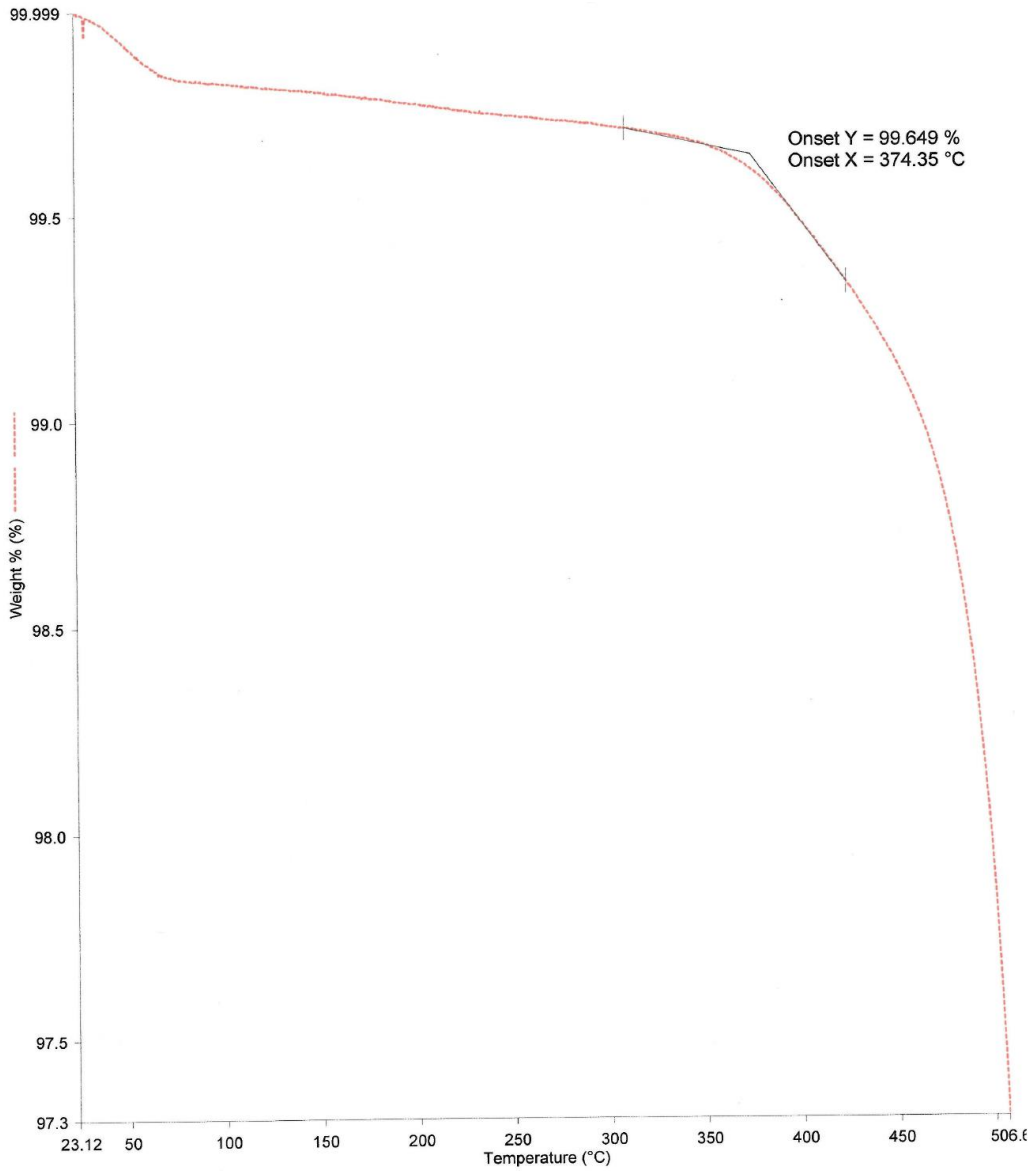

Figure S148. TGA trace of complex **11**. Onset = 374 °C.

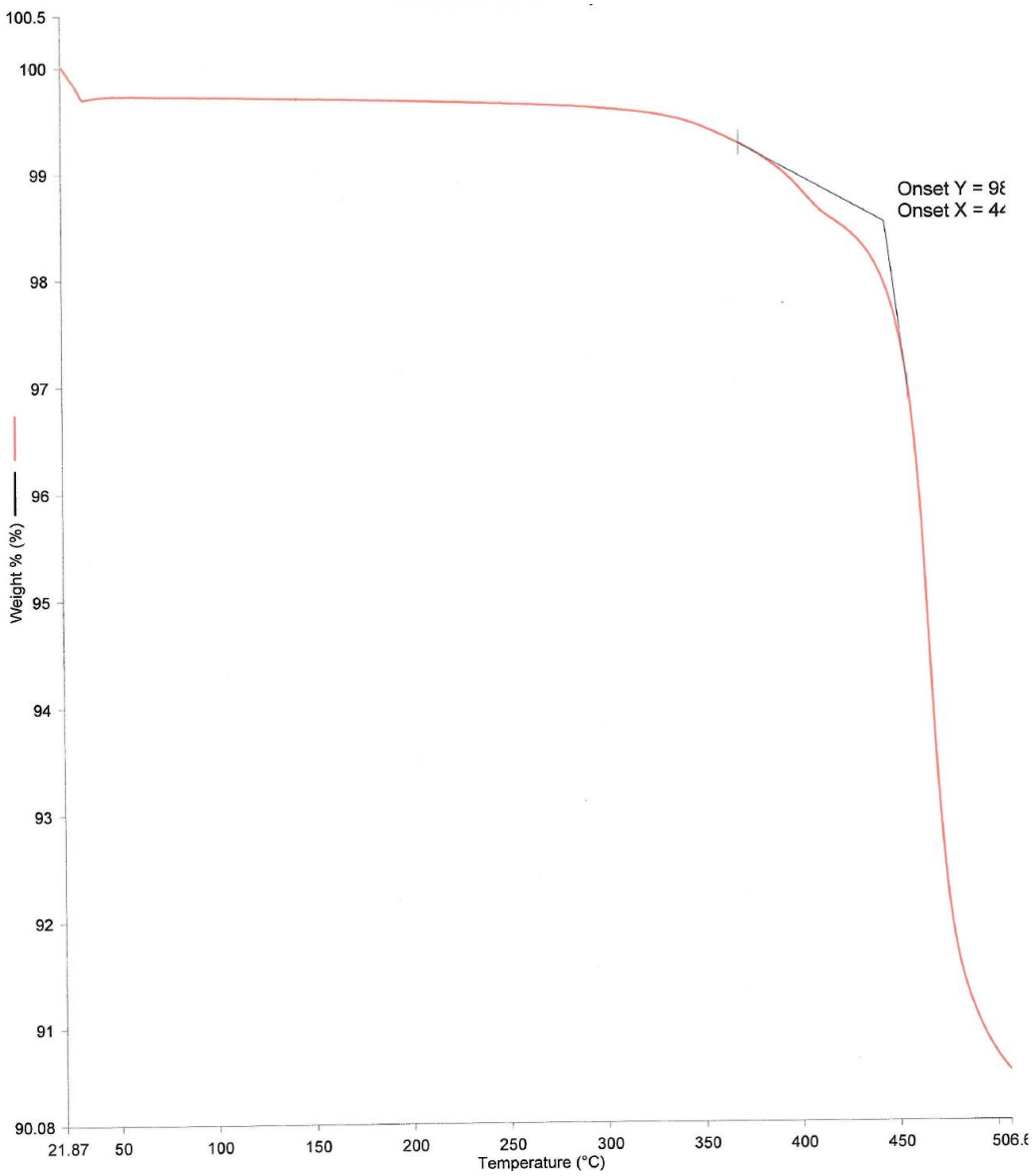

Figure S149. TGA trace of complex **12**. Onset = 440 °C.

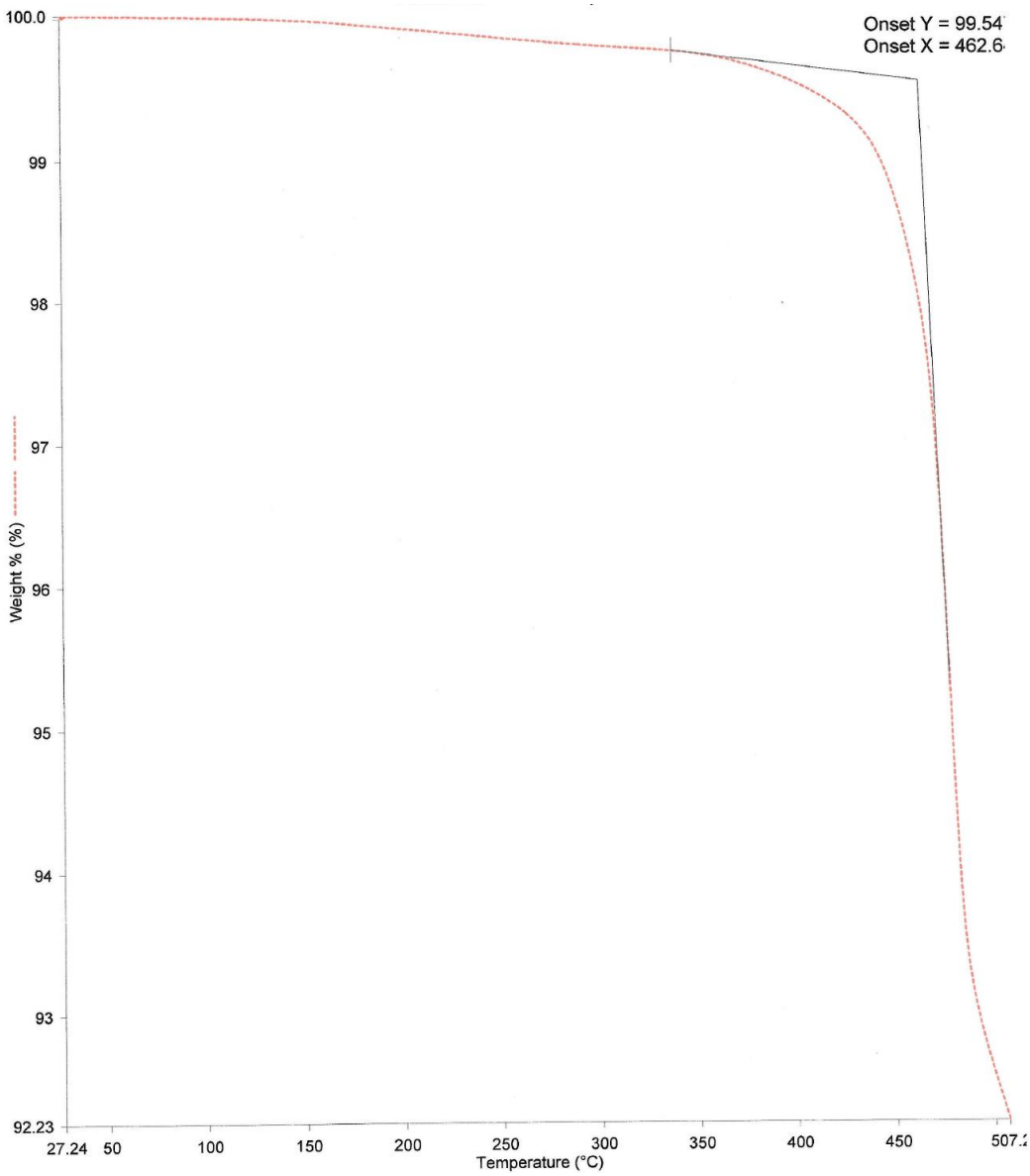

Figure S150. TGA trace of complex *meso* **13**. Onset = 463 °C.

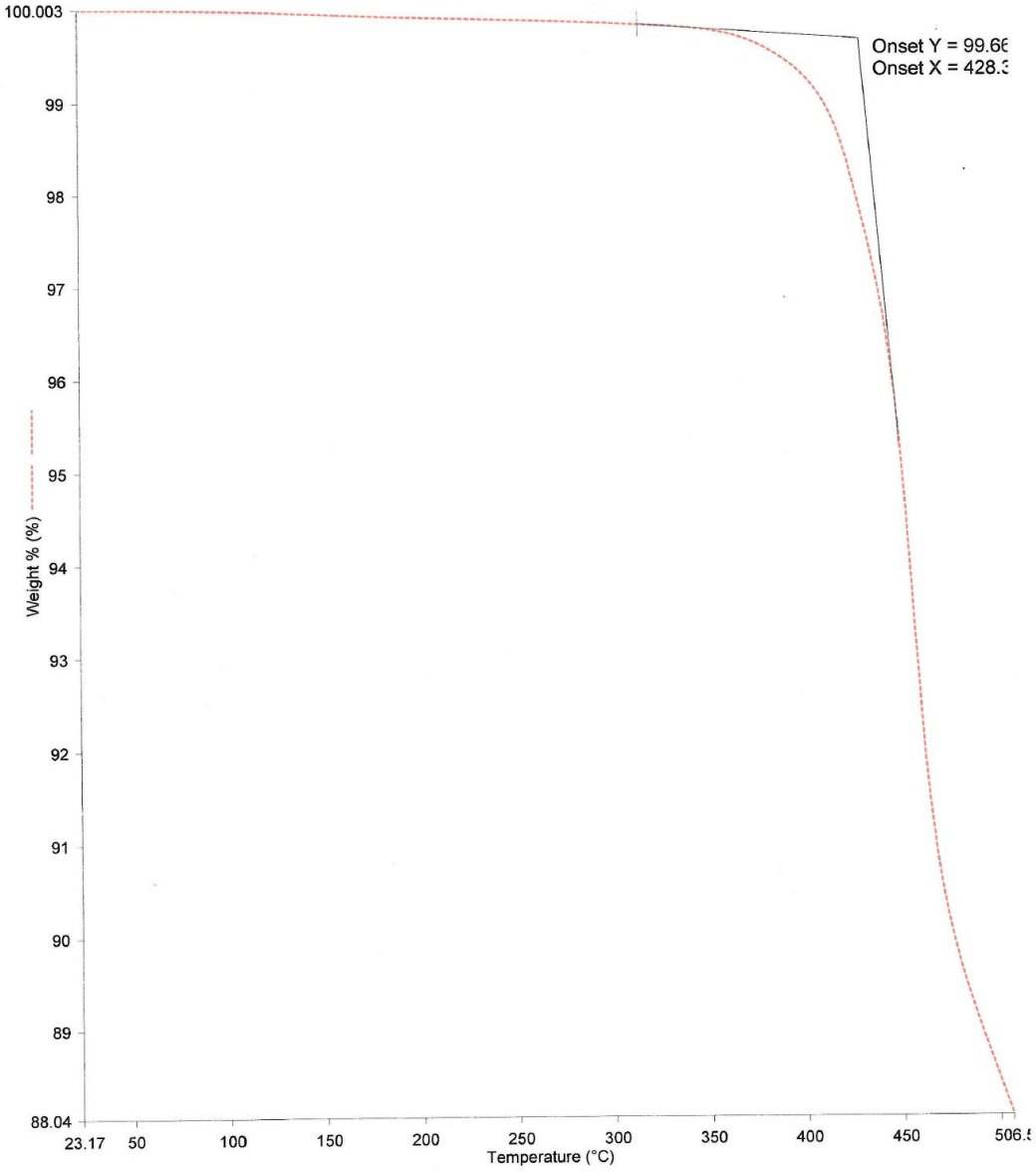

Figure S151. TGA trace of complex *rac* **13**. Onset = 428 °C.

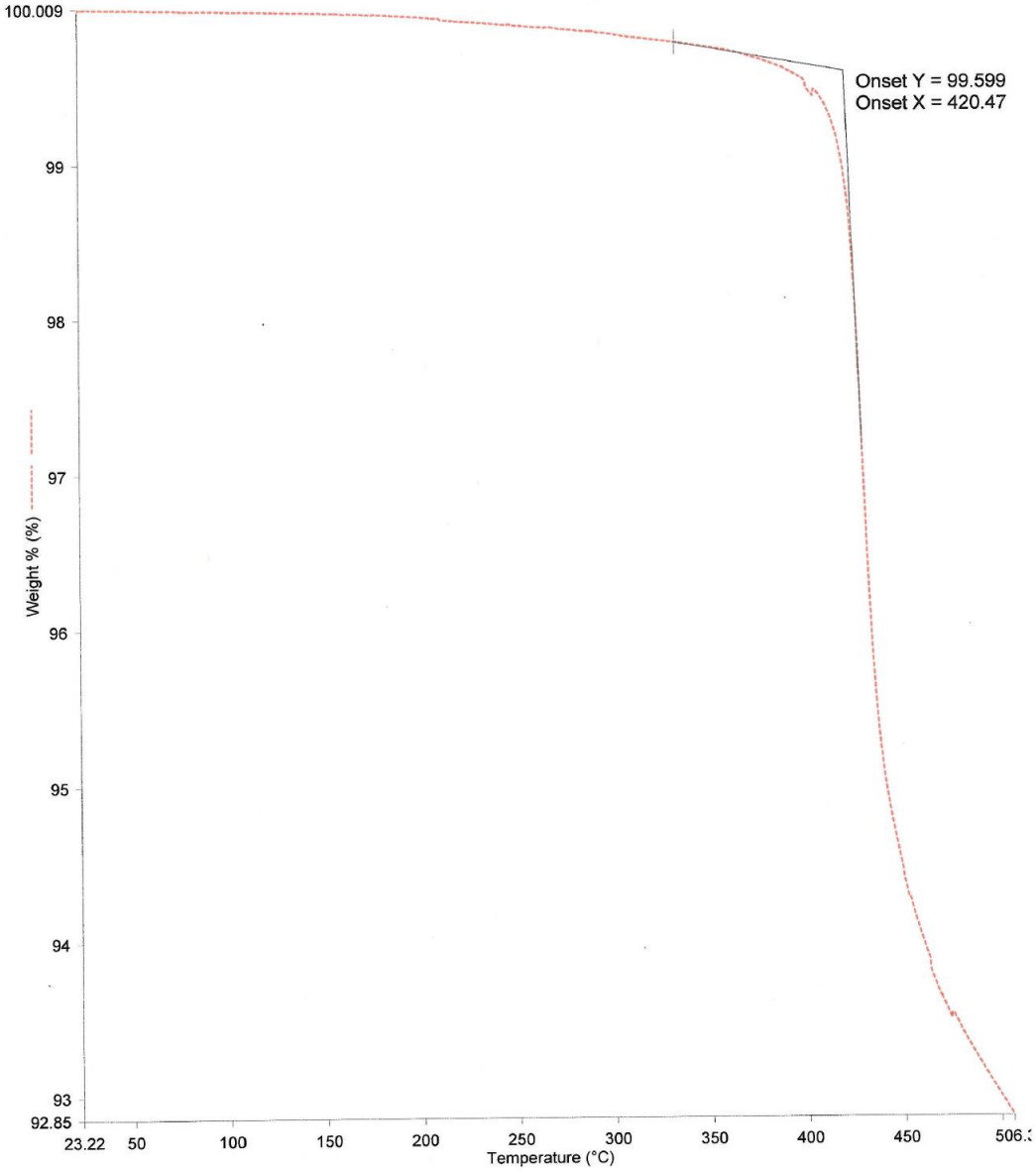

Figure S152. TGA trace of complex **14**. Onset = 420 °C.

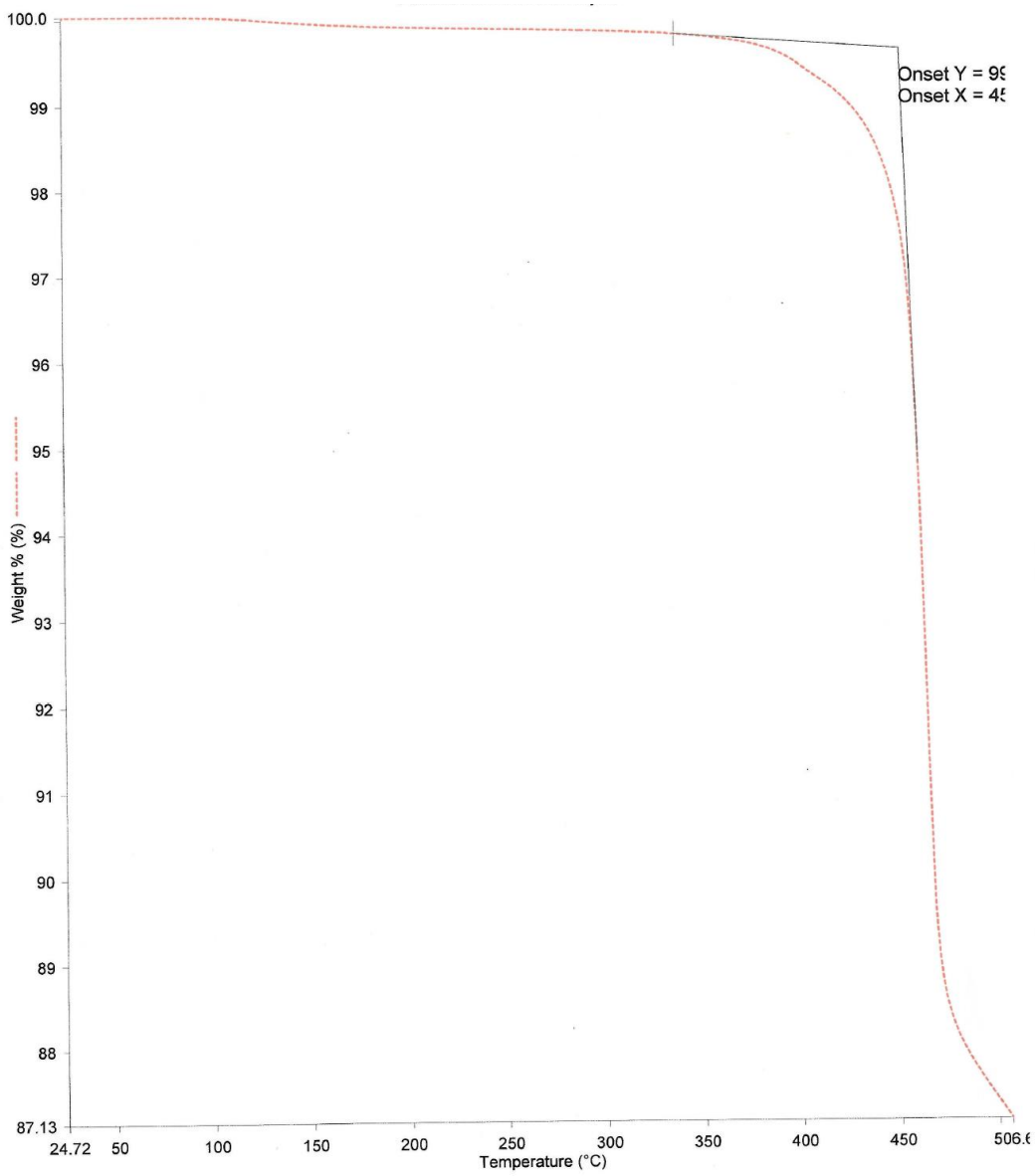

Figure S153. TGA trace of complex **15**. Onset > 450 °C.

Photophysics

Table S3. Tabulated absorption data for complexes **7–15** recorded in room temperature DCM solutions.

Complex	Isomer	λ_{abs} /nm (ε × 10^3 / $M^{-1}cm^{-1}$)
7	*mixture*	263 (77), 285sh (52), 310sh (30), 352 (15), 408 (7.5), 460 (4.3)
8	*mixture*	262 (70), 305sh (32), 345 (14), 380 (8.3), 400 (7.5), 455 (3.9)
9	*mixture*	261 (66), 281sh (50), 303sh (33), 345 (14), 400 (7.2), 453 (3.9)
10	*mixture*	262 (66), 281sh (50), 305sh (30), 347 (13), 377 (7.7), 401 (7.0), 451 (3.7)
11	*rac*	264 (80), 282 (70), 348 (19), 381 (11), 404 (10), 455 (5.5)
12	*meso*	265 (87), 281sh (81), 343 (25), 400 (11), 452 (5.4)
13	*meso*	255 (96), 274sh (79), 305sh (51), 336 (36), 384 (14), 430 (4.2), 460 (1.7)
	rac	255 (94), 276sh (73), 205sh (51), 335 (35), 386 (14), 430 (4.4), 460 (1.7)
14	*	252 (89), 272sh (77), 312sh (46), 331 (38), 382 (12), 429 (2.5), 457 (0.5)
15	*	239 (95), 259 (91), 291sh (44), 328 (21), 360 (13), 374 (11), 416 (3.3)
FIrpic	-	277 (50), 301 (34), 304 (33) 337sh (14), 357sh (8.9), 400 (6.2), 454 (0.8)[a]

[a]Values taken from ref 17. *Single diastereomer of unknown absolute configuration. sh = shoulder

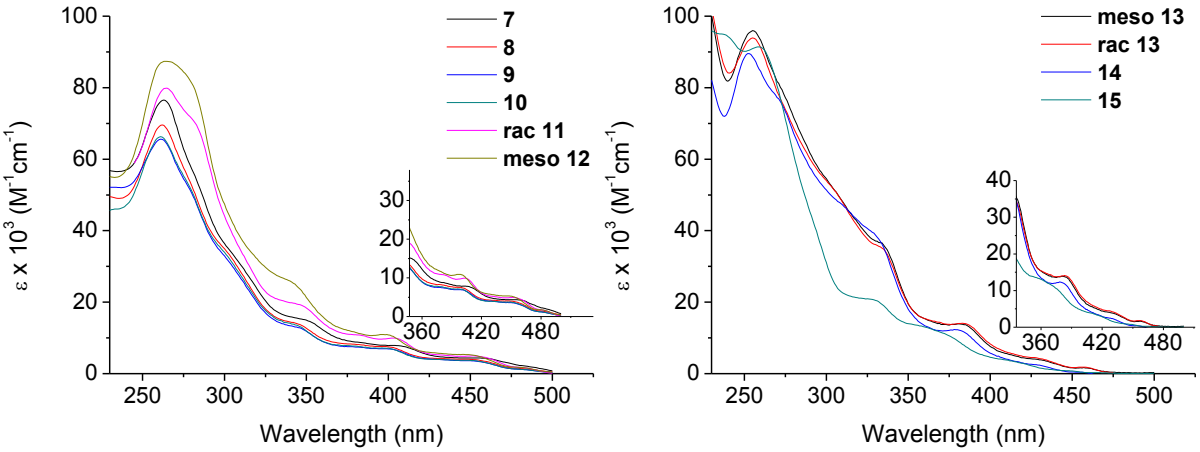

Figure S154. Absorption spectra of complexes **7–15** recorded in room temperature DCM solutions. Insets are expansions of the 350–500 nm regions.

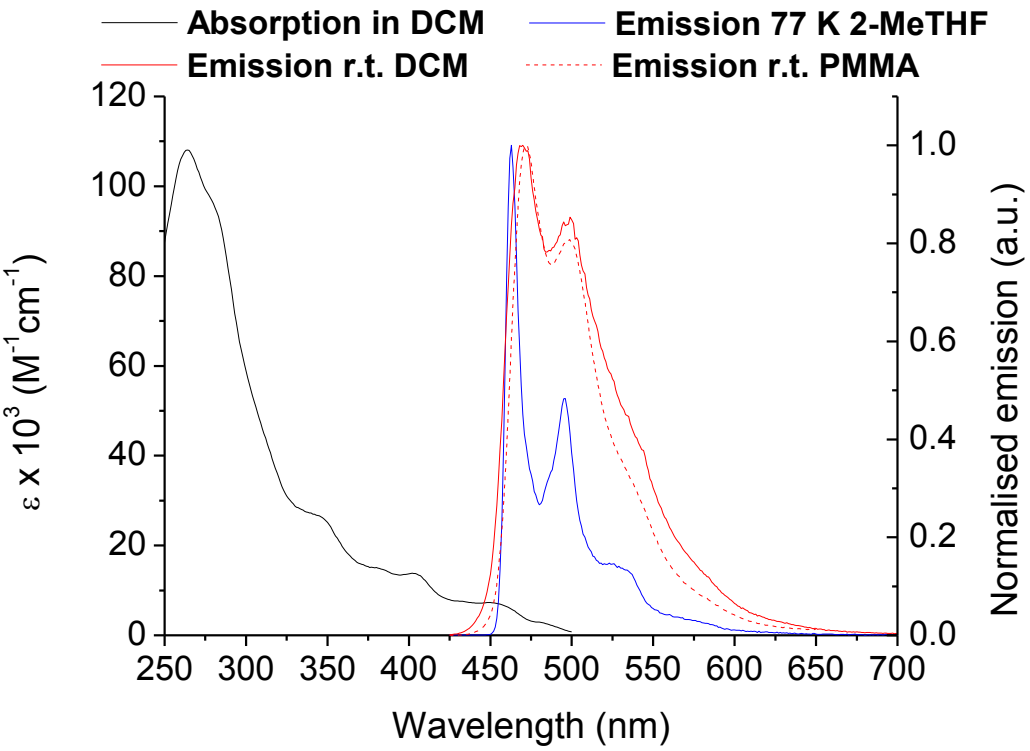

Figure S155. Spectral data for *rac* **13**.

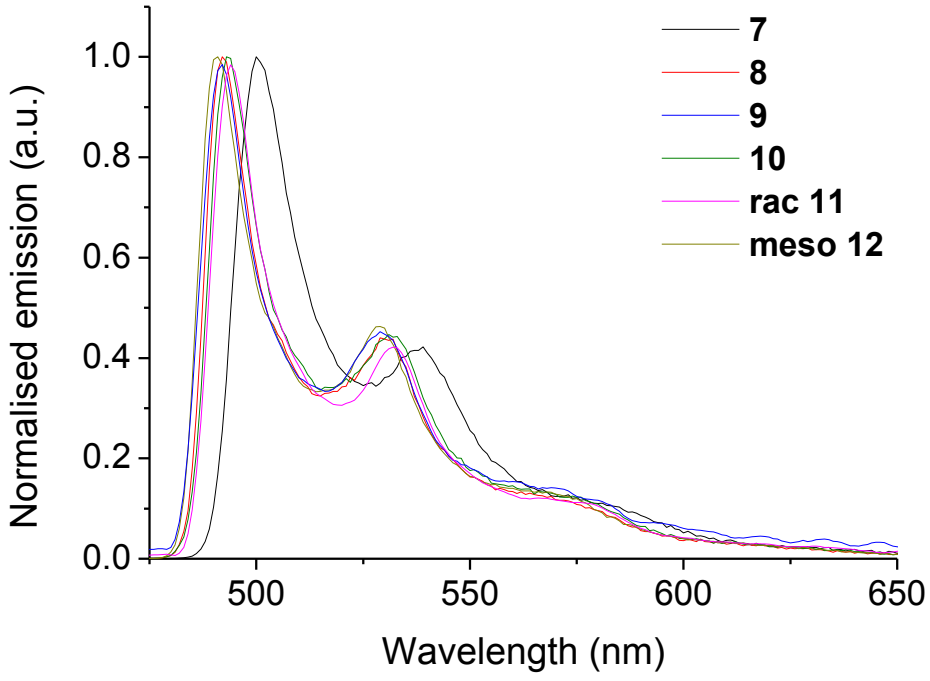

Figure S156. Normalised emission spectra of complexes **7**–**12** in 2-MeTHF glasses at 77 K (λ_{exc} 355 nm).

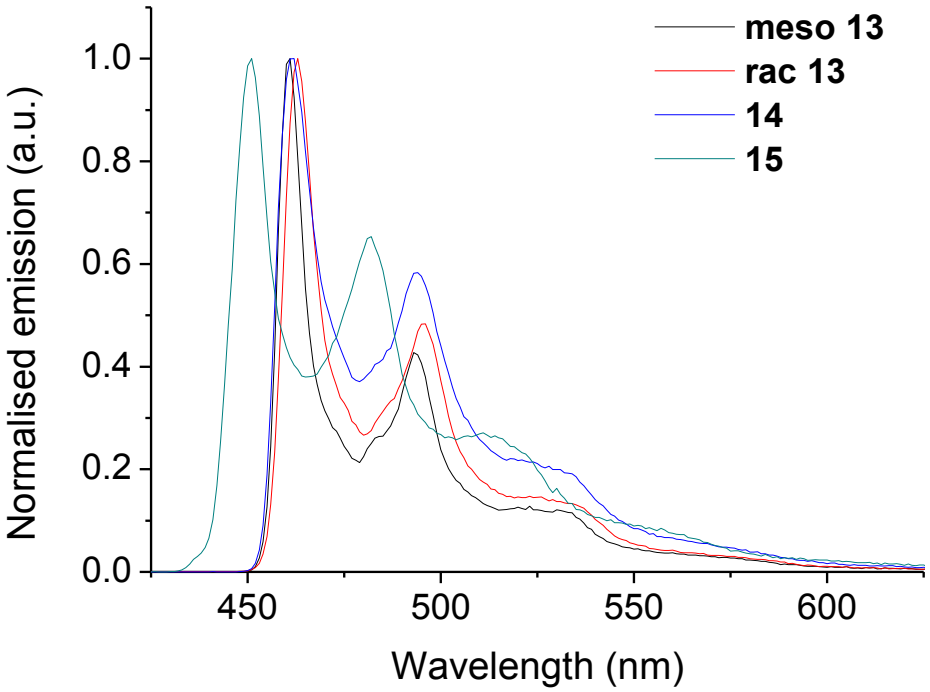

Figure S157. Normalised emission spectra of complexes **13**–**15** in 2-MeTHF glasses at 77 K (λ_{exc} 355 nm).

References

1 S. Sprouse, K. A. King, P. J. Spellane and R. J. Watts, *J. Am. Chem. Soc.*, 1984, 6647–6653.

2 V. N. Kozhevnikov, Y. Zheng, M. Clough, H. A. Al-Attar, G. C. Griffiths, K. Abdullah, S. Raisys, V. Jankus, M. R. Bryce and A. P. Monkman, *Chem. Mater.*, 2013, **25**, 2352–2358.

3 Gaussian 09, Revision A.02, M. J. Frisch, G. W. Trucks, H. B. Schlegel, G. E. Scuseria, M. A. Robb, J. R. Cheeseman, G. Scalmani, V. Barone, B. Mennucci, G. A. Petersson, H. Nakatsuji, M. Caricato, X. Li, H. P. Hratchian, A. F. Izmaylov, J. Bloino, G. Zheng, J. L. Sonnenberg, M. Hada, M. Ehara, K. Toyota, R. Fukuda, J. Hasegawa, M. Ishida, T. Nakajima, Y. Honda, O. Kitao, H. Nakai, T. Vreven, J. A. Montgomery, Jr., J. E. Peralta, F. Ogliaro, M. Bearpark, J. J. Heyd, E. Brothers, K. N. Kudin, V. N. Staroverov, R. Kobayashi, J. Normand, K. Raghavachari, A. Rendell, J. C. Burant, S. S. Iyengar, J. Tomasi, M. Cossi, N. Rega, J. M. Millam, M. Klene, J. E. Knox, J. B. Cross, V. Bakken, C. Adamo, J. Jaramillo, R. Gomperts, R. E. Stratmann, O. Yazyev, A. J. Austin, R. Cammi, C. Pomelli, J. W. Ochterski, R. L. Martin, K. Morokuma, V. G. Zakrzewski, G. A. Voth, P. Salvador, J. J. Dannenberg, S. Dapprich, A. D. Daniels, O. Farkas, J. B. Foresman, J. V. Ortiz, J. Cioslowski, D. J. Fox, Gaussian, Inc., Wallingford CT, 2009.

4 A. D. Becke, *J. Chem. Phys.*, 1993, **98**, 5648.

5 C. Lee, W. Yang and R. G. Parr, *Phys. Rev. B*, 1988, **37**, 785–789.

6 P. J. Hay and W. R. Wadt, *J. Chem. Phys.*, 1985, **82**, 270–283.

7 W. R. Wadt and P. J. Hay, *J. Chem. Phys.*, 1985, **82**, 284–298.

8 P. J. Hay and W. R. Wadt, *J. Chem. Phys.*, 1985, **82**, 293–310.

9 G. A. Petersson, A. Bennett, T. G. Tensfeldt, M. A. Al-Laham, W. A. Shirley and J. Mantzaris, *J. Chem. Phys.*, 1991, **94**, 6081–6090.

10 J. Melorose, R. Perroy and S. Careas, *J. Chem. Phys.*, 1988, **89**, 2193–2218.

11 A.-R. Allouche, *J. Comput. Chem.*, 2011, **32**, 174–182.
12 N. M. O'Boyle, A. L. Tenderholt and K. M. Langner, *J. Comput. Chem.*, 2008, **29**, 839–845.
13 L. Krause, R. Herbst-Irmer, G. M. Sheldrick and D. Stalke, *J. Appl. Crystallogr.*, 2015, **48**, 3–10.
14 G. M. Sheldrick, *Acta Crystallogr. A*, 2008, **A64**, 112–122.
15 O. V. Dolomanov, L. J. Bourhis, R. J. Gildea, J. A. K. Howard and H. Puschmann, *J. Appl.Crystallogr.*, 2009, **42**, 339–341.
16 G. M. Sheldrick, *Acta Crystallogr. C*, 2015, **71**, 3–8.
17 H. Benjamin, Y. Zheng, A. S. Batsanov, M. A. Fox, H. A. Al-Attar, A. P. Monkman and M. R. Bryce, *Inorg. Chem.*, 2016, **55**, 8612–8627.
18 R. Davidson, Y. Hsu, T. Batchelor and A. Beeby, *Dalton Trans.*, 2016, **45**, 11496–11507.
19 L.-O. Pålsson and A. P. Monkman, *Adv. Mater.*, 2002, **14**, 757–758.
20 D. G. Congrave, Y.-t. Hsu, A. S. Batsanov, A. Beeby and M. R. Bryce, *Organometallics*, 2017, **36**, 981–993.
21 N. Ai, A. Yoshinobu, O. Kazushi, S. Shimpei, I. Toshiya, I. Satoshi, US2005265686 (A1), 2005.
22 V. V. Il'in, O. V. Slavinskaya, Y. A. Strelenko, A. V. Ignatenko and V. A. Ponomarenko, *Bull. Acad. Sci. USSR, Div. Chem. Sci. English Transl.*, 1992, **40**, 2177–2180.
23 D. R. Martir, C. Momblona, A. Pertegás, D. B. Cordes, A. M. Z. Slawin, H. J. Bolink and E. Zysman-Colman, *ACS Appl. Mater. Interfaces*, 2016, **8**, 33907–33915.